The Snf2h and Snf2l nucleosome remodeling proteins co-modulate gene expression and chromatin organization to control brain development, neural circuitry assembly and cognitive functions.

Matías Alberto Alvarez-Saavedra,

Ph.D. Thesis.

This thesis is submitted to the Faculty of Graduate and Postdoctoral Studies in partial fulfillment of the requirements for the Doctorate in Philosophy in Cellular & Molecular Medicine at the University of Ottawa, Ottawa, Ontario, Canada.

Department of Cellular & Molecular Medicine,

Faculty of Medicine,

University of Ottawa.

The Snf2h and Snf2l nucleosome remodeling proteins co-modulate gene expression and chromatin organization to control brain development, neural circuitry assembly and cognitive functions.

Matías Alberto Alvarez-Saavedra,

Ph.D. Thesis.

Date of submission: 29th November 2013.

Internal Examiners: Drs. Diane Lagace, David Lohnes and Ruth Slack.

External Examiner: Dr. Jacques Côté, Université Laval, Québec, Canada.

Born in Santiago, Chile, May 06, 1980.

Ex nihilo nihil fit.

"Nothing comes from nothing."

Parmenides of Elea, Greek philosopher, founder of the Eleatic School of Philosophy.

This work gave rise to the following publication:

Snf2l regulates FoxG1-dependent progenitor cell expansion in the developing brain.
Yip D*, Corcoran C*, Alvarez-Saavedra M*, De Maria A, Rennick S, Mears A, Rudnicki M, Messier C, Picketts, DJ. *Developmental Cell* 2012, 22(4): 871-8. * = Joint first-authors.

And to the following submitted manuscripts:

Snf2h mediates histone dynamics to control cerebellar development and function.
Matías Alvarez-Saavedra, Yves De Repentigny, Edupuganti V. Raghu Ram, Keqin Yan, Alan J. Mears, Pamela S. Lagali, Michael S. Huh, Emile Hashem, Danton Ivanochko, Matthew A. Todd, Chelsea P. Corcoran, Juraj Kokavec, Romit Majumder, Valerie A. Wallace, Rashmi Kothary, Tomas Stopka, Eran Meshorer, Arthur I. Skoultchi and David J. Picketts.

Snf2h and Satb2-dependent chromatin regulation governs cortical development and maturation.
Matías Alvarez-Saavedra, Emile Hashem, Danton Ivanochko, Doo Yang, Keqin Yan, Yves De Repentigny, Gregory O. Cron, Rashmi Kothary, Teruyoshi Hirayama, Takeshi Yagi, Ilya Ioshikhes and David J. Picketts.

ABSTRACT

Chromatin remodeling enzymes are instrumental for neural development as evidenced by their identification as disease genes underlying human disorders characterized by intellectual-disability. In this regard, the murine *Snf2h* and *Snf2l* genes show differential expression patterns during embryonic development, with a unique pattern in the brain where Snf2h is predominant in neural progenitors, while Snf2l expression peaks at the onset of differentiation. These observations led me to investigate the role of Snf2h and Snf2l in brain development by using conditionally targeted Snf2h and Snf2l mice.

I selectively ablated Snf2h expression in cortical progenitors, cerebellar progenitors, or postmitotic Purkinje neurons of the cerebellum, while Snf2l was deleted in the germline. I found that Snf2h plays diverse roles in neural progenitor expansion and postmitotic gene expression control, while Snf2l is involved in the precise timing of neural differentiation onset. Gene expression studies revealed that Snf2h and Snf2l co-modulate the *FoxG1* and *En1* transcription factors during cortical and cerebellar neurogenesis, respectively, to precisely control the transition from a progenitor to a differentiated neuron. Moreover, Snf2h is essential for the postmitotic neural activation of the clustered *protocadherin* genes, and does so by functionally interacting with the matrix-attachment region protein Satb2. My neurobehavioral studies also provided insight into how Snf2h loss in cerebellar progenitors results in cerebellar ataxia, while Snf2h loss in cortical progenitors, or in postmitotic Purkinje neurons of the cerebellum, resulted in learning and memory deficits, and hyperactive-like behavior.

Molecularly, Snf2h plays an important role in linker histone H1e dynamics and higher order chromatin packaging, as evidenced by loss of chromatin ultrastructure upon Snf2h deletion in progenitor and postmitotic neurons. I further demonstrated that Snf2h loss in a neuronal cell culture model results in reduced H1e deposition, and that overexpression of human SNF2H or SNF2L upon Snf2h knockdown rescues this biochemical dysfunction. My experiments suggest that Snf2h and Snf2l are regulatory nucleosome remodeling engines that co-modulate the gene expression programs necessary for proper brain development, maturation and function.

ACKNOWLEDGEMENTS

Special thanks to Dr. Picketts for financial support during my stay in his laboratory. Also for intellectual freedom and great, long discussions.

Thanks to the members of my thesis advisory committee for important insight:
Drs. David Lohnes, Rashmi Kothary, Valerie Wallace and Robin Parks.

I'm also grateful to members of the Picketts lab for discussions and especially thankful to Mrs. Keqin Yan for technical assistance.

Thanks to Dr. Diane Lagace and Mirela Hasu at the University of Ottawa Behavioral Core for assistance with behavioral experiments and expert discussions.

I thank my wife Sulman Caballero for unconditional emotional support.

I dedicate this thesis to my mother Victoria Saavedra who inspired me to think freely ever since I can remember. Thank you Mamma!!

I also dedicate this thesis to the memory of my grandfather Sandalio "Lalo" Saavedra, and to my ancestors from the most southern oceans of Chile.

TABLE OF CONTENTS

ABBREVIATIONS

ACF = ATP-utilizing chromatin assembly and remodeling factor
ASH1 = absent, small, or homeotic 1
ATP = adenosine triphosphate
BAF = brahma-associated factor
BAP = brahma-associated protein
BMP = bone morphogenetic protein
BRG1 = Brahma-related factor 1
BRM = Brahma
CaPN = callosal projection neuron
CC = corpus callosum
CERF = CECR2-containing remodeling factor
CHD = chromodomain
CHRAC = chromatin accessibility complex
CNS = central nervous system
CPN = cortical projection neuron
CRC = chromatin remodeling complex
CTCF = CCCTC-binding factor
CThPN = corticothalamic projection neuron
CTIP2 = B-cell lymphoma/leukemia 11B
Cux = cut-like
DNA= deoxyribonucleic acid
E = embryonic
Emx = empty spiracles homeobox
En = engrailed
ESC = embryonic stem cell
FEZF2 = FEZ family zinc finger 2
FGF = fibroblast growth factor
FoxG1 = forkhead box G1
GC = granule cell
GNP = granule neuron progenitor
HDAC = histone deacetylase
ISWI = imitation switch
LHX2 = lim homeobox gene 2
LSD1 = lysine demethylase 1
Lys (K) = lysine
MATH1 = mouse atonal homolog 1
MBD = methyl-binding domain
mRNA= messenger RNA
MTA = metastasis associated
NoRC = nucleosome remodeling factor
NSC = neural stem cell
NTP = nucleotide triphosphate
NURD = nucleosome remodeling deacetylase
NURF = nucleosome remodeling factor

PAX6 = paired box gene 6
Pc = polycomb
PC = Purkinje cell
PTM = post-translational modification
RBBP = retinoblastoma binding protein
RNA = ribonucleic acid
RSF = remodeling and spacing factor
SANT = Swi3, Ada2, N-Cor, and TFIIIB
SATB2 = special AT-rich sequence-binding protein 2
ScPN = subcerebral projection neuron
Shh = sonic hedgehog
SLIDE = SANT-like ISWI domain
SMARCA1/5 = SWI/SNF-related, matrix-associated, actin-dependent regulator of chromatin, subfamily A, member 1/5
SNF2H = snf2-homolog
SNF2L = snf2-like
SOX5 = SRY-Box 5
SVZ = subventricular zone
SWI2/SNF2 = sucrose non-fermentation/mating type switching 2
Tbr1 = T-box, brain, 1
TRX = trithorax
qPCR = quantitative polymerase chain reaction
VZ = ventricular zone
WICH = WSTF-imitation switch
WNT = wingless-type MMTV integration site family
WSTF = Williams syndrome transcription factor

CHAPTER 1: GENERAL INTRODUCTION

1.1 The SWI2/SNF2 superfamily of ATP-dependent nucleosome remodeling enzymes

Chromatin regulation underlies all aspects of mammalian development and gene expression control, from a totipotent stem cell to the establishment and maintenance of complex neural networks. At least five processes control the assembly and dynamics of chromatin: DNA methylation/demethylation, histone post-translational modifications (PTMs), histone variant exchange, non-coding RNA regulation, and ATP-dependent chromatin remodeling (Guibert and Weber, 2013). Chromatin remodeling complexes (CRCs) play roles in all processes dealing with DNA, including DNA replication, gene activation/repression, DNA repair, histone variant exchange, and higher order chromatin structure. More than 30 different ATP-dependent CRCs have non-redundant roles in development, and can slide, eject or restructure nucleosomes to control gene expression and higher order chromatin packaging.

Evolutionary conserved SWI2/SNF2-like CRCs are classified into four main families: SWI/SNF, ISWI, CHD and INO80. They are expressed in nearly all tissues, and have diverse, yet specific roles in activating and repressing gene targets. Moreover, these roles have further diversified in higher eukaryotes to provide cell-type specific spatiotemporal control of gene expression (Narlikar et al., 2013).

The SWI2/SNF2 proteins all share a common SNF2 helicase/ATPase comprised of seven-conserved motifs common to nucleoside triphosphate (NTP)-binding proteins that include DNA and RNA helicases (Eisen et al., 1995). Subfamilies are further defined by the

degree of similarity between the ATPase domain and the presence of other conserved chromatin interacting motifs (Eisen et al., 1995). For example, SNF2 subfamily members have a conserved bromodomain that serves as an acetylated histone recognition module (Marmorstein and Berger, 2001). The imitation switch (ISWI) subfamily members have a HAND-SANT C-terminal domain juxtaposed to a SLIDE domain that further specifies nucleosomal substrate recognition (Grune et al., 2003). Chromodomain helicase DNA binding (Chd) subfamily members have two chromodomains involved in methylated histone tail recognition and some have PHD fingers implicated in methyl-lysine histone tail recognition (Woodage et al., 1997). Lastly, INO80 subfamily members have a conserved DBINO DNA-binding domain and are involved in variant histone H2AZ deposition (Bakshi et al., 2004; Mizuguchi et al., 2004). I will discuss the biological function of each of the four families of ATPases with a special emphasis on the ISWI family of CRCs **(Figure 1.1)**.

1.1.1 The SNF2/SWI2 proteins

The original member of the SNF2 subfamily of chromatin remodeling proteins, and the archetype for all SNF2 members, is the *Saccharomyces cerevisiae* (*S. cerevisiae)* SNF2 protein originally identified in yeast mutants deficient in mating type switching (SWI2), and sugar metabolism (sucrose non-fermentation, SNF2), hence collectively referred to as SWI2/SNF2 proteins (Abrams et al., 1986; Neigeborn and Carlson, 1984). Snf2 family proteins are DNA-dependent ATPases; ubiquitous in all eukaryotes; and also found in archae and bacteria (Ryan and Owen-Hughes, 2011). SWI2/SNF2 proteins were found to associate as multiprotein complexes with nucleosome remodeling activity and collectively named as

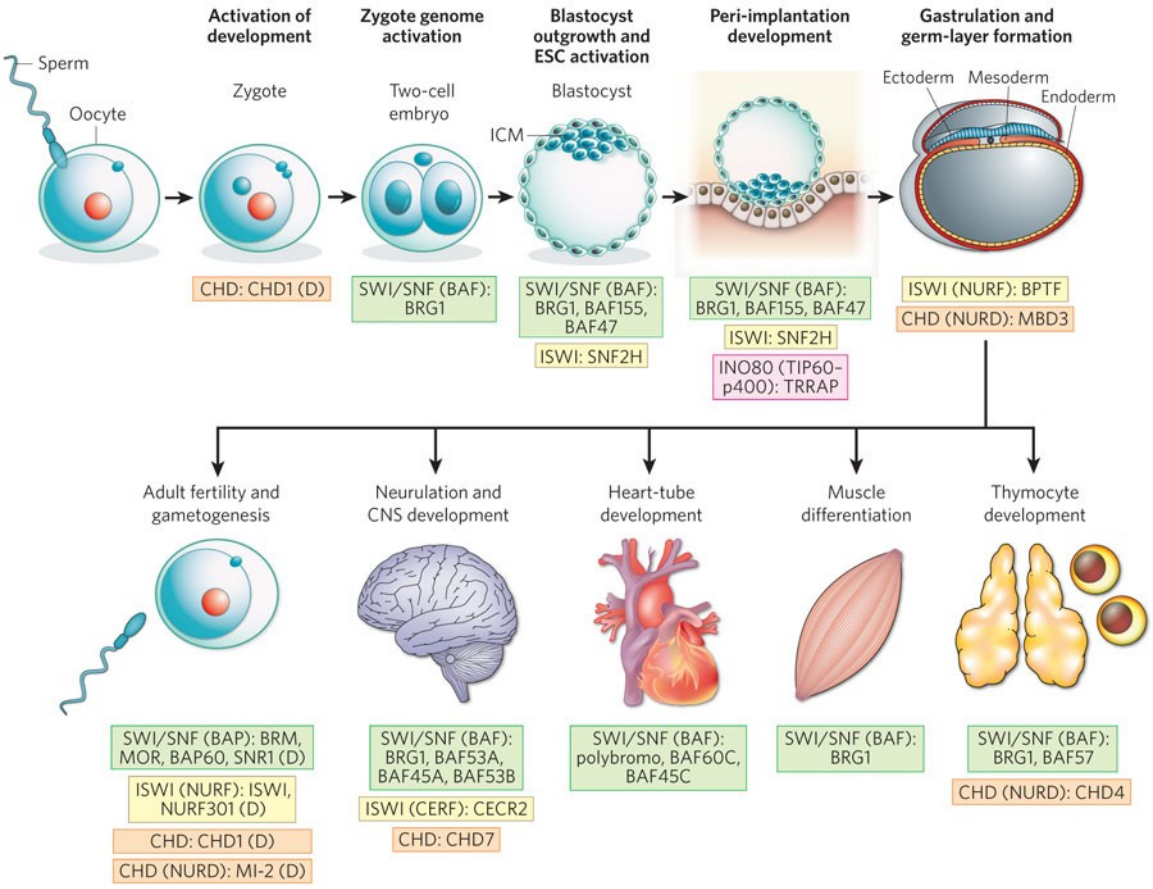

Figure 1.1 The four families of chromatin remodelers — SWI/SNF (green background), ISWI (yellow), CHD (orange) and INO80 (pink) — are required at distinct steps for the normal development of the development of embryos (implantation, gastrulation and organogenesis) and for the formation of gametes. The proteins known to be involved in mouse development are listed next to each developmental stage, together with the complex involved (and the name of the specific complex if known). In cases in which studies using mouse models have not been reported, proteins found to be involved in *Drosophila melanogaster* development are listed, as denoted by *(D),* although these results are not necessarily extrapolated to mammalian development. BAF complexes are involved in most of the developmental transitions depicted. The requirement for BAF complexes throughout development could reflect the many combinatorial possibilities of BAF complex composition. However, the apparent involvement of BAF complexes more than other chromatin-remodeling complexes could just reflect that these complexes are the most widely studied of the chromatin remodelers thus far. BAP, Brahma-associated proteins; BPTF, bromodomain PHD-finger transcription factor; CERF, CECR2-containing remodeling factor; CNS, central nervous system; ICM, inner cell mass; MOR, Moira; NURF, nucleosome-remodeling factor; SNR1, Snf5-related protein 1; TRRAP, transformation/transcription-domain-associated protein [printed with permission from {(Ho and Crabtree, 2010)}.

SWI2/SNF2 complexes (Cote et al., 1994). These proteins were found to participate in essential nuclear processes, including transcription and chromatin positioning (Hirschhorn et al., 1992; Peterson and Herskowitz, 1992; Yoshinaga et al., 1992).

The SWI2/SNF2 homolog found in *Drosophila melanogaster (Drosophila)* was named *Brahma (Brm)* for the Hindu god of fate, as it was first identified as a member of the trithorax group of genes that determine cell fate and patterning (Kennison and Tamkun, 1988). Mammals have two non-redundant paralogues, *Brm* and *Brahma-related gene 1 (Brg1)* (Khavari et al., 1993; Randazzo et al., 1994). *Brm*-null mice develop normally and show no overt phenotypes, while *Brg1*-null mice die at the peri-implantation stage (Bultman et al., 2000; Reyes et al., 1998). Moreover, maternal *Brg1* is necessary for zygotic genome activation at the two-cell stage embryo (Bultman et al., 2006). Brahma-associated proteins (BAP) were found to interact as multisubunit ATP-dependent CRCs and termed Brahma-associated factor (BAF) complexes (Dingwall et al., 1995). BAF complexes have diverse roles during mammalian development through combinatorial subunit composition exchange (Ho and Crabtree, 2010). For example, mouse embryonic stem cells (ESCs) have a specialized complex named esBAF, which has Brg1 (as catalytic subunit) and the Baf170 subunit, amongst others (Ho et al., 2009a; Ho et al., 2009b). As ESCs differentiate, the esBAF complex incorporates Brm and BAF60c (Ho et al., 2009a; Ho et al., 2009b). The BAF complexes further specialize: Brg1 is required for both neural stem cell (NSC) self-renewal and neural differentiation, but subunit composition further specifies the formation of two different complexes. A neuronal-progenitor-specific BAF (npBAF) complex contains Brg1 and subunits Baf45a and Baf53a, while a postmitotic neuron BAF (nBAF) complex contains Brg1 and subunits Baf45b and Baf53b (Lessard et al., 2007; Wu et al., 2007). This

specificity in subunit composition is necessary for neural development since Baf53a could not rescue the alterations in neural arborization associated with Baf53b loss (Wu et al., 2007). These studies highlight how spatiotemporal specificity of the BAF complexes arise from combinatorial assembly of their subunits which are necessary for neural development.

1.2 The Chromodomain (CHD) proteins

The CHD family is characterized by two chromodomains and has nine members further classified into three subfamilies: CHD subfamily 1 (CHD1 and CHD2); CHD subfamily 2 (CHD3 and CHD4); and CHD subfamily 3 (CHD5-9) (Hall and Georgel, 2007). The CHD domain is well known to interact with methylated histone tails (Flanagan et al., 2005; Woodage et al., 1997). Nevertheless, subfamily members have additional motifs that provide further substrate specificity: an AT-rich DNA binding motif; and PHD domains involved in methyl-lysine recognition (Pena et al., 2006).

1.2.1 CHD1 & CHD 2 (CHD subfamily I)

CHD subfamily I is distinguished by the presence of a DNA-binding domain that recognizes AT-rich sequences (Stokes and Perry, 1995). In yeast, *Chd1* was found to interact with components of the transcriptional elongation machinery and necessary for gene activation (Simic et al., 2003). In *Drosophila, Chd1* is more specific for gametogenesis as *Chd1*-null flies are sterile (McDaniel et al., 2008). This is due to the role for Chd1 in maternal H3.3 incorporation into the male pronucleus post-fertilization (Konev et al., 2007). *Drosophila Chd1* is also required for higher order chromatin structure, similar to the role for ISWI in chromatin organization (Bugga et al., 2013; Deuring et al., 2000). In mammals, Chd1 specifically recognizes trimethylated Lys 4 of Histone H3 to mediate recruitment of

post-transcriptional and pre-mRNA splicing factors (Sims et al., 2007). Chd1 is also essential for the hyperdynamic and open chromatin state of pluripotent ESCs and necessary for multi-lineage differentiation (Gaspar-Maia et al., 2009). Furthermore, Chd1 interacts with components of the transcriptional preinitiation complex to control genome wide gene expression (Lin et al., 2011). *Chd1* KO mice have not been generated, but a gene-trap *Chd2* KO mouse lacking the DNA-binding domain displays perinatal lethality due to severe growth delays during late embryogenesis (Marfella et al., 2006). Interestingly, the crystal structure of the Chd1 DNA-binding domain is now recognized to have additional SANT and SLIDE domains previously identified in ISWI ATPases (Ryan et al., 2011). The SANT and SLIDE domains were also identified in *CHD6-9,* and they are mutated in some forms of CHARGE syndrome (caused by mutations in *CHD7*) (Ryan et al., 2011). This coincides with recent findings that Chd1 and Isw1 (one of two yeast ISWI orthologues) control genome-wide nucleosome occupancy by preventing histone exchange within euchromatin (Gkikopoulos et al., 2011; Smolle et al., 2012). Moreover, yeast Chd1 and Isw1 were found to act in gene bodies, but highly enriched at nucleosome free regions (NFRs) where they bind to extended regions of DNA (Zentner et al., 2013). Nevertheless, its important to highlight that Chd1 assembles chromatin with a shorter nucleosome repeat length than the ISWI-containing ACF complex (Lusser et al., 2005). The ACF complex, but not Chd1, can also assemble chromatin containing histone H1 (Lusser et al., 2005). These experiments suggest that ISWI and Chd1-containing CRCs have non-redundant cooperative roles during gene activation and lineage specification through specific chromatin remodeling mechanisms *in vivo.*

1.2.2 The CHD3/Mi2α- and CHD4/mi2β-containing NURD complexes (CHD subfamily II)

The CHD4 protein was first discovered as the dermatomyositis-specific autoantigen Mi2 (Mitchell's autoimmune antibodies 2) (Seelig et al., 1995). Later, the CHD3 and CHD4 proteins were found to be part of multiprotein CRCs in frogs, mice and humans (Tong et al., 1998; Wade et al., 1998; Xue et al., 1998; Zhang et al., 1998). These CHD3- and CHD4-containing CRCs are now collectively known as the NuRD (nucleosome remodeling and histone deacetylase) complexes. The NuRD complexes interact with 4 main accessory subunits: histone deacetylases (HDAC1/HDAC2); methyl DNA binding proteins (MBD2, MBD3); Rbbp (retinoblastoma-associated binding protein) proteins Rbbp46/48; and one of three MTA (metastasis tumor antigen) proteins (MTA1-MTA3). In the NuRD complex, HDAC1/2 participate in the deacetylation process; Rbbp-46/48 participate in histone binding; MBD proteins recognize CpG-methylated or 5-hydroxymethylated residues; and CHD3 or CHD4 provide nucleosome remodeling activity (Bowen et al., 2004). The lysine-specific demethylase 1 (LSD1) protein also interacts with NURD, thus making a "super" multiprotein complex that has histone demethylase, histone deacetylase and chromatin remodeling enzymatic activity (Wang et al., 2009). The MTA proteins provide further specificity since they are found in distinct complexes, but their complex-specific roles are not well understood (Bowen et al., 2004; Yao and Yang, 2003).

Mi2 ablation during early *Drosophila* development is lethal through abnormal repression of homeotic genes (Kehle et al., 1998). Similarly, inactivation of Mbd3 in the mouse, a NuRD subunit, results in death during mid-gestation, due to the abnormal differentiation of the inner cell mass to an epiblast (Kaji et al., 2006; Kaji et al., 2007).

Moreover, NuRD complexes are implicated in T-cell and Schwann cell differentiation and are thought to be important for lineage commitment in mammalian cells (Srinivasan et al., 2006; Williams et al., 2004).

CHD5 is not considered part of the NuRD complexes and is preferentially expressed in the central nervous system (CNS) (Schuster and Stoger, 2002; Thompson et al., 2003). It was later characterized to be a human neuroblastoma tumor suppressor gene (Bagchi et al., 2007). However, *Chd5* ablation in the developing mouse neocortex inhibited neuronal differentiation and was shown to be required for silencing of Polycomb-repressed genes required for differentiation (Egan et al., 2013). However, Chd5 interacting subunits have not been characterized.

1.2.3 The CHD7 protein and CHARGE Syndrome (CHD subfamily III)

The most extensively studied member of subfamily III is CHD7, for which mutations in humans result in CHARGE syndrome, a multiple congenital anomaly condition characterized by ocular coloboma, heart defects, atresia of the choanae, retarded growth, genital hypoplasia, and characteristic ear abnormalities including deafness (Vissers et al., 2004). The *Drosophila Chd7* orthologue *kismet* is required for RNA polymerase II-driven elongation and counteracts Polycomb group repression by recruiting the ASH1 and Trithorax (Trx) histone methyltransferases to target loci (Schnetz et al., 2009; Srinivasan et al., 2005; Srinivasan et al., 2008). *Kismet* was also shown to be involved in axonal pruning, guidance and extension in the *Drosophila* CNS (Melicharek et al., 2010). In mice, *Chd7* ablation results in death around E10.5, while $Chd7^{-/+}$ embryos show signs of abnormal vestibular development, recapitulating the inner ear malformations observed in human CHARGE

syndrome patients (Hurd et al., 2007; Vissers et al., 2004). Human and frog *Chd7* are essential for the development of a multipotent, migratory, ectodermally-derived neural crest cell population that can give rise to craniofacial bones and cartilages; the peripheral nervous system (PNS); pigmentation; and cardiac structures (Bajpai et al., 2010). Chd7 physically interacts with the PBAF (polybromo- and BRG1-associated factor)-containing complex to regulate common target enhancers and transcriptionally modulate ES-specific genes (Bajpai et al., 2010). Moreover, *Chd7* plays a role in mouse adult neurogenesis in the SVZ of the hippocampus (Feng et al., 2013).

Unlike Chd7, not much is known about Chd6 or Chd9, but *CHD8* mutations have been associated to neurodevelopmental and autism-spectrum disorders (Neale et al., 2012; O'Roak et al., 2012a; O'Roak et al., 2012b; Talkowski et al., 2012). *Chd8* is highly expressed during mouse embryogenesis and also promotes the association of the tumor suppressor protein p53 and histone H1 to mediate inhibition of p53-dependent transactivation and apoptosis in human cells (Nishiyama et al., 2009; Nishiyama et al., 2012).

1.3 The INO80 proteins

In mammals, INOC1 and SRCAP (the mammalian orthologues of yeast Ino80 and Swr1, respectively) are the only chromatin remodeling subunits of multisubunit protein complexes characterized by having a conserved split ATPase domain (Jin et al., 2005). Swr1-containing CRCs were first characterized by their ability to incorporate the variant histone Htz1 in yeast (the mammalian H2A.Z orthologue) and later H2A.Z in mammals (Kobor et al., 2004; Mizuguchi et al., 2004; Ruhl et al., 2006; Wong et al., 2007). Ino80-containing CRCs are associated with DNA repair in plants and mammals, and also

associated with gene activation (Cai et al., 2007; Fritsch et al., 2004; Morrison et al., 2004; van Attikum et al., 2004). Yeast INO80 is also known to catalyze variant histone H2A.Z eviction and control genome-wide gene activation (Papamichos-Chronakis et al., 2011). Most interestingly, human mutations in SRCAP have been associated with the rare neurodevelopmental disorder Floating-Harbor Syndrome characterized by short stature, delayed osseous maturation, cognitive deficits, and a distinctive facial dysmorphology (Hood et al., 2012).

1.4 The ISWI proteins

ISWI proteins are distinguished by a HAND-SANT C-terminal domain juxtaposed to a SLIDE domain that provides nucleosome recognition specificity **(Figure 1.2)** (Boyer et al., 2002; Grune et al., 2003). The ISWI proteins were first isolated from *Drosophila* as part of three different complexes: NURF (nucleosome remodeling factor) (Tsukiyama et al., 1995; Tsukiyama and Wu, 1995); ACF (ATP-dependent chromatin assembly and remodeling factor) (Ito et al., 1997); and CHRAC (chromatin accessibility) complex (Varga-Weisz et al., 1997). ACF and CHRAC differ from other ISWI-containing CRCs because they share the ACF1 subunit. ACF consists of ISWI and ACF1, whereas CHRAC has two additional histone-fold subunits (Eberharter et al., 2001; Ito et al., 1997). Nevertheless, their *in vitro* biochemical properties are nearly identical (Eberharter et al., 2004; Hartlepp et al., 2005; Lusser et al., 2005; Maier et al., 2008). ISWI loss-of-function mutations in *Drosophila* results in three distinct phenotypic features: 1) abnormal inactivation of homeotic genes including *Engrailed* and *Ultrabithorax*; 2) death during the larval-pupal transition; and 3) alterations in higher order chromatin structure (Brasted, 1941; Deuring et al., 2000; Morata and Lawrence, 1975). *Drosophila* ISWI is also necessary for the self-renewal of ovarian

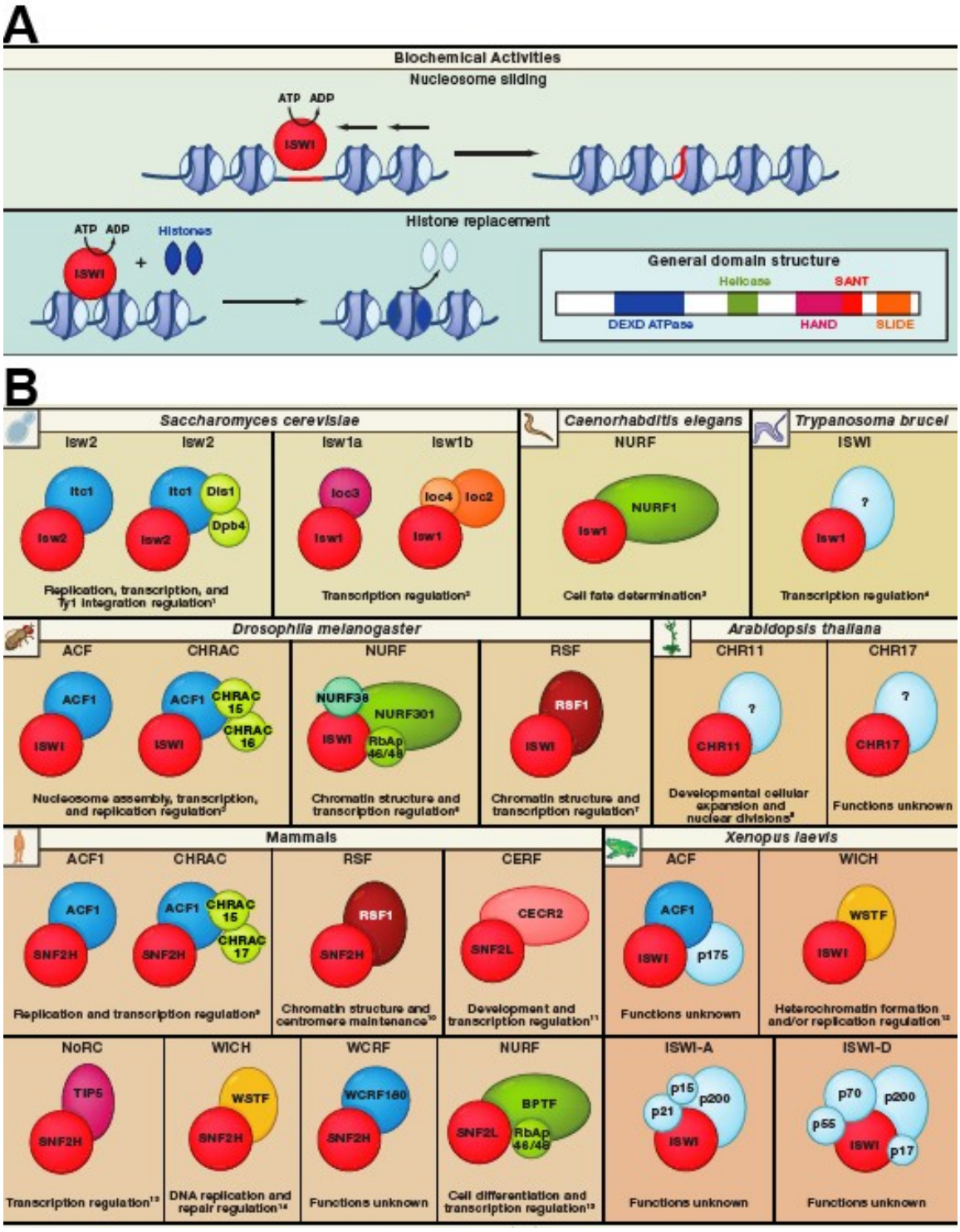

Figure 1.2 The ISWI family of ATP-dependent chromatin-remodeling enzymes comprises highly conserved protein complexes that utilize the energy of ATP hydrolysis to slide nucleosomes along DNA and/or replace histones within nucleosomes.

(A) All ATP-dependent chromatin-remodeling complexes, including the ISWI family, contain a conserved catalytic DEXD ATPase domain and a helicase domain. However, the

combination of three C-terminally located domains, known as HAND, SANT, and SLIDE, is unique to ISWI family members. The SANT domain (structurally related to the c-Myb DNA-binding domains) binds unmodified histone tails, the SLIDE (SANT-like ISWI domain) domain binds nucleosomal DNA near the dyad axis, and the HAND domain is implicated in both histone and DNA binding/recognition.
(B) Representative ISWI-containing protein complexes from multiple species are depicted with specific *in vivo* biological functions if known [printed with permission from {(Yadon and Tsukiyama, 2011)}.

germline stem cells (Xi and Xie, 2005). Importantly, some of these phenotypes have been associated with specific subunits or molecular mechanisms in *Drosophila*: a) *Nurf301* knockdown phenocopies the larval-pupal lethality and hypoactivation of homeotic genes (Badenhorst et al., 2002); b) *Acf1* loss-of-function results in abnormal heterochromatin formation and cell death during the larval-pupal stage (Chioda et al., 2010; Fyodorov et al., 2004); and c) knockdown of histone H1 partially mimics the decondensation of the male X chromosome in ISWI mutants (Corona et al., 2007; Siriaco et al., 2009). These observations highlight three essential roles for ISWI: 1) DNA replication and cell viability; 2) activation of segmentation and homeotic genes; and 3) higher order chromatin structure.

ISWI-containing CRCs have been found in yeast to humans **(Figure 1.2).** Yeast have 2 ISWI orthologues, *Isw1* and *Isw2*, which are subunits of three different CRCs (Iida and Araki, 2004; Tsukiyama et al., 1999; Vary et al., 2003). In *Caenorabditis elegans (C. elegans)*, the homolog *isw-1* interacts with *Nurf-1,* an orthologue of *Drosophila Nurf301* (Andersen et al., 2006). In *Xenopus,* the NURF complex is not known to exist, but three ISWI-containing CRCs have been described: ACF, CHRAC and WICH (Bozhenok et al., 2002; Guschin et al., 2000). ISWI is required for *Xenopus* gastrulation, neurulation and also in later stages for retinal differentiation (Dirscherl et al., 2005). Similarly, knockdown of *Xenopus WSTF* resulted in abnormal neural crest development (Barnett et al., 2012). Since ISWI is conserved throughout various CRCs, a study of their independent roles in higher organisms is possible, but technically challenging.

1.4.1 Mammalian ISWI

Mammals have two ISWI paralogues: *SNF2H* (*SNF2-homologue*; also referred to as *SMARCA5)* and *SNF2L* (*SNF2-like*; also referred to as *SMARCA1*) that are the orthologues of yeast *Isw1* and *Isw2* (Lazzaro and Picketts, 2001a). In mammals, Snf2h and Snf2l have been associated with the following functions and complexes: DNA replication and DNA repair (RSF, ACF, CHRAC and WICH) (Bozhenok et al., 2002; Collins et al., 2002; Lan et al., 2010; LeRoy et al., 1998; Poot et al., 2004; Poot et al., 2000; Sanchez-Molina et al., 2011); transcriptional regulation (WICH, NURF and CERF) (Banting et al., 2005; Barak et al., 2003; Yip et al., 2012); and heterochromatin formation (NoRC) (Postepska-Igielska et al., 2013; Strohner et al., 2001). Additionally, human SNF2H has also been associated with sister chromatin cohesion through the cohesin-NuRD (nucleosome remodeling and histone deacetylase) complex (Hakimi et al., 2002), making a total of six different Snf2h-containing CRCs in mammals. hNURF and the CERF (CECR2-containing remodeling factor) complexes are exclusive to the SNF2L catalytic subunit and are associated with cell differentiation (Barak et al., 2003; Landry et al., 2011; Lazzaro et al., 2006; Yip et al., 2012). In the mouse CNS, *Snf2h* expression is robust in neuronal progenitors, while *Snf2l* is expressed predominantly in terminally differentiated neurons (Lazzaro and Picketts, 2001a). Constitutive Snf2h loss in the mouse embryo results in death during the periimplantation stage due to growth arrest and cell death of the trophoectoderm and inner cell mass (Stopka and Skoultchi, 2003). Conversely, Snf2l loss does not result in embryonic lethality, but hyperproliferation and a larger brain (Yip et al., 2012). However, the role of Snf2h-containing CRCs during mammalian neuronal development remains largely uncharacterized.

1.5 Mammalian cortical development

Mammalian neocortical development occurs during embryogenesis as a series of symmetric and asymmetric cell divisions that populate the forebrain through the specification of cortical subtypes (Duckett and Pearse, 1968; Konig et al., 1977; McConnell and Kaznowski, 1991; Smart, 1984, 1985a; Smart and McSherry, 1982; Smart and Smart, 1982; Tan and Breen, 1993; Todd and Smart, 1982). During mouse mid-embryonic development (~E9.5), the telencephalic wall is composed of multipotent neuroepithelial cells that give rise to diverse progenitor populations (Smart, 1985a, b). These multipotent mitotic cells reside in the dorsal lateral ventricles of the forebrain in a region known as the ventricular zone (VZ), which gives rise to more restricted mitotic progenitors in the subventricular zone (SVZ) (McConnell and Kaznowski, 1991). The first neurons that exit the cell cycle migrate through the SVZ to form the preplate, which is later split into the subplate and the marginal zone (Wood et al., 1992). Cajal-Retzius cells, the first defined cortical lineage that is derived from the cortical gem first populates the upper plate or marginal zone (Konig et al., 1977; Raedler and Raedler, 1978; Zhao et al., 2006). Then, a spatiotemporal birth of layer-specific subtypes generates early-born neurons that populate layers V and VI, followed by late-born neurons that reside in layers II-IV (McConnell and Kaznowski, 1991; Todd and Smart, 1982). These layer-specific cellular populations have the intrinsic nature of forming specific neural networks that in turn control brain function.

1.5.1 Neocortical specification

Morphogens such as *sonic hedgehog (Shh)*, fibroblast growth factors and bone morphogenetic proteins, combined with the expression of patterning transcription factors (TFs) such as *engrailed*, combinatorially signal for the activation of developmental gene expression programs that will determine the fate of the neocortical pool. For example,

forkhead box G1 (FoxG1), LIM homeobox 2 (Lhx2), empty spiracles homologue 2 (Emx2) and paired box 6 (Pax6) will specify the fate of the neocortical pool (Bulchand et al., 2001; Caric et al., 1997; Dou et al., 1999; Hanashima et al., 2004; Monuki et al., 2001; Muzio et al., 2002; Stoykova et al., 2000). Both FoxG1 and Lhx2 are essential for cortical development since Lhx2 loss results in VZ agenesis, while FoxG1 deletion ablates projection neuron specification (Monuki et al., 2001; Muzio and Mallamaci, 2005). Similarly, Emx2 or Pax6 deletion results in agenesis of the neocortex (Muzio et al., 2002). These observations suggest that cell-type specific TFs govern the early spatiotemporal specification of nearly all neocortical subtypes. Nevertheless, a wide variety of layer-specific transcription factors that determine postmitotic projection neuron fate have been characterized and will be briefly discussed.

1.5.2 Cortical projection neurons

Two broad classes of cortical neurons evolved in the mammalian brain known as interneurons and cortical projection neurons (CPNs) (Molyneaux et al., 2007). Interneurons project locally, while CPNs differentiate into a wide variety of subtypes that extend axons to intracortical, subcortical and subcerebral targets (Molyneaux et al., 2007). CPNs are further classified according to their mature axonal projections. Callosal projection neurons (CaPNs) project to the contralateral cortex and mainly reside in layers II/III, but are also found in layers V and VI **(Figure 1.3)**. CaPNs are specified during embryonic development by the chromatin architectural TF Satb2, but their postmitotic arborization is also controlled by the homeobox-containing Cux1 and Cux2 TFs (Alcamo et al., 2008; Britanova et al., 2008; Cubelos et al., 2010). Corticothalamic projection neurons (CThPNs) mainly reside in layer VI and project to the thalamus **(Figure 1.3)**. CThPNs are genetically specified by a Tbr1-

a Commissural; callosal projection neurons

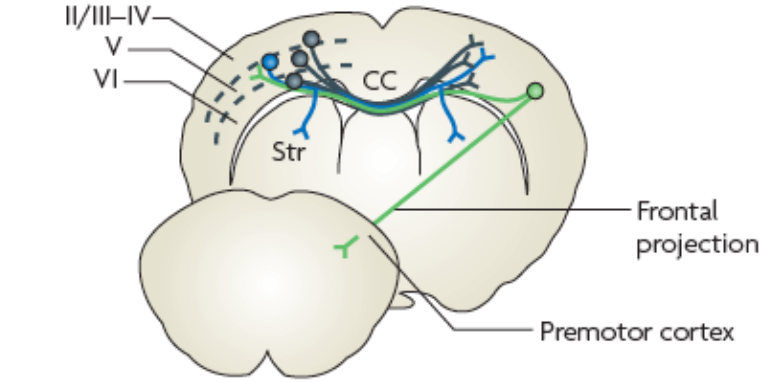

- Callosal neurons (layers II/III, V, VI)
- Callosal neurons with ipsilateral frontal projections (layer V)
- Callosal neurons with striatal projections (layer Va)

b Corticofugal; corticothalamic neurons

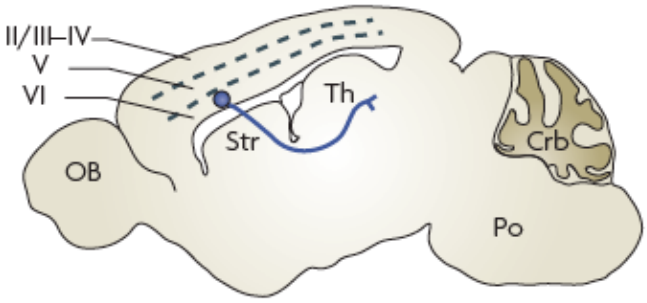

- Corticothalamic neurons (layer VI)

c Corticofugal; subcerebral projection neurons

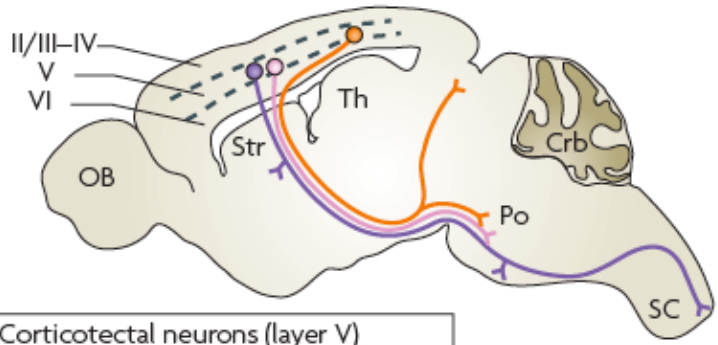

- Corticotectal neurons (layer V)
- Corticopontine neurons (layer V)
- Corticospinal motor neurons (layer V)

Figure 1.3 Projection neuron subtypes.
Classified by hodology, there are three basic classes of cortical projection neuron: associative, commissural and corticofugal. These are some of the principal subtypes: **Commissural:** Callosal projection neurons. Projection neurons of small to medium pyramidal size that are primarily located in layers II/III, V and VI, and extend an axon across the corpus callosum (CC) **(panel a).** At least three major types of callosal neuron can be classified. These maintain: single projections to the contralateral cortex (black); dual projections to the contralateral cortex and ipsilateral or contralateral striatum (blue); and dual projections to the contralateral cortex and ipsilateral frontal cortex (green). These never project axons to targets outside the telencephalon. Str, striatum.
Corticofugal (subcortical): Corticothalamic neurons. Projection neurons primarily located in cortical layer VI, with a smaller population in layer V, that projects subcortically to different nuclei of the thalamus (Th) **(panel b).** Subcerebral projection neurons. Also referred to as type I layer V projection neurons **(panel c).** These include pyramidal neurons of the largest size, which are located in deep-layer V and extend projections to the brainstem and spinal cord. They can be even further subdivided into several distinct projection neuron subtypes: Corticotectal neurons (orange) are located in the visual area of the cortex and maintain primary projections to the superior colliculus, with secondary collateral projections to the rostral pons (Po); corticopontine neurons (pink) maintain primary projections to the pons; and corticospinal motor neurons (purple) are located in the sensorimotor area of the cortex and maintain primary projections to the spinal cord, with secondary collaterals to the striatum, red nucleus, caudal pons and medulla. Many other subtypes of subcerebral projection neuron exist that send axons to different areas of the brainstem or have different combinations of collaterals, but are not depicted here for simplicity. Crb, cerebellum; OB, olfactory bulb; SC, spinal cord {printed with permission from (Molyneaux et al., 2007)}.

dependent mechanism that represses Fezf2 expression and specifies layer VI fate (Bedogni et al., 2010; Han et al., 2011; McKenna et al., 2011). Subcerebral projection neurons (ScPNs) reside in layer V and project to the optic tectum, brainstem or spinal cord and are specified by the TFs Sox5, Fezf2 and CTIP2 **(Figure 1.3)** (Arlotta et al., 2005; Chen et al., 2008; Kwan et al., 2008; Molyneaux et al., 2005).

CPN identity is controlled by a diverse, yet connected, genetic network of transcriptional regulators. For example, Tbr1 is a downstream target of CTIP2 and Satb2 for CaPN and ScPN specification in layers II-V (Srinivasan et al., 2012). Satb2 is TF involved in chromatin organization and gene expression control (Britanova et al., 2005; Britanova et al., 2008; Gyorgy et al., 2008). Loss of Satb2 expression during cortical development results in the re-activation of CTIP2 and abnormal axonal trajectory and fate specification (Alcamo et al., 2008; Britanova et al., 2008). Satb2 is also required for postmitotic CaPN arborization and mouse survival (Zhang et al., 2012). Satb2 binds to MAR regions within the CTIP2 locus to repress its expression and hence determine callosal versus subcerebral identity (Britanova et al., 2008). As a whole, these studies established a new paradigm where chromatin architectural proteins specify neuronal fate through repression of master regulatory TFs (Alcamo et al., 2008; Britanova et al., 2008).

1.6 Mouse cerebellar development

The CNS of the mouse embryo can be divided into four anatomical regions by ~E9: telencephalon and diencephalon (forebrain), mesencephalon (midbrain), and the metencephalon and myelencephalon (hindbrain). The mesencephalon is separated from the metencephalon by a midbrain/hindbrain boundary known as the isthmus. This complex

anatomical patterning is governed by signals derived from the isthmic organizer, an organizing center found within the isthmus (Liu and Joyner, 2001a; Wurst and Bally-Cuif, 2001). For example, the secreted molecules *Fgf8* and *Wnt1* are necessary for midbrain/hindbrain patterning (Chi et al., 2003; McMahon and Bradley, 1990). Similarly, the TFs *En1* and *Pax6* are also required for mesencephalon and metencephalon specification and are later followed by *En2* and *Pax5* expression (Liu and Joyner, 2001a). A complex genetic network of TFs including *En1, En2, Pax2, Lmx1b, Irx2* and *Gbx2* are necessary to sustain *Fgf8* expression in auto-regulatory feedback mechanisms (Li et al., 2002; Liu and Joyner, 2001a, b; Matsumoto et al., 2004; Matsunaga et al., 2002; Vernay et al., 2005). For example, *Otx2* and *Gbx2* demarcate *Fgf8* and *Wnt1* expression boundaries, but are not required for their induction (Broccoli et al., 1999; Rhinn et al., 1998). Similarly, *Fgf8* is necessary to repress *Otx2* expression and maintain posterior boundary identity (Foucher et al., 2006; Martinez et al., 1999). The spatiotemporal control of this genetic and signaling network specifies the cerebellar primordium by ~E12.5, when expansion and alignment of cerebellar progenitors commences **(Figure 1.4)**.

Cerebellar progenitors arise from the cerebellar primordium but there are two distinct germinal zones that give rise to all cerebellar lineages. First, a transient germinal epithelium known as the rhombic lip generates granule cells (GCs), neurons of the deep cerebellar nuclei (DCN) and unipolar brush cells (Englund et al., 2006; Fink et al., 2006; Machold and Fishell, 2005; Wang et al., 2005). The second germinal zone is known as the ventricular zone (VZ) that aligns next to the fourth ventricle. The VZ is where interneurons and Purkinje cells (PCs) are born (Altman and Bayer, 1985).

1.6.1 Granule and Purkinje cells of the cerebellum

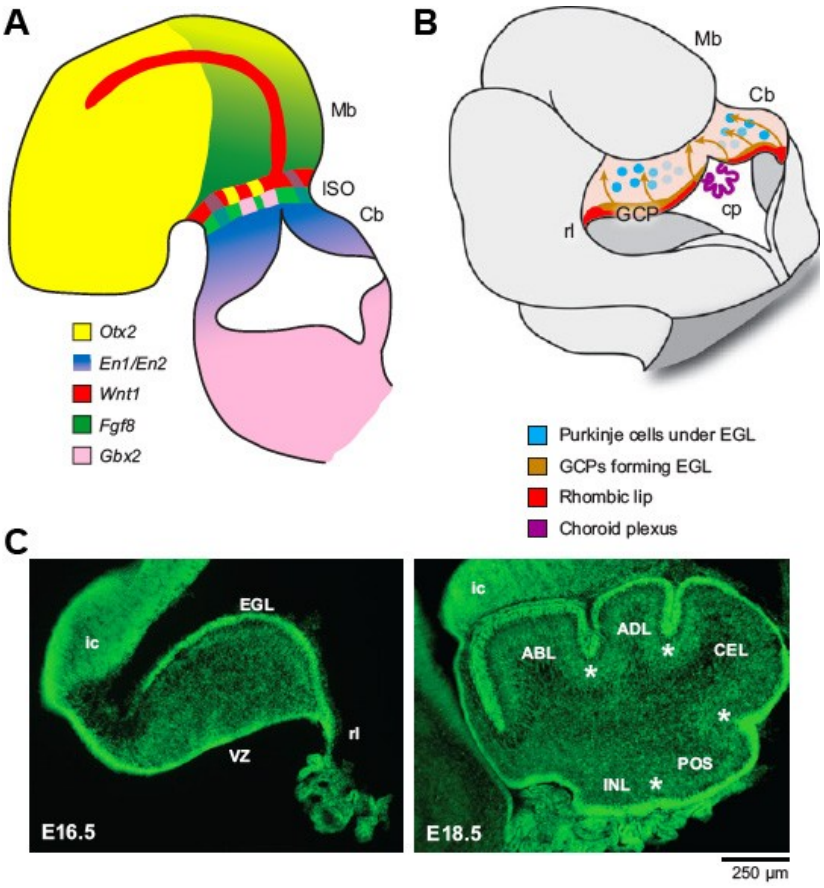

Figure 1.4 Complex genetic networks are required for cerebellar development and foliation. **(A)** Schematic diagram of the mouse embryo at approximately E9.5 showing the genes required for cerebellar morphogenesis. Mb, midbrain; ISO, isthmic organizer; Cb, cerebellum. **(B)** Schematic of an E12.5 cerebellum showing the tangential migration of granule cell precursors (GCPs) away from their origin in the rhombic lip. The GCPs migrate over the surface of the cerebellum. Below the surface, Purkinje cells (PC) are seen within the cerebellum. cp, choroid plexus; GCP, granule cell precursor; rl, rhombic lip. **(C)** The five cardinal lobes are formed at approximately embryonic day E17.5 in the mouse cerebellum. Sagittal sections through the E16.5 and cerebellum labeled with DAPI. The asterisks indicate the four fissures separating the cerebellum into five cardinal lobes. From anterior to posterior they are the preculminate, primary, secondary, and posterolateral fissures (Altman & Bayer, 1997). ic, inferior colliculus, EGL, external granular layer; rl, rhombic lip; VZ, ventricular zone; ABL, anterobasal lobe; ADL, anterodorsal lobe; CEL, central lobe; POS, posterior lobe; INL, inferior lobe {printed with permission from (Sillitoe and Joyner, 2007)}.

Granule neuron progenitors (GNP), the most abundant neuron of the brain, migrate from the rhombic lip towards the surface of the cerebellum and generate a mitotically active cell population known as the external granular layer (EGL) by ~E15 in the mouse (Fujita, 1967; Fujita et al., 1966). The EGL remains highly proliferative until ~P10 and disappears by ~P15 (Fujita, 1967; Fujita et al., 1966). At birth, GNPs exit the cell cycle, differentiate into granule cells (GCs) and migrate inwards guided by Bergmann glial fibers to form the internal granular layer (IGL). Here, GCs will reside through adulthood and establish their synaptic targets (Wang and Zoghbi, 2001). On the other hand, Purkinje cells (PCs) are specified and become postmitotic early in embryonic development around E11 to E13 (Miale and Sidman, 1961). Postmitotic PCs also migrate along radial glial fibers and form a transient multilayer below the EGL (Edwards et al., 1990; Morales and Hatten, 2006). At birth, PCs begin to align and form a monolayer across all cerebellar lobules coincident with lobule growth. This process known as foliation is intricately controlled by the *Engrailed* TFs and secreted factors such as *Shh* and *Bmp-4* during late embryonic and early postnatal stages **(Figure 1.4)** (Angley et al., 2003; Orvis et al., 2012; Wallace, 1999).

Foliation is a remarkable architectural, cellular and molecular masterpiece of mammalian brain development. Folia arise through morphogenetic and cellular matrix-based migrations that control the three-dimensional circuitry maturation of the adult cerebellum. The formation of cardinal lobes during late embryonic development, coupled to lobule foliation during the early postnatal stages, culminate in the formation of an evolutionary conserved structure composed of ten distinct lobules (Larsell, 1952; Larsell and Whitlock, 1952; Sudarov and Joyner, 2007). Its been proposed that PCs trigger anchor points for the subsequent folding of the lobules (Sudarov and Joyner, 2007). Nevertheless, the precise

epigenetic mechanisms that orchestrate the coordinated proliferation, migration, positioning and differentiation of the more than 10 different cell types that make up the adult cerebellum are just beginning to emerge. In this regard, the *Engrailed* TFs have been shown to play predominant roles during all stages of postnatal GC specification and maturation to control the three-dimensional patterning of afferent circuitry (Orvis et al., 2012; Sillitoe et al., 2008; Sillitoe et al., 2010). Nevertheless, the upstream modulators that control *Engrailed* expression are unknown.

1.6.2 Cerebellar topography

Classical studies have documented the existence of parasagittal stripes of enzymatic activity in the postnatal cerebellum (Scott, 1963). Additionally, axons underlying the white matter of the cerebellar cortex are arranged into anatomical bands (Voogd, 1967). Furthermore, the striped expression pattern of the antigen Zebrin II (ZII; coding for *Aldolase C*) has been extensively studied and is evolutionary conserved amongst mammalian species (Ahn et al., 1994; Brochu et al., 1990; Marzban and Hawkes, 2011). ZII is expressed in subsets of PCs that delineate afferent and efferent neural projections, forming arrays of parasagittal bands that extend rostrocaudally through the mammalian cerebellum **(Figure 1.5)** (Brochu et al., 1990). Additionally, a medial-lateral (M-L) and anterior-posterior (A-P) coordinate gene expression system is regulated by the *Engrailed* transcription factors (Sillitoe et al., 2010). The Engrailed proteins are essential for cerebellar foliation and afferent circuitry establishment (Cheng et al., 2010; Sillitoe et al., 2010). At a cognitive level, magnetic resonance imaging (MRI) studies suggest that cerebellar topography contains important genetic information for the development of sagittal stripes of physiological functional domains (Ellerman et al., 1994). Indeed, recent evidence supports the idea that

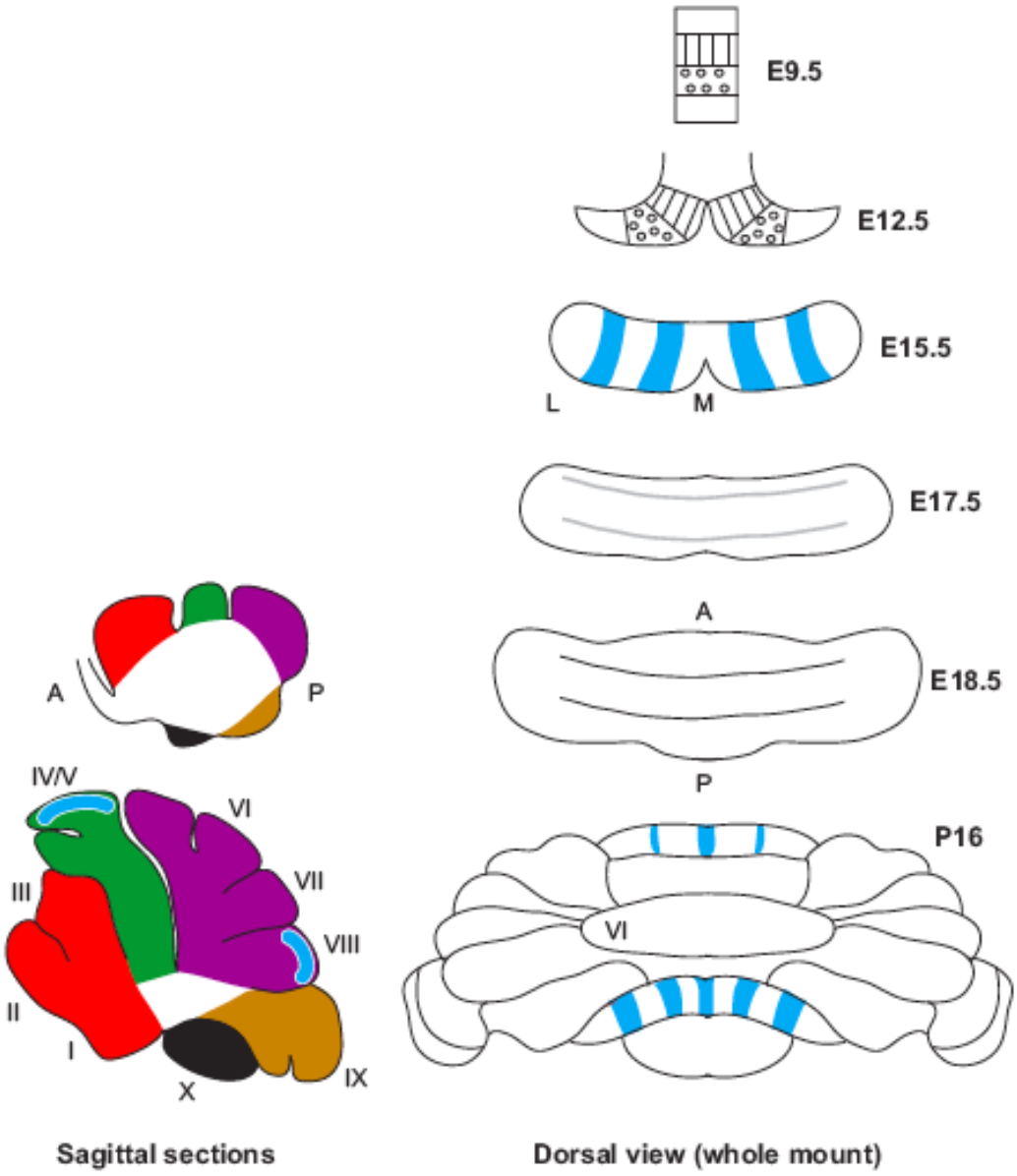

Figure 1.5 Two coordinate systems orchestrate cerebellar development.
Schematic diagrams showing dorsal views of the cerebellum changes in the anterior-posterior (AP) morphology and medial-lateral (ML) molecular coding from embryo to adult. Also shown are sagittal schematics illustrating the lobules in the AP axis. Roman numerals denote mature lobules. E, embryonic day; P, postnatal day; A, anterior; P, posterior; M, medial; L, lateral {printed with permission from (Sillitoe and Joyner, 2007)}.

cerebellar dysfunction not only underlies motor-related disorders, but also cognitive disorders including intellectual disability syndromes (Reith et al., 2013; Rogers et al., 2013; Sarachana and Hu, 2013; Tsai et al., 2012a).

1.7 RATIONALE & OBJECTIVES

Despite a good understanding of the *in vitro* biochemical properties of ISWI and its complexes, their *in vivo* roles remain poorly understood. In the murine CNS, *Snf2h* and *Snf2l* display dynamic patterns of expression, where *Snf2h* expression is robust in neural progenitors, while *Snf2l* is expressed predominantly in terminally differentiated neurons (Lazzaro and Picketts, 2001a). I thus hypothesized that Snf2h and Snf2l may regulate the transition of a progenitor to a differentiated neuron (at the cellular level); and compact chromatin for gene expression control (at the molecular level). To explore this hypothesis I proposed to characterize mice genetically ablated for *Snf2l*, *Snf2h*, or both genes in specific neural populations.

My studies employed diverse methods at the cellular, molecular, physiological, and ultrastructural levels to explore the function of mammalian ISWI-containing CRCs during cortical and cerebellar development, as well as upon deletion in postmitotic PCs of the cerebellum.

CHAPTER 2

Snf2l regulates Foxg1-dependent progenitor cell expansion in the developing brain

Darren J. Yip[1, 3, 6], Chelsea P. Corcoran[1, 3, 6], Matías Alvarez-Saavedra[1, 4, 6], Adriana DeMaria[1], Stephen Rennick[1, 3], Alan J. Mears[2, 4], Michael A. Rudnicki[1, 4], Claude Messier[5], and David J. Picketts[1, 3].

[1]Regenerative Medicine and [2]Vision Programs, Ottawa Hospital Research Institute, Ottawa, ON Canada K1H 8L6

Departments of [3]Biochemistry, Microbiology, and Immunology; and [4]Cellular and Molecular Medicine; and the [5]School of Psychology, University of Ottawa, Ottawa, ON, Canada

[6]These authors made equal contributions.

Microarray Accession Number: GSE34998

Key Words: Chromatin remodeling, neural development, ISWI, IPC, Snf2l, Foxg1

Statement of Contribution

Experimental design and execution of immunohistochemistry and immunofluorescence; confocal microscopy and analysis; FoxG1 promoter cloning and luciferase assays; FoxG1 western blotting; writing of results.

ABSTRACT

Balancing progenitor cell self-renewal and differentiation is essential for brain development and is regulated by the activity of chromatin remodeling complexes. Nevertheless, linking chromatin changes to specific pathways that control cortical histogenesis remains a challenge. Here we identify a genetic interaction between the chromatin remodeler Snf2l and Foxg1, a key regulator of neurogenesis. *Snf2l* mutant mice exhibit forebrain hypercellularity arising from increased *Foxg1* expression, increased progenitor cell expansion and delayed differentiation. We demonstrate that Snf2l binds to the *Foxg1* locus at mid-neurogenesis and that the phenotype is rescued by reducing *Foxg1* dosage, thus revealing that Snf2l and Foxg1 function antagonistically to regulate brain size.

INTRODUCTION

The development of the mammalian forebrain is a tightly regulated process that involves expansion of the neural progenitor pool followed by waves of asymmetric division to generate an array of specialized neuronal sub-types that comprise the six layers of the cortex (Gupta et al., 2002). The decision of precursor cells to self renew or differentiate is regulated by extrinsic factors and a cell intrinsic program largely mediated by neurogenic transcription factors (Gotz and Huttner, 2005; Guillemot, 2007; Shen et al., 2006b). The role of epigenetic factors in forebrain development is implicit based in part, on the rising number of neurodevelopmental disorders caused by mutations in genes encoding chromatin remodeling proteins (van Bokhoven and Kramer, 2010). Further, the use of mouse models and neural stem cell cultures have begun to elucidate the epigenetic mechanisms controlling neurogenesis (Berube et al., 2005; Fasano et al., 2009; Lessard et al., 2007; Lim et al., 2009; Molofsky et al., 2005; Molofsky et al., 2003). Nonetheless, the continued deciphering of the interplay between epigenetic regulators and neurogenic transcription factors is paramount to our understanding of forebrain development.

The mammalian *ISWI* chromatin remodeling proteins, Snf2h and Snf2l, are components of multiple protein complexes with diverse functions that include nucleosome assembly/spacing during replication and transcriptional regulation (Dirscherl and Krebs, 2004). In the developing brain, *Snf2h* expression is prevalent in progenitor cells whereas *Snf2l* expression increases during terminal differentiation (Barak et al., 2003; Lazzaro and Picketts, 2001b). Other studies suggest these genes may have distinct roles during neural development. Inactivation of *Snf2h* results in proliferation defects and embryonic lethality in mice whereas ectopic expression of *Snf2l* induces terminal differentiation of cultured

neuroblastoma cells (Barak et al., 2003; Stopka and Skoultchi, 2003). To further assess the *in vivo* requirement for Snf2l we used a conditional targeting approach to impair remodeling activity by the removal of the ATP-binding motif of the *Snf2l* gene. These *Snf2l* mutant mice exhibit deregulated *Foxg1* expression resulting in enhanced progenitor expansion, delayed neurogenesis and hypercellularity in the murine brain.

RESULTS & DISCUSSION

Hypercellularity in Snf2l-deficient mice

We utilized a conditional gene targeting approach by inserting loxP sites that flanked exon 6 (Fig. 1a). Exon 6 encodes the ATP-binding motif of the SNF2 domain that is critical for the chromatin remodeling activity of Snf2l containing protein complexes (Fig. 1a). To assess the impact of widespread early embryonic loss of *Snf2l* activity we bred $Snf2l^{f/f}$ mice to GATA1-Cre animals, which exhibit ubiquitous and early embryonic Cre activity (Mao et al., 1999). Unlike the embryonic lethality of *Snf2h*-null mice (Stopka and Skoultchi, 2003), the $Snf2l^{f/Y}$; GATA1-$Cre^{+/-}$ animals were healthy, fertile, and born at normal Mendelian ratios. As such, we bred the exon 6-deleted allele independent of Cre recombinase (hereafter named Ex6DEL).

The Ex6DEL male mice expressed a stable *Snf2l* transcript lacking exon 6 and produced a corresponding protein product reduced in size by 7 kDa (Fig. 1b and S1a). The mice displayed no overt phenotype and performed equally well to WT littermates in several behavior tests (Fig. S1b-d). The only gross morphological difference we observed was that the Ex6DEL animals had larger heads (Fig. S1e). Since Snf2l can promote neuronal

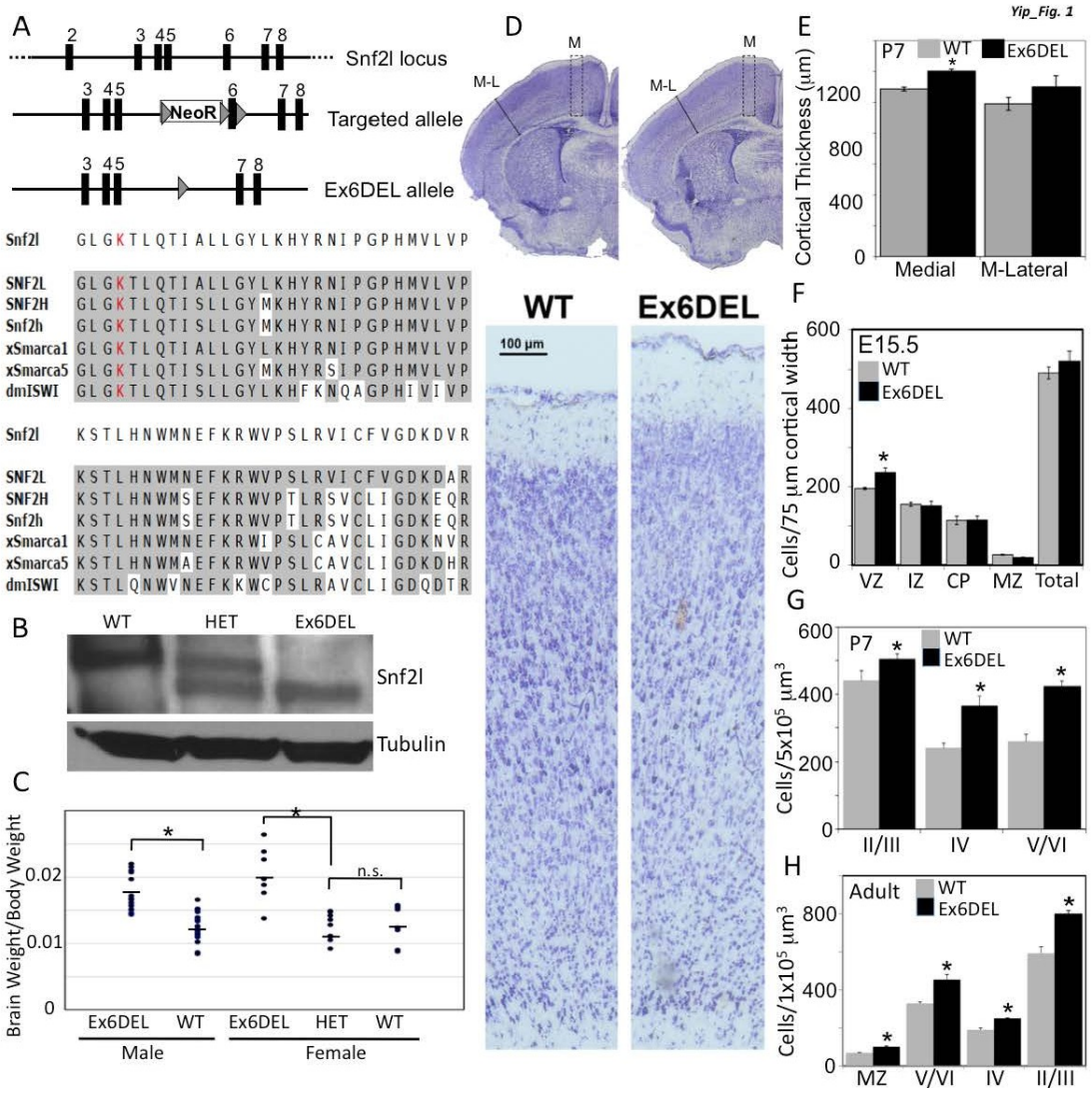

Figure 1. Increased brain mass and cell density in Ex6DEL mice. **(A)** Schematic of the Snf2l locus, targeted allele, and the Ex6DEL allele (LoxP sites, grey triangles; NeoR, neomycin resistance gene). Below, sequence conservation of the 60 amino acids encoded by exon 6. Lys residue critical for ATPase activity is red. **(B)** Snf2l immunoblot of E15.5 cortical extracts from WT, HET, and Ex6DEL mice. **(C)** Plot of brain weight to body weight ratios for Ex6DEL, WT, or HET mice. Brains from individual mice are represented by a dot with the mean indicated by a horizontal line. **(D)** Nissl stained P7 rostral coronal brain sections with high mag. images underneath and corresponding plot **(E)** of cortical thickness from medial and medial-lateral regions**. (F)** Cell counts from E15.5 cortical sections. **(G, H)** Cell counts within a fixed brain volume from P7 (G) or Adult (H) brains. MZ, medial zone; II/III, IV, V/VI: cortical layers II and III, IV, and V and VI, respectively; IZ, intermediate zone; VZ, ventricular zone; CP, cortical plate; For E-H, n=4; Bars correspond to the mean values while error bars indicate the Standard Error of the Mean (SEM); an asterisk (*****) represents a statistically significant change by a two-tailed paired Student t-test ($p_{value} \leq 0.05$) as compared to the WT sample unless otherwise indicated by brackets (n.s. - not significant).

differentiation *in vitro*, we reasoned that the loss of Snf2l activity might result in unfettered proliferation and increased brain size. Indeed, there was a 1.4-fold increase in the Ex6DEL brain:body mass ratio (Fig. 1c) that arose from an increased brain mass (0.65 g ± 0.18 g; n=29; aged 8-43 weeks) compared to WT littermates (0.48 g ± 0.06 g; n=26; $p=1.53x10^{-5}$), with no difference in body weight (Ex6DEL, 36.5g ± 6.8g; WT, 37.9g ± 7.6g; p=0.48). Homozygous Ex6DEL female mice showed a similar increase in brain:body mass ratio while heterozygous Ex6DEL females had normal ratios, suggesting that the Ex6DEL allele is not functioning as a dominant-negative or gain-of-function allele but is consistent with a loss-of-function phenotype (Fig. 1c). A similar analysis of multiple organs at a single age (11 weeks) showed that heart mass was the only other organ increased in size (Table S1). We conclude that the Ex6DEL mice have an increase in organ mass that primarily affects the brain.

To characterize the brains we measured cortical thickness at medial and medial-lateral positions in both rostral and caudal sections of P7 brains. A statistically significant increase in thickness throughout the medial region of the Ex6DEL cortex was observed (Fig. 1d, e and S1f). To determine if increased cortical thickness correlated with cell number we performed cell counts and observed hypercellularity within the cortex at several ages (Fig. 1f-h). Specifically, increased cell density were observed beginning embryonically at E15.5, although at this age statistical significance was restricted to the ventricular zone (VZ; Fig. 1f). At P7, cell density was increased in cortical layers II/III (Ex6DEL 504 ± 16 cells; WT 440 ± 22 cells; n=4; p=0.015), IV (Ex6DEL 364 ± 30 cells; WT 238 ± 16 cells; n=4; p=0.003), and V/VI (Ex6DEL 423 ± 16 cells; WT 258 ± 30 cells; n=4; p=0.001) (Fig. 1g). Similarly, the Ex6DEL adult cortex also showed increased

Similarly, the Ex6DEL adult cortex also showed increased cell density in the cortical layers (Fig. 1h). We conclude that *Snf2l* loss causes hypercellularity and an increased brain mass without significantly altering the structural morphology of the cortex.

Increased progenitor self renewal in developing brain of Ex6DEL mice

Increased cell numbers can arise from decreased cell death, changes in cell cycle kinetics, or increased self-renewal. We did not observe any differences in the proportion of apoptotic cells by TUNEL staining in WT or mutant mice indicating that altered cell survival is not the cause of the hypercellularity (Fig. S1g, h). As an initial measure of cell kinetics we stained for mitotic cells at E15.5 using antibodies to phospho-histone H3 (PH3). We observed a 2.9-fold increase in the proportion of mitotic cells in the VZ of Ex6DEL mice compared to control animals ($0.118 \pm 7.9x10^{-5}$ vs. 0.040 ± 0.002 per 125 μm^2, respectively; n=3; $p<0.05$) prompting us to investigate other cell cycle parameters (Fig. 2a, b). Next, we examined the proportion of S-phase cells by pulse-labeling cells with 5-bromo-2'-deoxyuridine (BrdU) at E13.5, 15.5, and 17.5 (Fig 2c, d). We observed a statistically significant increase in BrdU+ cells in the Ex6DEL neocortex at E13.5 (1.47-fold increase; n=4; p=0.0488) and at E15.5 (1.35-fold increase; n=6; p=0.0074). A similar trend, albeit not significant, was also observed at E17.5 (1.26-fold increase; n=3; p= 0.1503). An increased proportion of cells in both S- and M-phase suggest that proliferation is increased in the Ex6DEL animals.

Consistent with increased proliferation, we observed increased numbers of proliferating apical (Pax6+/BrdU+) and intermediate/basal (Tbr2+/BrdU+) progenitor cells (IPCs) in the Ex6DEL neocortex at E13.5 (Fig 2e, f and S2a). By E15.5, the level of

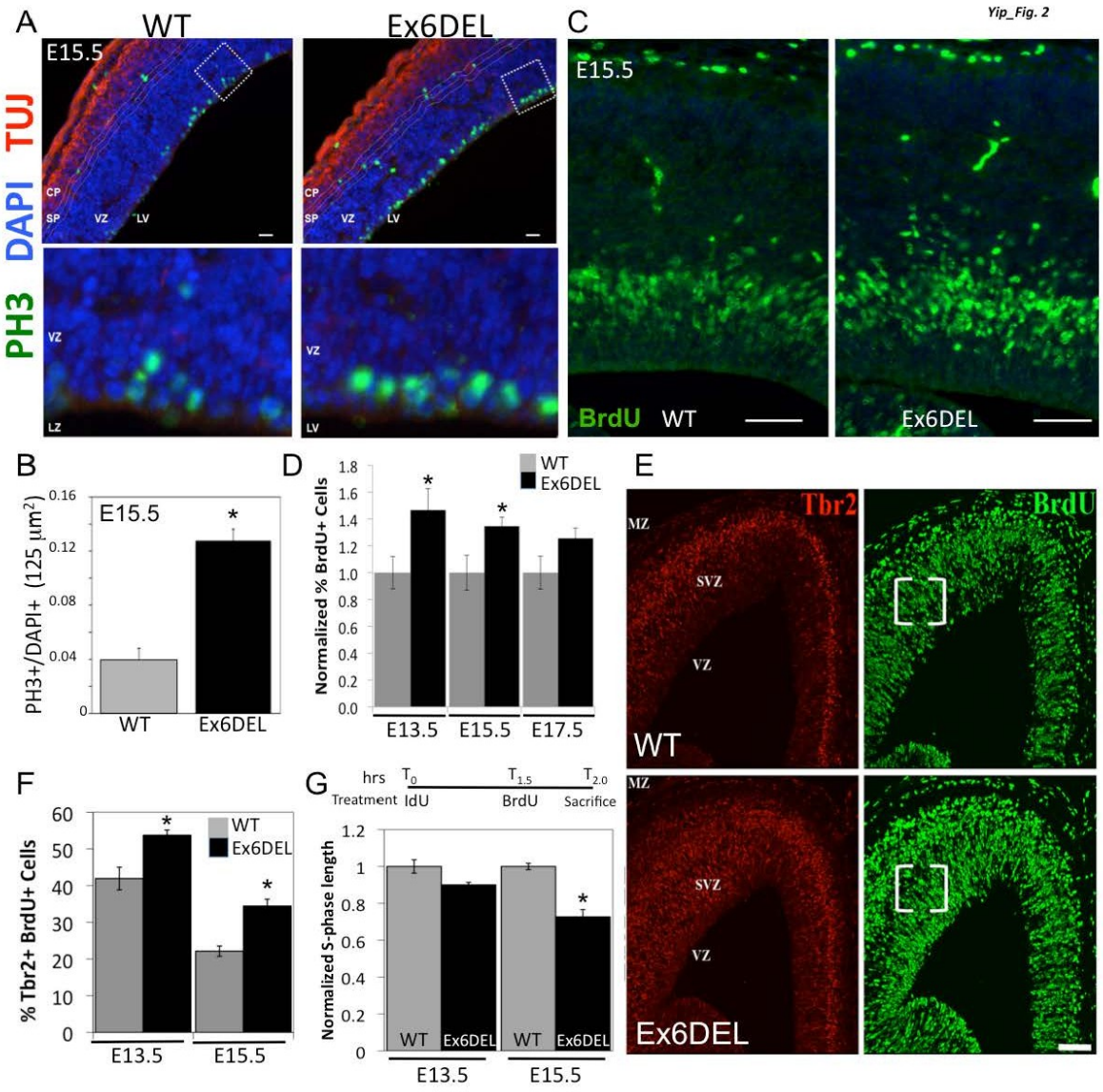

Figure 2. Ex6DEL forebrains have altered cell cycle kinetics. **(A)** E15.5 forebrain sections stained for terminally differentiated neurons (Tuj) and mitotic progenitors (PH3). Boxed regions are enlarged below. Scale bar = 30µm. **(B)** Quantification of PH3+ cells to total cells in the VZ of E15.5 embryos (n=3). **(C)** E15.5 cortical sections stained for BrdU after a 2-hr pulse (n=4; scale bar = 100 mm). **(D)** Normalized plot of the percentage of BrdU+ cells following a 2-hr BrdU pulse (n=3). **(E)** Tbr2 and BrdU double labeled E13.5 sections. Scale bar = 100 mm. The boxed regions are shown below at higher magnification (scale bar = 50 µm) and were representative of the images used to count the percentage of double-labeled cells (n=3) shown in **(F)**. **(G)** Schematic of IdU and BrdU injection times to determine S-phase length. Plot of normalized S-phase length (h) at E13.5 and E15.5 (n=3). For (B, D, F, G) bars represent Mean ± SEM; *p<0.05 by t-test.

proliferating apical progenitors was normal while IPC numbers (Tbr2+) remained increased (Fig. 2f). As a more direct assessment of cell cycle kinetics we used Idu/BrdU double labeling to measure S-phase length (Fukumitsu et al., 2006). We observed that S-phase length was significantly shorter in the Ex6DEL animals at E15.5 confirming that the progenitors cycled at a faster rate (Fig 2g). A similar trend was observed at E13.5, although significance was not attained.

To address the possibility that increased self-renewal also contributed to the increased number of proliferating progenitors, cells were pulse-labeled with BrdU at E12.5, or E16.5 and the brains harvested one day later for staining with Ki67 antigen, a protein expressed in all dividing cells. The number of BrdU+ Ki67+ double-labeled cells represents the proportion of progenitors that have remained in cycle. We observed a significant increase in the proportion of double-labeled cells in the mutant animals at E13.5 (WT: 39.2 ± 3.2%; Ex6DEL: 50.8 ± 4.2%; n=9; p=0.0056) suggesting that a greater fraction of progenitors undergo self-renewal within a 24-hour period (Fig. 3a, b). A similar increase was observed in the mutants at E17.5 (Fig. 3b). Taken together, the data demonstrate that increased hypercellularity observed in the Ex6DEL mice results from a combination of an increased progenitor cell cycle rate and enhanced self-renewal, primarily of IPCs.

Altered timing of neurogenesis and increased neuronal output

The altered proliferation of Ex6DEL progenitors coupled with the increased cortical thickness prompted us to examine the forebrain for changes in cortical lamination, the timing of neurogenesis, and the production of both deep (layer V, VI) and superficial (layers II-IV).

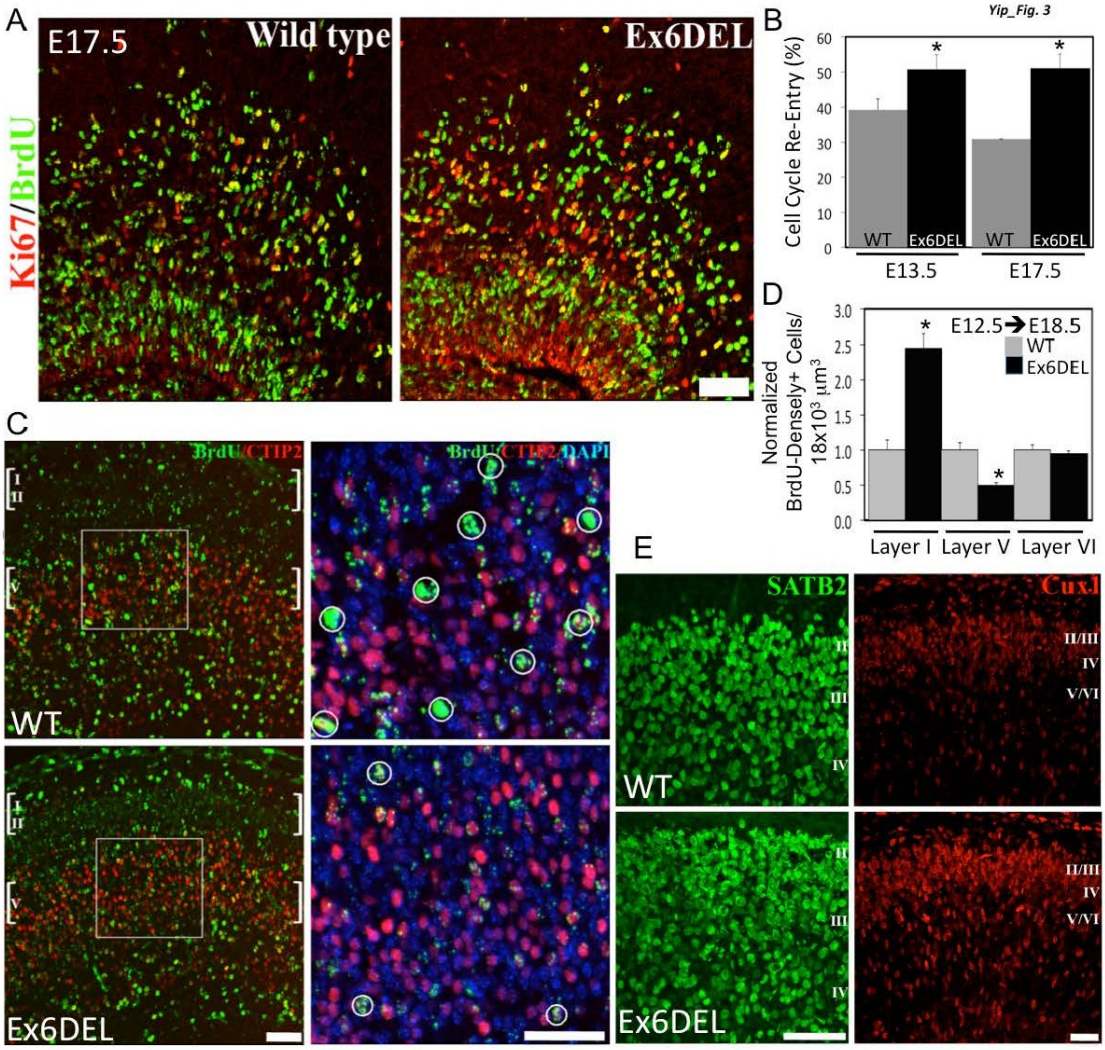

Figure 3. Delayed neurogenesis and increased neuronal output. **(A)** Cycling progenitors pulsed with BrdU at E16.5 then harvested at E17.5 and stained for Ki67 (red) and BrdU (green). Scale bar = 50 µm. **(B)** Plot from (A) of the percentage of cells re-entering the cell cycle (BrdU+, Ki67+; n=9). **(C)** E18.5 sections stained for CTIP2 and BrdU following neuronal birthdating at E12.5 (Scale bar = 50 mm). Boxed region is enlarged on right and brightly-fluorescent BrdU+ cells are circled (Scale bar = 20 mm). **(D)** The location of BrdU-densely+ cells from (C) were quantified and normalized to WT levels (n=3). **(E)** E18.5 sections stained for SATB2 and Cux1, markers of superficial neuronal layers (Scale bars = 50 mm). For (B, D) bars represent Mean ± SEM; *p<0.05 by t-test.

Staining with six different layer-specific markers at several stages (E15.5, 17.5, 18.5) revealed that marker was expressed in its correct each laminar position (see Fig. 3c, e; S2b, e; and S3b, c). Marker positive cell counts at E18.5 revealed that both early-born deep (Nurr1, CTIP2) and later-born superficial (Satb2, Cux1) neurons were increased in number (Fig. S2c, and S3a, d). Nonetheless, this was not true of all markers (eg. Foxp1) indicating that specific fate changes are likely occurring in the Ex6DEL mice. For example, alternate corticofugal neuronal identities within layer V/VI are characterized by CTIP2 and Tbr1 levels. We observed a qualitative increase in the proportion of $CTIP2^{high}/Tbr1^{low}$ expressing cells at E15.5 within layers V/VI (Fig S2e) that could be suggestive of a fate change (McKenna et al.). Similarly, at E17.5 the number of CTIP2+ cells in layer V remained high and we observed a reduction in Foxp1+ cells (Fig. S3b), which may be reflective of altered sensory motor projections (Surmeli et al., 2011). Taken together, these observations highlight that the Ex6DEL phenotype is complex with specific fate changes likely accompanying the increased neuronal output within the cortical layers.

The cortical plate is established by the successive birth of neurons that migrate to different layers. Layer I neurons are born at ~E11.5 followed around E12.5 by the production of layer VI and layer V neurons, respectively. Thus, a delay in cell cycle exit would be predicted to result in a shift in the timing of this sequence such that the production of "early" neurons will occur at later stages. To examine whether additional progenitor cell division(s) altered the timing of neurogenesis we pulse-labeled progenitors with BrdU at E12.5 then double labeled cells at E18.5 for BrdU and CTIP2, a marker of layer V-VI neurons. Brightly fluorescent BrdU-labeled cells (BrdU staining >75% of nucleus) are representative of cells born at E12.5. We observed a significant reduction in the number of

CTIP2/BrdU-double positive cells in layer V of the mutant cortex (Fig. 3c, d). Indeed, the majority of the brightly fluorescent cells in the Ex6DEL cortex resided within layers 1 and VI suggesting that the neurons "born" at E12.5 in the mutants were adopting fates that are characteristic of an earlier stage. Similar results were obtained for Nurr1 (Fig S2d). Thus, aberrant Snf2l function disrupts progenitor cell cycle kinetics, self-renewal decisions and alters the timing of neurogenesis that collectively, increases overall cell number in the developing Ex6DEL neocortex.

Foxg1 is misregulated in Ex6DEL mice

Gene profiling at E15.5 revealed a significant increase in the expression of *Foxg1* in the mutant cortex that was confirmed by qPCR (GSE34998; Table S2 and Fig 4a). *Foxg1*/*Brain factor-1* is a forkhead homeodomain transcription factor that controls NSC self-renewal, IPC expansion and the timing of neurogenesis (Fasano et al., 2009; Shen et al., 2006b; Siegenthaler and Miller, 2005; Siegenthaler et al., 2007). Mice deficient in *Foxg1* have a severe reduction in the size of the cerebral hemispheres as neural progenitors undergo premature differentiation, exhaust the progenitor pool at the expense of late-born neurons, and undergo lateral to medial re-patterning of Cajal-Retzius neurons (Dou et al., 1999; Hanashima et al., 2004; Muzio and Mallamaci, 2005; Xuan et al., 1995). Conversely, NSCs transduced with Foxg1-expressing lentiviral vectors increased the neural progenitor pool, delayed neurogenesis and increased neuronal output (Brancaccio et al., 2010). Thus, we postulated that increased *Foxg1* expression represented an excellent mechanism to explain the Ex6DEL phenotype. Consistent with this hypothesis, *Foxg1* protein levels were increased in the mutant animals compared to wild type mice (Fig 4b and S4a-c). Notably,

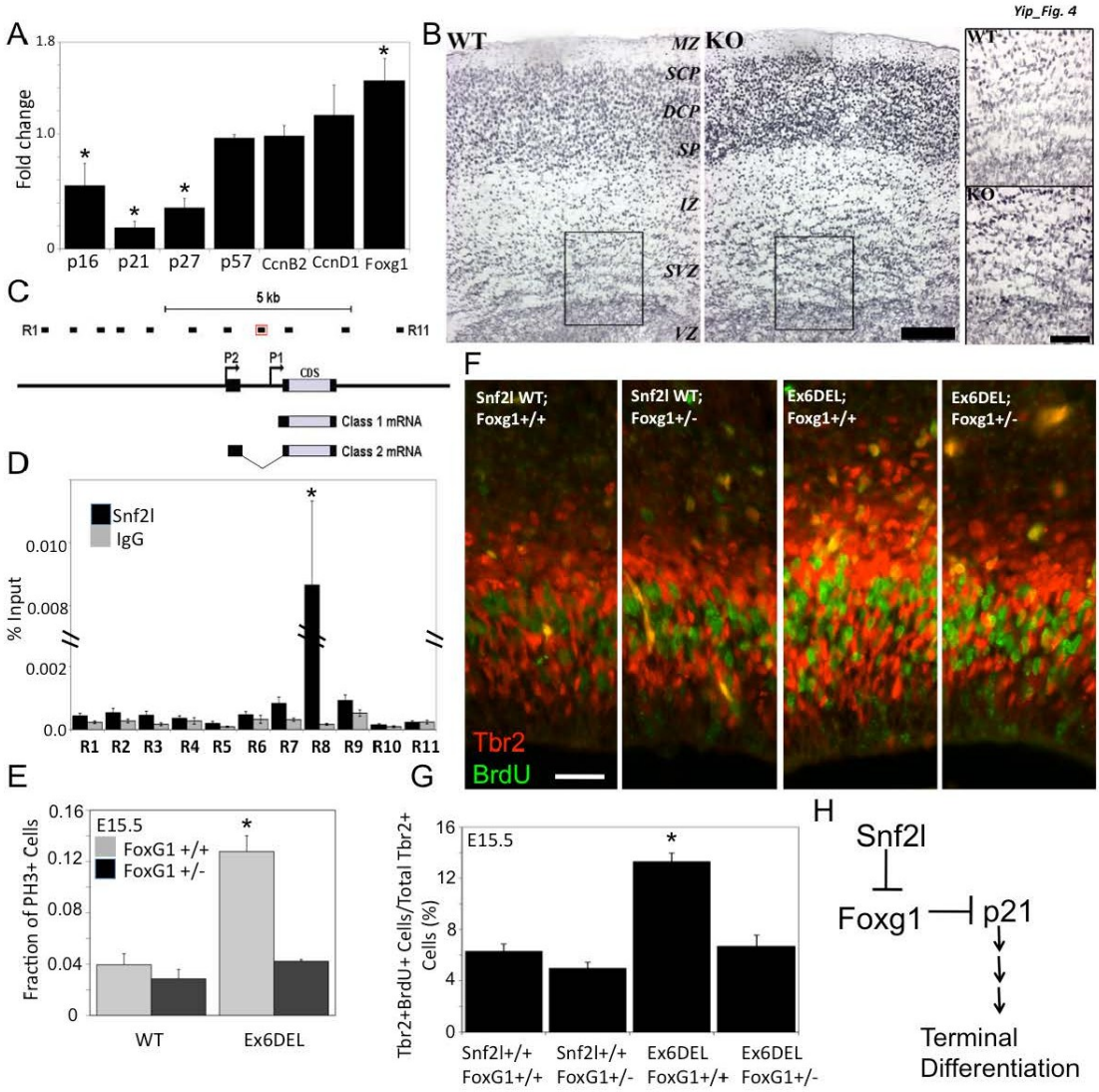

Figure 4. Foxg1 is misregulated in Ex6DEL mice. **(A)** qRT-PCR analysis of Foxg1, cdk inhibitors (Cdnk1a, 1b,1c, 2a), and cyclins (Ccnb2, Ccnd1) normalized to WT levels (n=3; bars represent mean ± SEM; * $p<0.05$ by t test). **(B)** Foxg1 immunohistochemistry of E17.5 cortical sections (scale bar = 50 mm). Boxed region within SVZ is enlarged on right (scale bar = 20 mm). **(C)** Schematic diagram of the Foxg1 locus showing the location of qPCR primer pairs R1-R11 used for ChIP analysis. P1 and P2 represent alternative promoters driving expression of class 1 and 2 Foxg1 transcripts, respectively. **(D)** ChIP analysis depicting the binding of Snf2l relative to % input across the Foxg1 locus. There was a significant level of Snf2l binding over IgG control at the R8 primer set ($p<0.012$ by t test). Each bar represents the mean ± SD from three biological replicates (each replicate represents a pool of E15.5 dissected cortices from 10 embryos) and two qPCR reactions from each replicate. **(E)** Proportion of mitotic (PH3+) cells in WT or Ex6DEL mice with normal (Foxg1 +/+) or reduced (Foxg1 +/-) Foxg1 dosage (n=3; bars represent mean ± SEM; * $p<0.05$ by t test; PH3 stained images are shown in Fig S3g). **(F)** E15.5 cortical sections from indicated genotype stained for Tbr2 (red) and BrdU (green) to identify cycling IPCs (scale

bar = 50 mm). **(G)** The proportion of Tbr2, BrdU-double labeled cells was rescued on the Foxg1 +/- background (n=3; bars represent mean ± SEM; * $p<0.05$ by t test). **(H)** Model suggesting that Snf2l represses Foxg1 expression allowing for p21 de-repression and the promotion of terminal differentiation.

the SVZ is comprised of a mixture of high and low Foxg1 expressing cells and the expression persists at a high level in the cortical plate (Fig 4b and S4b, c).

Recent studies have shown that Foxg1 mediates the repression of *Cdkn1a* (p21Cip1) to inhibit cell cycle exit and promote IPC expansion (Siegenthaler and Miller, 2005; Siegenthaler et al., 2007). Consistent with the increase in Foxg1 we observed a reduction in the expression of *Cdkn1a* in the mutant brains (Fig. 4a). We also assessed the expression of other cdk inhibitors and observed reduced expression of *Cdnk1b* (p27Kip1) and *Cdnk2a* (p16INK4a) but not *Cdnk1c* (p57Kip2). We conclude that the Ex6DEL mice have altered *Foxg1* expression that affects downstream target gene expression.

We reasoned that Snf2l complexes are recruited to the *Foxg1* locus to limit the expression level of the gene and promote terminal differentiation. To assess whether Snf2l is enriched at the *Foxg1* gene we performed chromatin immunoprecipitation (ChIP) assays. Chromatin isolated from cortices dissected from E15.5 embryos was incubated with a Snf2l antibody previously used to identify Snf2l target genes, or with sheep IgG as a negative control (Barak et al., 2003; Lazzaro et al., 2006). Eleven amplicons (R1-R11) were designed for qPCR that span the *Foxg1* gene (Fig. 4c). The results of these experiments (Fig. 4d) showed that Snf2l binding was specifically enriched at the region that encompasses the P1 promoter (R8, $p \leq 0.012$), which drives expression of the more abundant class 1 *Foxg1* transcript (Li et al., 1996). Luciferase reporter assays confirmed the importance of a 1.2 kb fragment for gene expression. While this fragment encompassed the R8 region, addition of Snf2l or Snf2h in the assay system did not have any effect indicating that the functionality may be context-dependent (Fig S4d-f). Nonetheless, we conclude that Snf2l binds to the *Foxg1* gene, consistent with a direct role for Snf2l-containing complexes in the regulation of

Foxg1 expression. These results further suggest that misregulation of *Foxg1* underlies the phenotype of Ex6DEL mice.

Reduction of Foxg1 rescues the Ex6DEL phenotype

If Snf2l-containing chromatin remodeling complexes are required to regulate *Foxg1* expression then we predicted that genetic reduction of *Foxg1* dosage should rescue the phenotype of the Ex6DEL mice. Ex6DEL mice were bred to *Foxg1* heterozygous mice and the resulting Ex6DEL; Foxg1+/- animals were examined at E15.5 for signs of genetic rescue. In this regard, we examined the proportion of mitotic cells and the fraction of IPCs. As shown in figure 4e and S4g, wild type and *Foxg1* heterozygous mice had no significant difference in the proportion of PH3+ cells (0.034 ± 0.003 vs. 0.033 ± 0.004 per fixed area). The Ex6DEL mice had a 3-fold increase in PH3+ cells (0.107 ± 0.006) but this was rescued in the Ex6DEL; Foxg1+/- animals (0.039 ± 0.002). Similarly, only the Ex6DEL mice showed a significant difference in the percentage of Tbr2/BrdU-double-positive cells in the VZ/SVZ of E15.5 cortical sections when compared to wild type or *Foxg1* heterozygous littermates (Fig. 4f and g). Remarkably, the increase in double positive cells was completely rescued when *Foxg1* dosage was reduced demonstrating that the increased IPC numbers was dependent on Foxg1 expression levels (Fig. 4f and g). Taken together, these data demonstrate that Snf2l functions in the same genetic pathway as Foxg1 to control the balance between progenitor proliferation and differentiation.

Modification of chromatin structure has emerged as a fundamental process controlling brain development through disease gene identification and a growing number of *in vitro* studies examining NSC proliferation and differentiation (Hamby et al., 2008; van

Bokhoven and Kramer, 2010). In this study we identify a genetic link between Foxg1 and the chromatin remodeling protein Snf2l that is important for regulating the balance between progenitor self-renewal and differentiation. We predict that Snf2l remodeling at the *Foxg1* gene results in its transcriptional repression and the subsequent de-repression of p21, thereby promoting the timely exit and terminal neuronal differentiation of progenitors that ultimately, controls brain size (Fig 4h). Studies in *Drosophila* and yeast demonstrate a well-documented role for ISWI in transcriptional repression often in association with the Sin3 repressive complex (Burgio et al., 2008; Fazzio et al., 2001). Other studies highlight a more global role for ISWI in chromatin compaction (Corona et al., 2007; Li et al., 2010). The Snf2l protein is part of two different complexes, CERF (Banting et al., 2005) and NURF (Barak et al., 2003), but which one regulates Foxg1 expression is unclear. The NURF complex is largely considered an activator of gene expression, while the function of the CERF complex remains unknown (Lazzaro et al., 2006; Wysocka et al., 2006). Since the Ex6DEL cortical phenotype is mild, the possibility exists that Snf2h-containing or other chromatin remodeling complexes may be providing some compensation. Indeed, future studies are required to delineate the specific roles of the ISWI-containing complexes in neural progenitor regulation. Nonetheless, an increased cortical cell density is most likely compensated by a reduction in another component of the tissue (eg. elaboration of neuronal projections). Additional studies will be required to define such changes although they may be related to corticofugal and sensory-motor projections as reflected by altered CTIP2- and Foxp1-positive cell numbers in the Ex6DEL animals.

Acknowledgements

We would like to thank J. Coulombe for technical assistance; and Drs. R. Kothary, L. Megeney, and V. Wallace for helpful discussions and comments on the manuscript. The HSFCSR provided partial financial support towards the purchase of the confocal microscope used in this study. DJY was funded by a OGSST award; CPC was an Ontario Graduate Scholarship recipient. DJP was funded by CIHR operating grants.

METHODS & SUPPLEMENTARY FILES

EXPERIMENTAL PROCEDURES

Generation and Maintenance of Ex6DEL Mice

A 4.84 kb *Kpn*I/*Xmn*I genomic fragment encompassing exon 6 of the m*Snf2l* gene was used to generate the targeting vector. A single loxP site was introduced distal to exon 6 (Pst1-EcoR1) and a Neo cassette flanked by loxP sites was inserted proximally (Xba1-Pst1) leaving short and long homologous arms of 1.6 kb and 2.6 kb, respectively. The targeting construct was electroporated into J1 ES cells, and G418-resistant clones were selected as described previously (Li et al., 1992). Homologous recombinants identified by Southern blot with probes located within exon 2 and exon 6, were utilized for blastocyst injection to generate exon 6 floxed mice. The exon 6 floxed line was bred to Gata1-Cre mice (Mao et al., 1999) to generate the Ex6DEL allele which was then maintained (independent of Cre) on a 129Sv background. Ex6DEL;Foxg1+/- mice were generated by crossing Ex6DEL mice to Foxg1-Cre knock-in animals (Hebert and McConnell, 2000). For timed mating purposes, the day of vaginal plug detection was counted as embryonic day 0.5 (E0.5). All experiments were approved by the University of Ottawa's Animal Care ethics committee adhering to the guidelines of the Canadian Council on Animal Care.

BrdU Labeling Experiments

Bromodeoxyuridine (BrdU) was administered by intraperitoneal injections (0.1 mg/g body weight) to time-mated females. For pulse labeling, pups were harvested 2 hours after a single injection. The percentage of BrdU+ cells to total VZ cells were counted and normalized to WT levels for all embryonic time points. For cell cycle re-entry experiments,

embryos pulse-labeled with BrdU at E12.5 or E16.5 were harvested one day later and stained for BrdU and the cell cycle marker Ki67. Cell cycle re-entry was determined as the proportion of cells that were BrdU+ and Ki67+ to the total number of BrdU+ cells. For neuronal birthdating experiments, BrdU was injected at E12.5 and offspring harvested at E18.5 for processing. BrdU+ cells were scored as densely labelled if BrdU comprised >75% of the nucleus. To determine S-phase length, iododeoxyuridine (IdU; 300 μg) was injected I.P. into pregnant mares at gestational days E13.5 and 15.5. This was followed, 1.5 hours (T_i) later, by a similar injection of BrdU (300 μg). The female was euthanized and the embryos removed 30 minutes after the second injection. These two separate analogs were differentially detected by mouse anti-BrdU/IdU (1:100; BD Biosciences) and rat anti-BrdU/CldU (1:200; Abcam) antibodies. Cells positive for IdU but not BrdU have exited S phase (L_c) but double-labeled cells remain in S phase (S_c). Length of S phase was calculated as: $T_s = T_i \times S_c/L_c$ as described elsewhere (Martynoga et al., 2005).

Immunofluorescent detection

Coronal brain sections (10 μm) were mounted on SuperFrost Slides (Fisher Scientific, ON, Canada) and frozen at -80^{o}C until use. Sections were washed five times in PBST (PBS with 0.1% Triton X-100), blocked (1 hr, room temperature) in 10% horse serum/PBST, and incubated (overnight, 4^{o}C) in primary antibodies. The following primary antibodies were used: rat anti-BrdU (1:400); mouse anti-SATB2 (1:10); rat anti-CTIP2 (1:500); rabbit anti-FoxP1 (1:400); rabbit anti-Ki67 (1:250; NCL-Ki67-P, Novocastro); rabbit anti-Phosphohistone H3 antibody (1:100; 06-570, Upstate); rabbit anti-TBR2 (1:250; ab23345, AbCam); rabbit anti-Nurr1 (1:500, Santa Cruz, CA, USA); mouse anti-beta III tubulin (Tuj; 1:400 dilution; 01409, Stem Cell Technologies); and mouse anti-NeuN (1:500; Millipore).

The following day, sections were washed five times in PBST and incubated (2 hrs, RT) with DyLight^{488}, DyLight^{594} or DyLight^{649}-conjugated secondary antibodies (1:1000, Jackson Immunoresearch, PA, USA). All sections were counterstained with the nuclear marker DAPI (Invitrogen). Coverslips were mounted with Dako Fluorescence Mounting Medium (Dako Canada, ON, Canada).

Image acquisition and processing

For IF experiments, tissue sections were examined and images captured using a Zeiss 510 laser scanning confocal microscope with UV (405nm), argon (488nm), helium/neon (546nm) and helium/neon (633nm) lasers. All images were acquired as 8µm Z-stacks (in 2µm intervals) and analyzed as projections using the LSM 510 Image Browser software (Zeiss). For cell density analysis, a 40 µm section was used to acquire 24 µm Z-stacks (in 2 µm intervals) which were used for 3D-reconstruction and cell counts. For counting of marker+ cells, we first determined the mean pixel intensity values using digital *x*-axis and *y*-axis pixel ovals placed within cortical brain regions or single cortical neurons (n>50). A digital oval (Φ100 pixels) was placed in immunoreactive negative brain regions and in adjacent "no primary" controls and the mean value was subtracted from the tissue under examination, thus generating a normalized immunoreactive positive intensity value that was used as the baseline to score a positive cell.

Chromatin immunoprecipitation

The ChIP assay was performed as described in the protocol from the Millipore ChIP Assay Kit (product #17-295) with some modifications. Cerebral cortex was dissected from E15.5 Snf2l$^{f/f}$ mice. The tissue was mechanically dissociated and cross-linked in 1% paraformaldehyde for 1 hour on ice. Tissue from approx. 10 embryos (4 x 10^7 cells) was

used for each experiment. Cells were lysed (50 mM Tris, 1 mM EDTA, 1% SDS, Roche Complete Mini protease inhibitor cocktail) on ice and then sonicated to generate fragments of 200 – 500 bp in length. Sepharose G slurry (25 µL; GE Biosciences) with 1 µg of either Sheep anti-Snf2l or Sheep IgG (Sigma) was used for IP. Quantitative PCR analysis was run on a MX3000P instrument (Stratagene) using Absolute™ QPCR SYBR® Green Mix (Thermo Scientific). The cycling conditions were: one cycle at 95°C for 10 min and 40 cycles of 95°C for 30 sec, 60°C for 30 sec, 72°C for 30 sec. Percent input of target DNA in the IP samples was calculated off a curve derived from serial dilutions of input chromatin.

Statistical Methods

For all data sets a minimum of 3 biological replicates (mice, embryos, or brains) were analyzed (n=3). For cell counts, the mean cell number was determined from a minimum of 3 sections from 3 biological replicates and, in most instances the data was normalized to WT. Unless indicated otherwise, histograms represent the Mean ± the Standard Error of the Mean (SEM). An asterisk (*) represents a statistically significant change by a two-tailed Student t-test ($p_{value} \leq 0.05$) as compared to the WT sample, unless indicated differently by the use of brackets.

Genotyping

The Ex6DEL mice were genotyped by multiplex PCR using primers that detected the exon 6 deletion using the following primers: intron-Forward 5'-ccatgtggggtccaggaatg -3'; exon6-Forward 5'-cctgggctggaaccatgatc-3'; and intron-Reverse 5'-gtatggacaagtgtgtgaagcc-3'. In order to determine the sex of embryos a PCR reaction with primers directed towards *Sry* was performed using the following primers, Forward 5'-ttgtctagagagcatggagggccatgtcaaa-3';

Reverse 5'-ccactcctctgtgacactttaggcctccga-3'. Heterozygous FoxG1 animals were identified by the presence of Cre-Recombinase using the following primers: Cre-Forward 5'-tgctctgtccgtttgccg-3' and Cre-Reverse 5'-actgtgtccagaccaggc-3'.

Behavior Testing

Naïve WT and Ex6DEL mice (~5 months old; n=8-12) were individually housed in a temperature-controlled room maintained on a 12hr day/night cycle (lights on at 7:00am) with unrestricted food and water unless stated otherwise. Mice underwent reference memory testing in the Morris water maze during four daily trials over 4-5 consecutive days as previously described (Choeiri et al., 2005; Mielke et al., 2006). For reverse trials, the platform was moved to the quadrant opposite to the one used for the initial experiments. Performance was measured by the time required to reach the platform and plotted as the mean ± SD. Average swimming velocity was measured to control for any motor deficits. Spontaneous alternation in a 4-arm maze was used to test spatial learning and memory as described (Choeiri et al., 2005). Delayed alternation was performed in the same apparatus. Mice were placed in the center of the maze and were allowed to make three unrestricted arm entries. On the fourth arm entry, a wooden block was placed in the entrance of the arm they had entered and remained in place for 30 seconds, effectively blocking the mice within that arm. The block was then removed and mice were free to enter any arm once again. The procedure of placing blocks in the entrance of the entered arm was repeated for each subsequent arm entry. The procedure was followed until 15 arm entries occurred or 30 minutes elapsed. Arm entries were recorded and successful alternations were defined as successive entry into a different arm of the maze. Percentage of alternation (ratio of actual to total possible alternations x 100) was calculated for each animal and plotted as the mean ±

SD. Operant learning was assessed in a bar-pressing task as described previously (Mielke et al., 2006). Briefly, mice were placed in the test cage for 30 minutes and the number of successful reinforcements was recorded. A reinforced trial was defined as a bar press followed within 30 s by the consumption of the reinforcer: a small 3 mg piece of pasta made of durum wheat. The mean number of reinforced bar presses per day ± SD was plotted.

Cortical Measurements

Coronal brain sections of P7 WT and Ex6DEL (n=3) mice were obtained with a Leica cryostat and Nissl stained. Measurements were performed using Image J software (http://rsbweb.nih.gov/ij) from pictures of the rostral and caudal cortex taken at medial and medial-lateral positions at 50x magnification. The width of the cortex was measured from the boundary of layer I and II to the underlying white matter. Mean values ± SEM are shown.

Protein Isolation and Immunoblots

Embryonic cortical extracts were homogenized in ice-cold RIPA buffer supplemented with protease inhibitor cocktail (Sigma), and incubated for 20 min on ice with gentle mixing. After pre-clearing by centrifugation (15 min at 17,000 x g), proteins were quantified by the Bradford method. Protein samples were resolved on 10% sodium dodecyl sulfate polyacrylamide gels under denaturing conditions, and blotted onto PVDF membranes (Immobilon-P; Millipore, MA, USA) by wet transfer for 2 hr at 80 V. Membranes were blocked (45 min, room temperature) with 5% skim milk in TBST (Tris-buffered saline containing 0.05% Triton X-100), and incubated (4°C, overnight) with the following antibodies: rabbit anti-FoxG1 (1:500, Abcam, ab18259), mouse anti-ß-Actin (1:30,000, Sigma, A1978) or mouse anti-FLAG-M5 (1:10,000, Sigma). Primary antibodies for Snf2l

have been described elsewhere (Lazzaro et al., 2006). Membranes were incubated (1 hr, room temperature) with ImmunoPure® HRP-conjugated goat anti-rabbit or anti-mouse IgG(H+L) secondary antibodies (1:5,000; Pierce, IL, USA). Membranes were washed 5 x 5 min in TBST after antibody incubations, and the signal was detected by chemiluminescence using the ECL-Plus kit (GE Healthcare). Pixel intensities for each blot were quantitated using ImageJ software (http://rsbweb.nih.gov/ij).

Immunohistochemical detection

Brain sections were washed five times with PBST, treated with 0.3% hydrogen peroxide in PBS for 20 min, blocked (1 hr, RT) in 10% horse serum/PBST, and incubated (overnight, 4^{o}C) in primary antibodies. The following primary antibodies were used: rabbit anti-FoxG1 (1:50, Abcam) and rabbit anti-pH3 (1:300, Millipore) as positive control. Sections were washed five times in PBST and incubated (2 hrs, room temperature) with biotinylated anti-rabbit IgG (H+L) secondary antibodies (1:300; Vector Laboratories, CA, USA). Immunodetection was accomplished using the HRP-ABC technique (Vector Laboratories) according to the manufacturer's instructions using a diaminobenzidine-nickel colored substrate. Immunohistochemistry images were acquired using a Zeiss Axiovert Observer Z1 epifluorescent/light microscope equipped with an AxioCam cooled-color camera (Zeiss, Oberkochen, Germany). The FoxG1 IHC, originally in grayscale, was quantitated using ImageJ software. 50 FoxG1^{high}- expressing cells were quantitated throughout all cortical layers. Background values were obtained from non-immunoreactive tissue in the lateral hypothalamus and subtracted from FoxG1-positive mean gray values.

Cell death analysis

To assess cell death a TUNEL assay was performed using the *in situ* Cell Death Detection Kit, TMR Red (Roche Diagnostics). The Apoptotic Index was calculated as the number of TUNEL+ cells divided by the total cell number (DAPI+) in a 100 □m section. The mean ± SEM were calculated from three biological replicates.

RT-PCR and qPCR

RNA from pelleted mammalian cells, or mechanically disrupted mouse tissues was isolated using Trizol Reagent (Invitrogen). Complimentary DNA sysnthesis was performed with 2.5-5 μg of total RNA was reverse transcribed as described (Yip and Picketts, 2003). Complimentary DNA products were used for PCR amplification under standard conditions for Snf2l (Forward 5'cctctcaacatgaaactggc 3', Reverse 5'tcacgcaaacatcccactct 3') and using *β-actin* as a positive control (Forward 5'ctgaaccctaaggccaaccgt 3', Reverse 5'ccgtcaggcagctcatagctcttc 3'). Reaction mixture contained [0.5-1 μL, cDNA, 1x PCR buffer, 0.2 mM dNTPs, 0.5 mM primers (each) and Taq DNA polymers] for 24-30 cycles of 94^{o}C for 30s, 56-60^{o}C (depending on primer pair) for 30s, 72^{o}C for 1 min, followed by 10 min at 72^{o}C.

RNA for quantitative realtime RT-PCR experiments was isolated using RNeasy Plus Midi kit from Qiagen (Mississauga,ON). Total RNA (2.5-5 μg) was used to synthesize cDNA as described (Yip and Picketts, 2003). Quantitative PCR was then performed with a Mx 3000 realtime cycler (Stratagene) using the ABsolute QPCR SYBR Green Mix (Thermo Scientific). PCR conditions were as follows; 10 minutes at 95^{o}C followed by 35 cycles of 30 seconds at 95^{o}C, 30 seconds at 60^{o}C and 30 seconds at 72^{o}C. Primers were as follows: *Cdnk2a* (Forward 5'-aagcgaactcgaggagagc-3'; Reverse 5'-gtacgaccgaaagagttcg-3'), *Cdnk1a* (Forward 5'-gtccaatcctggtgagtcc-3'; Reverse 5'-gttttcggccctgagatgt-3'), *Cdnk1b* (Forward

5`-cctgactcgtcagacaattcc-3', Reverse 5'-tgttctgttggccctttg-3'), *Cdnk1c* (5`-cagatgcccagcaagttctc-3', Reverse 5'-ctctccaaacgtggctcct-3'), *Ccnb2* (Forward 5'-ctagctcccaaggatcgtcc-3', Reverse 5'-gttctccctgtcctcgttatctat-3'), *Ccnd1* (Forward 5`-cggatgagaacaagcagacc-3', Reverse 5`-gagggtgggtggaaatga-3'), and *Foxg1* (Forward 5'-ctactccctcaacccctgct-3', Reverse 5'-cagacagtcccccagacagt-3'). All data was normalized to *Gapdh* (Forward 5'-tgaaaggggtcgttgatgg-3', Reverse 5'-aaaatggtgaaggtcggtgt-3') and *18S* (Forward 5'-cggctaccacatccaagg-3', Reverse 5'-ctggaattaccgcggct-3') RNA expression levels and calculated using the delta delta CT (ddCt) method defined as fold change = 2^-(Ex6DEL(CT)- Wt(CT)).

Microarray Analysis

RNA was isolated from WT and Ex6DEL dissected E15.5 cortices using an RNeasy Mini Kit (Qiagen, Mississauga,ON). The cDNA synthesis, labelling and microarray hybridization was performed using the 3DNA Array 900 Cy3/Cy5 kit (Genisphere, Hatfield PA) with one sample pair performed under dye-flip conditions. The hybridization was performed on MEEBO 38.5k arrays obtained from Microarrays Inc (Huntsville, AL). The microarray was scanned using a Scan Array Express scanner and analyzed using the Pro Scan Array Express software package (Perkin Elmer). Data was background subtracted and LOWESS normalized to generate $\log_2$ ratio (test/reference). The dataset was submitted to the NCBI Gene Expression Omnibus (GEO) repository with accession number GSE34998.

Luciferase Assays

The mouse FoxG1 promoter region was amplified via PCR from 100ng of BAC RP23-305D23 (CHORI, Oakland, USA) using Elongase enzyme mix (Invitrogen, ON, Canada)

and cloned into the KpnI and XhoI sites of the pGL4.23 vector (Promega, WI, USA). The 4.5kb-WT-FoxG1 and 3.5kb-Δ1-FoxG1 constructs expanded base pairs -4550 to +22 and -4550 to -1179, respectively (+1 = translation start site). Primers used are as follows: *mFoxG1*(-4.5kb)-KpnI-F 5'-cgtggtacctcccacatgtcaagaggtca-3' ; *mFoxG1*(+22)-XhoI-R: 5'-cgtctcgagtcctatctcccatgtccagc-3'; *mFoxG1*(-1179)-XhoI-R 5'-cgtctcgagttctgtggaggccttcca-3'. Underlined sequences denote introduced restriction sites used for cloning into pGL4.23. All clones were verified via DNA sequencing. Neuro-2A cells were grown on 24-well plates and transfected with 50ng of the pRL-TK vector (pGL4.74, Promega), 150ng of the pGL4.23 vector containing either the 4.5kb-WT-FoxG1 or 3.5kb-Δ1-FoxG1 amplicons and 600ng of *hSNF2L* or *hSNF2H* full-length cDNAs using Lipofectamine 2000 (Invitrogen). For Luciferase and Renilla activity measurements, cell lysates were prepared 24 hrs post-transfection and processed using the Dual Glo® Luciferase Assay System (Promega) according to the manufacturer's instructions. Readings were acquired using the GloMax 96 Plate Luminometer with the dual injection system (Promega). All Luciferase values are normalized to the Renilla value of each sample, and then double normalized to pGL4.23-empty Luciferase expression.

SUPPLEMENTARY FIGURES

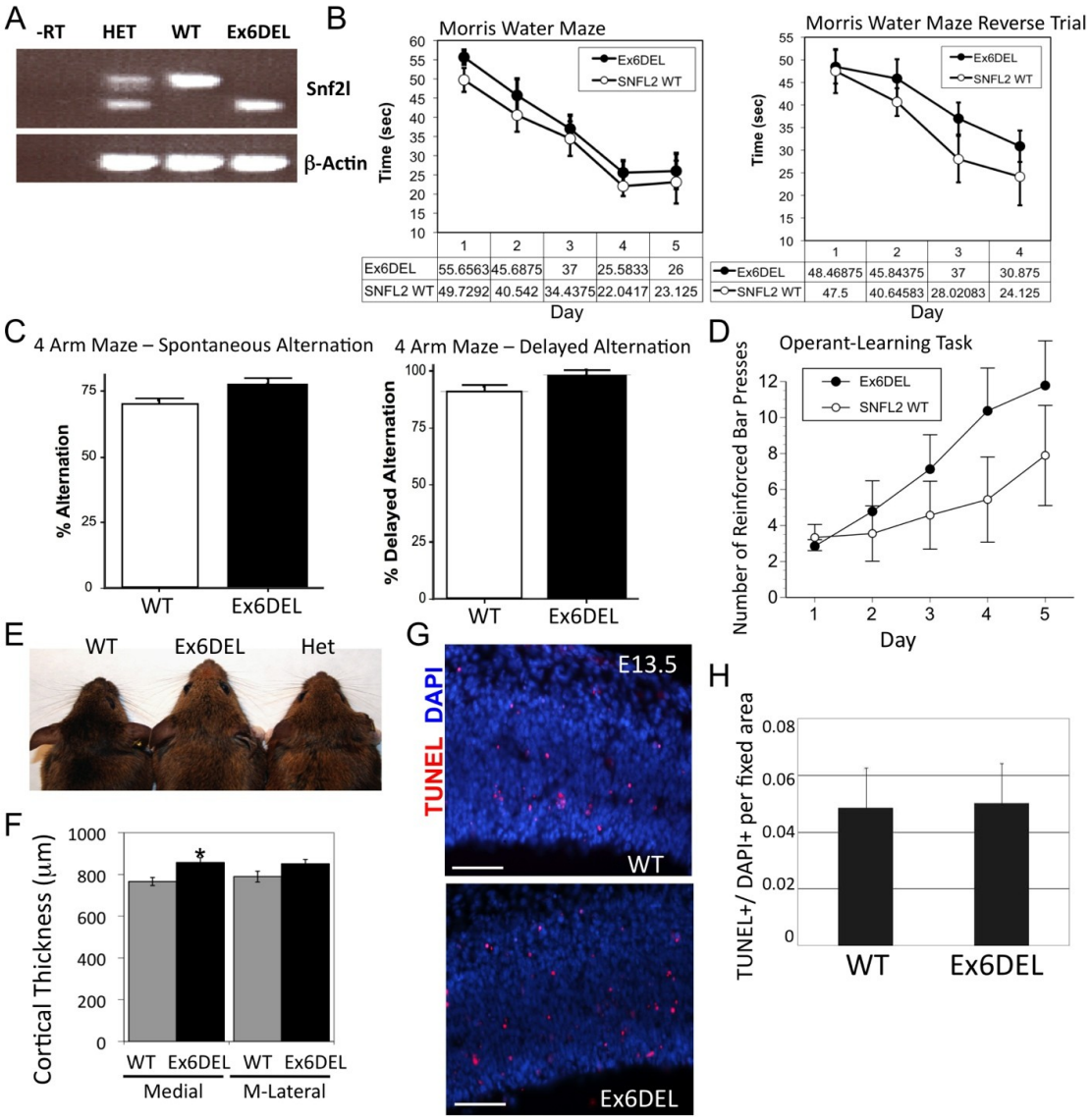

Figure S1. Ex6DEL mice have larger heads yet no overt phenotype. **(A)** RT-PCR analysis and segregation of the normal and targeted (lacking exon 6) Snf2l transcripts from WT, HET or Ex6DEL mice. -RT, no RT control. **(B)** Graphs depicting mean animal performance of daily trials in the Morris water maze (n=12 WT; n=8 Ex6DEL). For the Reverse Trial, the platform was placed in the quadrant opposite the one used for the initial test. **(C)** Plot of the percentage of spontaneous or delayed alternations in a 4-arm maze. Successful alternations were defined as successive entries into three different arms. Successful delayed alternation is defined as entry into a different arm of the maze following block removal. Values represent the mean ± SD (n=9). **(D)** Operant conditioning test that scored the number of bar presses in which the animal retrieved the food reward within 30s over a testing time of 30 min. Values represent daily mean scores ± SD (n=9). **(E)** Photographs depicting that

Ex6DEL mice (P30) have larger heads compared to WT or heterozygous (Het) littermates. **(F)** Cortical thickness measurements of caudal brain sections (n=3). Measurements are from the medial and medial-lateral regions (see Fig 1d) and represent the mean ± SEM (n=3; *, $p \leq 0.05$ by t test). **(G)** The TUNEL assay was performed on E13.5 sections from WT or Ex6DEL brains and then immunostained for TUNEL+ cells (red) as a measure of cell death and counterstained with DAPI (blue). Scale bar = 10□□m. **(H)** The graph depicts the number of TUNEL+ cells as a proportion of total cell counts (DAPI+) and demonstrates that there was no significant difference between WT and Ex6DEL animals (n=4; Mean ± SEM; t test).

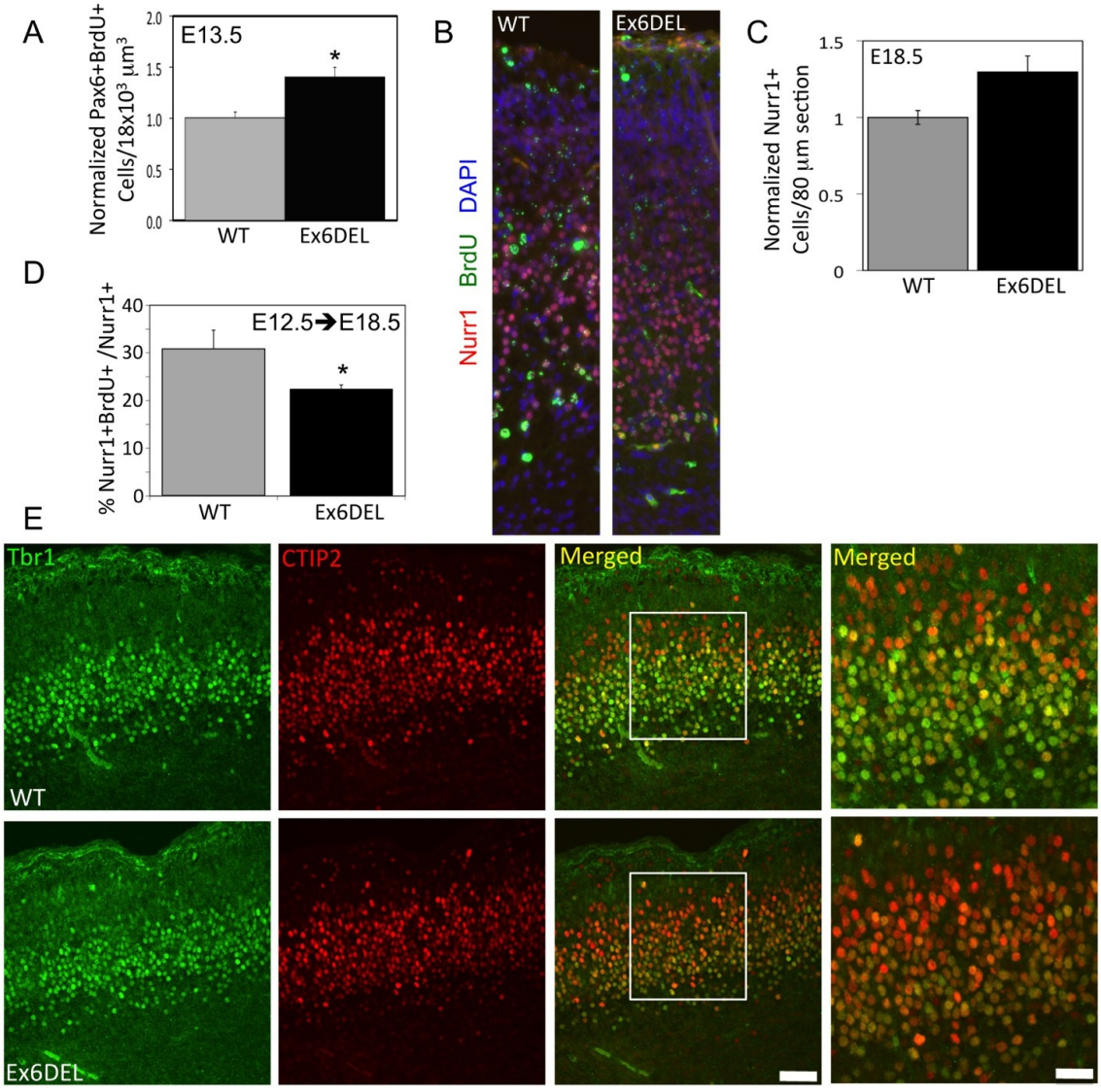

Figure S2. Increased neuronal output in Ex6DEL mice. **(A)** Plot of the proportion of cycling apical progenitors (Pax6+, BrdU+/total BrdU+) at E13.5 normalized to WT levels (n=3; Mean ± SEM; * $p<0.05$ by t test). **(B)** E18.5 sections (80 □m width) stained for Nurr1 and BrdU following neuronal birthdating at E12.5 **(C)** Normalized quantification of Nurr1+ cells at E18.5 from sections represented in B (n=3; Mean ± SEM; $p=0.058$ by t test). **(D)** Quantification of Nurr1+/BrdU+ neurons as a fraction of total Nurr1+ cells stained at E18.5 following neuronal birthdating with BrdU at E12.5 (n=3; *p-value = 0.02 by t test). **(E)** E15.5 sections stained for CTIP2 and Tbr1 demonstrate a qualitative increase in the proportion of $CTIP2^{high}/Tbr1^{low}$ cells in the Ex6DEL mice. Scale bar = 50 □m.

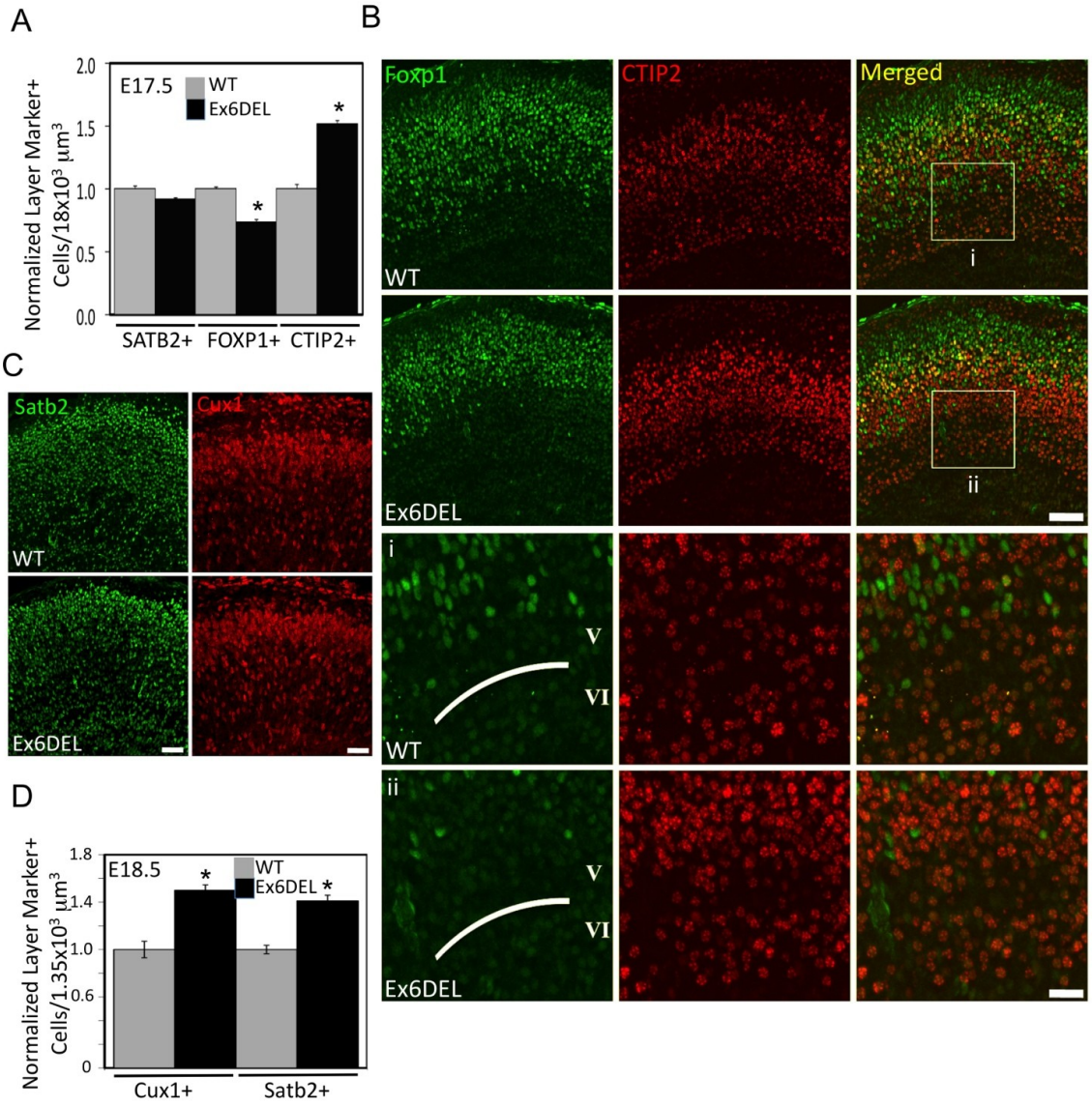

Figure S3. Layer marker cell counts are altered in Ex6DEL mice. **(A)** Normalized cell counts for SATB2, FOXP1, and CTIP2 cell layer markers at E17.5. Bars represent Mean ± SEM; *p<0.05 by t test. **(B)** E17.5 cortical sections stained for Foxp1 (green) and CTIP2 (red). Scale bar = 50 □m. Boxed regions i and ii shown below highlight the reduction in FOXP1 staining and increased CTIP2 staining in layer V. **(C)** Representative low magnification images of Satb2 at E17.5 and Cux1 at E18.5. Scale bar = 50 □m. **(D)** Normalized cell counts of the proportion of Cux1 or Satb2 positive cells within layers II/II at E18.5 as depicted in Figure 3e. Bars represent Mean ± SEM; *p<0.05 by t test.

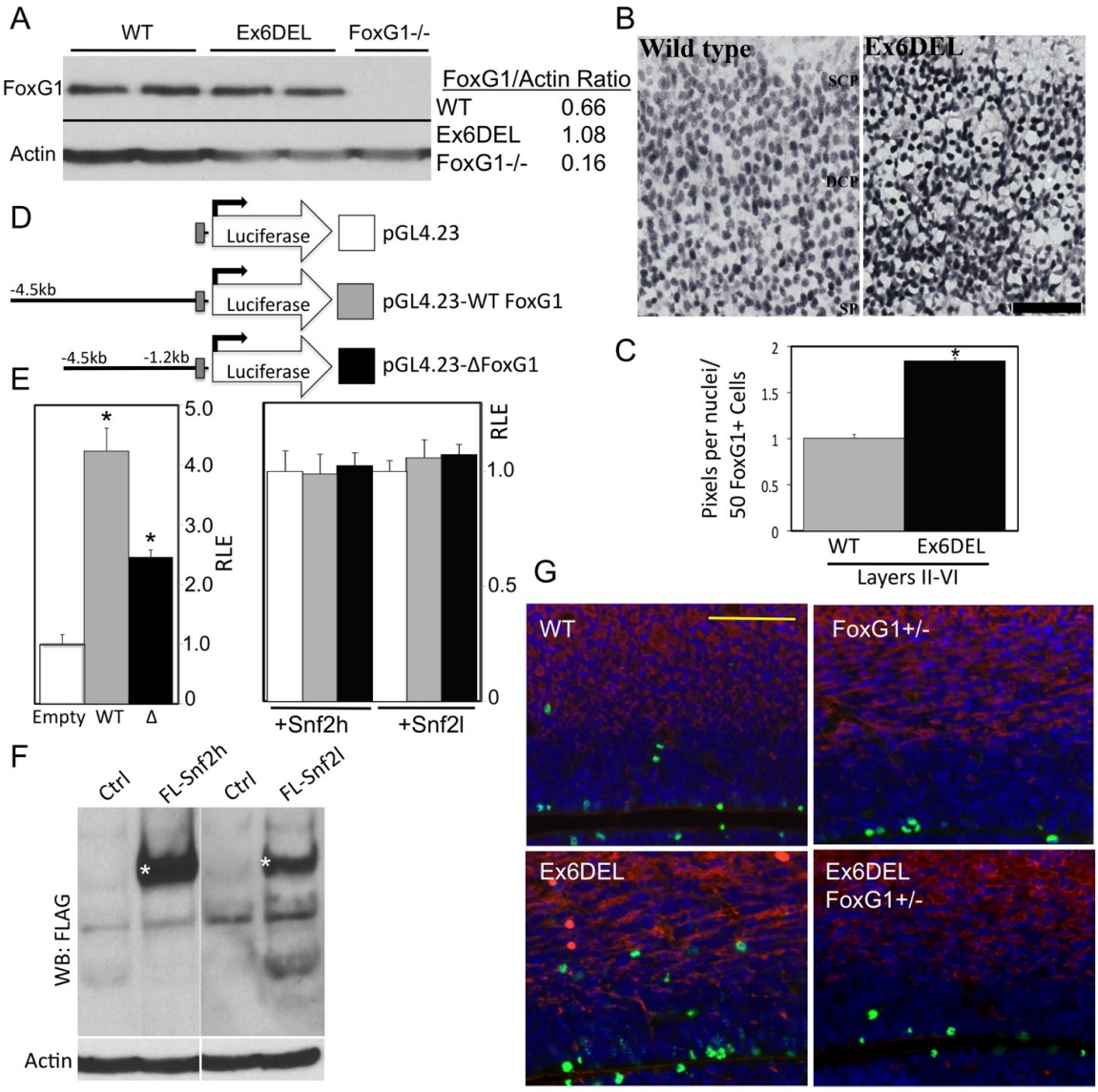

Figure S4. Increased Foxg1 expression alters cell number. **(A)** Immunoblot of Foxg1 protein levels from E15.5 cortical extracts. Table on right depicts the Foxg1/actin densitometric ratio and highlights the increased Foxg1 expression levels in the Ex6DEL mice. **(B)** Magnified image of E15.5 cortical plate immunostained for Foxg1 (see lower mag. image in Fig 4b). Scale bar = 20 □m. **(C)** Normalized pixel counts for 50 Foxg1+ cells from the cortical plate demonstrates that the Ex6DEL mice have increased levels. * represents $p \leq 0.05$. **(D)** Schematic diagram of the luciferase constructs containing a basal promoter (grey box; pGL4.23) and either 4.5 kb of the Foxg1 upstream sequence (pGL4.23-WT Foxg1) or the same region lacking the first 1.2 kb containing the Snf2l binding site (pGL4.23-ΔFoxg1). **(E)** Relative Luciferase Expression (RLE) following transfection into Neuro-2A cells of the three plasmids and normalized to pGL4.23 (left graph). The graph on the right represents RLE after co-transfection of either Snf2l or Snf2h expression plasmids. The values are normalized to the expression level of each vector without the ISWI plasmid demonstrating that co-transfection of Snf2l or Snf2h has minimal effects. **(F)** Immunoblot with M5

antibody to detect Flag-tagged Snf2l or Snf2h expression following transfection. The white asterisk denotes the location of the tagged protein. Actin was used as a loading control. **(G)** E15.5 cortical sections from WT, Foxg1+/-, Ex6DEL, or Ex6DEL; Foxg1+/- animals stained with PH3 (green) to label mitotic progenitors. Differentiated post-mitotic neurons are stained with Tuj (red). Yellow scale bar = 125 μm. Quantification of this experiment is presented in Fig 4e.

CHAPTER 3

Snf2h and Satb2-dependent chromatin regulation governs cortical development and maturation.

Matías Alvarez-Saavedra[1,3], Emile Hashem[1,3], Danton Ivanochko[1], Doo Yang[4], Keqin Yan[1], Yves De Repentigny[1], Gregory O. Cron[5], Rashmi Kothary[1,4], Teruyoshi Hirayama[6], Takeshi Yagi[6], Ilya Ioshikhes[4] and David J. Picketts[1,4].

[1]Regenerative Medicine Program; and [2]Vision Program, Ottawa Hospital Research Institute, Ottawa, ON, Canada K1H 8L6;

Departments of [3]Cellular and Molecular Medicine; [4]Biochemistry, Microbiology & Immunology; and [5]Radiology, University of Ottawa, Ottawa, ON, Canada;

[6]KOKORO Biology Group, Laboratories for Integrated Biology, Graduate School of Frontier Biosciences, Osaka University, Suita 565-0871, Japan.

Statement of Contribution

All experimental design; immunohistochemistry and immunofluorescence; confocal and light microscopy analysis; molecular biology and cell culture experiments; behavioral analysis; writing of manuscript.

ABSTRACT

The neocortex provides the brain with the cellular diversity and connectivity controlling higher order cognitive functions. Genetic abnormalities affecting cortical development convey neural circuitry assembly alterations that underlie cognitive disorders. However, the epigenetic mechanisms involved in cortical development and differentiation are poorly characterized. Here we show that the chromatin remodeler Snf2h drives embryonic cortical expansion through *FoxG1* and *Satb2* gene regulation; and postmitotic neural arborization by clustered *protocadherin* gene expression control. Telencephalon-specific *Snf2h* cKO embryos have impaired FoxG1 and Satb2 expression, resulting in increased cell death and cortical hypoplasia. Mutant mice survive into adulthood, but postmitotic neurons display arborization deficits, reduced clustered *protocadherin* gene expression and agenesis of the corpus callosum, resulting in cognitive dysfunction. We show that both Snf2h and Satb2 mediate the transcriptional regulation of the clustered *Pcdh* isoforms in a cell culture model, and both molecules can partially rescue *Pcdh* gene activation upon Snf2h knockdown. Thus, a single nucleosome remodeler, coupled to the Satb2-chromatin architectural protein, trigger progenitor and postmitotic gene expression programs to control the development and maturation of the mammalian cortex.

INTRODUCTION

The proper wiring of the mammalian brain is necessary for cognitive control, including linguistics, motor functions, emotions, memory and associative processing. The six neuronal layers of the cerebral cortex project directly or indirectly to all brain structures, connect the cerebral hemispheres and provide the neural diversity that is necessary for higher order cognitive skills (Kwan et al., 2012). Indeed genetic mutations affecting the development and/or function of the neocortex results in a wide array of neurobehavioral alterations and is the cause of numerous intellectual-disability syndromes. This is indicated by the growing number of genes encoding chromatin remodeling proteins as the cause of a wide range of developmental disorders associated with intellectual disability (Rangasamy et al., 2013). However, the epigenetic mechanisms mediating neocortical development and maturation remain largely unknown.

Gene expression is ultimately regulated at the level of chromatin, where ATP-dependent chromatin remodeling complexes (CRCs) control DNA replication, DNA accessibility, chromosome structure and ultimately gene expression. More than 30 different genes encode for the catalytic subunits of CRCs in mammals, and multiple DNA-protein binding domains further specify and diversify their strategies to interact with nucleosomes (Narlikar et al., 2013). The ISWI (Imitation of Swi2/Snf2) nucleosome remodeler is part of several complexes that catalyze DNA-dependent chromatin remodeling in all eukaryotic species. The first ISWI-containing complexes were isolated from *Drosophila melanogaster* as NURF (nucleosome-remodeling factor), ACF (chromatin-assembly factor) and CHRAC (chromatin accessibility complex) [reviewed in (Erdel and Rippe, 2011)]. ISWI plays roles in DNA replication, homeotic gene expression regulation, and higher order chromatin

structure (Erdel and Rippe, 2011). Mammals possess two ISWI orthologs, *Snf2h* and *Snf2l* (also known as *SMARCA5* and *SMARCA1,* respectively), which have divergent patterns of expression in the developing mouse embryo (Lazzaro and Picketts, 2001a). Snf2h-null embryos die during the peri-implantation stage due to hypoproliferation of the inner cell mass and trophoectoderm (Stopka and Skoultchi, 2003), while Snf2l-null mice survive normally, but display hyperproliferation of cortical progenitors, resulting in an enlarged brain (Yip et al., 2012). However, the role of Snf2h-containing CRCs in the developing brain remains unknown.

In mammals, neocortical development occurs during embryogenesis as a series of symmetric and asymmetric cell divisions in the neuroepithelium of the ventricular zone (VZ) and subsequent specification to cortical projection neurons or interneuron subtypes (Kwan et al., 2012). A spatiotemporal inside-to-outside model of neurogenesis results in the formation of the six mammalian cortical layers that establish the cortical networks that control brain function. We have recently shown that one of the two *Drosophila* ISWI orthologs*, Snf2l,* controls cell cycle exit through FoxG1 dosage to modulate neuronal output and cortical differentiation (Yip et al., 2012). We therefore interrogated the role of the second *Drosophila* ISWI ortholog, *Snf2h*, during neocortical development by conditional deletion. We determined that Snf2h-dependent gene activation mediates progenitor and postmitotic transcriptional programs to establish the development and maturation of the mouse cortex.

RESULTS

Snf2h loss during cortical progenitor expansion results in FoxG1 and Satb2 hypoactivation and increased cell death.

In order to investigate the role of Snf2h in the developing neocortex, we ablated Snf2h expression with Emx1-Cre and FoxG1-Cre driver mice (Eagleson et al., 2007; Guo et al., 2000). Survival curves revealed that *Snf2h* cKO by FoxG1-Cre (*Snf2h* cKO-FoxG1 hereon) mice did not survive past birth, but *Snf2h* cKO by Emx1-Cre (*Snf2h* cKO-Emx1 hereon) mice had a normal lifespan as they survived normally past two years of age (not shown). The lethality of *Snf2h* cKO-FoxG1 mice likely arises from the ~50% reduction of FoxG1 mRNA levels in the FoxG1-Cre hypomorphic background (Eagleson et al., 2007). As such, we used the *Snf2h* cKO-Emx1 mouse model to assess the role of Snf2h in cortical development. First, we validated the spatiotemporal specificity of the Emx1-Cre driver by breeding to the ROSA-STOP-lacZ reporter line, where lacZ was activated after ~E10 predominantly in the dorsal telencephalon of reporter mice (Supplementary Fig. 1). We next assessed the steady-state mRNA levels from E13.5 mutant and control cortical extracts by qRT-PCR. As expected, Snf2h expression was reduced ~2.1-fold in the mutant cortex, while Snf2l expression was unaffected in the mutant cortex relative to controls (Figure 1A). We have previously shown that Snf2l represses the expression of the Forkhead Box G1 transcription factor (TF) during the late stages of corticogenesis (Yip et al., 2012), so we assessed the expression of FoxG1; Satb2, a matrix-attachment region (MAR)-binding protein that specifies the callosal projection neuron lineage by ~E14 (Alcamo et al., 2008; Britanova et al., 2008); and Early B-cell factor 3 (Ebf3), a TF that specifies the Cajal-Retzius lineage (Chiara et al., 2012).

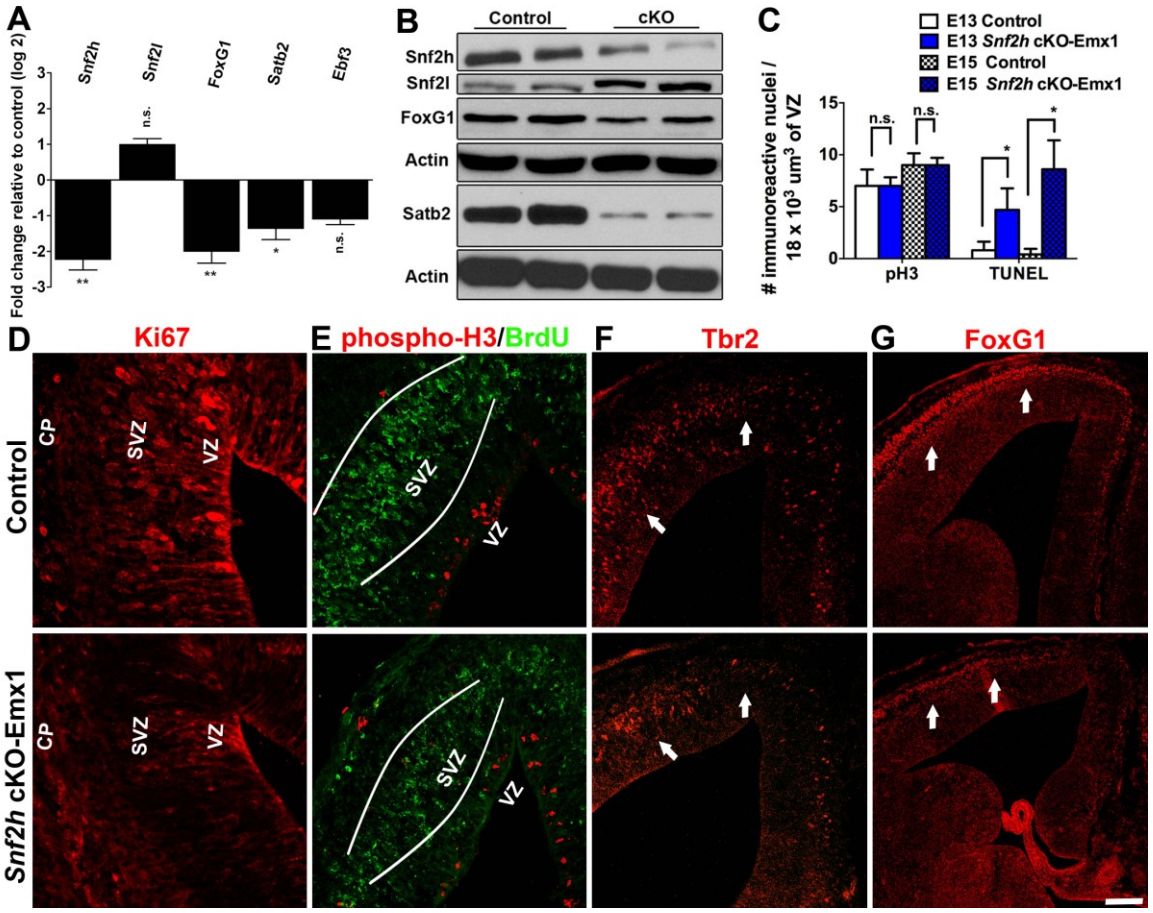

Figure 1. Snf2h loss during neocortical expansion results in FoxG1 deactivation and cell death. **(A)** qRT-PCR expression for Snf2h, Snf2l, FoxG1, Satb2 and Ebf3 from mutant and control cortical extracts at E13.5. **P*<0.05, n=3, student's t-test. **(B)** Western blotting for Snf2h, Snf2l, FoxG1, Satb2 and Actin, as loading control, from mutant and control cortical extracts at E15.5. **(C)** Quantitation of pH3+; or TUNEL+ cells through the VZ of mutant and control embryos at E13.5 and E15.5. Five cubic bins were scored and averaged per embryo. **P*<0.05, n=3, student's t-test. **(D)** Confocal Z-stacks immunolabeled for Ki67 (red), a marker of proliferating cells, through the mutant and control neocortex at E13.5. VZ = ventricular zone; SVZ = subventricular zone; CP = cortical plate. **(E)** Confocal Z-stacks double-immunolabeled for BrdU (green); and phospho-Histone H3 (pH3; red) through the mutant and control neocortex after a 2-hr BrdU pulse. Note the reduction of BrdU+ cells in the mutant SVZ. **(F)** Confocal Z-stacks immunolabeled for Tbr2 (red), a marker of basal progenitors, through the mutant and control neocortex at E15.5. Arrows highlight domains of Tbr2+ precursors that are reduced in mutant embryos. **(G)** Confocal Z-stacks immunolabeled for FoxG1 (red) through the mutant and control neocortex at E15.5. Note the robust expression of FoxG1 in postmitotic neurons of the cortical plate (arrows), whereas the mutant neocortex displays a reduced population of FoxG1+ neurons (arrows).

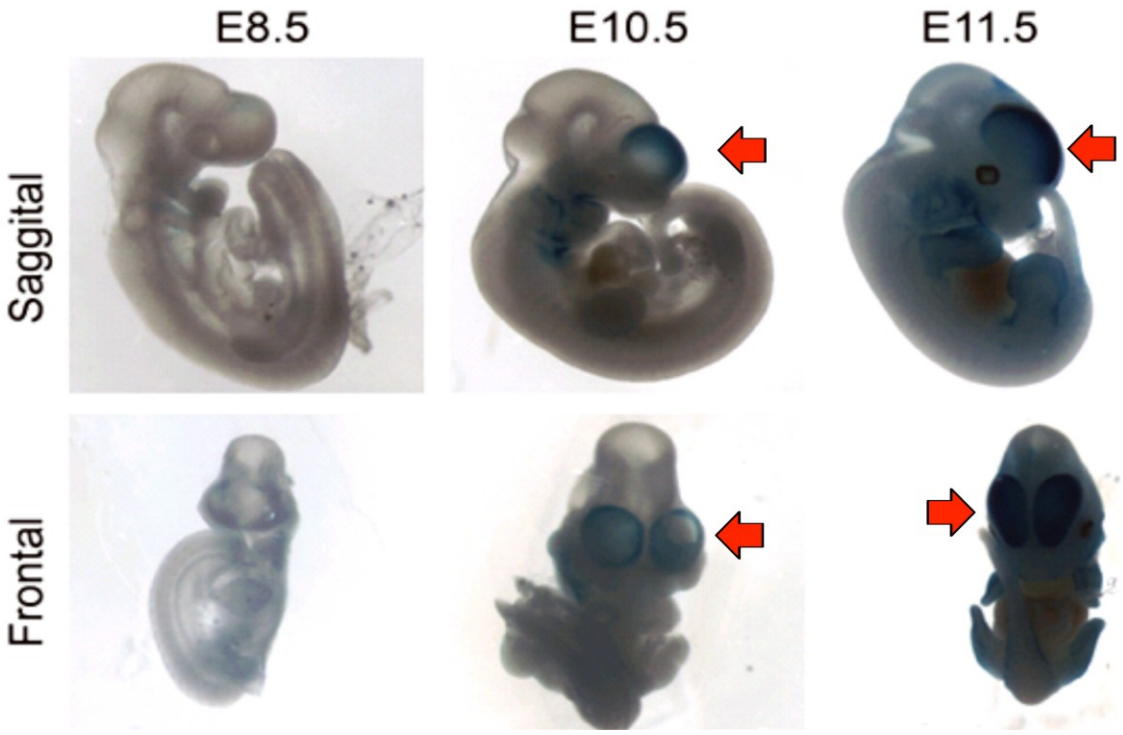

Supplementary Figure 1. Emx1-Cre driver mice functionally target the developing telencephalon. Emx1-Cre driver mice were bred to ROSA-STOP-LacZ mice that activate lacZ expression upon Cre deletion. Note the expression of LacZ (blue-colored product) predominantly in the developing telencephalon after ~E10.5 (arrows) in Emx1-Cre$^{-/+}$::ROSA-STOP-lacZ$^{-/+}$ mice.

We found an ~1.81 and ~1.43 reduction of FoxG1 and Satb2 mRNA levels, respectively, while Ebf3 expression levels were unaffected (Fig. 1A). We further demonstrate the downregulation of Snf2h, FoxG1 and Satb2 proteins, while Snf2l levels were significantly upregulated in in E15.5 mutant cortical extracts relative to controls (Fig. 1B).

Snf2h is well known to play a role in DNA replication, so we assessed the number of proliferating cortical progenitors in the developing neocortex. We quantitated the number of mitotic (phospho-histone H3+) and apoptotic (TUNEL+) progenitors at E13.5 and E15.5. We observed a normal number of cells going into mitosis in the mutant VZ at both time points, while apoptotic cells were highly increased at both time points in the mutant VZ and SVZ relative to controls (Figure 1C). However, we detected a lower number of proliferating Ki67+ cells in the mutant VZ by E13.5; and reduced BrdU+ cells in the mutant SVZ after a 2-hr pulse relative to control littermates (Figures 1D-E). By E15.5, Tbr2+ basal progenitors were also reduced in the mutant SVZ (Figure 1F); and reduced FoxG1+ neurons were present in the mutant cortical plate relative to controls (Figure 1G). We conclude that Snf2h plays a key role in the early expansion of cortical progenitors in part by the genetic activation of master TFs involved in cell fate decisions, including FoxG1 and Satb2 (Alcamo et al., 2008; Britanova et al., 2008; Kumamoto et al., 2013).

Snf2h loss in the neocortex reduces the output of callosal and corticofugal projection neurons.

The cortical plate is established through successive rounds of neurogenesis that further resolves into the six cortical layers of the mammalian brain (Kwan et al., 2012). Neurons of the same laminar location share a common date of birth. For example, Layer I

(Cajal-Retzius) neurons are born around E11, while layer V and VI (corticofugal and corticothalamic projection) neurons are produced between E12 and E14 (Molyneaux et al., 2007). Subsequently, layer II-IV (callosal projection) neurons are produced from ~E15 to ~E17 (Fame et al., 2011). We assessed whether the enhanced neocortical cell death in *Snf2h* cKO-Emx1 embryos affected the generation of postmitotic projection neurons by birth. Early- and late-born cortical neurons were birthdated with a single BrdU injection at E13.5 and E15.5, respectively, and pups were analyzed at birth (P0). We co-labeled the neonatal cortex with BrdU to label birthdated cells; and markers of corticofugal projection neurons (layers V-VI; anti-Sox5); or callosal projections neurons (layers II-IV; anti-Satb2 and anti-Cux1). We quantitated the number of brightly fluorescent BrdU-labeled cells (BrdU staining >75% of nucleus) that co-localized with each of the layer markers. We found more than a ~2-fold decrease of Satb2+ or Cux1+ late-born neurons in the mutant neocortex relative to controls when birthdated at E15.5 (Figures 2A & 2C). Similarly, we found a ~2-fold decrease of Sox5+/BrdU+ early-born neurons in the mutant neocortex relative to controls when birthdated at E13.5 (Figures 2B & 2C). Nissl-stained sagittal sections reveal the cortical hypoplasia of *Snf2h* cKO-Emx1 mice relative to controls by birth (Figure 2D), while whole mount brains highlight the severe cortical hypoplasia of adult mice, which is further aggravated upon deletion of the Snf2l homologue (Figure 2F). We further show the significant reduction of Snf2h+ neurons throughout the mutant cortex relative to controls at birth (Figure 2E). Thus far, we conclude that Snf2h is intricately involved in the early expansion of the cortical progenitor pool to specify early-born and late-born cortical

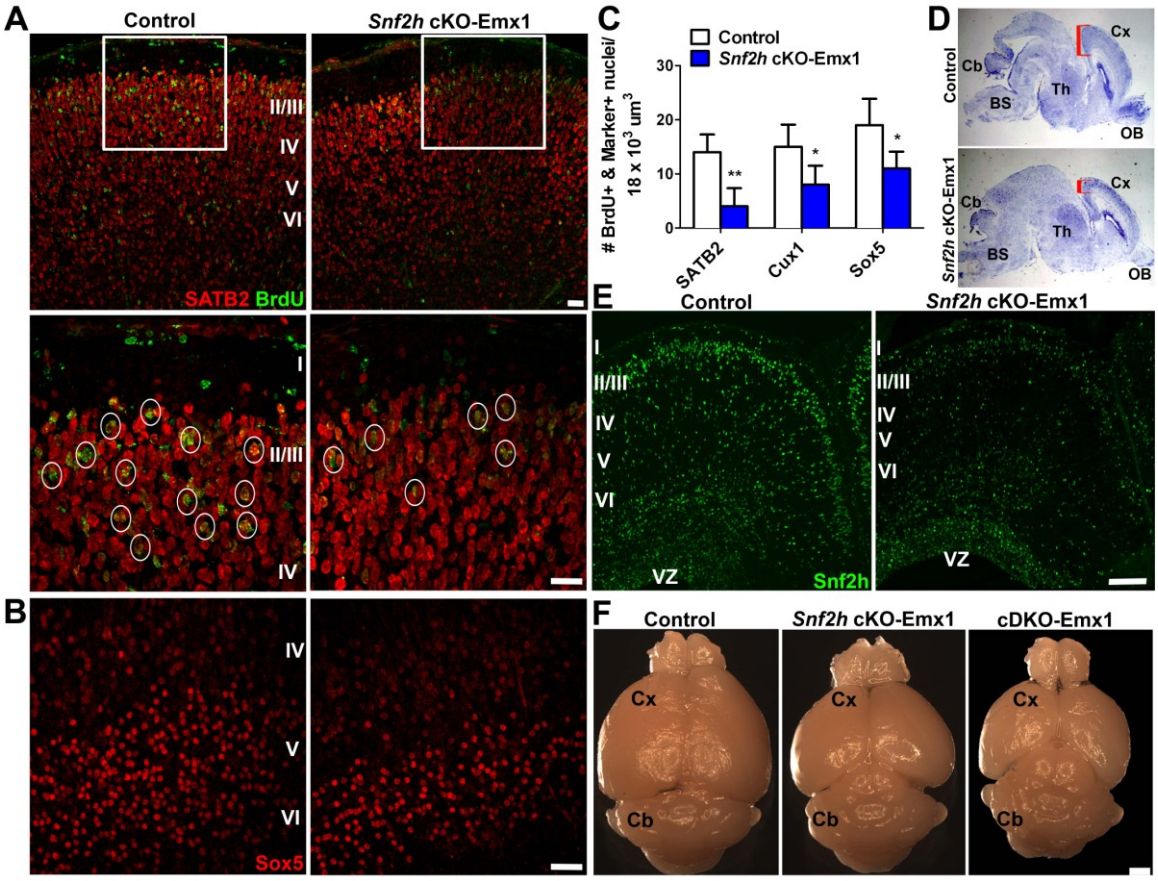

Figure 2. Snf2h loss in the neocortex results in cortical hypoplasia due to lower production of callosal and corticofugal projection neurons. **(A)** Confocal Z–stacks through the BrdU birthdated (BrdU injected at E15.5, embryos killed at P0) mutant and control cortex co-labeled with BrdU (green); and Satb2 (red), a marker of callosal projection neurons. Boxes are enlarged in bottom panels. Note the lower number of BrdU-densely stained neurons (>75% BrdU in the nucleus) in the mutant cortex relative to controls (circles). Roman numerals denote the six cortical layers. **(B)** Confocal Z–stacks immunolabeled for Sox5 (red) at birth, a marker of corticofugal projections neurons. **(C)** Quantitation of BrdU-densely stained and marker-positive neurons from E15.5 BrdU-birthdated (for Satb2 and Cux1); or E13.5 BrdU-birthdated (for Sox5) embryos. 5 cubic bins were scored and averaged per embryo. **P*<0.05, n=3, student's t-test. **(D)** Nissl staining of sagittal sections through the mutant and control brain at P1. Note the reduced cortical area of mutant neonates (brackets). OB = olfactory bulb; Cx = cortex; Th = thalamus; SC = superior colliculi; Cb = cerebellum; BS = brain stem. **(E)** Confocal Z–stacks immunolabeled for Snf2h (green) at birth. Note the reduced number of Snf2h+ cells in the mutant neocortex. VZ = ventricular zone. **(F)** Whole mount top view images of *Snf2h* cKO-Emx1, cDKO-Emx1 and control brains at P40. Note the dramatic cortical hypoplasia in *Snf2h* cKO-Emx1 mice, which is further aggravated upon *Snf2l* deletion in cDKO-Emx1 mice.

subtypes by activating *FoxG1* and *Satb2,* while *Snf2l* represses FoxG1 to promote cortical differentiation and terminate neurogenesis (Yip et al., 2012).

Snf2h cKO-Emx1 mice display cognitive deficits and hyperactivity-like behavior.

We reasoned that the reduction in cortical size of *Snf2h* cKO-Emx1 mice likely resulted in cognitive alterations. We performed a battery of neurobehavioral tests in adult mutant and control littermates to assess learning and memory (Morris water maze; fear conditioning); anxiety-related symptoms (elevated plus maze; social interactions); and sensorimotor learning (rotarod; pole test). The Morris water maze showed no differences between mutant and control littermates in in the time needed to reach a platform during 9 days of training (Figure 3A); and no differences in the time spent in all quadrants at day 10 after training (Figure 3B). In the fear conditioning assay, mice are exposed to a novel cue ("cue tone"), followed by a foot-shock ("context"), and the "fear" response is measured ("conditional response") (Maren, 2001). *Snf2h* cKO-Emx1 mice had a normal response to the cue tone compared to controls, but a reduced response to the context, suggestive of impaired associative learning skills (Figure 3C).

In the elevated platform assay, mutant mice showed an increased percentage of total entries into the closed arms, and lower entries into the open arms relative to control littermates (Figure 3D), suggestive of "reduced anxiety" or alternatively interpreted as hyperactive-like symptoms. The social interaction assay measures the preference of mice to interact with a stranger mouse rather than with an inanimate object. *Snf2h* cKO-Emx1 mice spent more time interacting with a stranger mouse compared to control littermates (Figure 3E), also suggestive of hyperactive-like symptoms.

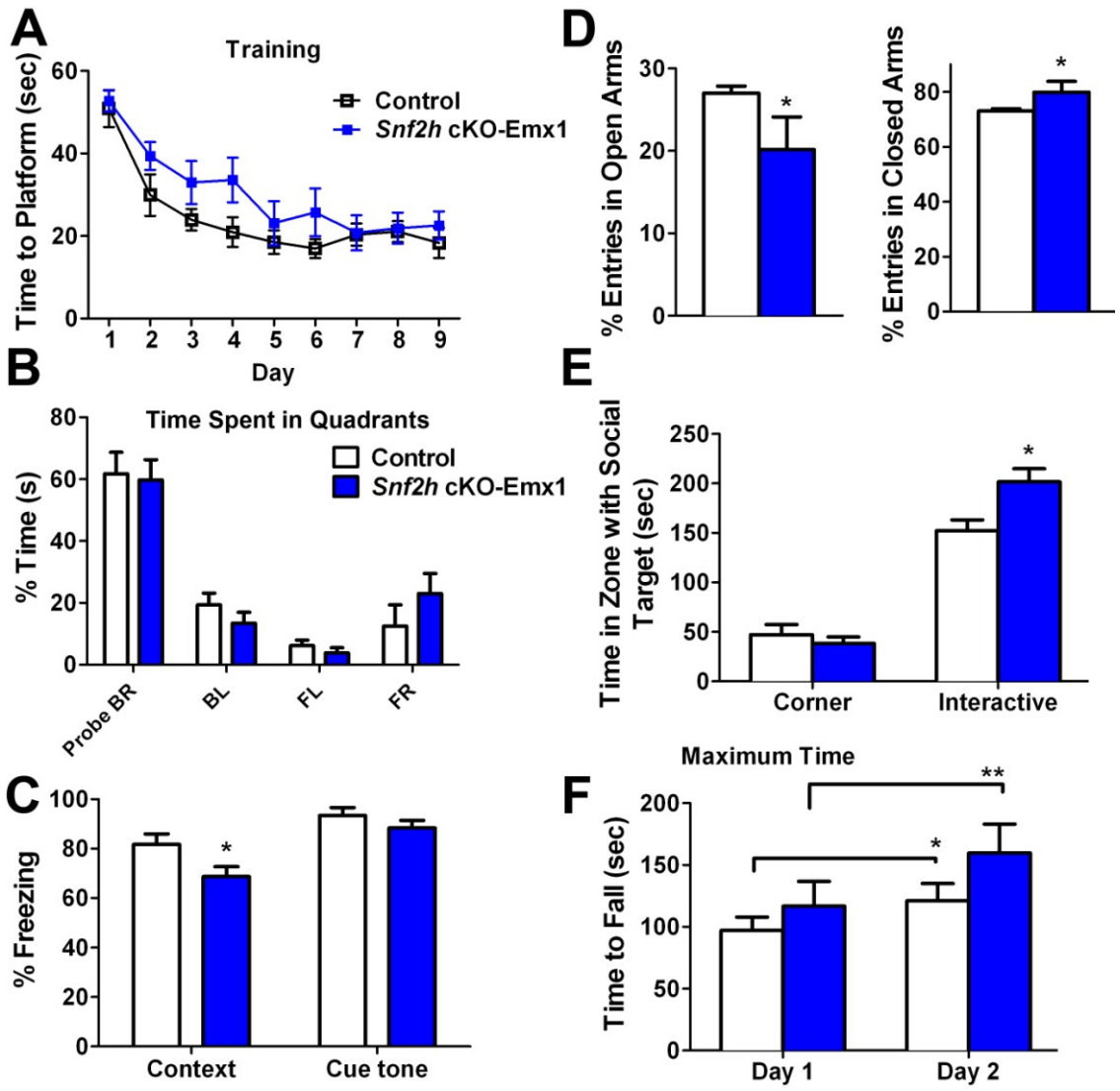

Figure 3. Snf2h cKO-Emx1 mice display cognitive deficits and hyperactive-like behavior. **(A)** Morris water maze training sessions. The time it took the mice to reach the platform was recorded. No statistical significant differences were detected between genotypes during 9 days of training. **(B)** Trial day 10 in the Morris water maze reveals no differences in the % time it took mutant and control mice to reach the different platforms. **(C)** The fear-conditioning assay reveals that mutant mice responded normally to the cue tone after training, but have a reduced context-dependent response relative to controls. **P*<0.05, one-way ANOVA. **(D)** The elevated plus maze reveals that mutant mice have a higher percentage of total entries into the closed arms, but a lower percentage of entries into the open arms relative to controls. **P*<0.05, one-way ANOVA. **(E)** The social interaction assay reveals that mutant mice spent more time interacting with a stranger mouse than an inanimate object relative to controls. **P*<0.05, one-way ANOVA. **(F)** The amount of time it took the mice to fall off the rotating rod was recorded from training day 1 and day 2 for adult mutant and control littermates. **P*<0.05, ***P*<0.01, one-way ANOVA.

The rotarod assay measures balance as well as motor learning. Mutant mice displayed a significantly enhanced ability to stay in the rotarod compared to controls in the second day of a two-day trial, while both strains improved their performance on the second day relative to the first day trial (Figure 3F). Lastly, the pole test measures sensorimotor abilities where no differences were found between mutant and control littermates (Supplementary Fig. 2). As a whole, these experiments suggest that *Snf2h* cKO-Emx1 mice have impaired associative, but not spatial learning, increased hyperactive-like symptoms, and enhanced motor skills. These findings are suggestive of an autism spectrum-like disorder.

Snf2h activates clustered protocadherin gene expression to control neural arborization.

Neural diversity underlies the complexity of neuronal networks. We set out to identify the transcriptional networks altered in the neocortex of *Snf2h* cKO-Emx1 mice at birth, when neural maturation commences. We isolated P0 cortical RNA extracts from mutant and control mice and hybridized them to mouse genome Affymetrix Gene 1.0 ST microarrays. After a stringent filtering analysis (>1.5-fold change, $P<0.01$), we only identified 45 downregulated and 20 upregulated genes in the Snf2h-null neocortex relative to controls (Table 1). Gene ontology (GO) analysis reveals enrichment for downregulated genes involved in cell adhesion and transcriptional control in the mutant cortex relative to controls (Table 1). Various isoforms from the *Protocadherin-ß (Pcdh-ß*) cluster are predominantly downregulated in the mutant cortex (Table 1). The clustered *Pcdh* locus encodes 58 related cadherin-like transmembrane proteins, some of which exhibit isoform-specific homophilic adhesion and are combinatorially expressed in single neurons (Figure

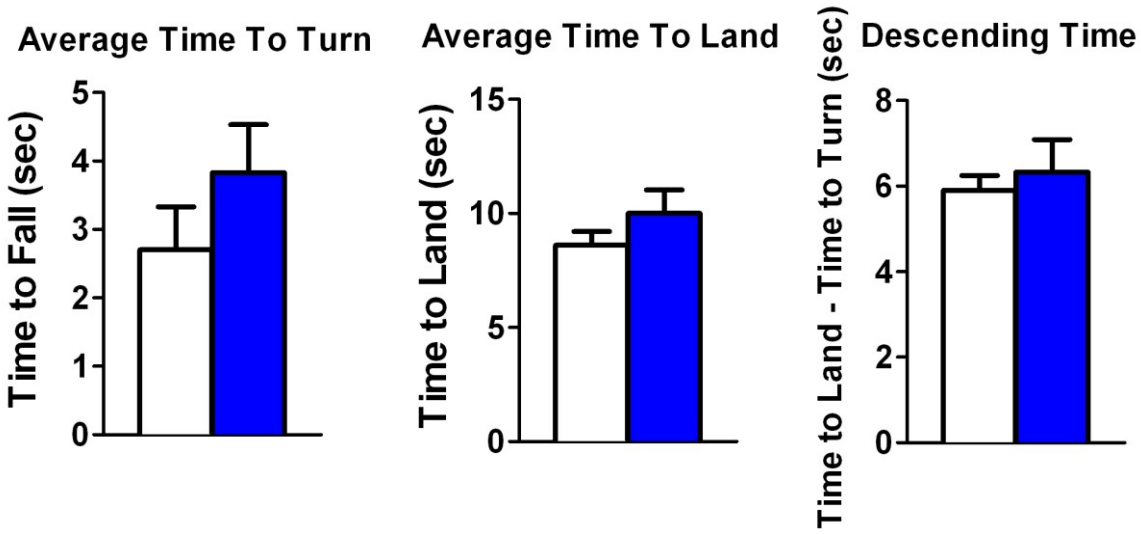

Supplementary Figure 2. Snf2h cKO-Emx1 mice do not display sensorimotor alterations in the pole test. *Snf2h* cKO-Emx1 and control littermates were assessed for sensorimotor control in the pole test at 4-6 months of age. Average time to turn; average time to land; and average descending time for at least 8-10 mice per genotype is shown as ± SEM. No significant differences were found between genotypes.

Affymetrix ID	Accession	Gene Symbol	cKO Avg	CT Avg	Fold change	Homophilic cell adhesion	cell-cell adhesion	regulation of transcription,DNA-dependent	regulation of RNA metabolic process	regulation of transcription	cell adhesion	biological adhesion	transcription	adult behavior
10357328	GENSCAN00000042301	---	8.30	9.16	0.55									
10359999	ENSMUST00000082677	---	3.39	4.13	0.60									
10363455	NM_025273	Pcbd1	8.18	8.95	0.59					■				
10399588	ENSMUST00000079237	Zfp125	8.69	9.35	0.64									
10405927	NM_001048204	Zfp455	5.64	6.23	0.66			■	■	■			■	
10409970	NM_001136496	Zfp935	8.17	8.77	0.66			■	■	■			■	
10442194	NM_172486	Zfp677	5.12	5.76	0.64			■	■	■			■	
10455080	NM_053134	Pcdhb9	6.35	7.06	0.61	■					■	■		
10455112	NM_053142	Pcdhb17	6.97	7.64	0.63	■					■	■		
10455118	NM_053143	Pcdhb18	7.76	8.39	0.64	■					■	■		
10455123	NM_053144	Pcdhb19	7.33	8.07	0.60	■					■	■		
10455128	NM_053145	Pcdhb20	7.67	8.27	0.66	■					■	■		
10455135	NM_053146	Pcdhb21	6.97	7.66	0.62	■					■	■		
10457203	ENSMUST00000108936	---	7.90	8.49	0.67									
10476941	ENSMUST00000076007	---	7.02	7.67	0.63									
10479192	BC099528	Gm14410	10.07	10.68	0.65			■	■	■			■	
10479195	BC099528	OTTMUSG00000016609	10.07	10.68	0.65			■	■	■			■	
10479198	BC099528	Gm14410	10.07	10.68	0.65			■	■	■			■	
10479203	BC080301	2210418O10Rik	7.81	8.48	0.63			■	■	■			■	
10479217	NM_001177568	Gm14420	8.99	9.58	0.66			■	■	■			■	
10479228	NM_001177399	Etohi1	9.06	9.84	0.58			■	■	■			■	
10490273	NM_001100416	OTTMUSG00000016609	10.07	10.68	0.65			■	■	■			■	
10490276	BC080301	2210418O10Rik	7.81	8.48	0.63			■	■	■			■	
10490294	NM_001164689	Gm14326	9.88	10.50	0.65			■	■	■			■	
10490302	NM_001162922	Zfp931	5.45	6.46	0.50			■	■	■			■	
10493995	NM_009112	S100a10	10.71	11.31	0.66									
10500345	NR_001579	Terc	8.91	9.59	0.63									
10501208	NM_008184	Gstm6	5.97	6.61	0.64									
10510176	NM_053124	Smarca5	7.40	8.11	0.61			■	■	■				
10510215	NM_001083918	Gm13139	6.66	7.26	0.66			■	■	■			■	
10511810	NM_008899	Pou3f2	8.61	9.33	0.61									
10518361	NM_053124	Smarca5-ps	7.88	8.56	0.63			■	■	■				
10544106	ENSMUST00000121946	---	5.64	6.23	0.67									
10544523	NR_004419	Rny1	8.15	8.74	0.66									
10550409	NM_007676	Psg16	5.82	6.53	0.61									
10552358	NM_001034893	Zfp936	5.78	6.59	0.57			■						
10552363	NM_001034893	Zfp936	5.79	6.52	0.60			■						
10562651	NM_001242388	9830147E19Rik	5.67	6.86	0.44									
10562657	NM_001008427	Gm5595	5.45	6.83	0.38			■	■	■			■	
10570634	BC150794	Gm15319	6.56	7.31	0.59									
10577388	NM_001177408	4930467E23Rik	6.66	7.29	0.64									
10579054	NM_001039553	4930467E23Rik	6.51	7.20	0.62									
10579060	NM_001177408	4930467E23Rik	6.33	7.04	0.61									
10589994	NM_001164789	Eomes	8.33	9.11	0.58			■	■	■			■	
10598032	---	---	9.44	10.03	0.66									
10367024	NM_009312	Tac2	8.05	7.41	1.56			■						
10372648	NM_017372	Lyz2	7.91	7.30	1.53									
10391798	NM_001131020	Gfap	9.12	8.28	1.78						■			
10424119	NM_010930	Nov	9.41	8.75	1.58									
10428388	NM_172815	Rspo2	8.73	8.14	1.51									
10432278	NM_001013741	Ddn	8.50	7.88	1.54			■						
10462231	NM_145831	Dmrt2	8.26	7.64	1.54									
10473483	NM_001011852	Olfr1029	5.94	5.27	1.58									
10483624	NR_002854	Dlx1as	9.10	8.47	1.55			■						
10507326	ENSMUST00000083251	---	4.06	3.25	1.75									
10536505	NM_008591	Met	9.65	8.93	1.65									■
10540233	NM_182808	Fam19a1	10.71	10.09	1.53									
10542355	NM_010128	Emp1	9.43	8.77	1.58									
10543921	NM_172892	Slc13a4	8.58	7.98	1.52			■						
10566934	NM_053247	Lyve1	8.83	8.23	1.52									
10582888	ENSMUST00000099047	---	9.12	8.08	2.06									
10582890	---	---	7.53	6.72	1.76									
10586865	NM_009022	Aldh1a2	8.50	7.81	1.62									
10593756	NM_145129	Chrna3	9.00	8.10	1.87									■
10606178	NR_001463	Xist	12.42	11.54	1.84			■	■					

Table 1. List of altered genes from the Snf2h cKO-Emx1 cortex. 2 microarrays per genotype were averaged from wild type and mutant cortical extracts obtained at P0. Each sample per genotype is a pool of 3 cortices from individual pups. Deregulated genes denote $P < 0.01$. Yellow highlights fold-change for *Pcdh-ß* genes, while blue highlights fold-change for *Snf2h (Smarca5).*

4A) (Hirayama and Yagi, 2013). Stochastic and combinatorial expression of *Pcdh* isoforms is thought to underlie the diversity and complexity of neural network assembly. Thus, we analyzed the expression of multiple clustered *Pcdh*-α, *-ß,* and -γ isoforms by qRT-PCR from the adult cortex. P60 cortical extracts show that the mutant neocortex displays altered expression of multiple *Pcdh-α*, *Pcdh-ß and Pcdh-*γ isoforms relative to control littermates (Figure 4B). Similarly, we observed that cortical and hippocampal neurons from *Snf2h* cKO-Emx1 mice have lower *Pcdh-ß15* expression levels by *in situ* hybridization (Figure 4C). These results suggest that Snf2h is necessary for the activation of the clustered protocadherin isoforms in postmitotic neurons of the mammalian brain.

The protocadherin superfamily of surface proteins control neural diversity and connectivity (Hirayama and Yagi, 2013). Deregulation of *Pcdh* isoform expression results in abnormal neuronal arborization and altered dendritic self-avoidance (Ledderose et al., 2013; Lefebvre et al., 2012; Wang et al., 2002b; Weiner et al., 2005). *Pcdh-γ*-null olfactory bulb neurons have severely reduced dendritic arbors (Ledderose et al., 2013). Indeed, the *Pcdh-γ* isoforms are thought to promote neuronal arborization through a FAK/PKC/MARCK2-dependent signaling pathway (Garrett et al., 2012). We assessed the functional significance of *Pcdh* gene deregulation in *Snf2h*-null cortical neurons with two methodologies: I) Golgi-Cox staining; and II) transmission electron microscopy (TEM). Golgi-Cox staining reveals the atrophied arborization and reduced basal and apical dendrites of cortical projection neurons of the adult mutant cortex relative to controls (Figures 4D & 4E). Similarly, TEM reveals that mutant axons display a higher incidence of actin filament crossover events in cortical projection neurons as early as E18.5 (Figure 4F). We conclude that Snf2h is

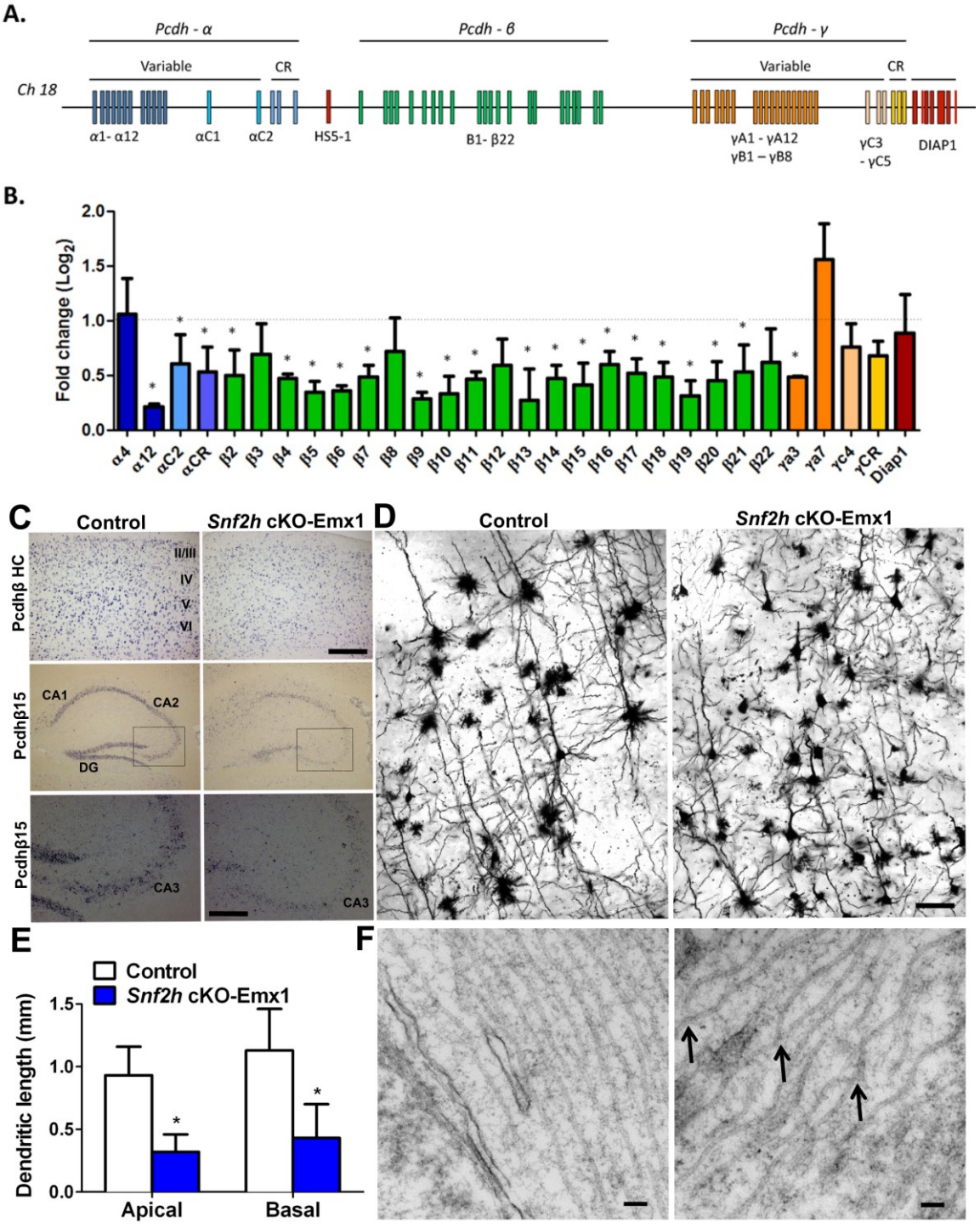

Figure 4. Snf2h drives clustered protocadherin gene expression to control neuronal arborization and axon ultrastructure. **(A)** Schematic diagram of the clustered protocadherin genes. CR = constant region; HS = hypersensitive site. **(B)** qRT-PCR fold-change expression changes in the adult mutant cortex relative to control littermates at P60. Triplicate samples were averaged from 3 independent cortical preparations per genotype and normalized to L32

expression. *P<0.05, student's t-test. **(C)** In situ hybridization for a *Pcdh-ß-HC* extracellular constant domain (HC); and for *Pcdh-ß15* through the mutant and control cortex and hippocampus at P60. Note reduced expression of *Pcdh-ß-HC* and *Pcdh-ß15* within cortical and hippocampal mutant neurons. **(D)** Light microscopy Z-stacks of Golgi-Cox stained cortical projection neurons through the *Snf2h* cKO-Emx1 and control cortex at P60. Note the abnormal arborization of mutant neurons. **(E)** Dendritic length measurements from apical and basal dendrites from cortical projections neurons through the *Snf2h* cKO-Emx1 and control cortex at P60. *P<0.05, n=3, student's t-test. **(F)** Transmission electron microscopy (TEM) images through axons from *Snf2h* cKO-Emx1 and control cortical projection neurons at E18.5. Arrows denote a higher incidence of actin filament "cross-over" events in mutant axons.

necessary for the proper activation of *Pcdh* isoforms to mediate postmitotic neuron arborization and cytoskeletal ultrastructure.

Snf2h mediates corpus callosum assembly.

Callosal projection neurons (CaPNs) are a diverse subtype of projection neurons that connect the hemispheres of the cerebral cortex through the corpus callosum and play multiple roles in cognition (Fame et al., 2011). We next investigated whether the reduced number of CaPNs (SATB2+ and Cux1+ cells) and the abnormal arborization of surviving neurons resulted in neural assembly deficits, using the corpus callosum as readout. First, we immunolabeled P40 coronal brain sections through rostral, medial and caudal regions from mutant and control brains with myelin associated glycoprotein (MAG), a cell membrane glycoprotein expressed in myelinated axons that connect the hemispheres. We did not detect differences in myelinated MAG+ axons through the rostral brain, while a >2-fold reduction in myelinated MAG+ axons were observed in medial and caudal regions of the mutant corpus callosum relative to controls (Figures 5A & 5B).

To visualize the neural assembly alterations of *Snf2h* cKO-Emx1 mice, we performed magnetic resonance imaging (MRI) of adult *Snf2h* cKO-Emx1 and control littermates. The corpus callosum is severely reduced in mutant mice relative to control littermates along all planes of the adult brain (Figure 5C). We conclude that the abnormal assembly of the corpus callosum is due to lower production of CaPNs during embryonic development, in combination with altered clustered *Pcdh* isoform regulation in surviving CaPNs.

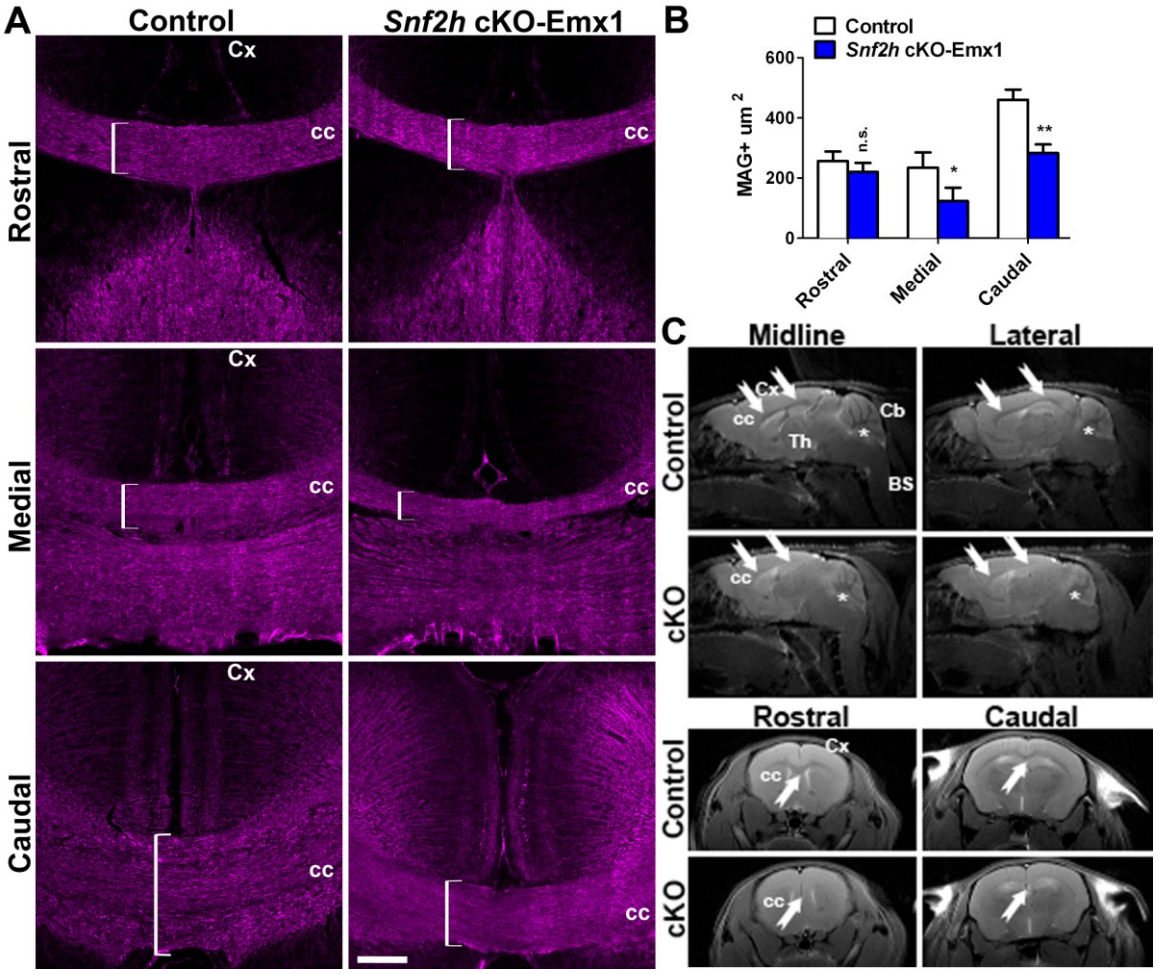

Figure 5. Snf2h cKO-Emx1 mice have an underdeveloped corpus callosum. **(A)** P40 rostral, medial and caudal coronal sections through the corpus callosum of mutant and control mice immunolabeled for myelin-associated glycoprotein (MAG) (magenta), a marker of myelinated neuronal axons. Note the reduction of MAG+ axons in the medial and caudal brain (brackets). Cc = corpus callosum; Cx = cortex. **(B)** Quantitation of myelinated MAG+ axons through the corpus callosum at P40. 5 cubic bins were scored and averaged per section. **P*<0.05, n=3 per region per genotype, student's t-test. **(C)** Magnetic resonance imaging (MRI) from *Snf2h* cKO-Emx1 and control mice at P200. Sagittal (top panels) and coronal (bottom panels) scans across the brain highlight the reduction of corpus callosum white matter (seen as gray; arrows) in mutant mice relative to control littermates. Also note a modest reduction in white matter content through the mutant cerebellum (seen as gray; asterisks). cc = corpus callosum; Cx = cortex; Th = thalamus; Cb = cerebellum; BS = brain stem. 3 animals were scanned in sagittal, coronal and transversal planes per genotype.

Snf2h and Satb2 functionally interact to control clustered Pcdh gene expression.

Satb2 is essential for the embryonic specification of CaPNs and for their postmitotic arborization (Alcamo et al., 2008; Britanova et al., 2008; Zhang et al., 2012). Satb2 has recently been found to functionally interact with the proto-oncogene Ski to repress Ctip2 expression and promote CaPN fate (Baranek et al., 2012; Srinivasan et al., 2012). The overlapping neuronal phenotypes upon Snf2h and Satb2 deletion in the neocortex prompted us to assess whether Snf2h and Satb2 functionally interact to control clustered *Pcdh* gene activation. For this end, we employed a retinoic-acid-Neuro2A differentiated cell culture system and assessed the effects of short interference (si)-RNA mediated knockdown of Snf2h; human (h) SNF2H overexpression; hSATB2 overexpression; and hSNF2H, or hSATB2 reintroduction after siSnf2h knockdown ("rescue"). siSnf2h knockdown resulted in the significant upregulation of *Pcdh-ß11, Pcdh-ß13,* and *Pcdh-ß14* isoforms, while *Pcdh-ß15, Pcdh-ß16, Pcdh-ß21* and *Diap1* (a gene downstream of the cluster) were significantly downregulated in knockdown (KD) relative to siScrambled (siScr) controls (Figure 6A). However, siScr + hSNF2H overexpression resulted in the opposite effect: downregulation of *Pcdh-ß5, Pcdh-ß11, Pcdh-ß13,* and *Pcdh-ß14* isoforms, while *Pcdh-ß15, Pcdh-ß16, Pcdh-ß21* and *Diap1* were significantly upregulated relative to siScr + empty vector controls (Figure 6A). Most interestingly, siSnf2h KD and simultaneous hSNF2H or hSATB2 overexpression resulted in the restoration of *Pcdh-ß11* and *Pcdh-ß15* expression, whereas siScr + hSATB2 overexpression resulted in the downregulation of *Pcdh-ß13* and *Pcdh-ß16* expression (Figure 6A).The restoration of *Pcdh-ß11* and *Pcdh-ß15* expression upon hSNF2H or hSATB2 overexpression in siSnf2h KD Neuro2A cells suggest that Snf2h and Satb2 may be working in a common genetic pathway.

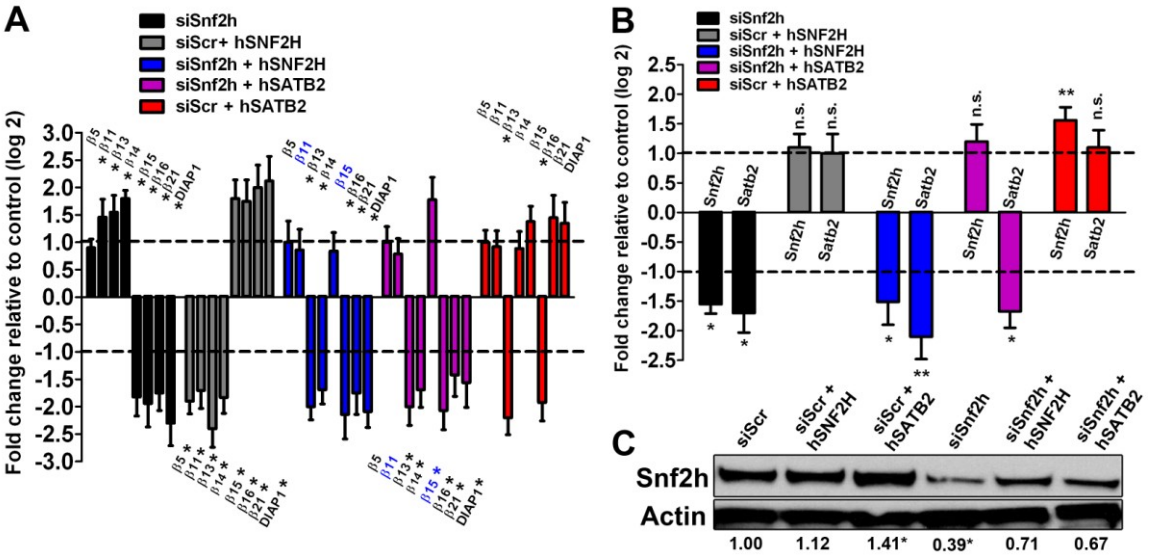

Figure 6. Snf2h and Satb2 functionally interact and co-regulate clustered protocadherin gene activation. **(A)** qRT-PCR analysis of *Pcdh-ß* isoforms and the 3' gene *Diap1* in a retinoic-acid differentiated Neuro2A cell culture model upon siSnf2h knockdown (KD); human (h) SNF2H or hSATB2 overexpression; or siSnf2h KD + SNF2H or hSATB2 overexpression ("rescue"). Blue idenotes *Pcdh-ß* isoforms rescued by both hSNF2H and hSATB2 overexpression upon siSnf2h KD. **P*<0.05, n=3, student's t-test. **(B)** qRT-PCR analysis for endogenous Snf2h and Satb2 expression upon siSnf2h knockdown (KD); hSNF2H and hSATB2 overexpression; or siSnf2h KD + SNF2H or hSATB2 overexpression ("rescue"). Note that hSATB2 overexpression restores Snf2h expression in siSnf2h KD cells + hSATB2 overexpression. Similarly, Snf2h is upregulated exclusively in siScr + hSATB2 overexpression-treated cells. **P*<0.05, n=3, student's t-test. N.s. = not significant. **(C)** Western blotting for Snf2h upon siSnf2h KD; hSNF2H and hSATB2 overexpression; or siSnf2h KD + SNF2H or hSATB2 overexpression ("rescue"). Note that both hSNF2H and hSATB2 overexpression restores Snf2h expression in siSnf2h treated cells. Also note that Snf2h is upregulated exclusively in siScr + hSATB2 overexpression-treated cells, and not in siScr + hSNF2H overexpression-treated cells,. Values denote densitometry values from 3 independent lanes. **P*<0.05, n=3, student's t-test.

We next assessed whether hSNF2H or hSATB2 overexpression resulted in the upregulation of their own transcription. We screened Snf2h and Satb2 mRNA steady-state levels by qRT-PCR with mouse specific primer sets, where we found that siSnf2h treatment resulted in a ~1.6-fold reduction of Snf2h mRNA levels 48 hrs after knockdown, while Satb2 levels were similarly reduced by ~1.7-fold relative to siScr controls (Figure 6B). hSNF2H overexpression alone did not alter endogenous Snf2h or Satb2 mRNA levels, while hSNF2H overexpression in siSnf2h KD cells did not restore endogenous Snf2h nor Satb2 mRNA expression (Figure 6B). However, hSATB2 overexpression resulted in the restoration of endogenous Snf2h mRNA levels (~1.1-fold) in siSnf2h treated cells, while it did not rescue Satb2 levels (Figure 6B). Moreover, hSATB2 overexpression further augmented Snf2h mRNA levels in siScr cells by ~1.55-fold, whereas Satb2 mRNA levels were unaffected (Figure 6B). We next assessed whether hSATB2 overexpression enhanced Snf2h protein synthesis as observed at the transcriptional level. Indeed, hSATB2 overexpression resulted in the upregulation of endogenous Snf2h protein in both siSnf2h (KD + rescue) and siScr treated cells (overexpression), whereas hSNF2H overexpression did not alter endogenous Snf2h protein levels in siScr controls, but upregulated its own expression in siSnf2h + hSNF2H treated cells (KD + rescue) (Figure 6C). We conclude that Satb2 works genetically upstream of Snf2h; and that through upregulation of endogenous Snf2h expression provides the partial rescue of the clustered *Pcdh* isoforms observed upon siSnf2h knockdown in Neuro2A differentiated cells.

DISCUSSION

Snf2h activates FoxG1 to drive neocortical expansion.

Snf2l deletion results in FoxG1 upregulation, hyperproliferation and delayed differentiation of cortical progenitors (Yip et al., 2012). Here we reveal that Snf2h is necessary for FoxG1 activation and neocortical expansion. Snf2h loss resulted in increased cell death and a lower production of FoxG1+ postmitotic neurons in the cortical plate by mid-neurogenesis. FoxG1 is necessary for the appropriate spatiotemporal expansion and differentiation of nearly all cortical subtypes and early postnatal development of hippocampal neurons (Kumamoto et al., 2013; Tian et al., 2012). Our studies suggest that Snf2h and Snf2l evolved to antagonistically modulate FoxG1 expression to establish postmitotic cortical identity and proper neuronal output, thus controlling proper brain size (Yip et al., 2012). ISWI preferentially binds near the transcriptional start site (TSS) of target genes genome-wide and mediates the expression of essential homeotic genes such as *Engrailed* and *Ultrabithorax* in *Drosophila* (Deuring et al., 2000; Sala et al., 2011). However, the precise chromatin-associated mechanisms of how Snf2h and Snf2l antagonistically co-modulate target loci remain to be elucidated.

Snf2h and Satb2 mediate clustered Pcdh gene activation.

The clustered *Pcdh* genes were first identified as a *cadherin-related neuronal receptor (Cnr)* gene family in the mouse brain (Kai et al., 1997; Kohmura et al., 1998). The mouse and human genes are organized into three tandemly linked clusters, *Pcdh-α, Pcdh-β* and *Pcdh-γ* (Hirayama and Yagi, 2013). The *Pcdh-α* and *Pcdh-γ* clusters are composed of 14 and 22 variable-region exons, respectively and a common set of constant-region exons (Hirayama and Yagi, 2013). Conversely, the *Pcdh-β* cluster is composed of 22 tandemly arranged single-exon genes that lack a constant region with common exons (Hirayama and Yagi, 2013). Theoretically, the multiple clustered *Pcdhs* could generate more than 3×10^{10}

possible variations in each neuron and 12,720 types of cis-tetramers per neuron (Yagi, 2012). Our studies reveal that Snf2h ablation results in a predominant downregulation of *Pcdh-β* isoforms *in vivo*. Previous studies using genetically modified clustered *Pcdh* alleles showed that clustered *Pcdh* isoforms are transcribed from promoters upstream of each variable exon (Tasic et al., 2002). A cluster control region (CCR) is sufficient for *Pcdh-β* transcriptional activation *in vivo* (Yokota et al., 2011). This CCR is located downstream of the last *Pcdh-γ* constant-region exon and only affects *Pcdh-β* cluster transcription, even though the ~300kb *Pcdh-γ* cluster lies between these two regions. We envision that the clustered *Pcdhs* provide a molecular basis for the neuronal complexity that contributes to the development of complex neural networks, which is ultimately controlled at the chromatin level.

Chromosomal *cis* and *trans* interactions provide further complexity into the regulation of gene expression. These interactions are mediated by CCCTC-binding protein (CTCF) and the cohesin complex (Guo et al., 2012). Forebrain-specific conditional *CTCF* KO mice only survive until ~1-month of age, have abnormal expression of *Pcdh* isoforms, altered neural arborization and lower frequency of excitatory postsynaptic currents (Hirayama et al., 2012). CTCF interacts with the cohesin complex to establish *Pcdh-α* promoter choice, single neuron diversity and lineage specification (Guo et al., 2012). Mice heterozygous for *Nipped-B-like,* which promotes cohesin loading onto DNA, also shows a significant downregulation of *Pcdh* expression and cortical hypoplasia (Kawauchi et al., 2009). Similarly, ablation of cohesin-SA1, which binds to the TSSs of the clustered *Pcdhs,* results in decreased expression of *Pcdh* isoforms and brain hypoplasia (Cuadrado et al., 2012; Remeseiro et al., 2012). Snf2h directly interacts with the hRAD21 subunit of the

cohesin complex (Hakimi et al., 2002). Thus, we propose that Snf2h is playing an important role as part of the cohesin complex, amongst other complexes (e.g. WSTF), to activate the clustered *Pcdh* genes and provide the ATP-dependent chromatin remodeling activity necessary to activate the clustered *Pcdh* isoforms.

Epigenetic control of callosal projection neuron diversity.

CaPN dysgenesis is one of few pathologies consistently identified in autism spectrum disorders (Egaas et al., 1995; Frazier and Hardan, 2009; Vidal et al., 2006). *Snf2h* cKO-Emx1 mice have partial agenesis of the corpus callosum, learning and memory deficits, and display increased hyperactive-like behavior. Indeed, absence of CaPN connectivity in humans is associated with defects in higher-order associative tasks, such as abstract reasoning and problem solving (Paul et al., 2007). CaPNs make up a vast and diverse neuronal population that requires precise epigenetic control for their specification and connectivity, thus allowing for the association and integration of ipsilateral and contralateral cortical hemispheres. Our work highlights how a single nucleosome remodeler, as part of multiple CRCs, triggers gene expression programs essential for neural progenitor expansion and postmitotic maturation.

Satb2 is essential for the specification of CaPNs, and Satb2 ablation after CaPN specification results in abnormal arborization during postnatal stages, similar to the *Snf2h* cKO-Emx1 phenotype (Alcamo et al., 2008; Britanova et al., 2008; Zhang et al., 2012). The Satb1 homolog interacts with Snf2h and ACF, subunits of the CHRAC and ACF nucleosome remodeling complexes to mediate nucleosome positioning over long-range chromatin domains (Yasui et al., 2002). Kohwi-Shigematsu and colleagues postulated that Satb1 acts as

a “landing platform” to control these long-range chromatin remodeling reactions (Yasui et al., 2002). Our findings reveal that overexpression of either SNF2H or SATB2 can rescue *Pcdh-ß* isoform expression upon Snf2h knockdown, and that overexpression of hSATB2 upregulates Snf2h expression itself, suggestive of an auto-regulatory feedback mechanism. Recent studies also suggest that variant histone H2A.Z deposition may promote Snf2h-dependent gene activation (Coleman-Derr and Zilberman, 2012a; Goldman et al., 2010; Zentner and Henikoff, 2013; Zentner et al., 2013). We envision a chromatin environment where Snf2h catalyzes the remodeling of target TSS containing H2A.Z-containing nucleosomes, anchored by Satb2 and CTCF-mediated regulatory domains. In this scenario, Satb2-dependent chromatin anchoring and Snf2h-dependent chromatin remodeling activates the FoxG1 locus to mediate progenitor expansion, whereas clustered *Pcdh-ß* gene activation controls postmitotic arborization and neural assembly. Upon Snf2h loss, target genes are hypoactivated, resulting in transcriptional silencing and progenitor cell death; or abnormal postmitotic arborization and cognitive dysfunction. Future high-throughput sequencing binding studies for Snf2h and Satb2 in primary neuronal models will provide further insight into the “logistics” of Snf2h and Satb2-mediated chromatin control to govern genome-wide homeostasis.

ACKNOWLEDGEMENTS

We are grateful to Dr. Diane Lagace and Mirela Hasu at the University of Ottawa Behavioral Core for assistance with behavioral experiments and expert discussions. M.A.-S. thanks D.J.P. for funding. This work was funded by operating grants from the Canadian Health Research Institutes to D.J.P. (MOP97764; MOP84412).

MATERIALS & METHODS

Generation of Snf2h$^{fl/fl}$ mice

Snf2h$^{exon5fl/exon5fl}$ (Snf2h$^{fl/fl}$) mice were generated through homologous recombination in WW6 ES cells as described (Stopka and Skoultchi, 2003). Briefly, a 6.0 kb fragment of the Snf2h gene containing exons 4 through 8, into which loxP sites were inserted 5' and 3' of exon 5, was cloned into the pEasyFlirt vector (a gift of Dr. M.P. Lisanti, University of Manchester, UK). This vector has a neomycin resistance gene flanked by Frt sites, which was removed in mice generated from correctly targeted ES cells by breeding to *Flp1* recombinase mice (Raymond and Soriano, 2010). *Snf2h$^{fl/fl}$* mice were viable, fertile and did not exhibit any gross behavioral abnormalities. Cre-mediated deletion of *Snf2h* exon 5 was tested by breeding to ZP3-Cre mice (Lewandoski et al., 1997) for which embryos homozygous for a deleted exon 5 died *in utero,* as previously described (Stopka and Skoultchi, 2003).

Mouse Breeding

Snf2h$^{fl/fl}$ mice were backcrossed for 6 generations to a C57Bl/6 background and bred with C57Bl/6 Emx1-Cre$^{-/+}$ or FoxG1-Cre heterozygous mice (Berube et al., 2005; Hebert and McConnell, 2000) that also carried a *Snf2h* null allele (Stopka and Skoultchi, 2003), thereby generating *Snf2h* cKO mice by Emx1-Cre (*Snf2h*$^{-/fl}$::Emx1-Cre$^{-/+}$ or *Snf2h*$^{-/fl}$::FoxG1-Cre$^{-/+}$) and control littermates that carried only one functional copy of *Snf2h* (*Snf2h*$^{-/fl}$ or *Snf2h*$^{+/fl}$::Cre$^{-/+}$) or both functional alleles (*Snf2h*$^{+/fl}$). These three control genotypes showed no overt phenotypes, reproduced normally and lived into adulthood and were used interchangeably as controls, except where indicated. For *Snf2l* ablation, we used a previously characterized germline *Snf2l^{Exon6}* deleted mouse line that survives normally into adulthood (Yip et al., 2012), thus generating *Snf2l-/y::Snf2h* cKO (cDKO-Emx1) and *Snf2l-+::Snf2h*

cKO-Emx1 compound heterozygotes. For embryo staging, embryonic day 0.5 (E0.5) was defined as noon of the day a vaginal plug was observed after overnight mating. Animals were kept in an animal house under SPF (specific pathogen-free) conditions in a 12/12 light:dark cycle with water and food *ad libitum.* The University of Ottawa Animal Care and Use Committee approved all experiments. C57Bl/6 and FVBN/J wild type mice were purchased from Charles River (Montreal, QC, Canada). Emx1-Cre mice were obtained from The Jackson Laboratory (Stock # 005628; Bar Harbor, MA, USA).

Behavioral Analysis

All behavioral tests were completed in the Behavior Core Facility at the University of Ottawa using standardized protocols. Animals were habituated to the testing room at least 1 hour before testing. Female and male mice were assessed independently at 4-6 months old, for which we did not observe sex-specific differences in behavior. For behavioral assays, one-way ANOVA was used for at least 8-10 mice per genotype. The values are presented as the mean ± SEM.

Morris Water Maze

The water maze pool was maintained at 22 ± 1°C. A white platform was submerged 1 cm below the water's surface in the center of the target quadrant. Mice were randomly placed on one of the starting points in one of four quadrants and given 60 s to find the hidden platform. Mice that did not find the platform at the end of the 60 s period were manually guided to the platform and allowed to rest for 20 s. Each mouse had 4 trials per day for 10 consecutive days. An animal was scored as successfully finding the platform if it succeeded in two of four trials per day. In the visual assays, mice were placed on one of four quadrants and

allowed to find the visible platform in 60 s. The swimming path of mice was recorded with automated video detection software (Ethovision, Wageningen, Netherlands).

Elevated Plus Maze

Animals were habituated to the test room for at least 2 days prior to test. Animals were placed in the center of a maze consisting of two arms (each arm 5 cm wide x 60 cm long) enclosed by ~15 cm high walls, and two open arms (each arm 25 x 7.5 cm, with a raised 0.5 cm lip at edges) elevated 1 meter above ground and with equidistant arms from the center of the platform. The amount of time the animals spent in the open or closed arms, the total number of entries and the total distance traveled were recorded for 10 min using video detection software (Ethovision).

Social Interactions

A control mouse is placed in the corner of an open field box (under dim red light) that measures 45 cm long on each side x 45 cm high and containing a 5.5 x 9.6 cm wire mesh rectangular cage. The mouse is given 5 mins to explore the arena and then removed. A few seconds later, a test mouse (or social target), of the same strain, age and gender is placed inside the rectangular wire mesh cage and the control mouse placed back in the arena. The time the social target interacts with the control mouse in 5 min trials is recorded using Ethovision 7 XT automatic tracking software. Total distance traveled, time spent in 2 corners across the wire mesh cage and velocity is also recorded.

Fear Conditioning

On the first day (training), the animal is placed in the fear conditioning apparatus for a total

of 6 minutes. After the first two minutes in the apparatus a tone is played for 30 sec ending with a 2-sec shock. One minute following the shock, the tone is played again for 30 sec ending with a 2-sec foot shock. For the remaining two minutes there is no tone or shock. The freezing behavior of the animal is recorded throughout the 6 minutes. This is the training in which the mouse receives 2 exposures to the tone followed by the shock and this occurs in a novel context, which is the conditioning box. On the 2nd day, contextual conditioned fear testing begins. This measures the fear associated with being in the same environment where the shock was delivered (done ~24hrs after training). The mouse is placed in the same apparatus with all the same lighting and room conditionings for 6 minutes and freezing behavior is recorded.

Rotarod

Mice were trained and tested on the accelerated rotarod (rod diameter 3cm) for 300 seconds for five times before measurements (IITC, Woodland Hills, CA, USA). Starting speed was set at 4 RPM and maximum speed at 40 RPM. The latency to fall from the rotarod was recorded. If animals were able to stay on the rod for 300 sec, the latency to fall recorded was 300 sec. The animals received 4 trials per day, with a trial interval of 30 min, for 2 consecutive days.

Pole Test

Mice were placed head-upward on the top of a rough surfaced vertical pole (8mm diameter x 55 cm tall) and the time for descending recorded. The time required for the mouse to turn downward after placing and the total time on the pole until the mouse reaches the bottom is recorded. Mice were trained for 2 days before test. 5 trials were averaged on day 3.

BrdU-birthdating

Timed-pregnant females were injected intraperitoneally with 100 µg/g body weight of 5-bromo-2′-deoxyuridine (BrdU; Sigma) and pups killed at indicate times. For BrdU-pulse labeling, timed-pregnant females were injected with BrdU and killed 120 minutes later. For BrdU immunodetection, sections were incubated in 2N HCl for 10 min at 37°C, rinsed in 0.1 M sodium borate, pH 8.3, blocked and incubated overnight at 4°C with rat monoclonal anti-BrdU antibody 1:500 (Abcam #6326). For BrdU-birthdating of lower- and upper-layer cortical neurons, pregnant dams were injected with a single BrdU dose (100µg/g body weight) at E13.5 and E15.5, respectively, and pups killed at birth. The average number of immunopositive cells was determined from five separate fields under ×40 magnification in confocal Z-stacks (or cubic bins) of 18 x 10^3 μm^3.

TUNEL assay

Sections were examined for DNA fragmentation with the TUNEL *in situ* cell death detection kit (Roche Applied Science, ON, Canada) according to the manufacturer's instructions. The average number of TUNEL-positive cells was determined from five separate fields under ×40 magnification in 18 x 10^3 μm^3 cubic bins.

Histology

Nuclei were visualized using cresyl violet staining in 20µm frozen sections. Sections were cleared in Xylene and mounted with Permount.

Golgi-Cox Staining

Golgi staining was completed using FD Rapid GolgiStain Kit (FD NeuroTechnologies). Briefly, adult mice were intracardially perfused with 4% paraformaldehyde in 0.1M PBS and

stained according to the manufacturer's instructions. Tissues were sectioned at 60µm and mounted on gelatin-coated slides. Morphology of apical and basal dendrites of cortical projection neurons were analyzed using ImageJ software (rsbweb.nih.gov/ij/).

Immunofluorescent histochemistry

For embryonic tissue, 16µm sections were used. For postnatal brains, 40µm free-floating sections were used. Sections were washed four times in PBST (PBS with 0.1% Triton X-100), blocked (1 hr, room temperature) in 10% horse serum/PBST, and incubated (overnight, 4 ºC) in primary antibodies. The following primary antibodies were used: rabbit anti-Snf2h (1:500; Abcam 72499); rat anti-BrdU (1:300; Abcam #6326); rabbit anti-phospho histone H3 (pH3; 1:200; Millipore #06-570); rabbit anti-FoxG1 (1:300; Abcam #18259); mouse anti-SATB2 (1:50; Abcam #51502); rabbit anti-Cux1 (1:100; Santa Cruz); rabbit anti-Sox5 (1:200; Santa Cruz); mouse anti-MAG (1:500; Millipore). The following day, sections were washed five times in PBST and incubated (2 hrs, room temperature) with DyLight^{488}, DyLight^{594} or DyLight^{649}-conjugated mouse pre-adsorbed secondary antibodies (1:1000, Jackson Immunoresearch, PA, USA) against the IgG domains of the primary antibodies. All sections were counterstained with the nuclear marker DAPI (Invitrogen). Sections were mounted on slides with Dako Fluorescence Mounting Medium (Dako Canada, ON, Canada).

In situ hybridization

Brain were rapidly removed and embedded in O.C.T. compound and quickly frozen in isopentane cooled with liquid nitrogen. 10-12 µm sections were obtained through the sagittal brain and hybridization as described previously (Noguchi, 2009; Schaeren-Wiemers, 1993). Digoxigenin (DIG)-labeled RNA probes were synthesized from cDNA clones using the DIG RNA Labeling Mix (Roche) and with previously published probes (Hirayama, 2013).

Western blotting

Cortical extracts were quickly dissected from individual embryos and snap frozen in dry ice. Extracts were then homogenized in ice-cold RIPA buffer supplemented with protease inhibitor cocktail (Sigma #8340), and incubated for 20 min on ice with gentle mixing. After pre-clearing by centrifugation (15 min at 17,000 x g), proteins were quantified by the Bradford method. Protein samples were resolved on sodium dodecyl sulfate polyacrylamide gels under denaturing conditions using Bis-Tris 4-12%, Tris-Acetate 3-8% gradient gels (NuPage, Invitrogen); or homemade linear gels and blotted onto PVDF membranes (Immobilon-P; Millipore, MA, USA) by wet transfer for 1-2 hrs at 90V. Membranes were blocked (45 min, room temperature) with 5% skim milk in TBST (Tris-buffered saline containing 0.05% Triton X-100), and incubated (4°C, overnight) with the following antibodies: rabbit anti-Snf2h (1:4000; Abcam #72499); sheep anti-Snf2l (1:2000) (Barak et al., 2003); mouse monoclonal anti-Snf2l 1:1000 (Alvarez-Saavedra M & Picketts DJ, *unpublished*); mouse anti-ß-Actin (1:30,000; Sigma); rabbit anti-FoxG1 (1:1000; Abcam #18259); or mouse-anti Satb2 (1:500; Abcam #51502). Membranes were incubated (1 hr, room temperature) with ImmunoPure® HRP-conjugated goat anti-rabbit; anti-mouse; or anti-sheep IgG (H+L) secondary antibodies (1:50,000; Pierce, Rockford, IL). Membranes were washed 5 x 5 min in TBST after antibody incubations, and the signal was detected using the Pierce Supersignal West Fempto chemiluminescence substrate (Pierce). Western blots were quantitated using ImageJ software (rsbweb.nih.gov/ij/). At least 2 separate gels were immunoblotted with cortical extracts from independent litters and used for quantitation. Densitometry values are presented as the mean ± SEM.

Reverse Transcription

Cortical extracts were quickly dissected from mutant and control littermates and RNA was isolated using Trizol (Invitrogen) according to the manufacturer's instructions. Glycogen (Ambion) was used as carrier at 20 µg/µl. 1µg of total RNA was reverse-transcribed using SuperScriptIII (Invitrogen) and random primers (Promega). cDNA was diluted 1:15 and 1µl was used per qPCR reaction. All primers were analyzed by melt curve analysis after qPCR amplification and also in agarose electrophoresis for detection of single amplicons. Primers are listed below. The ΔΔCt method was used to compare fold-change. L32 and 18S mRNAs were used as normalizers. Triplicate or quadruplicate samples were performed per reaction and a minimum of 3-4 mice analyzed per genotype. Student's *t*-test was used for statistical significance.

Quantitative Real-Time PCR

qPCR analysis was carried out using the SYBR Green Advantage qPCR premix (Clontech) and run under the following conditions: one cycle at 95°C for 1 min, and 45 cycles at 95°C for 10 sec, 60°C for 10 sec, and 72°C for 20 sec. The following primers were used:

Gene Name	Sequence (5' to 3')	Product Length
Pcdh a4[1]	forward; GATTCAAGGGACAGAGAGG	93
Pcdh a12[1]	forward; AGTCTCCCTCCTGTGTTAGG	111
Pcdh ac2[1]	forward; CAACAGGCAACTCACCG	121
Pcdh a4 to ac2[1]	reverse; CGAGGCAGAGTAGCGCC	
Pcdh aCR[1]	forward; AGAGCAGGCATGCACAGC	200
	reverse; GACTGTTTGGGGTTGCC	
Pcdh ga3[1]	forward; CTCACAGATTTACTTGAAACGAAAGAAGACC	134
Pcdh ga7[1]	forward; GATTTTCAAGAATGTAAGGGTGAAGC	128
Pcdh gc4[1]	forward; GTCCACCCTCTGATCTTCTC	121
Pcdh ga3 to gc4[1]	reverse; CAGGTGCCAGTTTCATCACC	
Pcdh gCR[1]	forward; CTGGCGTTTCTCTCAAGCCC	109
	reverse; CATGGCTTGCAGCATCTCTG	
Diap1[1]	forward; CAGTCTTCTAGAAGCTCTGCAGTC	126
	reverse; CTCCGAGGCTAGCAGAGATG	
Pcdh b2	forward; CAGGCTGGGTCCACAATTAGG	109
	reverse; TGCAGCGAGTTCCTCTACCT	
Pcdh b3[1]	forward; TTTGTTTTTCTGGGTGGGTCTC	101
	reverse; GATCCGTCGCTAAATTGGCTA	
Pcdh b4	forward; AGGTTCCCGAGAATTTCCCC	111
	reverse; AGTCCAACTTTTTGCTTAGACGG	
Pcdh b5	forward; CAGGCAAGTGATTCCTTTCCT	103
	reverse; ATTGCTGTTTGTCATGGTCAGA	
Pcdh b6	forward; TCTGGGTTTCAGGGTAGGGG	174
	reverse; GTCTCCACATCTAGCTGCAAG	
Pcdh b7	forward; GTGCAGGTGTCCGATGTCAA	191
	reverse; GGAGATTAACGAGGAGAGTGGC	
Pcdh b8	forward; GGTGTGTTCAATTCAGAACGGA	135
	reverse; AGGTCAGAGACCGTGATTGTG	
Pcdh b9	forward; ACTGCTCTTGAGAATACCAGAGA	132
	reverse; AGGACGTGAAAATAAGGGTTGG	
Pcdh b10	forward; CCTTGATGCCTTAGTTGCCAC	171
	reverse; TACGGAGTTGCCTCAAAATCC	
Pcdh b11	forward; GCTCTGGGGCAACTAGATATTC	101
	reverse; GGCCAGTTCTCCAACCCTG	
Pcdh b12	forward; CACTGCTCTTGATGGCGGAT	162
	reverse; GCAGAGACCATGACAACTAAGG	
Pcdh b13	forward; TGCAAGACAAGGCAAGTGATG	82
	reverse; GCATGGCATACTGAATTGATCCT	
Pcdh b14	forward; GGGAGCAACACGGTTCAAAAC	175
	reverse; GAGGTGACCCACTGTCCATAG	
Pcdh b15	forward; TTACTGCTCAGTCCGCTTACT	138
	reverse; TGCAGCGCGATAAATCTGAAAT	
Pcdh b16[1]	forward; GTTCTGGGATGGTTTGGAAATGTAC	130
	reverse; GACCTCGTTGTGTTTGAGCATTG	
Pcdh b17	forward; TCAGGAAAATGCACGCTGTTA	81
	reverse; GCTGGTAAGAGCAGATAGCATC	
Pcdh b18	forward; AGGCAAGTGCTATTTCTCTTCC	173
	reverse; TCACAAACCACCCTAGTTCTCT	
Pcdh b19	forward; ATTGGTCCGAGTGGAGGTCAT	79
	reverse; TGGAACCGTCACTTCATAGAACA	
Pcdh b20	forward; TCTTTGCGCTATTCTGTAGCAG	187
	reverse; GATCCAGTCGCTCATTCAGGA	
Pcdh b21	forward; AGCAGCGAACCCTGTATATTGC	157
	reverse; TTCCTGGAGTAGCACTTTCTGA	
Pcdh b22[1]	forward; AACTATGGTAGGCAACCAGATGATC	80
	reverse; GAATACAGAGAGCGAAATGTGACG	

Microarrays

Gene expression profiling was performed on RNA isolated from P0 cortical extracts from *Snf2h* cKO-Emx1 and wild type control mice. RNA samples were sent to the Genome Quebec Innovation Centre (Montreal, QC, Canada) for hybridization onto Affymetrix Mouse Gene 1.0 ST microarrays. Two replicates were ran per genotype, each a pool of 3 embryos per genotype. The microarray data were normalized using robust multi-array average (RMA) with Affymetrix Power Tool and FlexArray 1.6. The output was summarized by gene level and log transformed. Differentially expressed genes were analyzed by Significance Analysis of Microarray (SAM). Genes were scored as differentially expressed on an array if it demonstrated a *P*-value <0.01, and had sufficient detectable signals across all replicates (A value (log_2) >7). All raw and processed data has been deposited into the GEO database (GSE001234).

Image acquisition and processing

Tissue sections were examined and images captured using a Zeiss 510 laser scanning confocal microscope with UV (405nm), argon (488nm), helium/neon (546nm) and helium/neon (633nm) lasers. All images were acquired as 8 or 30µm Z-stacks (in 1-2µm intervals) and analyzed as projections using the LSM 510 Image Browser software (Zeiss, Oberkochen, Germany). Epifluorescent and light microscopy images were acquired with a Zeiss Axiovert Observer Z1 epifluorescent/light microscope equipped with an AxioCam cooled-color camera (Zeiss). Images were exported to Adobe Photoshop CS5 (Adobe Systems Inc., San Jose, CA, USA) and further processed for contrast when necessary.

Transmission electron microscopy (TEM)

E18.5 embryos were collected under a stereomicroscope, cut into sections of 1-2 mm thickness through cortical regions and fixed for at least 4 hrs to overnight in Karnovsky's fixative (4% paraformaldehyde, 2% glutaraldehyde and 0.1 M cacodylate in phosphate-buffered saline, pH 7.4) at 4ºC. These specimens were subsequently washed twice in 0.1 M cacodylate buffer for 1h and once overnight at room temperature. Sections were then post-fixed with 1% osmium tetroxide in 0.1 M cacodylate buffer for 1 h at 4ºC, and washed twice for 5 min in water. The specimens were dehydrated twice for 20 min for each step in a graded series of ethanol from water through 30%-50%-70%-85%-95% ethanol and twice for 30 minutes in 100% ethanol (molecular sieves were used to dehydrate ethanol), followed by twice for 15 min in 50% ethanol/50% acetone and twice for 15 min in 100% acetone. Sections were infiltrated in 30 % spurr/acetone for 15 h (overnight) then in 50% spurr/acetone for 6 h and in fresh 100% spurr resin overnight. Spurr was changed twice a day for three days at room temperature. All infiltration steps were carried out on a rotator. Sections were then embedded in fresh liquid spurr epoxy resin and polymerized overnight at 70ºC. Ultrathin sections (80nm) from the cortex were collected onto 200-mesh copper grids and let dried overnight before staining. Grids were stained with 2% aqueous uranyl acetate and with Reynold's lead citrate. Sections were observed under a transmission electron microscope (Hitachi 7100). All ultrastructural analysis was based on at least three mice per genotype.

Toluidine blue staining

Semi-thin sections of 0.5 µm were stained with 1% toluidine blue and 2% Borate in distilled water. Histological samples were scanned with a MIRAX MIDI automated scanning light microscope (Zeiss) and images processed with Zeiss MIRAX Viewer software (Zeiss).

Magnetic Resonance Imaging

MRI was performed with a General Electric/Agilent MR901 7T small animal MRI scanner using a 72 mm inner diameter radiofrequency transmit coil and mouse brain surface receive coil (Rapid MR International). Axial, coronal, and sagittal images were acquired with a 2D T2-weighted fast spin echo pulse sequence with the following parameters: echo time=25 ms, repetition time=3 s, echo train length=8, bandwidth=15.6 kHz, field of view=2 cm; slice thickness=0.7 mm, matrix size = 256 x 256 x 15, number of averages=6-8, scan time per orientation=9.5-13 min, in-plane spatial resolution=78 microns.

Vector Construction

SNF2H cDNA comprising the entire open reading frame was cloned into the pCI-neo expression vector (Promega Corp. Madison, WI) then amplified with the SNF2H-BamHI-Fwd (5'-AAAAGGATCCATGTCGTCCGCGGCCGAGCC) and SNF2H-XhoI-Rev (5'-AAAACTCGAGTAGTTTCAGCTTCTTTTTTCTTCC) primers and directionally subcloned into the pBRIT-LoxP-NTAP and pBRIT-LoxP-CTAP vectors, following restriction digest with BamHI and XhoI. All clones were verified by sequencing at McGill University and Génome Québec Innovation Centre (Montreal, QC, Canada).

siRNA-mediated knockdown in Neuro2A cells

Neuro2A cells were freshly obtained from ATCC (Manassas, VA, USA) and grown in DMEM medium containing 10% FBS and no antibiotics. Briefly, cells were seeded in media containing 30 μM retinoic acid (RA) at a confluency of ~50-60% for 72 hrs; and then transfected using Lipofectamine 2000 (Invitrogen) with 50nM siSnf2h (Thermo Scientific, Ottawa, ON, Canada; siGENOME, mouse *Smarca5*, D-041484-03); 50 nM siScrambled (siGENOME non-targeting siRNA #1, D-001210-01-05); or simultaneously treated with

siScrambled; or siSnf2h + 1ug of hSNF2H (described above); or 1ug of hSATB2 plasmids (Origene # RC216909). Total proteins were collected as described above and analyzed by immunoblotting.

Statistics

Group statistical analysis was performed via the two-tailed Student's *t*-test, expect for behavioral experiments were one-way ANOVA was used. $P<0.05$ was accepted as statistically significant. At least 3-4 mice from each genotype were used for evaluation. The values are presented as the mean ± SEM.

CHAPTER 4

Snf2h mediates histone dynamics to control cerebellar development and function.

Matías Alvarez-Saavedra[1,3], Yves De Repentigny[1], Edupuganti V. Raghu Ram[5], Keqin Yan[1], Alan J. Mears[2], Pamela S. Lagali[1], Michael S. Huh[1], Emile Hashem[1,4], Danton Ivanochko[1,4], Matthew A. Todd[1,4], Chelsea P. Corcoran[1], Juraj Kokavec[6], Romit Majumder[7], Valerie A. Wallace[2,4], Rashmi Kothary[1,4], Tomas Stopka[6], Eran Meshorer[5], Arthur I. Skoultchi[7] and David J. Picketts[1,4].

[1]Regenerative Medicine Program & [2]Vision Program, Ottawa Hospital Research Institute, Ottawa, ON, Canada K1H 8L6;

Departments of [3]Cellular and Molecular Medicine; and [4]Biochemistry, Microbiology & Immunology, University of Ottawa, ON, Canada;

[5]Department of Genetics, The Alexander Silberman Institute of Life Sciences, The Hebrew University of Jerusalem, Jerusalem, Israel.

[6]Institute of Pathologic Physiology, First Faculty of Medicine, Charles University in Prague, Prague, Czech Republic;

[7]Department of Cell Biology, Albert Einstein College of Medicine, Bronx, NY, USA.

Statement of Contribution

All experimental design; immunohistochemistry and immunofluorescence; confocal and light microscopy analysis; molecular biology and cell culture experiments; behavioral analysis; writing of manuscript.

ABSTRACT

Chromatin compaction controls the establishment of postmitotic neuronal gene expression programs, but the epigenetic mechanisms remain largely uncharacterized. Snf2h and Snf2l are ATP-dependent chromatin remodeling proteins that assemble, reposition, and space nucleosomes. Here we demonstrate that *Snf2h* conditional knockout mice have a dramatic reduction in histone H1, H2A and H2A variants that compromises chromatin ultrastructure and transcriptional processes within the cerebellum. Impaired histone dynamics limits granule neuron progenitor expansion resulting in cerebellar hypoplasia. Additionally, aberrant expression of transcription factors, including *Engrailed*, contributes to impaired Purkinje neuron development and sensorimotor dysfunction. Considering the severe cerebellar atrophy, these animals survive to young adulthood from *Snf2l* compensation that restores *Engrailed-1* expression. Similarly, postmitotic Purkinje-specific *Snf2h* ablation affects chromatin organization and dendritic arborization but alters cognitive skills rather than sensorimotor control. As a whole, this work provides novel insight into ISWI-mediated histone dynamics and chromatin organization with respect to cerebellar development and function.

INTRODUCTION

The importance of epigenetic regulation to brain development is recognized by the increasing number of developmental disorders caused by mutations in genes that encode proteins that modify or remodel chromatin structure (Lasalle et al., 2013). Nonetheless, discerning precise mechanisms has proven challenging since these proteins impact all nuclear processes from transcription and replication to higher order chromatin compaction. Genome wide epigenetic profiling experiments have supported the hypothesis that neurogenesis is accompanied by the transition of a highly dynamic chromatin environment within progenitor cells to a more restrictive epigenetic landscape that dictates gene expression programs specific to each lineage (Hawkins et al., 2010; Xie et al., 2013; Zhu et al., 2012). Chromatin restriction involves the expansion of repressive histone marks such as H3K9Me3 and H3K27Me3, increased DNA methylation and a reduction in the distribution of the histone variant H2A.Z within gene bodies slated for silencing (Creyghton et al., 2008; Hattori et al., 2013). Concomitant with these histone and DNA modifications, chromatin compaction also requires regular nucleosome spacing and the inclusion of the linker histone H1 (Diesinger and Heermann, 2008; Robinson et al., 2008; Routh et al., 2008).

The repositioning of nucleosomes is catalyzed by evolutionary conserved multiprotein chromatin remodeling complexes (CRCs) that include a SNF2-domain containing catalytic subunit related to the Swi2/Snf2 family (Hauk and Bowman, 2011). One such class of ATP-dependent nucleosome remodelers is the ISWI family, first identified in yeast (Elfring et al., 1994). Mammals have two ISWI homologues *SNF2H* (*SNF2-homologue*; *SMARCA5)* and *SNF2L* (*SNF2-like*; *SMARCA1*) that are the orthologs of yeast *Isw1* and *Isw2* genes (Lazzaro and Picketts, 2001a). ISWI can assemble regularly spaced

nucleosomal arrays *in vitro* alone, or within a diverse number of protein complexes many of which contain a BAZ-family transcription factor(Erdel and Rippe, 2011). ISWI complexes regulate many nuclear processes including DNA replication and repair (ACF, CHRAC, and WICH), transcriptional regulation (NURF, RSF, and CERF), and nucleolar structure and function (NoRC) (Erdel and Rippe, 2011). ISWI inactivation in Drosophila also highlighted a role in higher order chromatin structure (Deuring et al., 2000). Despite a good understanding of the *in vitro* biochemical properties of ISWI and its related complexes, their *in vivo* roles remain poorly understood.

In the murine central nervous system (CNS), *Snf2h* and *Snf2l* display dynamic patterns of expression, where *Snf2h* expression peaks in neuronal progenitors, while *Snf2l* is expressed predominantly in terminally differentiated neurons (Lazzaro and Picketts, 2001a). For this reason, we postulated that Snf2h and Snf2l might regulate the transition of a progenitor to a differentiated neuron via its different complexes to restrict and compact chromatin while poising other genes for expression. In this regard, *Snf2l*-null mice exhibit hypercellularity of cortical progenitors and delayed differentiation, resulting in a larger brain (Yip et al., 2012). However, *Snf2h*-null mice die at the peri-implantation stage due to growth arrest of the trophoectoderm and inner cell mass, thereby preventing the study of Snf2h in mammalian brain development (Stopka and Skoultchi, 2003). To overcome this problem we describe the generation of an *Snf2h* targeted allele that facilitated its characterization during brain development. Our studies reveal that Snf2h is essential for proper cerebellar development by the transcriptional regulation of key developmental gene expression programs. We additionally reveal that Snf2h mediates histone H1 dynamics to control

genome wide gene expression and higher order chromatin structure in neural progenitors and postmitotic neurons alike, thereby underlying proper cerebellar development and function.

RESULTS

Snf2h and *Snf2l* are developmentally regulated in cerebellar lineages

The closely related mammalian ISWI genes, *Snf2h* and *Snf2l,* display complementary expression patterns that suggest they have distinct roles during tissue development (Lazzaro and Picketts, 2001a). During the postnatal development of the cerebellum we observed similar dynamic changes in Snf2h and Snf2l protein levels (Figures 1A-B). Snf2h levels peaked during the period of granule neuron progenitor proliferation (P7; Sillitoe and Joyner, 2007), whereas Snf2l levels increased as a function of cerebellar maturity with peak expression at P21 (Figure 1A-B). Expression of both proteins was maintained in adulthood (P90). To examine cell lineage expression, cerebellar sections (P0-P40) were immunofluorescently labeled for the ISWI proteins and the Purkinje cell (PC) marker Calbindin. Snf2h is present in GNPs and PCs throughout cerebellar development while Snf2l is primarily expressed in PCs (Figures 1C-D and Supplementary Fig. S1A). We conclude that Snf2h and Snf2l protein levels are dynamically modulated in PCs during mid and late cerebellar development.

Snf2h cKO mice develop cerebellar ataxia and die prematurely

To investigate the significance of ISWI expression changes within the cerebellum we proceeded to generate *Snf2h* conditional null mice based on our previous work showing that *Snf2h* germline knockout mice die at the peri-implantation stage

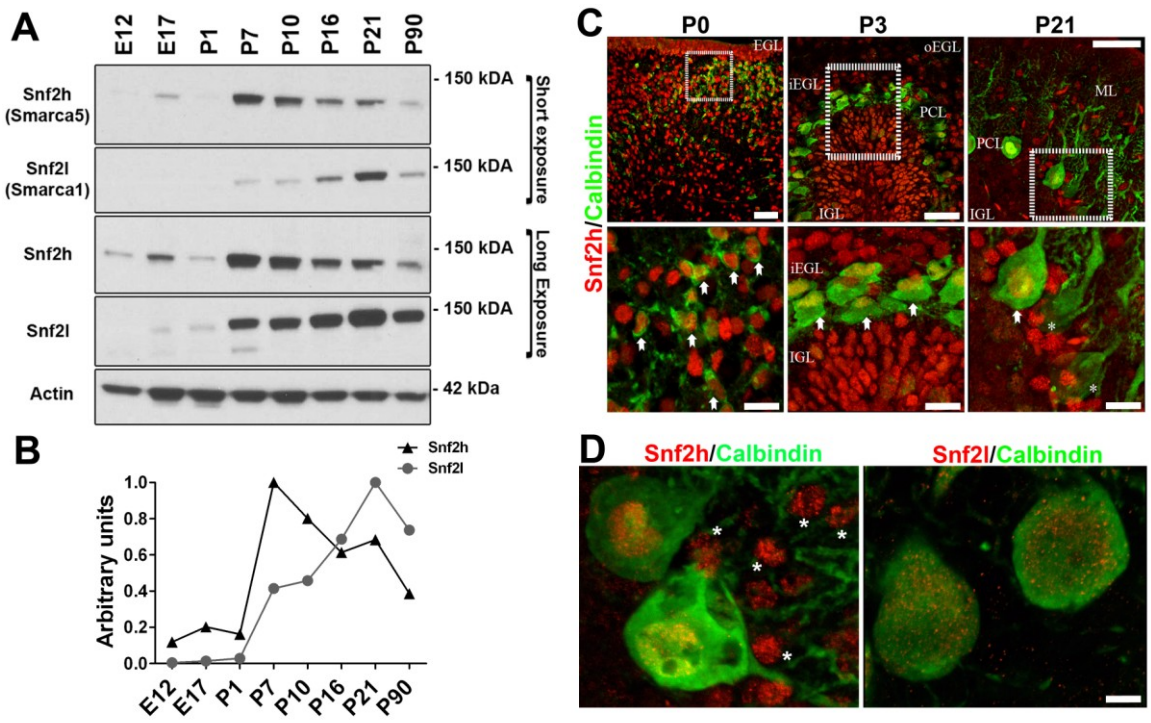

Figure 1. The mammalian ISWI homologues, Snf2h and Snf2l, are dynamically expressed in the developing cerebellum. **(A)** Snf2h and Snf2l immunoblots of wild type (WT) cerebellar extracts, except for E12 and E17 where hindbrain extracts were used. Actin served as loading control. E=embryonic day; P=postnatal day. **(B)** Plot of relative Snf2h and Snf2l expression during cerebellar development. Peak expression was normalized to 1. **(C)** Confocal Z-stacks through the WT cerebellar vermis co-labeled with Snf2h (red) and Calbindin (green), a marker of the Purkinje cell (PC) lineage at the ages indicated. Boxed areas are enlarged at bottom. Arrows denote Snf2h+ PCs. Asterisks denote Snf2h negative PCs. EGL = external granule layer; IGL = internal granule layer; PCL = Purkinje cell layer; o = outer; i = inner. Scale bars = 20µm (top panels); 10µm (bottom panels). **(D)** Confocal Z-stacks of the P40 WT cerebellar vermis co-labeled with Calbindin (green) and Snf2h (red, left panel); or Snf2l (red, right panel). Asterisks denote Snf2h+ cerebellar interneurons. Scale bar = 5µm.

(Stopka and Skoultchi, 2003). As such, we inserted loxP sites flanking exon 5, which encodes the evolutionary conserved ATP-binding pocket critical for remodeling activity (Figures 2A-B) (Corona et al., 1999). *Snf2h*$^{-/fl}$ mice were bred with a Nestin-Cre driver line that demonstrated Cre expression in neural progenitors as early as E11 within the developing forebrain, hindbrain, and spinal cord (Supplementary Figs. S1B-G) (Berube et al., 2005). *Snf2h*$^{-/fl}$*::*Nestin-*Cre*$^{-/+}$ conditional knockout mice (*Snf2h* cKO hereon) were born at normal Mendelian ratios, but were smaller with a significant reduction in body weight observed by P7 (Figure 2C), and half the size of control littermates by P20 (Figure 2D). Brains isolated from these animals were reduced in size with striking cerebellar hypoplasia (Figure 2E and Supplementary Fig. S2). Immunoblots of cerebellar extracts confirmed an ~90% reduction in total Snf2h protein levels (Figure 2F). As an assessment of cerebellar function, three different behavioral assays demonstrated that *Snf2h* cKO mice have severe sensorimotor defects (Figure 2G). Moreover, we observed ataxia-like symptoms that began at ~P15, became severe by ~P20, and clearly contributed to the impaired motor skills and premature death of *Snf2h* cKO animals at ~P40 (Figure 2H and Supplementary Movies S1-S5).

Reduced GNP proliferation and aberrant PC development underlie the cerebellar hypoplasia of Snf2h cKO mice

Since previous studies have highlighted a role for Snf2h-containing CRCs during DNA replication (Bozhenok et al., 2002; Poot et al., 2000), we assessed whether the cerebellar hypoplasia in *Snf2h* cKO mice resulted from poor GNP proliferation. BrdU-pulse labeling was used to identify cells in S-phase and phosphorylated histone H3 (pH3) immunolabeling to identify mitotic cells. We observed a significant reduction in both the

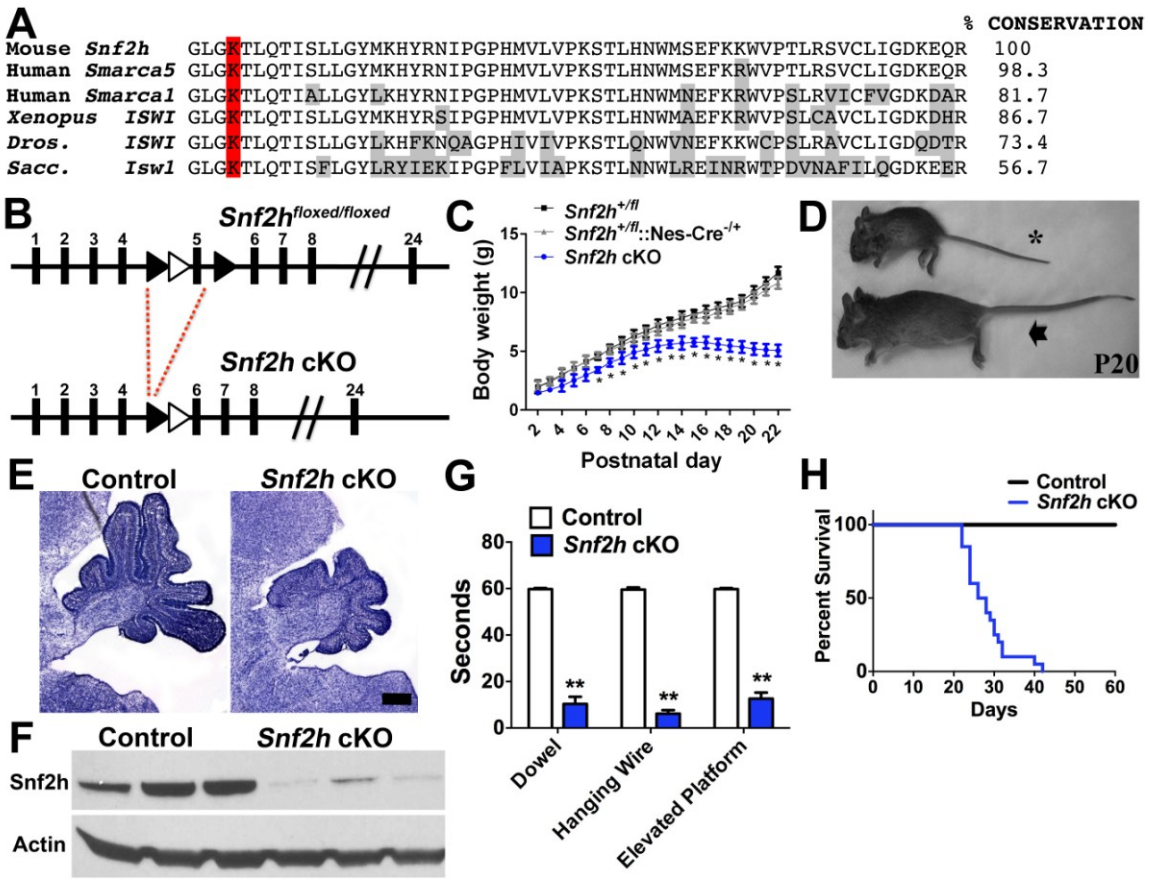

Figure 2. Snf2h deficient mice develop cerebellar hypoplasia, ataxia-like symptoms and die prematurely. **(A)** Amino acid sequence conservation of exon 5 from the *Snf2h* gene that encodes for part the ATP-binding motif of the SNF2 domain. Lysine residue (red) is essential for catalytic activity across species. Conserved changes are boxed grey. *Xenopus = Xenopus laevis; Dros. = Drosophila melanogaster; Sacc. = Saccharomyces cerevisiae.* **(B)** Schematic of the *Snf2h* targeting strategy (LoxP sites, black arrowheads; Frt sites = white arrowheads). **(C)** Total body weights from *Snf2h* cKO and control mice from P2 to P22. **P*<0.05, student's t-test. **(D)** Photos of mutant (asterisk) and control (arrow) littermates at P20. **(E)** Nissl staining through the mutant and control cerebellar vermis at P7. Scale bar = 50µm. **(F)** Snf2h immunoblot from *Snf2h* cKO and control cerebellar extracts at P0. Actin served as loading control. **(G)** Dowel, hanging wire and elevated platform assays reveal sensorimotor abnormalities in *Snf2h* cKO mice at P20-P25 relative to control littermates. ***P*<0.01, student's t-test. **(H)** Kaplan-Maier survival curves of *Snf2h* cKO mice and control littermates. *Snf2h cKO* mice were not viable under standard laboratory conditions after ~P45. *Also refer to Supplementary Figs. S1-S2.*

number of pH3+ cells and BrdU+ cells within the GNP pool of mutant cerebella at E17 and at birth (Figure 3A). The decreased GNP pool was accompanied by an increased number of apoptotic cells as assessed by TUNEL staining (Figure 3A). GNP proliferation remained low at P7, as demonstrated by the thin EGL layer and reduced number of pH3+ and BrdU+ cells (Figure 3B and Supplementary Figs. S3A-B). Reduced proliferation in the *Snf2h* mutant cerebella is in stark contrast to *Snf2l* deficient animals where we observed hypercellularity and delayed differentiation of cortical progenitors (Yip et al., 2012). Despite the poor proliferation, BrdU-birthdating experiments showed an equivalent proportion of differentiated granule cells (GCs) in the IGL of *Snf2h* cKO mice relative to wild type cerebella, suggesting that the timing of differentiation is unaltered in mutant animals (Supplementary Fig. S3C). From these experiments we conclude that the reduced lobule foliation in *Snf2h* cKO cerebella results from poor proliferation and enhanced cell death of GNPs.

GNP proliferation is dependent on mitogenic factors secreted by Purkinje cells (PCs), so we used Calbindin staining to examine the cell number and development of this lineage. Calbindin+ cells were counted across all lobules within confocal stacked images using a moving 20mm^3 window. Despite an obvious reduction in cerebellar size, we observed no differences at P3 suggesting that the birth and early survival of PCs are not affected (Figure 3C). However, the mutant animals showed a progressive decline in PC numbers along with an abnormal morphology comprising multiple rows of Calbindin+ cell bodies with dendrites that appeared disorganized and not strictly directed towards the apical surface (Figures 3C-E and Figure S3D). This staining pattern was in stark contrast to wild type PCs, which resided in a single cell layer with dendrites extending towards

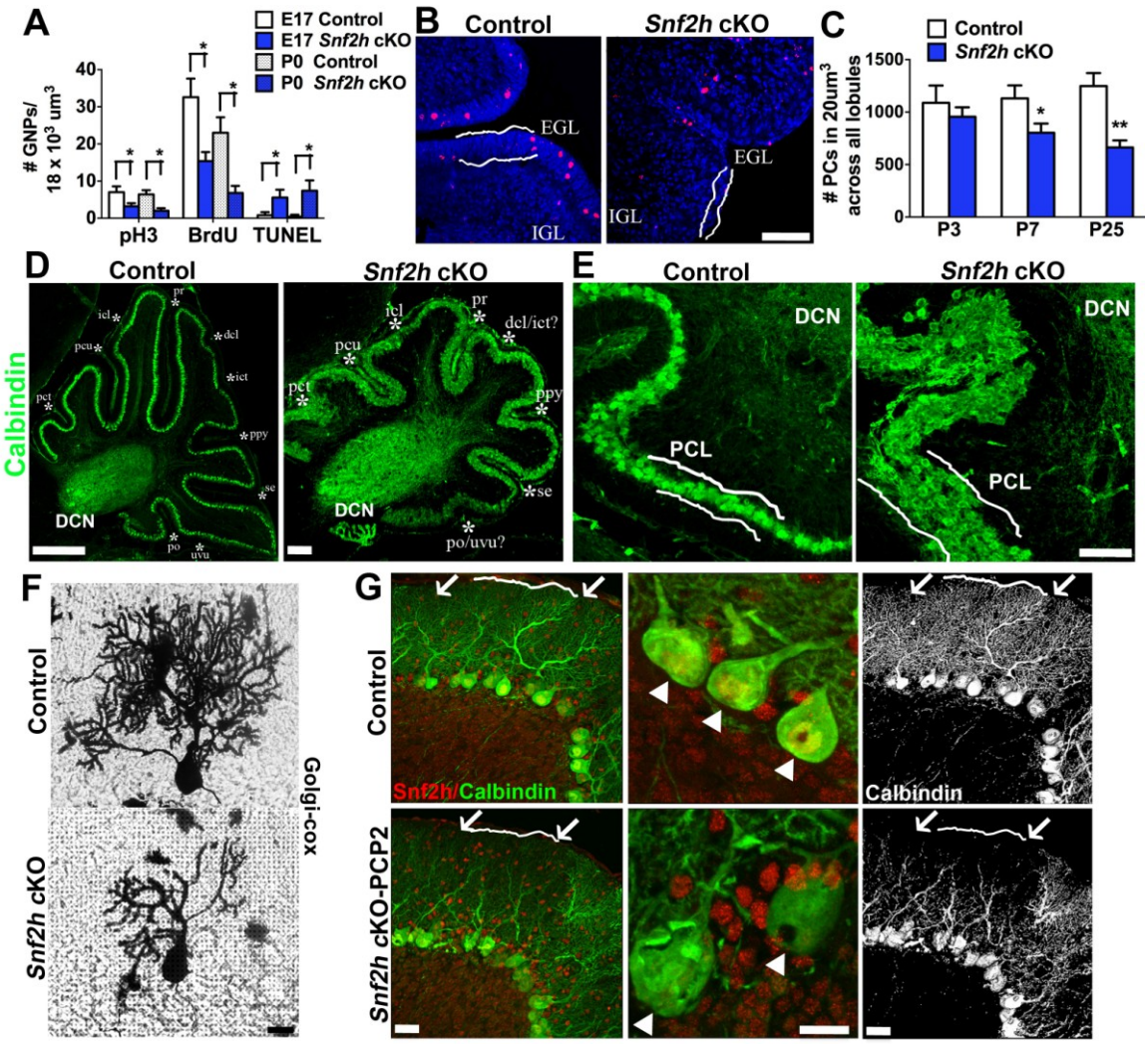

Figure 3. Abnormal granule neuron progenitor expansion and aberrant Purkinje cell development in Snf2h cKO mice. **(A)** Quantitation of BrdU+, phospho-histone H3+, or TUNEL+ cells within the EGL of *Snf2h* cKO mice and control littermates at E17 and P0. **P*<0.05, student's t-test. **(B)** Confocal Z-stacks of pH3 immunolabeling (red) from *Snf2h* cKO mice and control littermates at P7. DAPI (blue) labels all nuclei. Note the severe EGL reduction in the mutant cerebellum (white lines). Scale bar = 50µm. **(C)** Quantitation of PCs from *Snf2h* cKO mice and control littermates at P3, P7, and P25. **P*<0.05, ***P*<0.01, student's t-test. **(D-E)** Confocal Z-stacks through the cerebellar vermis from *Snf2h* cKO mice and control littermates at P7 stained with Calbindin (green). Note the multiple layers of PCs. PCL = Purkinje cell layer; DCN = deep cerebellar nuclei; Latin abbreviations denote the 10 fissures of the mammalian cerebellum. Scale bars = 100µm (D); 50µm (E). **(F)** Confocal Z-stacks of PCs stained with the Golgi-Cox method from *Snf2h* cKO mice and control littermates at P20. Scale bar = 10µm. **(G)** Confocal Z-stacks through the cerebellar vermis from *Snf2h* cKO-PCP2 mice and control littermates at P40. Arrows denote reduced PC dendrites in mutant mice that do not reach the pial surface (white lines). Arrowheads denote Snf2h immunoreactivity within control PCs that is absent in mutant PCs (middle panels). Pseudocolored Calbindin (silver) immunoreactivity is shown in rightmost panels.

Scale bars = 20μm (left and rightmost panels); 10μm (middle panels). *Also refer to Supplementary Fig. S3.*

the apical surface (Figures 3D-E and Supplementary Fig. S3D). Golgi-Cox staining at P20 revealed poorly developed dendritic trees of *Snf2h* cKO PCs compared to WT littermates (Figure 3F). Moreover, PC-specific ablation of Snf2h using the PCP2-Cre driver line that becomes active after P10 (Barski et al., 2000) demonstrated that reduced dendritic arborization was a cell autonomous defect (Figure 3G).

Taken together, our results suggest that the underdeveloped cerebellum in *Snf2h* cKO mice results from the combination of poor GNP proliferation and altered PC maturation. Moreover, the massive reduction in GNPs and the progressive decline in PC number likely contribute to the progressive ataxia and early death in these animals.

Snf2h loss leads to deregulation of evolutionary conserved transcriptional regulators

In *Drosophila*, ISWI binding is enriched at transcriptional start sites where it influences gene transcription by repositioning nucleosomes (Sala et al., 2011). We reasoned that altered nucleosome spacing within key developmental genes might alter their expression and impair cerebellar maturation. Array hybridization of RNA isolated from mutant and control cerebella identified 110 genes differentially expressed at P0 that increased to 2916 transcripts at P10 (p-value <0.01, n=4 per genotype; GEO accession # GSE42371). GO term analysis using the DAVID online tool (http://david.abcc.ncifcrf.gov/) revealed significant enrichment ($p<0.05$) for downregulated genes associated with transcriptional regulation, cell adhesion and pattern specification (Supplementary Table S1). Validation of the array results by qRT-PCR confirmed that the expression of the transcription factors *Rfx3, Uncx, Cbp, Math1, Pax6, En2*, *En1;* the signaling factor *Bmp4;* and the cell adhesion molecules *Pcdhß6* and *Pcdhß17* were all significantly downregulated (~1.5-2.5-fold) in the mutant cerebella

(Figure 4A). Moreover, we observed a ~2.6-fold downregulation of *Snf2h*, while *Snf2l* levels were unperturbed in mutant cerebella (Figure 4A). While most genes analyzed remained downregulated at P10 (Supplementary Table S1), we observed an unexpected increase in *En1* (~1.9-fold), *Bmp4* (~2.1-fold), and *Snf2l* (~1.7-fold) mRNA levels (Figure 4A), the latter suggesting that Snf2l may be compensating for Snf2h loss in the activation of some targets. In this regard, P10 immunoblots demonstrated that Snf2l protein levels were increased by ~2.3-fold whereas Snf2h protein was down ~2-fold (Figures 4B-B'). Furthermore, we observed a ~2-fold downregulation of En2 protein levels, while En1 levels showed no significant changes relative to control littermates (Figure 4C). We conclude that Snf2h loss results in the reduced expression of multiple developmentally important transcription factors. One notable exception was the increase in *En1* expression that occurred at P10.

Snf2l upregulation provides partial compensation for Snf2h loss

En1 and *En2* homeobox genes are essential for cerebellar patterning and foliation (Sillitoe et al., 2010). During early postnatal development they adopt distinct expression patterns with *En1* and *En2* expressed in Purkinje and granule cells, respectively (Wilson et al., 2011). Given that *Snf2l* expression is limited to PCs (Figure 1D), we reasoned that upregulation of *En1* but not *En2* might occur from Snf2l compensation. To determine the interactions at the *En1* gene *in vivo*, we performed ChIP assays for Snf2h and Snf2l with wild type cerebellar extracts at P7, when Snf2h levels are at their peak; and at P21, when Snf2l levels reach their maximal level. An IgG ChIP was used as a control. *En1* occupancy was analyzed by qPCR with primer pairs corresponding to the intragenic

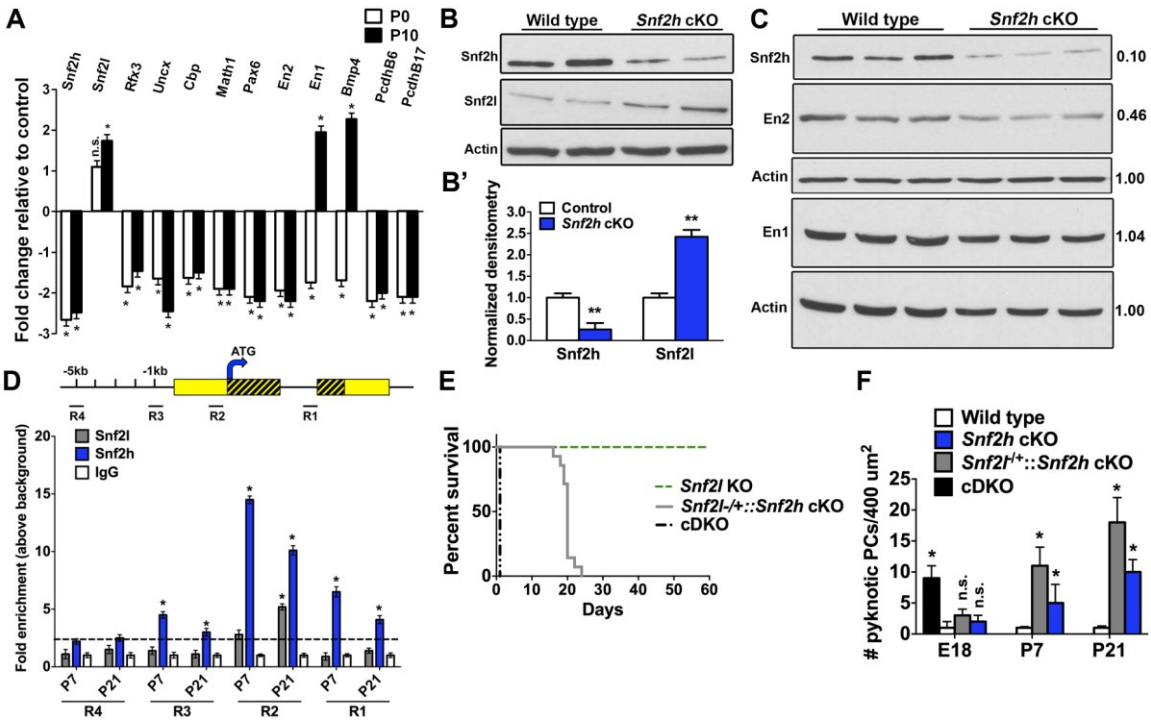

Figure 4. Snf2h and Snf2l co-modulate the Engrailed-1 locus during cerebellar development. **(A)** qRT-PCR analysis of select transcription factors and cell adhesion genes from *Snf2h* cKO and control cerebella at P0 and P10. Note the dynamic upregulation of *Snf2l, Engrailed-1 (En1)* and *Bmp4* in the mutant cerebellum at P10. **P*<0.05, student's t-test. n.s. = not significant. **(B)** Immunoblots for Snf2h and Snf2l from *Snf2h* cKO and control cerebellar extracts at P10. Actin served as loading control. **(B')** Quantitation of Snf2h and Snf2l immunopixels shown in B as normalized to Actin. ***P*<0.01, student's t-test. **(C)** Immunoblots for Snf2h, En2 and En1 from *Snf2h* cKO and control cerebellar extracts at P20. Actin served as loading control. Numbers represent relative expression levels in the mutant cerebellum relative to wild type levels as normalized to Actin. **(D) Top:** Schematic diagram of the mouse *En1* locus indicating primer set locations. Yellow boxes = 5' and 3' untranslated regions (UTRs); striped yellow boxes = coding regions; black lines = non-coding regions; ATG = start codon; kb = kilobases. **Bottom:** ChIP-qPCR from WT cerebellar extracts for the *En1* locus reveals Snf2h enrichment throughout the gene (R3, R2, and R1) at P7 and P21. Snf2l enrichment occurs only in the 5'-UTR (R2) at P21. **P*<0.05, student's t-test. **(E)** Kaplan-Maier curves of *Snf2l* KO, *Snf2l-/+::Snf2h* cKO and *cDKO* mice. *cDKO* mice die at birth. **(F)** Quantitation of pyknotic PC nuclei from control, *Snf2h cKO*, *Snf2l-/+::Snf2h* cKO and *cDKO* mice at E18, P7, and P21, as revealed by toluidine blue staining. Note the progressive death of mutant PCs upon loss of the mammalian ISWI proteins. **P*<0.05, student's t-test. *Also refer to Supplementary Table S1.*

region (R1), the 5'-UTR (R2), the proximal promoter (R3), and an upstream region (R4; Figure 4D). Snf2h binding showed the greatest enrichment at R2 at both time points with maximal binding observed at P7 (Figure 4D, blue bars). At P21, we also observed significant binding of Snf2l at R2 (Figure 4D, grey bars), suggesting that the ISWI proteins co-regulate En1 transcription at this time and that increased *Snf2l* expression at P10 is providing functional compensation in the *Snf2h cKO* animals. To further test this possibility, we asked whether reducing *Snf2l* levels would increase the severity of the phenotype. Indeed, removal of one copy of *Snf2l* on the *Snf2h cKO* background (*Snf2l*$^{-/+}$*::Snf2h cKO*) resulted in a more severe ataxic phenotype and death by ~P25 (Figure 4E and Movie S6). Moreover, the *Snf2l*$^{-/y}$*::Snf2h*$^{-/fl}$*::*Nestin-*Cre*$^{-/+}$ conditional double knockout (cDKO) mice had the most severe phenotype resulting in death at birth (Figure 4E), which is comparable to the lethality of *En1* knockout mice (Wurst et al., 1994). As a second measure, we quantitated the number of pyknotic PCs at E18, P7, and P21, observing a progressive and Snf2l dose-dependent effect on the number of dying PCs (Figure 4F). We conclude that Snf2l upregulation in *Snf2h* cKO mice provides partial functional compensation by extending lifespan through restoration of *En1* expression, amongst other genes. Nonetheless, the progressive decline of these animals suggests that Snf2h-specific transcriptional deficits and/or chromatin structure alterations accumulate that cannot be resolved by Snf2l upregulation alone.

Snf2h loss perturbs chromatin organization

Studies in yeast and *Drosophila* have demonstrated multiple roles for ISWI complexes in higher order chromatin compaction by repositioning nucleosomes to mediate linker DNA length and by facilitating histone H1 deposition (Corona et al., 2007; Deuring et

al., 2000; Siriaco et al., 2009). To assess chromatin organization in *Snf2h* cKO mice we examined nuclear ultrastructure of cerebellar neurons by transmission electron microscopy (TEM). TEM images of E18 mutant animals revealed that GNPs and PCs display numerous densely stained clumps within the euchromatin, a dispersed nucleolar region, chromatin loops, and structures indicative of nuclear invaginations or micronuclei that, collectively, indicate that the chromatin structure is highly disorganized (Figure 5A). Moreover, we observed that the altered chromatin organization is augmented in cDKO mice at E18 (Figure 5A, far right panel) and is progressive, both temporally and in a Snf2l-dose dependent manner (Figure 5B-G). This was confirmed by quantitation of pixel intensity within the euchromatin (Figure 5H). Not surprisingly, the number of pyknotic cells increased dramatically in older *Snf2h cKO* animals (see Figure 4F) resulting in a >3-fold decrease in the number of PCs by the time of their death (Figure 5I). Indeed, many pyknotic nuclei and cell "ghosts" were clearly visible in *Snf2h* cKO mice at P21 (5B-E). Collectively, these experiments demonstrate a progressive disorganization of the chromatin structure that correlates with the progressive death of PCs, loss of GNPs and the ataxic phenotype.

Snf2h mediates histone deposition during cerebellar development

To explain the nature of the chromatin disorganization we noticed that several histone genes within the *Hist1* gene cluster were altered in our gene expression arrays at P10 (Supplementary Table S2). Expression changes in core histones were analyzed by qRT-PCR at P0 and P10 with a range of varying patterns detected including genes consistently increased (H1c), consistently decreased (H1a, H2A.Z), or only changed at

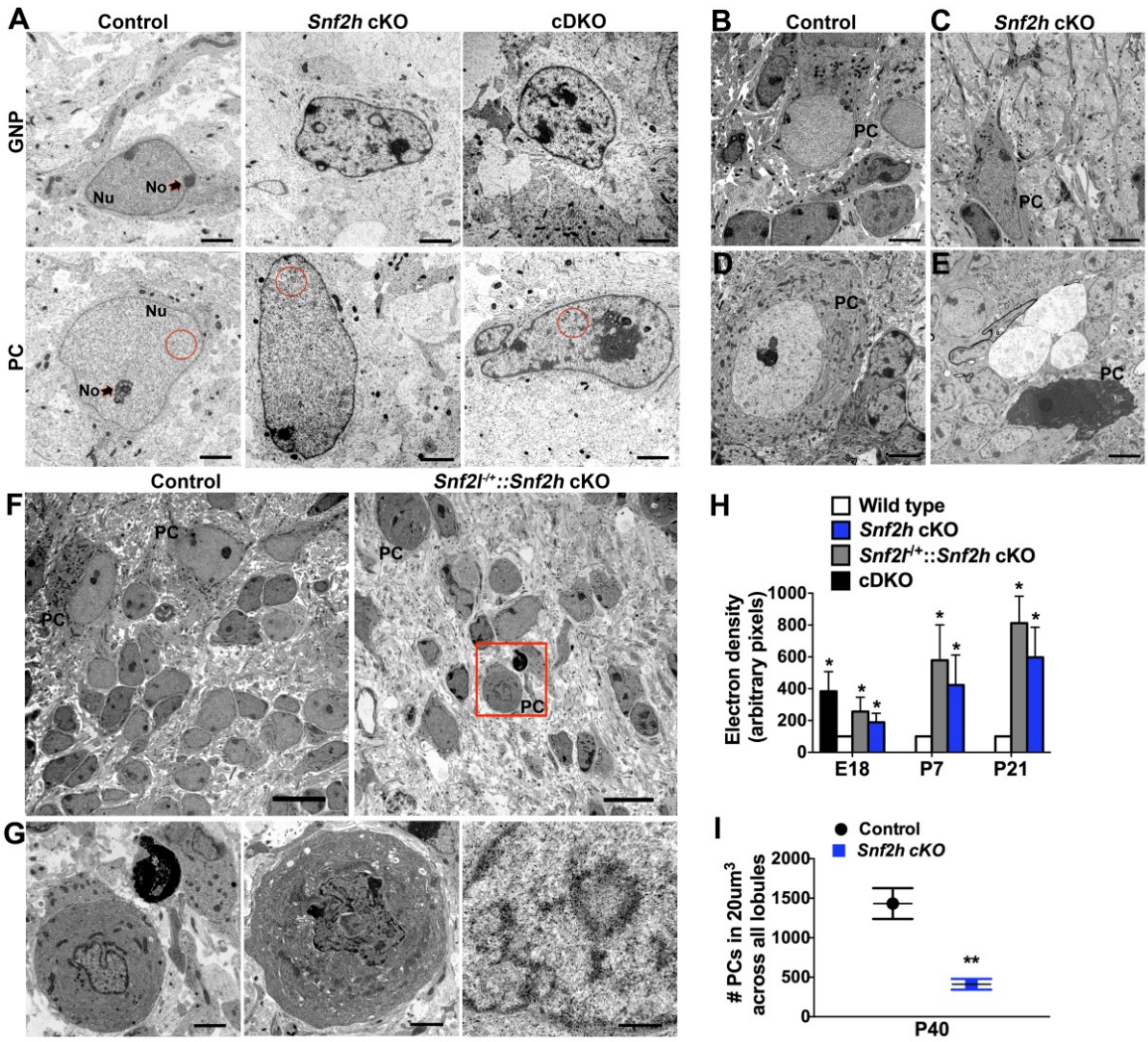

Figure 5. Snf2h is essential for higher order chromatin structure. **(A)** Transmission electron microscopy (TEM) of GNPs and PCs through the cerebellar vermis from control, *Snf2h* cKO and cDKO mice at E18. Red circles denote representative areas used for electron density pixel measurements. Nu = nucleus; No = nucleolus. Scale bars = 2µm. **(B-C)** TEM of control and *Snf2h* cKO mice through the cerebellar vermis at P7. Note the abnormal morphology of mutant PCs. PC = Purkinje cell. Scale bars = 2µm. **(D-E)** TEM of control and *Snf2h* cKO mice through the cerebellar vermis at P21. Note the pyknotic PCs and "cell ghosts" in mutant cerebella. Scale bars = 2µm. **(F)** TEM through the cerebellar vermis from control and *Snf2l-/+::Snf2h* cKO mice at P7, revealing the aggravation of chromatin ultrastructure abnormalities within PCs upon additional removal of one *Snf2l* copy. Boxed area is enlarged in bottom leftmost panel. Scale bars = 10µm. **(G)** Representative images from pyknotic *Snf2l-/+::Snf2h* cKO PC nuclei highlighting nuclear ultrastructural abnormalities relative to control PCs. Scale bars = 2µm (left and middle panel); 500nm (rightmost panel). **(H)** Electron density quantitation through euchromatic regions of PC nuclei from control, *Snf2h* cKO, *Snf2l-/+::Snf2h* cKO and cDKO mice at the indicated ages. Note the progressive increase in electron density in PCs upon loss of the mammalian ISWI

proteins. *P<0.05, student's t-test. **(I)** Distribution of PCs from *Snf2h* cKO and control littermates at P40. **P<0.01, student's t-test.

the later postnatal time (Figure 6A). Despite this broad fluctuation in the transcript levels of individual histone genes, we were uncertain that this would affect protein levels or impinge on chromatin structure since mammalian cells contain several histone gene clusters and multiple gene copies within each cluster (Marzluff et al., 2002). Nonetheless, we analyzed the histone proteins by immunoblot following acid extraction from mutant and control cerebella at P2 and P9. At P2, histones H1, H2A, and H4 were present at levels equivalent to wild type mice while histone H2B was slightly reduced and histone H3 showed a marginal increase (Figure 6B). In addition, there were no changes in the histone variants γ-H2AX, H2AZ, and macro-H2A (Figure 6B). Surprisingly, we observed striking changes in histones at P9 with almost complete loss of histone H2A and the histone H2A variants; moderate histone H1 and H4 loss; while histone H2B and H3 showed no change (Figure 6B). Furthermore, acute knockdown of Snf2h by siRNA treatment in Neuro2A cells showed a similar dramatic decrease in H2A levels, but only a modest decrease in H1 and increased H2B levels, while the histone variant H2AZ and total histone H3 were unaffected (Supplementary Fig. S4). The consistent drop in histone H2A and H1 levels suggest that these histones may be the primary target for Snf2h in the regulation of histone dynamics.

To further decipher the *in vivo* role of Snf2h in chromatin dynamics, we performed fluorescence recovery after photobleaching (FRAP) experiments using an H1e-GFP-tagged construct transfected into Neuro2A cells prior to Snf2h knockdown (Gerlitz et al., 2007; Melcer et al., 2012). Snf2h knockdown, but not siScrambled control, resulted in ~30% cell death upon transfection after 72 hours (not shown). Therefore, to avoid any non-specific effects of cell death on H1e dynamics, all FRAP experiments

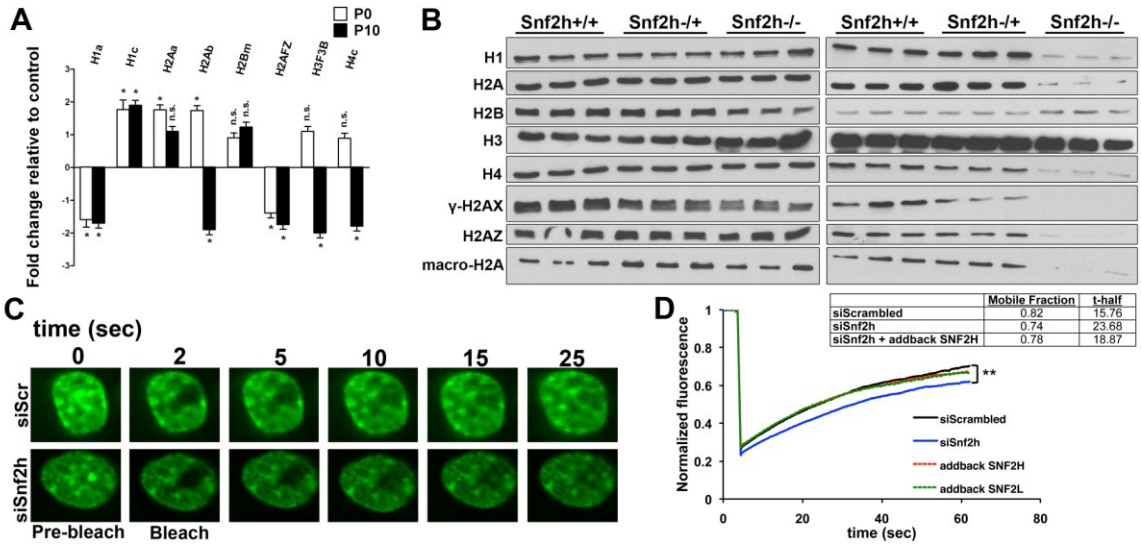

Figure 6. Snf2h loss results in deregulation of histone gene expression and altered histone H1e dynamics. **(A)** qRT-PCR gene expression analysis of representative core histones and histone variants from *Snf2h* cKO and control cerebella at P0 and P10. **P*<0.05, student's t-test. n.s.=not significant. **(B, C)** Immunoblots of P2 (left panels) and P9 (right panels) acid-extracted cerebellar extracts for histones H1, H2A, H2B, H3, H4; and H2A variants H2AX, H2AZ and macroH2A. **(C)** FRAP images of H1e-GFP in siScrambled (top) and siSnf2h (bottom) Neuro2A treated cells at the indicated time points. **(D)** Mean normalized FRAP curves of siScrambled, siSnf2h, siSnf2h + addback human SNF2H and siSnf2h + addback human SNF2L Neuro2A treated cells. The difference between recovery curves of siScrambled and siSnf2h is significant and indicated by two asterisks (***P* = 0.008). Both SNF2H and SNF2L rescue siSnf2h FRAP mobile fractions relative to siScrambled levels. Error bars were omitted for clarity. Inset: mobile fractions and t-half values for the experiments indicated. *Also refer to Supplementary Figs. S4-S5 and Supplementary Table S2.*

were performed at the 48h time point. The cell nucleus in both siScrambled control and siSnf2h-treated cells appeared normal in size and shape at the time of the experiments (Figure 6C). The siSnf2h-treated cells displayed a ~10% reduction in histone H1e-GFP mobility and an ~50% increase in the half maximal recovery time (t-half) compared to the siScrambled controls, thus demonstrating the slower dynamics of H1e deposition upon Snf2h depletion (Figure 6D and Supplementary Movies S7-S8). To demonstrate that the observed effect was specific to Snf2h, we restored the mobility of H1e-GFP by co-transfecting a human SNF2H expression construct that is not targeted by the siRNA treatment (Figure 6D). Conversely, knockdown of Snf2l did not alter H1e-GFP dynamics (Supplementary Fig. S5A). However, exogenous expression of human SNF2L was able to rescue H1e dynamics following Snf2h knockdown (addback SNF2L), which is indicative of the functional compensation we have observed in *Snf2h* cKO mice (Figure 6D). Similar experiments were performed with H2A-RFP constructs transfected into Neuro2A cells, but we did not observe any alterations in the dynamics of this core histone (Supplementary Fig. S5B). This was surprising, but may be a reflection of the slower exchange rate of H2A (Higashi et al., 2007) and/or the large reduction in endogenous H2A levels upon Snf2h knockdown, which when replaced by H2A-RFP may mask the sensitivity of the FRAP analysis.

Taken together, these experiments suggest that the general disorganization of the chromatin we observed at the ultrastructural level in *Snf2h* cKO mice is caused, in part, by altered histone gene transcription and histone H1/H2A deposition that eventually culminates in reduced levels of many core histones and histone variants over a one week period in the developing cerebellum.

Snf2h loss in postmitotic PCs results in chromatin disorganization and cognitive impairments

To confirm that the chromatin disorganization resulted from the cell autonomous loss of Snf2h, we once again made use of the *Snf2h* cKO-PCP2 mice. Sections from P50 mice were examined for chromatin ultrastructure changes by TEM. Similar to the *Snf2h cKO* mice, we observed chromatin disorganization in *Snf2h* cKO-PCP2 animals that were not present in wild type littermates (Figure 7A) but were augmented when *Snf2l* was also deleted (cDKO-PCP2; Supplementary Fig. S6). Consistent with the *Snf2h* cKO quantitation results, pixel intensity measurements confirmed an increased electron density within mutant PC nuclei (Figure 7B), and a progressive loss of PCs as the animals aged which was further enhanced in cDKO-PCP2 animals (Figure 7C).

While we had noted earlier that *Snf2h* cKO-PCP2 mice had reduced PC dendritic arborization (Figure 3G), they do not develop ataxia-like symptoms. Given that the PC has traditionally been associated to motor control, the lack of an obvious sensorimotor phenotype was puzzling. Nevertheless, recent reports have revealed that the PC also plays a role in higher order cognitive skills (Reith et al., 2013; Tsai et al., 2012a). Hence, we assessed the performance of *Snf2h* cKO-PCP2 mice in a cohort of behavioral assays. In the open field assay that measures anxiety-related symptoms, *Snf2h* cKO-PCP2 mice exhibit increased time spent in the large and small centers relative to controls, but showed no differences in the total distance traveled (Figure 7D-F). Interestingly, we observed an enhanced ability to maneuver in the rotating rotarod (Figure 7G), but no additional sensorimotor or spatial learning deficits (Supplementary Fig. S7). In the fear conditioning assay, mice are exposed to a novel cue ("cue tone"), followed by a foot-shock and the

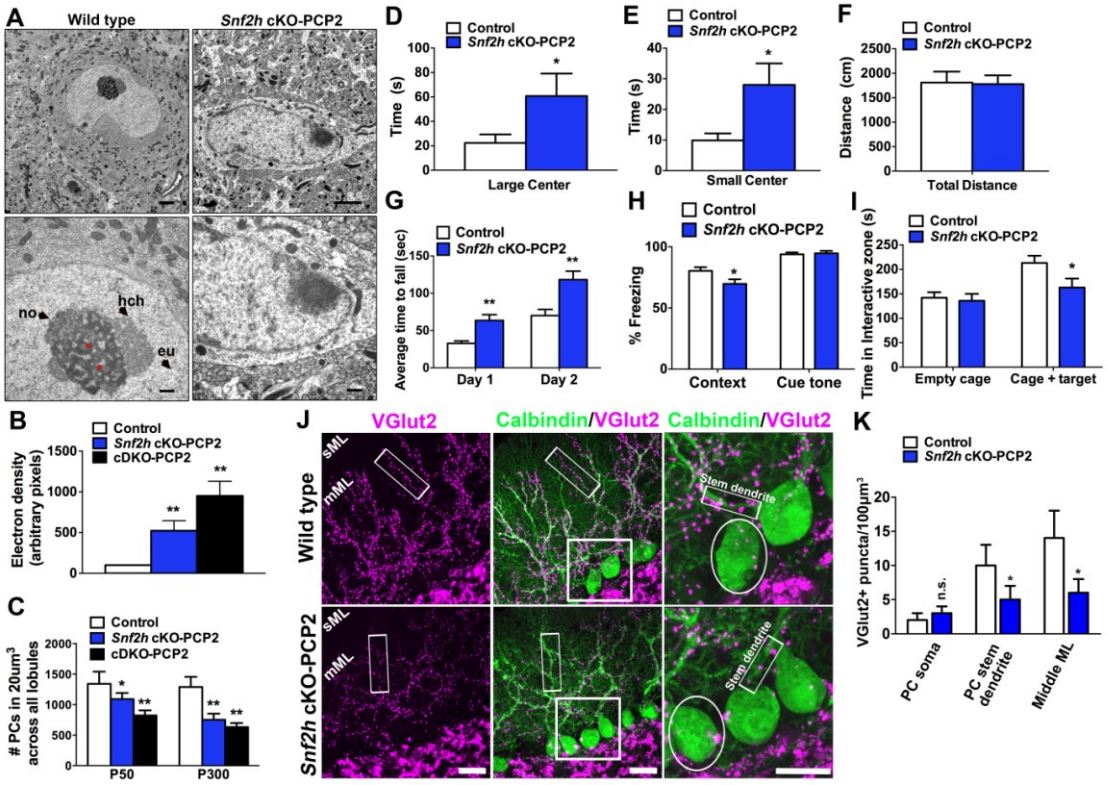

Figure 7. Snf2h deletion in postmitotic Purkinje cells results in chromatin ultrastructural alterations, cognitive deficits and progressive cell death. **(A)** TEM of PCs through the cerebellar vermis of *Snf2h* cKO-PCP2 mice and control littermates at P50. Higher magnification is provided in lower panels. Note the loss of nucleolar, heterochromatin and euchromatin ultrastructure and increased electron density within mutant PC nuclei. No = nucleolus; eu = euchromatin; hch = heterochromatin; stars denote nucleolar dense fibrillar centers. Scale bars = 2µm (top panels); 500nm (bottom panels). **(B)** Electron density quantitation of euchromatic regions of PC nuclei from control, *Snf2h* cKO-PCP2 and cDKO-PCP2 mice at P50. ***P*<0.01, student's t-test. **(C)** Quantitation of PCs from *Snf2h* cKO-PCP2, cDKO-PCP2 mice and control littermates at the indicated ages. Note the progressive death of PCs by P300. **P*<0.05, ***P*<0.01, student's t-test. **(D-F)** *Snf2h* cKO-PCP2 exhibit increased time spent in the large (D) and small center (E) of the open field assay, but no difference in the total distance traveled in 10-min assays (F) relative to controls (**P*<0.05, 1-way ANOVA). **(G)** *Snf2h* cKO-PCP2 exhibit enhanced ability to stay on the rotarod after 5 sessions of training relative to controls (**P*<0.05, 1-way ANOVA). **(H)** *Snf2h* cKO-PCP2 exhibit no differences in freezing response during training, but a decreased freezing response in context-dependent learning relative to controls (**P*<0.05, 1-way ANOVA). **(I)** *Snf2h* cKO-PCP2 exhibit less time spent interacting with stranger mice in a controlled social environment relative to controls (**P*<0.05, 1-way ANOVA). **(J)** *Snf2h* cKO-PCP2 and control littermate P50 coronal sections through the posterior zone (lobule aIX) of the cerebellum co-labeled with Calbindin (green) and VGlut2 (magenta). Note the reduced number of pre-synaptic excitatory VGlut2+ climbing fiber afferents onto Purkinje arbors (rectangles). Square boxes are enlarged on the rightmost panels. sML = superficial molecular layer; mML= middle molecular layer; Scale bars = 20µm. **(K)** Quantitation of VGlut2+

puncta larger than 2μm^3 around the PC soma, through the PC stem dendrite, and the mML in 100μm^3 bins from control and *Snf2h* cKO-PCP2 mice at P50. **P*<0.05, student's t-test. *Also refer to Supplementary Figs. S6-S7.*

"fear" response is measured ("conditional response") (Maren, 2001). *Snf2h* cKO-PCP2 mice had a normal response to the cue tone compared to controls, but a reduced response to the context, suggestive of impaired associative learning skills (Figure 7H). Lastly, the social interaction assay measures the preference of mice to interact with a stranger mouse than with an inanimate object. *Snf2h* cKO-PCP2 mice spent less time interacting with the stranger mouse than control littermates (Figure 7I). We conclude that the loss of Snf2h in postmitotic PCs does not result in motor deficits, but contrarily in enhanced motor skills, hyperactive-like behavior and cognitive deficits.

To assign a physiological correlate to the cognitive alterations in *Snf2h* cKO-PCP2 mice, we assessed the number of excitatory pre-synaptic terminals onto PC arbors by immunolabeling with the vesicular glutamate transporter-2 (VGlut2) that labels climbing fibers originating from olivary neurons within the brain stem (Gebre et al., 2012). We quantitated the number of VGlut2+ puncta around the PC soma, within the PC stem dendrite, and in the middle molecular layer. We did not detect any VGlut2+ puncta in the superficial molecular layer and no differences around the PC soma, but significantly lower VGlut2+ puncta in the middle molecular layer and around the PC stem dendrite in *Snf2h* cKO-PCP2 mice compared to WT littermates (Figure 7J-K). The reduction in VGlut2+ pre-synaptic terminals onto PC arbors suggests that this deficit contributes to the altered cognition of *Snf2h* cKO-PCP2 mice.

DISCUSSION

Ablation of Snf2h results in the loss of functional ACF/CHRAC, WICH, and NoRC remodeling complexes that, collectively, has a major impact on the dynamics and organization of chromatin. Indeed, altered chromatin dynamics and organization impaired

GNP proliferation, the transcription of key cerebellar patterning genes, and the morphological maturation of PCs during cerebellar morphogenesis. As a result, these mice developed cerebellar ataxia that resulted in their premature death.

Higher order chromatin packaging requires Snf2h

Chromatin condensation is dependent on nucleosome repeat length and the incorporation of the linker histone H1 (Robinson et al., 2008; Routh et al., 2008). *In vitro* studies have shown that ISWI protein complexes assemble and evenly space nucleosomes on a chromatin template (Erdel and Rippe, 2011), while loss of ISWI function in Drosophila results in reduced histone H1 levels and the decondensation of the X chromosome (Corona et al., 2007; Deuring et al., 2000; Siriaco et al., 2009). Other studies have noted a requirement for NoRC in the formation of perinucleolar heterochromatin structures (Postepska-Igielska et al., 2013). Our work indicates that Snf2h also mediates the dynamics of histone H1, H2A and its variants. Recent studies have demonstrated that the C-terminal tail of histone H2A is required for histone H1 loading and for Snf2h-dependent nucleosome translocation (Vogler et al., 2010). This raises the idea that interactions between the C-terminal H2A tail and Snf2h promotes histone H1 loading onto chromatin and H2A variant exchange. Within progenitor cells these functions could mark genes for expression upon differentiation (H2A.Z loading) while establishing the restrictive chromatin environment (through histone H1 loading) that accompanies neuronal differentiation (Efroni et al., 2008; Meshorer et al., 2006).

Snf2h loss hampers GNP proliferation

A key feature of the developing postnatal cerebellum is the massive expansion of GNPs, a critical event in cerebellar foliation (Sillitoe and Joyner, 2007). We demonstrate that the reduced cerebellar size in *Snf2h* cKO mice results from poor GNP proliferation. Several studies have implicated ACF/CHRAC and WICH complexes in the replication of heterochromatin (Bozhenok et al., 2002; Poot et al., 2000). The WICH complex acts behind the replication fork to re-establish the local chromatin environment while the ACF/CHRAC complex is recruited as part of the DNA damage checkpoint response to collapsed replication forks (Sanchez-Molina et al., 2011; Yoshimura et al., 2009). Indeed, defective replication of heterochromatin is known to result in DNA damage, mitotic catastrophe and cell death, which can have a significant effect on cell number during the proliferative phase of tissue growth (Huh et al., 2012). This would be consistent with our findings of micronuclei and increased TUNEL staining in *Snf2h* cKO mice. Alternatively, the reduction of histones H1 and H2A may be sufficient to induce cell cycle arrest, as found with H3 ablation studies in yeast (Gossett and Lieb, 2012). However, we cannot rule out the possibility that reduced expression of Engrailed and/or other GNP-enriched transcription factors (TFs) are the main cause of impaired growth, since mouse models null for *Pax6, Math1, NeuroD1* or *En2* also result in cerebellar hypoplasia (Ben-Arie et al., 1997; Cho and Tsai, 2006; Engelkamp et al., 1999; Joyner et al., 1991). Regardless, our experiments demonstrate that Snf2h is intricately involved in the proliferation of GNPs and the subsequent foliation of the cerebellum during the postnatal period.

Snf2h loss compromises Purkinje cell development and function

We demonstrate that Snf2h is important for maturation and function of PCs that are essential for cerebellar function. We show that dendritic arborization was compromised

using two different Cre-driver lines (Nestin-Cre and PCP2-Cre) to ablate Snf2h. In the Nestin model, the poor arborization in *Snf2h* cKO mice resulted in severe sensorimotor deficits that are likely due to the combined loss of PCs and GNPs. Conversely, the *Snf2h* cKO-PCP2 model presented with cognitive abnormalities reminiscent of the Purkinje-specific *Tsc1* mouse model with autistic-like features (Tsai et al., 2012a). Moreover, poor dendritic arborization affected PC afferent circuitry development as evidenced by the reduced number of excitatory VGlut2+ climbing fiber afferents present in *Snf2h* cKO-PCP2 mice. In this regard, dendritic defects and aberrant synaptic plasticity are common phenotypes for mouse models inactivated for chromatin remodeling proteins or subunits (Nogami et al., 2011; Shioda et al., 2011; Zhou et al., 2006). Most recent evidence shows that epigenetic regulation of synaptic plasticity extends beyond development, since synaptic plasticity deficits can be rescued by re-introduction of the missing chromatin remodeling complex subunit in postmitotic neurons (Vogel-Ciernia et al., 2013). Similar studies are required to dissect the individual roles of *Snf2h*-associated subunits to synaptic plasticity and cognitive control.

ISWI proteins stabilize transcription states in neurons

We surmise that the dendritic defects arise from aberrant transcription of target genes, particularly given the rampant increase in deregulated genes between birth and P10 (110 genes at P0 vs. ~3000 genes at P10). Work from *Drosophila* indicates that ISWI interacts at genes ~300bp downstream of the TSS where it localizes nucleosomes into positions that stabilize a transcriptional (active or repressed) state (Gkikopoulos et al., 2011; Sala et al., 2011). Similarly, we observed enrichment for both Snf2h and Snf2l in a similar position on the *En1* gene. The specific positioning of nucleosomes around the TSS and

within the gene body by Snf2h may also facilitate the loading of H2A.Z in progenitors, which acts to "poise" genes for expression upon differentiation (Creyghton et al., 2008). An inability to load H2A.Z may account for the poor activation we observed for many genes. It is also possible that Snf2h and Snf2l are required to impart exquisite transcriptional control of developmentally important genes, as suggested by the function of known targets (Dirscherl et al., 2005; Landry et al., 2008; Yip et al., 2012). For example, *Foxg1* levels determine whether a progenitor undergoes self-renewal or differentiation (Siegenthaler et al., 2008) and *Snf2l* mutant mice had increased Foxg1 expression that enhanced progenitor proliferation and increased brain size (Yip et al., 2012). Similarly, the interaction of both Snf2h and Snf2l at the *En1* gene (co-modulation) may regulate its expression levels and/or recruitment to target loci to control PC maturation, as has been observed for Olig2 and Brg1 during oligodendrocyte differentiation (Yu et al., 2013). Indeed, the compensatory upregulation of Snf2l in *Snf2h* cKO mice and the more severe phenotype after removal of *Snf2l* alleles supports such a model of gene target co-modulation. Delineating the epigenetic regulation of neuronal development is crucial to our understanding of intellectual-disability disorders caused by mutations in epigenetic modifiers, including chromatin-remodeling enzymes. As a whole, our findings highlight the complexity and diversity of Snf2h-containing CRCs during the development of the mammalian cerebellum, and their roles in progenitor and postmitotic neurons alike to govern histone dynamics and chromatin organization.

ACKNOWLEDGEMENTS

We are grateful to Dr. Diane Lagace and Mirela Hasu at the University of Ottawa Behavioral Core for assistance with behavioral experiments and expert discussions. We thank Dr.

Alexandra Joyner for anti-Pan Engrailed antibodies. M.A.-S. thanks D.J.P. for funding. This work was funded by operating grants from the Canadian Health Research Institutes to D.J.P. (MOP97764; MOP84412).

AUTHOR CONTRIBUTIONS

M.A.-S. designed all experiments and performed the phenotypic and molecular characterization of the *Snf2h* cKO-Nestin, cDKO-Nestin, *Snf2h* cKO-PCP2 and cDKO-PCP2 mice with K.Y., E.H., D.I., M.S.H. and M.A.T. providing technical support. P.L. and C.P.C. established the $Snf2h^{fl/fl}$ breeding colony and made some initial phenotypic observations. Y.D.R. and R.K. performed and analyzed TEM experiments. E.V.R.R. & E.M. performed and analyzed FRAP experiments. A.M. and V.A.W. performed and analyzed microarray results. The $Snf2h^{fl/fl}$ and $Snf2h^{-/+}$ mice were generated and provided by T.S., J.K., R.M., and A.S. D.J.P. supervised the project and discussed results. M.A.-S. & D.J.P wrote the paper with input from all authors.

METHODS & SUPPLEMENTARY FILES

EXPERIMENTAL PROCEDURES

Generation of Snf2h$^{fl/fl}$ mice

Snf2h$^{exon5fl/exon5fl}$ (Snf2h$^{fl/fl}$) mice were generated through homologous recombination in WW6 ES cells as described (Stopka and Skoultchi, 2003). Briefly, a 6.0 kb fragment of the Snf2h gene containing exons 4 through 8, into which loxP sites were inserted 5' and 3' of exon 5, was cloned into the pEasyFlirt vector (a gift of Dr. M.P. Lisanti, University of Manchester, UK). This vector has a neomycin resistance gene flanked by Frt sites, which was removed in mice generated from correctly targeted ES cells by breeding to *Flp1* recombinase mice (Raymond and Soriano, 2010). *Snf2h$^{fl/fl}$* mice were viable, fertile and did not exhibit any gross behavioral abnormalities. Cre-mediated deletion of *Snf2h* exon 5 was tested by breeding to ZP3-Cre mice (Lewandoski et al., 1997) for which embryos homozygous for a deleted exon 5 died *in utero,* as previously described (Stopka and Skoultchi, 2003).

Mouse Breeding

Snf2h$^{fl/fl}$ mice were backcrossed for 6 generations to a C57Cl/6 background and bred with a C57Bl/6 Nestin-Cre$^{-/+}$ heterozygous mice (Berube et al., 2005) that also carried a *Snf2h* null allele (Stopka and Skoultchi, 2003), thereby generating *Snf2h* cKO mice by Nestin-Cre (*Snf2h*$^{-/fl}$::Nes-Cre$^{-/+}$ or *Snf2h* cKO) and control littermates that carried only one functional copy of *Snf2h* (*Snf2h*$^{-/fl}$ or *Snf2h*$^{+/fl}$::Nes-Cre$^{-/+}$) or both functional alleles (*Snf2h*$^{+/fl}$). These three control genotypes showed no overt phenotypes, reproduced normally and lived into adulthood and were used interchangeably as controls, except were indicated. We also bred *Snf2h$^{fl/fl}$* mice to the PCP2-Cre driver line (Barski et al., 2000) that lived normally into

adulthood and showed no gross behavioral abnormalities. For *Snf2l* ablation, we used a previously characterized germline $Snf2l^{Exon6}$ deleted mouse line that survives normally into adulthood (Yip et al., 2012), thus generating *Snf2l-/y::Snf2h* cKO (cDKO) and *Snf2l-/y::Snf2h* cKO-PCP2 (cDKO-PCP2), as well as *Snf2l-/+::Snf2h* cKO and *Snf2l-+::Snf2h* cKO-PCP2 compound heterozygotes. Our multiple breeders generated a total of six (6) different ISWI conditional knockout lines that were all analyzed for this article. For embryo staging, embryonic day 0.5 (E0.5) was defined as noon of the day a vaginal plug was observed after overnight mating. Animals were kept in an animal house under SPF (specific pathogen-free) conditions in a 12/12 light:dark cycle with water and food *ad libitum*. The University of Ottawa Animal Care and Use Committee approved all experiments. C57Bl/6 and FVBN/J wild type mice were purchased from Charles River (Montreal, QC, Canada). PCP2-Cre mice were obtained from The Jackson Laboratory (Stock # 004146; Bar Harbor, MA, USA).

Behavioral Analysis

All behavioral tests were completed in the Behavior Core Facility at the University of Ottawa using standardized protocols. Animals were habituated to the testing room at least ~1 h before testing. Behavioral assays were performed irrespective of sex for *Snf2h* cKO mice and tested between P20-P25. For *Snf2h* cKO-PCP2 mice, female and male mice were assessed independently at 4-6 months old, for which we did not observe sex-specific differences in behavior, thus showed combined data. For behavioral assays, one-way ANOVA was used for at least 10 mice per genotype. The values are presented as the mean ± SEM.

Suspended wire test

Mice were suspended by their forepaws on a 2 mm wire, and the amount of time they remained on the wire was recorded.

Dowel test

Mice were placed in the center of a horizontal pole (1cm diameter) and the time mice remained on the pole was recorded. If mice walked across and off the dowel, they were placed back onto the dowel. Trials lasted for a maximum of 2 min.

Elevated Platform

Mice were placed in the center of a 15-cm^2 round elevated platform 50-cm above the ground and the time mice remained on the platform was recorded. Student's *t*-test was used for statistical significance.

Rotarod

Mice were trained and tested on the accelerated rotarod (rod diameter 3cm) for 300 seconds for five times before measurements (IITC, Woodland Hills, CA, USA). Starting speed was set at 4 RPM and maximum speed at 40 RPM. The latency to fall from the rotarod was recorded. If animals were able to stay on the rod for 300 sec, the latency to fall recorded was 300 sec. The animals received 4 trials per day, with a trial interval of 30 min, for 2 consecutive days.

Pole Test

Mice were placed head-upward on the top of a rough surfaced vertical pole (8mm diameter x 55 cm tall) and the time for descending recorded. The time required for the mouse to turn downward after placing and the total time on the pole until the mouse reaches the bottom is

recorded. Mice were trained for 2 days before test. 5 trials were averaged on day 3.

Open Field

Animals were placed in the center of a 45 x 45 x 45-cm chamber equipped with photobeams (Noldus) to record activity during a 10-min test period.

Elevated Plus Maze

Animals were habituated to the test room for at least 2 days prior to test. Animals were placed in the center of a maze consisting of two arms (each arm 5 cm wide x 60 cm long) enclosed by ~15 cm high walls, and two open arms (each arm 25 x 7.5 cm, with a raised 0.5 cm lip at edges) elevated 1 meter above ground and with equidistant arms from the center of the platform. The amount of time the animals spent in the open or closed arms, the total number of entries and the total distance traveled were recorded for 10 min using video detection software (Ethovision, Wageningen, Netherlands).

Social Interactions

A control mouse is placed in the corner of an open field box (under dim red light) that measures 45cm long on each side x 45cm high and containing a 5.5 x 9.6cm wire mesh rectangular cage. The mouse is given 5 mins to explore the arena and then removed. A few seconds later, a test mouse (or social target), of the same strain, age and gender is placed inside the rectangular wire mesh cage and the control mouse placed back in the arena. The time the social target interacts with the control mouse in 5 mins trials is recorded using Ethovision 7 XT automatic tracking software. Total distance traveled, time spent in 2 corners across the wire mesh cage and velocity is also recorded.

Fear Conditioning

On the first day (training), the animal is placed in the fear conditioning apparatus for a total of 6 minutes. After the first two minutes in the apparatus a tone is played for 30 sec ending with a 2-sec shock. One minute following the shock, the tone is played again for 30 sec ending with a 2-sec foot shock. For the remaining two minutes there is no tone or shock. The freezing behavior of the animal is recorded throughout the 6 minutes. This is the training in which the mouse receives 2 exposures to the tone followed by the shock and this occurs in a novel context, which is the conditioning box. On the 2^{nd} day, contextual conditioned fear testing begins. This measures the fear associated with being in the same environment where the shock was delivered (done ~24hrs after training). The mouse is placed in the same apparatus with all the same lighting and room conditionings for 6 minutes and freezing behavior is recorded.

BrdU-birthdating

Timed-pregnant females were injected intraperitoneally with 100μg/g body weight of 5-bromo-2′-deoxyuridine (BrdU; Sigma) and pups killed at indicate times. For BrdU-pulse labeling, timed-pregnant females were injected with BrdU and killed 60 or 120 minutes later. For BrdU immunodetection, sections were incubated in 2N HCl for 10 min at 37°C, rinsed in 0.1 M sodium borate, pH 8.3, blocked and incubated overnight at 4°C with rat monoclonal anti-BrdU antibody 1:300 (Abcam #6326). The average number of immunopositive cells was determined from five separate fields under ×40 magnification in confocal Z-stacks (or cubic bins) of 18 x 10^3 μm^3.

TUNEL assay

Sections were examined for DNA fragmentation with the TUNEL *in situ* cell death detection kit (Roche Applied Science, ON, Canada) according to the manufacturer's instructions. The average number of TUNEL-positive cells was determined from five separate fields under ×40 magnification in cubic bins.

Histology

Nuclei were visualized using cresyl violet staining in 20µm frozen sections. Sections were cleared in Xylene and mounted with Permount.

Golgi-Cox Staining

Golgi staining was completed using FD Rapid GolgiStain Kit (FD NeuroTechnologies). Briefly P20 mice were intracardially perfused with 4% paraformaldehyde in 0.1M PBS and stained according to the manufacturer's instructions. Tissues were sectioned at 100 µm and mounted on gelatin-coated slides. Morphology of apical and basal dendrites of cerebellar Purkinje neurons were blindly analyzed with Neurodigitech software (Neurodigitech LLC, San Diego, CA, USA).

Immunofluorescent histochemistry

For embryonic tissue, 20µm sections were used. For postnatal brains, 40µm free-floating sections were used. Sections were washed four times in PBST (PBS with 0.1% Triton X-100), blocked (1 hr, room temperature) in 10% horse serum/PBST, and incubated (overnight, 4 ºC) in primary antibodies. The following primary antibodies were used: rabbit anti-Snf2h (1:250, Abcam #72499); rabbit anti-Snf2l (1:100, Abcam #37003); mouse anti-NeuroD1 (1:500, Abcam #60704); mouse anti-Calbindin (1:200, Sigma C9848); rabbit anti-Calbindin (1:300, Sigma C2724); rabbit anti-GFP (1:1000, Molecular Probes); mouse anti-BrdU (1:100, DAKO); rat anti-BrdU (1:300; Abcam #6326); rabbit anti-phospho histone H3 (pH3;

1:200; Millipore #06-570); rabbit anti-Engrailed- (1:500; Abcam #32817); rabbit anti-Pax6 (1:200; Covance #PRB-278P); mouse anti-NeuN (1:200, Millipore #MAB377); guinea pig anti-VGlut2 (1:1000, Millipore #AB2251); rabbit anti-pan-Engrailed (gift of Dr. Alexandra Joyner, Memorial Sloan-Kettering Cancer Center, NY, USA); The following day, sections were washed five times in PBST and incubated (2 hrs, room temperature) with DyLight^{488}, DyLight^{594} or DyLight^{649}-conjugated mouse pre-adsorbed secondary antibodies (1:1000, Jackson Immunoresearch, PA, USA) against the IgG domains of the primary antibodies. All sections were counterstained with the nuclear marker DAPI (Invitrogen). Sections were mounted on slides with Dako Fluorescence Mounting Medium (Dako Canada, ON, Canada).

X-Gal Staining

Staged embryos were quickly dissected and rinsed in 0.1M PBS, pH 7.4 and fixed for 30 minutes. X-Gal staining was performed as previously described (Berube et al., 2005).

Western Blotting

Cerebellar or hindbrain (for E12 and E17 time points only) extracts were quickly dissected from individual pups and snap frozen in dry ice. Cerebella were then homogenized in ice-cold RIPA buffer supplemented with protease inhibitor cocktail (Sigma), and incubated for 20 min on ice with gentle mixing. After pre-clearing by centrifugation (15 min at 17,000 x g), proteins were quantified by the Bradford method. Protein samples were resolved on sodium dodecyl sulfate polyacrylamide gels under denaturing conditions or using Bis-Tris 4-12% and Tris-Acetate 3-8% gradient gels (NuPage, Invitrogen) and blotted onto PVDF membranes (Immobilon-P; Millipore, MA, USA) by wet transfer for 1-2 hrs at 90V. Membranes were blocked (45 min, room temperature) with 5% skim milk in TBST (Tris-buffered saline containing 0.05% Triton X-100), and incubated (4°C, overnight) with the

following antibodies: rabbit anti-Snf2h (1:4000; Abcam #72499); sheep anti-Snf2l (1:2000) (Barak et al., 2003); mouse monoclonal anti-Snf2l 1:1000 (Alvarez-Saavedra M & Picketts DJ, *unpublished*); mouse anti-ß-Actin (1:30,000, Sigma); rabbit anti-Engrailed-1 (1:2000, Millipore), or mouse anti-Engrailed 4G11 (1:20, Developmental Studies Hybridoma Bank). Membranes were incubated (1 hr, room temperature) with ImmunoPure® HRP-conjugated goat anti-rabbit or goat anti-mouse IgG (H+L) secondary antibodies (1:30,000; Pierce, Rockford, IL). Membranes were washed 5 x 5 min in TBST after antibody incubations, and the signal was detected using the Pierce Supersignal West Fempto chemiluminescence substrate (Pierce). Western blots were quantitated using ImageJ software (rsbweb.nih.gov/ij/). At least 2 separate gels were immunoblotted with cerebellar extracts from independent litters and used for quantitation.

Chromatin Immunoprecipitation (ChIP)

Cerebella was isolated from C57Bl/6 wild type mice and cell pellets resuspended in 50 mM HEPES-KOH, pH 7.5, 140 mM NaCl, 1 mM EDTA, 1% Triton X-100, 0.1% sodium deoxycholate, 0.1% SDS and protease inhibitor cocktail and incubated on ice for ~30 min. Cells were then sonicated for 100 cycles (30 sec pulse, 30 sec rest intervals) to an average size of ~500-800bp using a 4°C sonicator (Bioruptor® UCD-200, Diagenode, Inc., Sparta, NJ). After sonication, cell debris was pelleted by centrifuging 2 min, 4°C at 8000 x *g*. Supernatant was collected and a 20 µl input sample was analyzed on a 2% agarose gel to verify chromatin size. Additionally, 100 µl of recovered chromatin was used for DNA quantitation and as qPCR positive control (Input). GammaBind Plus Sepharose Beads (GE Healthcare, Piscataway, NJ, USA; Cat. No. 17-0886-01) were blocked with BSA (100 ng/µl beads; New England Biolabs, Ipswich, MA) and salmon sperm DNA (100 ng/µl beads;

Invitrogen) for 30 min at RT. Beads were washed 3 times with RIPA buffer (50 mM Tris-Cl, pH 8, 150 mM NaCl, 2 mM EDTA, pH 8, 1% NP-40, 0.5% sodium deoxycholate, 0.1% SDS with protease inhibitor cocktail) and resuspended in 2 volumes of RIPA. Pre-clearing of recovered chromatin was performed by incubating with 100 µl of blocked GammaBind Plus Sepharose Bead slurry for 30 mins at 4ºC. Beads were centrifuged for 2 min, 4°C at 8000 x *g*, and pre-cleared chromatin was recovered and further diluted 1:10 in RIPA for immunoprecipitation. Immunoprecipitation was performed overnight at 4 ºC by incubating ~50 µg of pre-cleared chromatin with 2 µg of the following rabbit antibodies from Abcam: anti-Snf2h; anti-Snf2l; anti-histone H3; or rabbit IgG (Jackson Immunoresearch). We also used anti-H3K9Ac; and anti-H3K9Me3 as internal controls (not shown). Immune complexes were captured with 120 µl of blocked GammaBind Plus Sepharose Bead slurry for 2 hrs at 4ºC. Beads were then collected by centrifuging for 2 min at 8000 x *g*. Beads were washed three times with 20 mM Tris-Cl, pH 8, 150 mM NaCl, 0.1% SDS, 1% Triton X-100 and 2 mM EDTA, pH 8, and once with 20 mM Tris-Cl, pH 8, 500 mM NaCl, 0.1% SDS, 1% Triton X-100 and 2 mM EDTA, pH 8. DNA was eluted with 150 µl of elution buffer (1% SDS, 100 mM $NaHCO_3$) for 15 min at RT. Eluted DNA was further diluted in 2 volumes of elution buffer and incubated overnight at 65°C with 100 µg of proteinsase K (Invitrogen) for cross-link reversal. The DNA was then phenol-chloroform extracted and resuspended in 100 µl of TE, pH 8 (10 mM Tris-Cl, pH 8, 1 mM EDTA, pH 8). 1 µl ($1/100^{th}$) of DNA was used per reaction for quantitative PCR analysis. Triplicate samples were ran per reaction and a minimum of 2 independent ChIP experiments were carried per time point.

Quantitative Real-Time PCR

For qPCR analysis of ChIP DNA, PCRs were carried out using the SYBR Green Advantage qPCR premix (Clontech) and run under the following conditions: one cycle at 95°C for 1 min, and 45 cycles at 95°C for 10 sec, 60°C for 10 sec, and 72°C for 20 sec. All primers were analyzed by melt curve analysis after qPCR amplification. Primers are listed below:

Mouse Gene	Application	5' to 3'
Uncx-Ex2-F	qRT-PCR	GCGTTCAATGAGAGCCACTA
Uncx-Ex3-R	qRT-PCR	CCCTTTTTGGTGTTCTCCTTC
Rfx3-Ex3-F	qRT-PCR	GCTCAGGTGCAGTATGTGGA
Rfx3-Ex4-R	qRT-PCR	CTGGGCAGAACTTCCTTGAG
Crebbp Ex2-F	qRT-PCR	ACACAGGTTTCCCCACAAAT
Crebbp Ex3-R	qRT-PCR	CTAACTGGGGGTTCACTCCA
Bmp4-Ex1-F1	qRT-PCR	TGATACCTGAGACCGGGAAG
Bmp4-Ex2-R	qRT-PCR	CCTGGGATGTTCTCCAGATG
En1-F1	qRT-PCR	TCACAGCAACCCCTAGTGTG
En1-R1	qRT-PCR	TATAGCGGTTTGCCTGGAAC
En2-F1	qRT-PCR	GACTCGGACAGCTCTCAAGC
En2-R1	qRT-PCR	GCCGCTTGTCCTCTTTGTTA
Pax6-Ex2F	qRT-PCR	TCAGCTTGGTGGTGTCTTTG
Pax6-Ex3R	qRT-PCR	AGCACCTGGACTTTTGCATC
Snf2h-Ex4F	qRT-PCR	ACACCGTAGAACGGAGCAAG
Snf2h-Ex5R	qRT-PCR	AGACTTGGGAACCAAAACCA
Atoh1-F2	qRT-PCR	GCTTCCTCTGGGGGTTACTC
Atoh1-R2	qRT-PCR	CTGTGGGATCTGGGAGATGT
Snf2l-Ex4-F	qRT-PCR	CCACAGGCGTACAGAACAAG
Snf2l-Ex5-R	qRT-PCR	GCGGTCCTCCTTTCACAT
Pcdhb6-F	qRT-PCR	CCCTCGATGCCTTAGTTGTC
Pcdhb6-R	qRT-PCR	CAAAATCCAGTGCCCCTTTA
Pcdhb17-F	qRT-PCR	AGCTACTCGCTGTTGCCTTC
Pcdhb17-R	qRT-PCR	GGTGAGCCTTGGTCTATTGC
Hist1h2aa-F	qRT-PCR	GGGAACTACGCACAACGAAT
Hist1h2aa-R	qRT-PCR	TAATGCGCGTCTTCTTGTTG
Hist1h1a-F	qRT-PCR	CATCACCACCAAGGTGTCAG
Hist1h1a-R	qRT-PCR	TTGGAAACTGCAGGCTTCTT
H2AZ-Ex4-F	qRT-PCR	CGTATCACCCCTCGTCACTT
H2AZ-Ex5-R	qRT-PCR	TCAGCGATTTGTGGATGTGT
Hist1h1c-F	qRT-PCR	AACCCCAGGCTAAGAAGGC
Hist1h1c-R	qRT-PCR	TGGCTTTACGGCTTTAGACGC
Hist1h2bm-F	qRT-PCR	CCTGAGCCAACGAAGTCCG
Hist1h2bm-R	qRT-PCR	GCACTTGCTTTAGCACCTTGT
Hist1h2ab-F	qRT-PCR	ATTCAGGCTGTCTTACTTCCGA
Hist1h2ab-R	qRT-PCR	TTTCCAGGCTTAATGACTTTCCG
H3F3B-F	qRT-PCR	AAGCAGACCGCTAGGAAGTC
H3F3B-R	qRT-PCR	GTAACGACGGATCTCTCTCAGA
Hist1h4c-F	qRT-PCR	ATGTCTGGACGTGGTAAGGGT
Hist1h4c-R	qRT-PCR	CCTGGATGTTATCACGGAGAAC
En2-5kbpromo-F	ChIP-qPCR	TTTTTGGGTGCCATCTTCTC
En2-5kbpromo-R	ChIP-qPCR	CCCTCCAGGTGTTACAGAGG
En1-P3F	ChIP-qPCR	CTTCATGCCCTCTTAAGTCC
En1-P3R	ChIP-qPCR	CGGGACTTTGCGGATAAATA
En2-1kbpromo-F	ChIP-qPCR	GGTTCCTGTCACCAAGCTG
En2-1kbpromo-R	ChIP-qPCR	CGCAACCTGAGACACTTTCA
En2-I1-F	ChIP-qPCR	AGGCAGTTGGAAGGACACAC
En2-I1-R	ChIP-qPCR	CCTGAGGATGGCAGAGAGTT

Reverse Transcription

Cerebella were quickly dissected from mutant and control littermates and RNA was isolated using Trizol (Invitrogen) according to the manufacturer's instructions. Glycogen (ambion) was used as carrier. 1µg of total RNA was reverse-transcribed using SuperScriptIII (Invitrogen). cDNA was further diluted 1:25 and 1µl was used per qPCR reaction. All primers were analyzed by melt curve analysis after qPCR amplification. Primers are listed below. The ΔΔCt method was used to compare fold-change. L32 and 18S mRNAs was used normalizers in separate experiments. Triplicate samples were ran per reaction and a minimum of 3 mice were analyzed per genotype. Student's *t*-test was used for statistical significance.

Microarrays

Gene expression profiling was performed on RNA isolated from dissected cerebella tissue of P0 or P10 *Snf2h* cKO and wild type control mice. RNA samples were labeled with Cy5 or Cy3 using 3DNA Array 900 kits (Genisphere, Hatfield, PA) following the manufacturer's instructions. *Snf2h* cKO and control samples were then cohybridized to MEEBO 38.5K arrays (Microarrays Inc., Huntsville, AL, Canada). A total of four replicates were performed for P0 and three for P10 and in both cases the labeling dyes were flipped for at least one replicate to counter dye bias. Probe-specific signals were quantified using the ScanArray express (Perkin Elmer, Waltham, MA). On the resulting raw background subtracted signals intra-array normalization (correcting for Cy5/Cy3 bias) was performed with global loess, inter-array normalization with the quantile method and statistical analysis via the WEBARRAY online tool (http://www.webarraydb.org/webarray/index.html). M ($\log_2$ ratio of *Snf2h* cKO/control signal) and A values ($\log_2$ average signal strength) were then

determined for all probes. A probe (gene) was scored as differentially expressed on an array if it demonstrated a *P*-value <0.01, and had sufficient detectable signals across all replicates (A value (log_2) >7). All raw and processed data has been deposited into the GEO database (GSE42371).

Image acquisition and processing

Tissue sections were examined and images captured using a Zeiss 510 laser scanning confocal microscope with UV (405nm), argon (488nm), helium/neon (546nm) and helium/neon (633nm) lasers. All images were acquired as 10-30μm Z-stacks (in 1-2μm intervals) and analyzed as projections using the LSM 510 Image Browser software (Zeiss, Oberkochen, Germany). Epifluorescent and light microscopy images were acquired with a Zeiss Axiovert Observer Z1 epifluorescent/light microscope equipped with an AxioCam cooled-color camera (Zeiss). Images were exported to Adobe Photoshop CS5 (Adobe Systems Inc., San Jose, CA, USA) and further processed for contrast when necessary.

Acid-based histone extraction

Histones were acid-extracted from P2 and P9 *Snf2h* cKO and control cerebella or from Neuro2A cells after siRNA treatment. Briefly, cerebellar tissue was quickly dissected and separated from the inferior and superior colliculi and brain stem and snap frozen on dry ice. Then, tissue was homogenized in TEB+ buffer (0.1M PBS, 0.5% Triton X-100, 5mM sodium butyrate, 0.02% NaN3 complemented with protease inhibitors cocktail [Sigma]), lysed on ice for 20 mins, and centrifuged for 10 minutes at 2,000 rpm at 4°C. Then, the supernatant was discarded and the pellet resuspended in 0.2N HCl at a cell density of 4 $X10^7$ cells/ml overnight with stirring at 4°C. Samples were then centrifuged for 10 minutes at

2,000 rpm at 4°C and supernatant containing free histones collected and quantitated for western blotting. The following antibodies were used from Active Motif: histone H1 1:4000 (#61201); histone H2A 1:4000 (#39209); histone H2B 1:4000 (#39125) or macro-H2A1 1:1000 (#39593); from Abcam: Histone H3 1:20,000 (ab1791); histone H4 1:5000 (ab10158); histone H2AZ 1:5000 (ab4174); or γ-H2AX (phospho-Serine S139) 1:2000 (#9718, Cell Signaling Technology, MA, USA). 3-5μg of total histones were loaded unto 15% SDS-PAGE linear gels and immunoblotted as described above.

Vector Construction

Human SNF2L cDNA comprising the entire open reading frame (+exon1/-exon13/+NLS) was amplified from a pcDNA3 expression plasmid (Lazzaro et al., 2008) in a two-step process. The 5' end of SNF2L cDNA was amplified with SNF2L-EcoRI-Fwd (5'-TAAGGAATTCATGGAGCA-3') and SNF2L-XhoI-Rev-internal (5'-ACCTCTCGAGCTATGT-3') primers, followed by purification of the PCR products, restriction digest by EcoRI and XhoI, and directional subcloning into the pBRIT-LoxP-NTAP and pBRIT-LoxP-CTAP retroviral plasmid vectors, which have been previously described (Todd and Picketts, 2012). The remaining 3' sequence of SNF2L was then subcloned non-directionally following amplification with SNF2L-XhoI-Fwd-internal (5'-ATAGCTCGAGAGGTAG-3') and SNF2L-XhoI-Rev (5'-ATGCTCGAGGGATTTCACCTTCTTG-3) primers and a restriction digest with XhoI. Similarly, SNF2H cDNA comprising the entire open reading frame was cloned into the pCI-neo expression vector (Promega Corp. Madison, WI) then amplified with the SNF2H-BamHI-Fwd (5'-AAAAGGATCCATGTCGTCCGCGGCCGAGCC) and SNF2H-XhoI-Rev (5'-AAAACTCGAGTAGTTTCAGCTTCTTTTTTCTTCC) primers and directionally

subcloned into the pBRIT-LoxP-NTAP and pBRIT-LoxP-CTAP vectors, following restriction digest with BamHI and XhoI. All clones were verified by sequencing at McGill University and Génome Québec Innovation Centre (Montreal, QC, Canada).

siRNA knockdown on Neuro2A cells

Neuro2A cells were freshly obtained from ATCC (Manassas, VA, USA) and grown in DMEM medium containing 10% FBS, L-glutamine and 1X Penicillin/Streptomycin. Briefly, cells were grown to a confluency of ~80% and transfected using Lipofectamine 2000 (Invitrogen) with 75nM siSnf2h (Thermo Scientific, Ottawa, ON, Canada; siGENOME, mouse *Smarca5*, D-041484-03); 75 nM siScrambled (siGENOME non-targeting siRNA #1, D-001210-01-05); or 75nM siSnf2l (OriGene Technologies, Inc, Rockville, MD, USA; *Smarca1* (mouse) # SR421862B). Total proteins or acid-extracted histones were collected as described above and analyzed by immunoblotting.

Fluorescence recovery after photobleacing (FRAP)

Neuro2A cells were grown in DMEM medium containing 10% FBS, L-glutamine and 1X Penicillin/Streptomycin. H1e-GFP plasmid has been previously described (Gerlitz et al., 2007). FRAP experiments were conducted essentially as described (Melcer et al., 2012). Cells were grown in 8-well μ-slides (ibidi LLC, Martinsried, Germany) and transfected with H1e-GFP plasmid together with 75 nM of each of the siRNAs using Lipofectamine 2000 (Invitrogen). For human SNF2H and human SNF2L "addback" studies, pBRIT-FLAG-hSNF2H or pBRIT-FLAG-hSNF2L was added to the transfection mix. Photobleaching studies were performed using a Revolution spinning disk (CSUX, Yokogawa, Japan) and an EMCCD high-speed imaging system (Andor Technology, Belfast, UK) equipped with a FRAPPA module (Andor Technology) and with solid-state lasers mounted on an Olympus

IX81 fully automated microscope. During the entire imaging process, cells were maintained under controlled CO_2, temperature and humidity using an environmental chamber (Life Imaging Services, Basel, Switzerland). Bleaching was performed with a 60X oil objective (NA=1.4). Images were captured every 250 ms using an EMCCD iXon+ camera (Andor, UK). Typically 240 post-bleach images were collected. Data from more than 20 cells were collected per experiment. For H2A-RFP FRAP, images were captured every 1s and typically 360 post-bleach images were collected. All FRAP experiments were performed at least three times and plots for one representative experiment are shown. Data processing was performed using the easyFRAP program (Rapsomaniki et al., 2012), based on the double normalization method (Phair et al., 2004). Curve fitting was performed using MATLAB's non-linear least-squares function. The method to calculate fully normalized recovery curves has been described previously (Ellenberg et al., 1997). This method was used to estimate the mobile protein fraction and t-half of protein. Two-tailed student's *t*-test was used to compare the significance of differences between different FRAP curves (Nissim-Rafinia and Meshorer, 2011).

Transmission electron microscopy (TEM)

Cerebella (E18, P7 and P21) were collected under a stereomicroscope, cut into sections of 1-2 mm thickness through the cerebellar vermis region and fixed for at least 4 hrs to overnight in Karnovsky's fixative (4% paraformaldehyde, 2% glutaraldehyde and 0.1 M cacodylate in phosphate-buffered saline, pH 7.4) at 4ºC. These specimens were subsequently washed twice in 0.1 M cacodylate buffer for 1h and once overnight at room temperature. Sections were then post-fixed with 1% osmium tetroxide in 0.1 M cacodylate buffer for 1 h at 4ºC, and washed twice for 5 min in water. The specimens were dehydrated twice for 20 min for

each step in a graded series of ethanol from water through 30%-50%-70%-85%-95% ethanol and twice for 30 minutes in 100% ethanol (molecular sieves were used to dehydrate ethanol), followed by twice for 15 min in 50% ethanol/50% acetone and twice for 15 min in 100% acetone. Sections were infiltrated in 30 % spurr/acetone for 15 h (overnight) then in 50% spurr/acetone for 6 h and in fresh 100% spurr resin overnight. Spurr was changed twice a day for three days at room temperature. All infiltration steps were carried out on a rotator. Sections were then embedded in fresh liquid spurr epoxy resin and polymerized overnight at 70ºC. Ultrathin sections (80nm) from the cerebellar vermis were collected onto 200-mesh copper grids and let dried overnight before staining. Grids were stained with 2% aqueous uranyl acetate and with Reynold's lead citrate. Sections were observed under a transmission electron microscope (Hitachi 7100). All ultrastructural analysis were based on at least three mice per genotype of the same age for each group examined. Electron density was quantitated using ImageJ software (rsbweb.nih.gov/ij/). Briefly, a digital 150 (*x*-axis) × 200 (*y* axis)-pixel oval was placed within PC nuclei and the mean intensity values were determined. A digital circle (Φ 200 pixels) was placed in a background control region outside of the nucleus and the mean value was subtracted, thus generating a normalized pixel intensity value. Values were normalized to 100 for wild type PC nuclei. At least 20 PCs were quantitated per genotype.

Toluidine blue staining

Semithin sections of 0.5 μm were stained with 1% toluidine blue and 2% Borate in distilled water. Histological samples were scanned with a MIRAX MIDI automated scanning light microscope (Zeiss) and images processed with Zeiss MIRAX Viewer software (Zeiss).

Statistics

Group statistical analysis was performed via the two-tailed Student's *t*-test. $P<0.05$ was accepted as statistically significant. At least 3 mice from each genotype were used for evaluation. The values are presented as the mean ± SEM.

SUPPLEMENTARY FIGURES

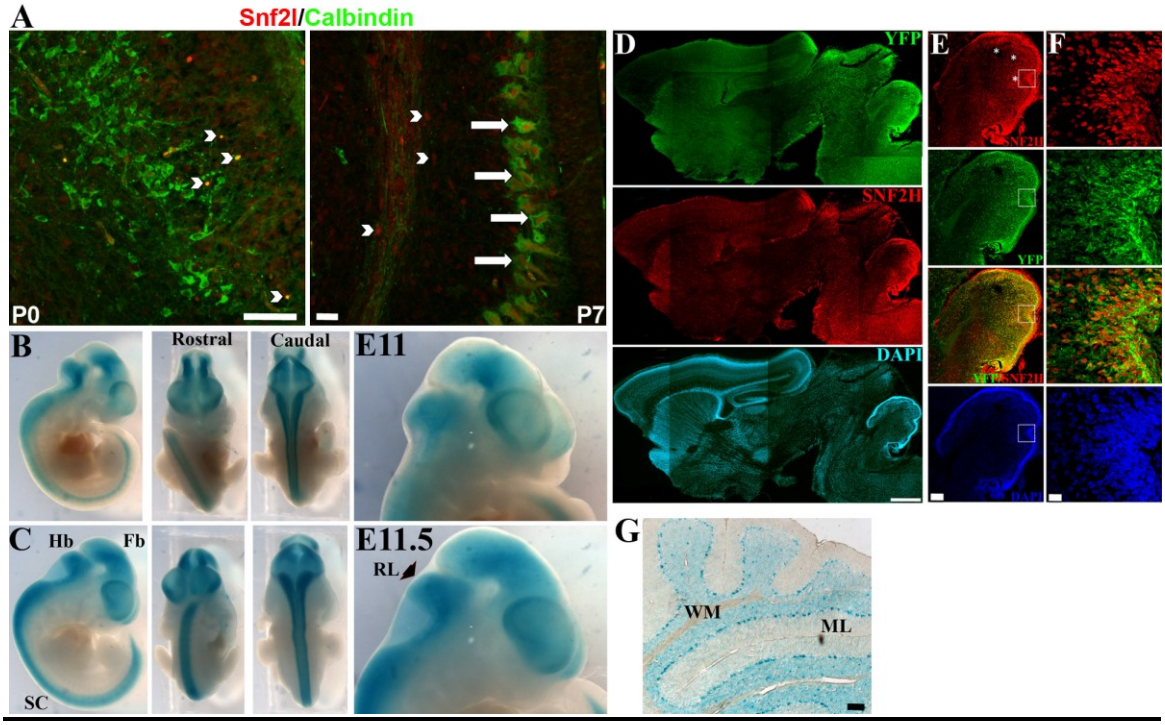

Figure S1. Snf2l is expressed in Purkinje neurons and efficacy of Nestin-Cre deletion to CNS progenitors. **(A)** Wild type cerebellar sections through the cerebellar vermis at P0 and P7 co-labeled with Snf2l (red) and Calbindin (green) antibodies. Note that Snf2l is not expressed in PCs at P0, but in a different Calbindin+ cell lineage (arrowheads), while that at P7 Snf2l is robustly expressed in PCs (arrows) and in cells close to the white matter (arrowheads). Scale bar = 20µm. **(B-C)** ROSA-STOP-LacZ reporter mice were bred to Nestin-Cre mice and X-gal staining performed at the times indicated. Fb = forebrain; Hb = hindbrain; SC = spinal cord; RL = rhombic lip. **(D)** ROSA-STOP-EYFP reporter mice were bred to Nestin-Cre mice and P0 midbrain sagittal sections co-labeled with Snf2h (red) and YFP (green). DAPI (cyan) labels all nuclei. Note robust Snf2h expression in hindbrain areas. Scale bar = 200µm. **(E-F)** 3D rendered confocal Z-stacks through the cerebellar vermis reveals robust co-localization of Snf2h (red) and YFP (green) in nearly all cerebellar progenitors. DAPI (blue) labels all nuclei. Asterisks denote 3 of the 4 principal fissures of the neonatal developing cerebellum (Orvis et al., 2012). Boxed areas are enlarged in (e). Scale bars = 100µm (d); 5µm (e). **(G)** ROSA-STOP-lacZ::Nestin-Cre reporter mice stained with X-Gal at P30, highlighting robust lacZ expression in Purkinje and granule neurons. ML = molecular layer; WM = white matter. Scale bar = 50µm. *Related to Figures 1 and 2.*

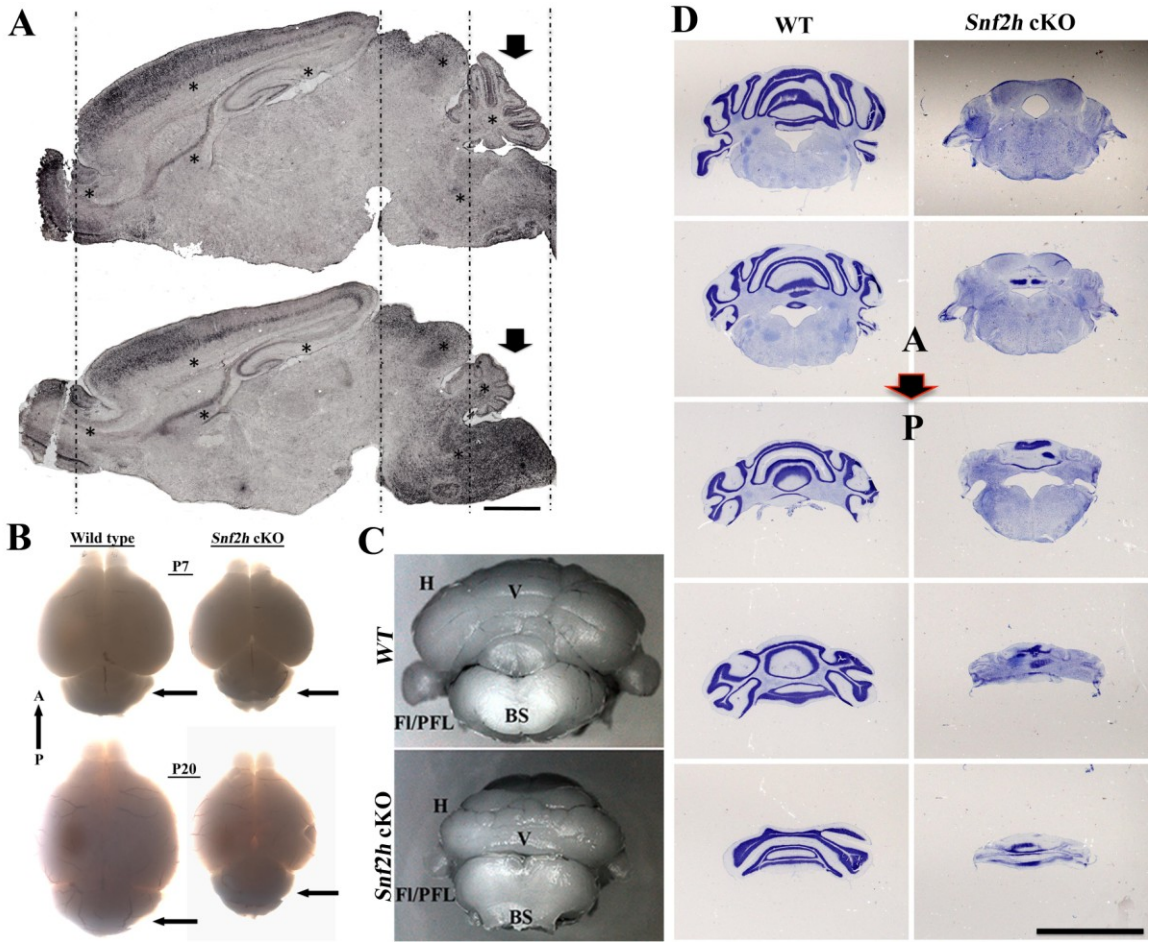

Figure S2. Snf2h cKO by Nestin-Cre produces cerebellar hypoplasia. **(A)** Snf2h immunohistochemistry through the cerebellar vermis at P7 from *Snf2h* cKO and control littermates. Arrows highlight the cerebellar hypoplasia. Asterisks denote regions of robust Snf2h immunoreactivity. Dashed lines delineate the approximate boundaries of the olfactory bulb, midbrain and hindbrain between both genotypes. Scale bar = 200µm. **(B)** Top view of whole brains from P7 and P20 *Snf2h* cKO and control littermates. Arrows highlight the cerebellar hypoplasia. A= anterior; P = posterior. **(C)** Lateral view of whole mount cerebella from P40 *Snf2h* cKO and control littermates. V = vermis; H = hemisphere; FL/PFL = flocculus/paraflocculus; BS = brain stem. **(D)** Nissl stain of transversal sections through the cerebellum from P40 *Snf2h* cKO and control littermates. A = anterior; P = posterior. Scale bar = 500µm. *Related to Figure 2.*

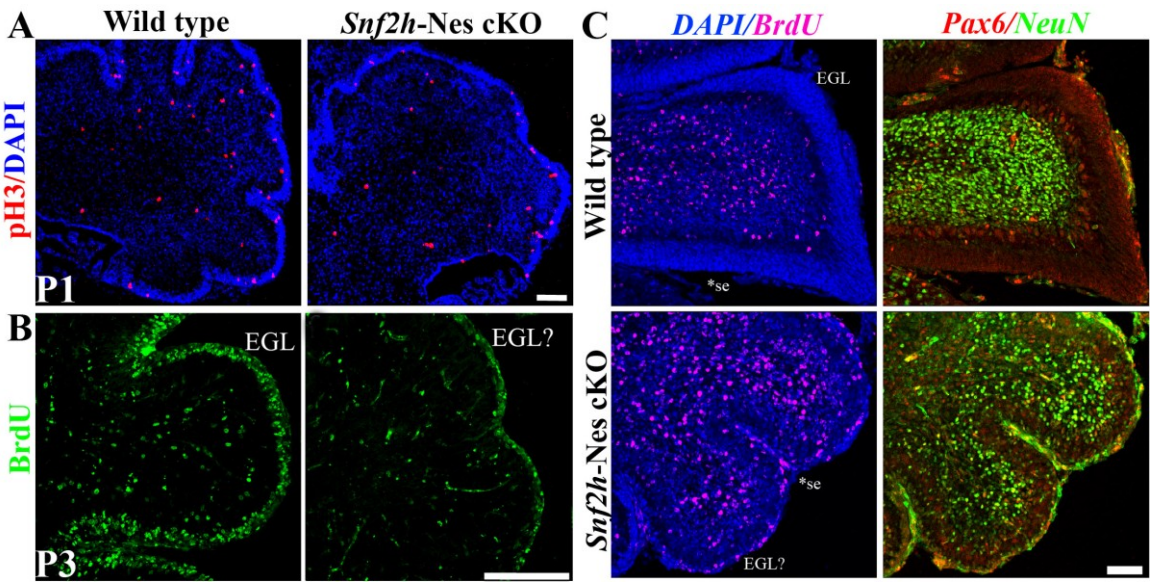

Figure S3. Snf2h loss results in GNP hypoproliferation, but normal differentiation of granule neurons. (A) *P1 sections trough the cerebellar vermis from Snf2h cKO and control littermates immunolabeled* for phospho-Histone H3 (red; pH3). DAPI (blue) stains all nuclei. **(B)** P3 sections trough the cerebellar vermis from *Snf2h* cKO and control mice that had been injected with BrdU 2-hrs before killing. Note the lower number of BrdU+ cells in the external granule layer (EGL) of mutant mice. **(C)** *Snf2h* cKO and control littermates were BrdU-birthdated at E18 and killed 7 days later at P7. Sections through the cerebellar vermis were triple-labeled with BrdU and Pax6, a marker of granule neurons, and NeuN, a marker of postmitotic neurons. Note the equivalent number of differentiated cells in mutant vs. control cerebella. Scale bars = 50μm. *Related to Figure 3.*

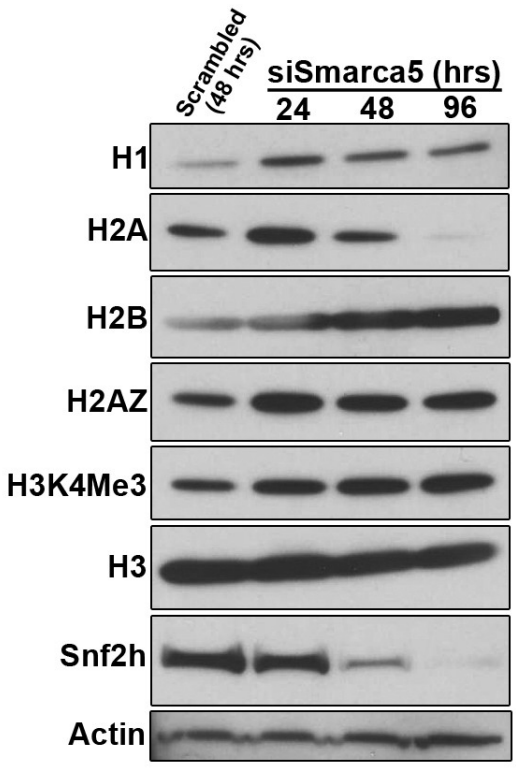

Figure S4. Snf2h siRNA knockdown in Neuro2A cells modestly affects histone H1 and depletes histone H2A. siScrambled and siSnf2h were transiently transfected into Neuro2A cells and acid-extracted histones were prepared at the times indicated. Note that Snf2h levels are rapidly downregulated 48 hrs after knockdown, whereas histone H1 is only modestly affected. Conversely, histone H2A is nearly depleted 96-hrs after knockdown. *Related to Figure 6.*

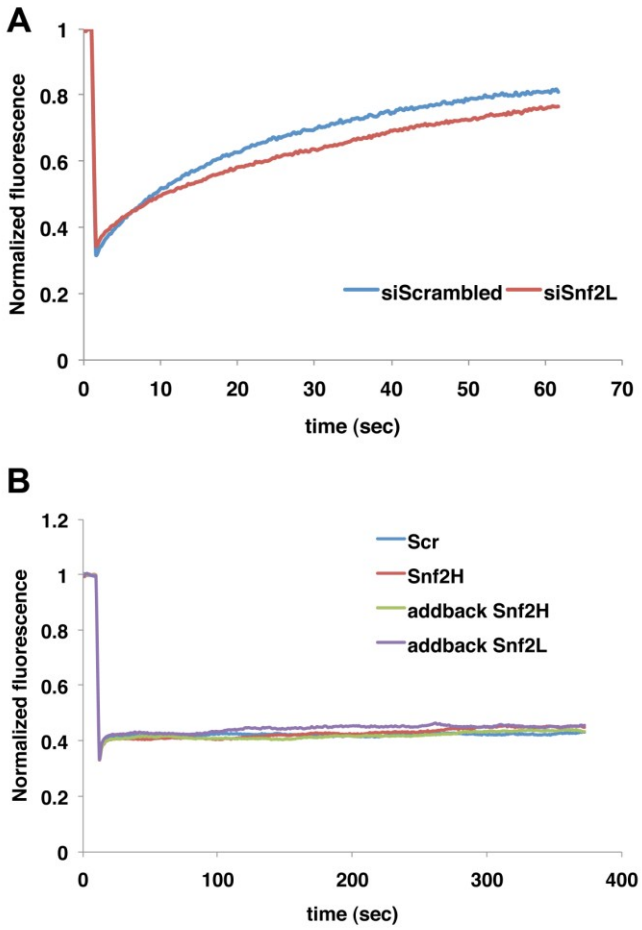

Figure S5. Snf2l does not affect H1e-GFP mobility and H2A-RFP mobility is unaffected by Snf2h knockdown, or Snf2h and Snf2l overexpression. **(A)** H1e-GFP FRAP recovery curves from Neuro2A cells 48-hrs after siSnf2l transfection. **(B)** H2A-RFP FRAP recovery curves from Neuro2A cells 48-hrs after siSnf2h knockdown alone, siSnf2h knockdown + human SNF2H (addback) or siSnf2h knockdown + human SNF2L co-transfection. *Related to Figure 6.*

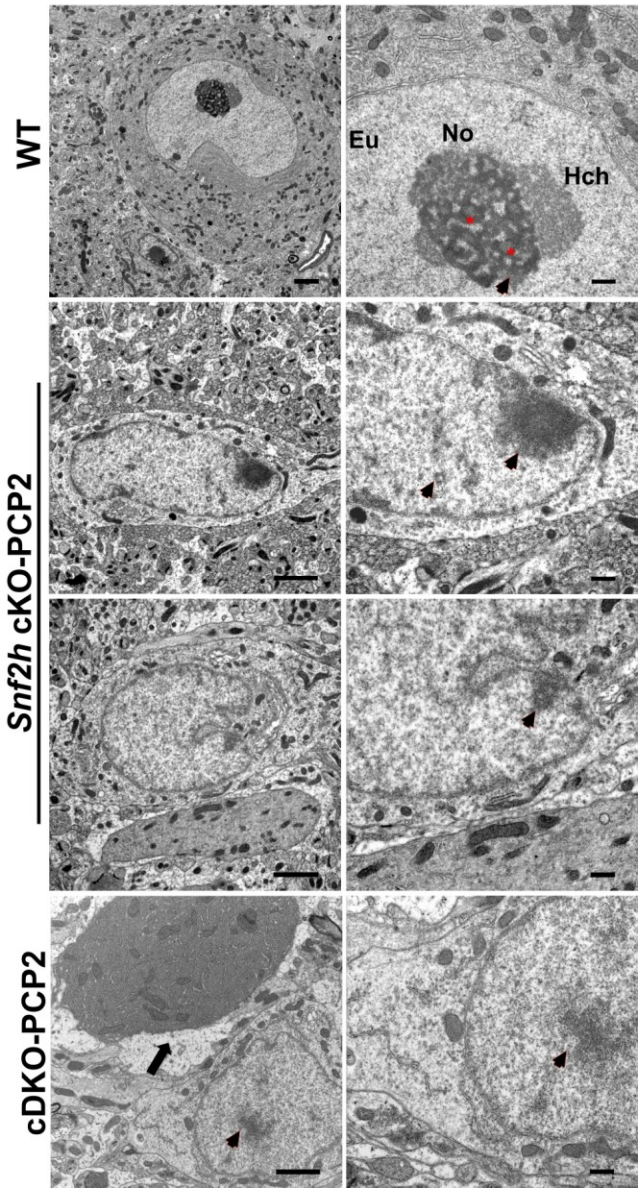

Figure S6. Snf2l deletion aggravates the chromatin ultrastructural alterations observed in Snf2h cKO-PCP2 mice. Transmission electron microscopy (TEM) of PCs through the cerebellar vermis of *Snf2h* cKO-PCP2, cDKO-PCP2 and control mice at P50. Higher magnification are provided to the right of each panel. Note the loss of nucleolar, heterochromatin and euchromatin ultrastructure and increased electron density within mutant PC nuclei. Arrowheads denote electron-dense chromatin clumps in mutant PC nuclei. Arrow denotes pyknotic nuclei in cDKO-PCP2 mice. No = nucleolus; eu = euchromatin; hch = heterochromatin; stars denote dense fibrillar centers. Scale bars = 2μm (left panels); 500nm (right panels). *Related to Figure 6.*

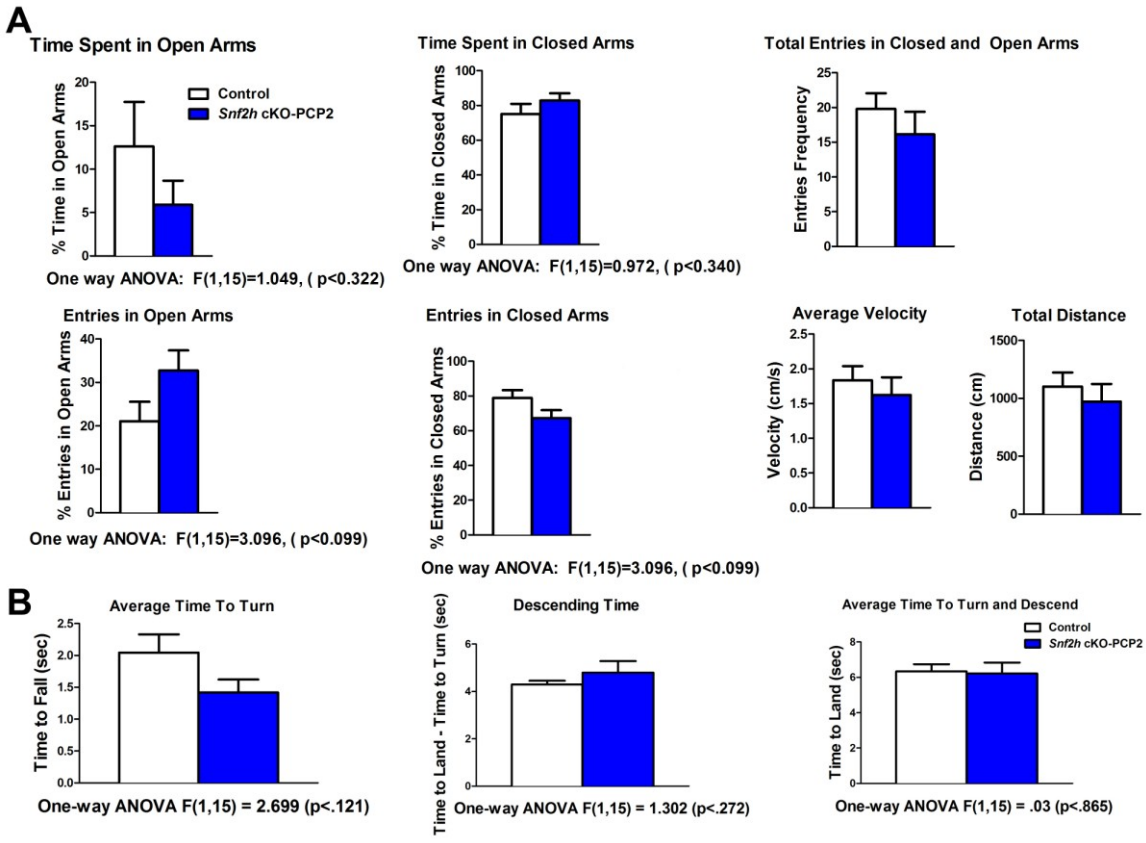

Figure S7. Snf2h cKO-PCP2 mice do not display gross sensorimotor abnormalities. *Snf2h* cKO-PCP2 do not exhibit gross sensorimotor abnormalities in the **(A)** elevated platform or **(B)** pole test relative to controls (n=10-14; one-way ANOVA). *Related to Figure 7.*

SUPPLEMENTARY TABLES

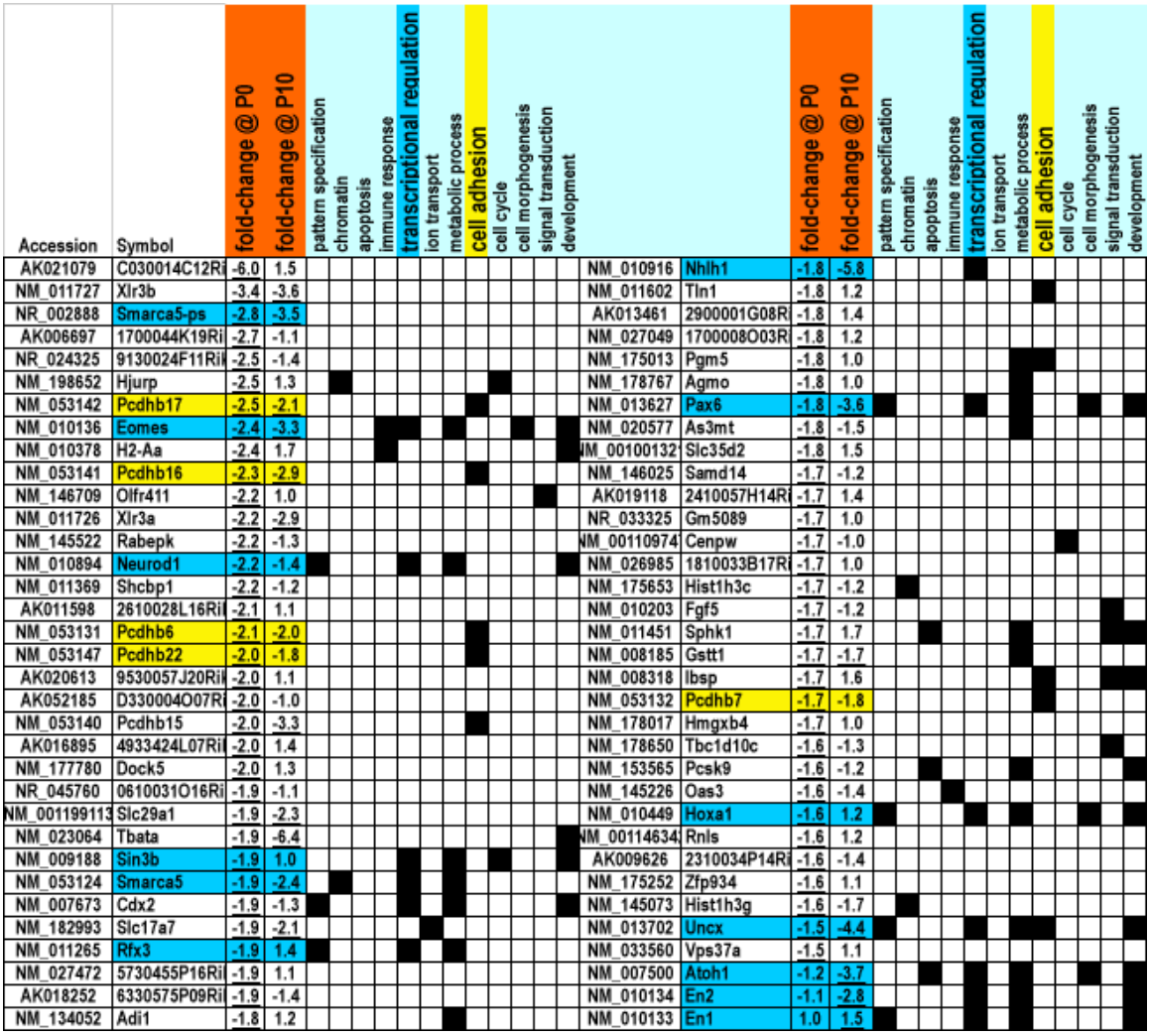

Accession	Symbol	fold-change @ P0	fold-change @ P10	pattern specification	chromatin	apoptosis	immune response	transcriptional regulation	ion transport	metabolic process	cell adhesion	cell cycle	cell morphogenesis	signal transduction	development
AK021079	C030014C12Ri	-6.0	1.5												
NM_011727	Xlr3b	-3.4	-3.6												
NR_002888	Smarca5-ps	-2.8	-3.5												
AK006697	1700044K19Ri	-2.7	-1.1												
NR_024325	9130024F11Ri	-2.5	-1.4												
NM_198652	Hjurp	-2.5	1.3	■								■			
NM_053142	Pcdhb17	-2.5	-2.1								■				
NM_010136	Eomes	-2.4	-3.3				■	■		■			■		■
NM_010378	H2-Aa	-2.4	1.7				■								■
NM_053141	Pcdhb16	-2.3	-2.9								■				
NM_146709	Olfr411	-2.2	1.0											■	
NM_011726	Xlr3a	-2.2	-2.9												
NM_145522	Rabepk	-2.2	-1.3												
NM_010894	Neurod1	-2.2	-1.4	■				■		■					■
NM_011369	Shcbp1	-2.2	-1.2												
AK011598	2610028L16Ri	-2.1	1.1												
NM_053131	Pcdhb6	-2.1	-2.0								■				
NM_053147	Pcdhb22	-2.0	-1.8								■				
AK020613	9530057J20Ri	-2.0	1.1												
AK052185	D330004O07Ri	-2.0	-1.0												
NM_053140	Pcdhb15	-2.0	-3.3								■				
AK016895	4933424L07Ri	-2.0	1.4												
NM_177780	Dock5	-2.0	1.3												
NR_045760	0610031O16Ri	-1.9	-1.1												
NM_001199113	Slc29a1	-1.9	-2.3												
NM_023064	Tbata	-1.9	-6.4												■
NM_009188	Sin3b	-1.9	1.0					■		■		■			■
NM_053124	Smarca5	-1.9	-2.4	■				■		■					
NM_007673	Cdx2	-1.9	-1.3	■				■		■					■
NM_182993	Slc17a7	-1.9	-2.1						■						
NM_011265	Rfx3	-1.9	1.4	■				■		■					
NM_027472	5730455P16Ri	-1.9	1.1												
AK018252	6330575P09Ri	-1.9	-1.4												
NM_134052	Adi1	-1.8	1.2							■					
NM_010916	Nhlh1	-1.8	-5.8												
NM_011602	Tln1	-1.8	1.2								■				
AK013461	2900001G08Ri	-1.8	1.4												
NM_027049	1700008O03Ri	-1.8	1.2												
NM_175013	Pgm5	-1.8	1.0								■				
NM_178767	Agmo	-1.8	1.0								■				
NM_013627	Pax6	-1.8	-3.6	■				■		■			■		■
NM_020577	As3mt	-1.8	-1.5							■					
NM_00100132	Slc35d2	-1.8	1.5												
NM_146025	Samd14	-1.7	-1.2												
AK019118	2410057H14Ri	-1.7	1.4												
NR_033325	Gm5089	-1.7	1.0												
NM_00110974	Cenpw	-1.7	-1.0									■			
NM_026985	1810033B17Ri	-1.7	1.0												
NM_175653	Hist1h3c	-1.7	-1.2	■											
NM_010203	Fgf5	-1.7	-1.2												■
NM_011451	Sphk1	-1.7	1.7		■						■				■
NM_008185	Gstt1	-1.7	-1.7								■				
NM_008318	Ibsp	-1.7	1.6								■				■
NM_053132	Pcdhb7	-1.7	-1.8								■				
NM_178017	Hmgxb4	-1.7	1.0												
NM_178650	Tbc1d10c	-1.6	-1.3												■
NM_153565	Pcsk9	-1.6	-1.2		■						■				
NM_145226	Oas3	-1.6	-1.4			■									
NM_010449	Hoxa1	-1.6	1.2	■				■		■			■		■
NM_00114634	Rnls	-1.6	1.2												
AK009626	2310034P14Ri	-1.6	-1.4												
NM_175252	Zfp934	-1.6	1.1												
NM_145073	Hist1h3g	-1.6	-1.7		■										
NM_013702	Uncx	-1.5	-4.4	■				■		■	■				■
NM_033560	Vps37a	-1.5	1.1												
NM_007500	Atoh1	-1.2	-3.7		■			■		■			■		■
NM_010134	En2	-1.1	-2.8					■		■					■
NM_010133	En1	1.0	1.5	■				■		■					■

Table S1. List of downregulated genes at P0 and corresponding gene expression changes at P10 from Snf2h cKO cerebella. Blue highlights transcription factors and yellow highlights cell adhesion molecules, some of which were validated by qRT-PCR. Note that ~110 genes were deregulated at P0, while ~3,000 genes were deregulated by P10. 3 microarrays per genotype were averaged from wild type and mutant cerebellar extracts from P0 and P10 cerebellar extracts. Underlined values denote $P < 0.05$. Also refer to GEO database (GSE42371). *Related to Figure 4.*

Oligo ID	Symbol	M	log2	A	t	P
NM_178197	Hist1h2bh	**0.25**		14.65	1.79	**0.143801**
NM_175655	Hist1h4f	**0.45**	**1.65**	11.96	2.86	**0.043149**
NM_030609	Hist1h1a	**0.10**		8.41	0.78	**0.476888**
NM_175660	Hist1h2ab	**-0.50**		7.46	-1.31	**0.256655**
NM_013548	Hist1h3f	**0.17**		7.35	1.17	**0.303699**
NM_178193	Hist1h4b	**-0.04**		6.97	-0.13	**0.904670**
NM_178210	Hist1h4j	**-0.27**		14.77	-1.54	**0.195698**
NM_178198	Hist1h2bj	**0.18**		13.93	1.28	**0.265287**
NM_145713	Hist1h1d	**-0.41**		7.15	-1.61	**0.178751**
NM_178183	Hist1h2ak	**0.33**		12.89	2.16	**0.093760**
NM_175663	Hist1h2ba	**-0.13**		11.94	-0.58	**0.588573**
NM_178206	Hist1h3h	**0.19**		13.92	1.32	**0.253692**
NM_178192	Hist1h4a	**0.38**	**1.58**	12.84	2.78	**0.047375**
NM_178193	Hist1h4b	**0.29**		12.04	1.89	**0.127598**
NM_178208	Hist1h4c	**0.66**	**1.82**	10.64	4.44	**0.010149**
NM_175656	Hist1h4i	**0.33**		11.28	1.83	**0.138558**
NM_178211	Hist1h4k	**0.23**		11.19	1.32	**0.255250**
NM_015787	Hist1h1e	**0.42**		8.77	1.94	**0.121511**
NM_145713	Hist1h1d	**0.30**		6.83	0.56	**0.605403**
NM_178200	Hist1h2bm	**0.07**		14.44	0.48	**0.653053**
NM_175664	Hist1h2bb	**0.11**		11.85	0.62	**0.567143**
NM_175659	Hist1h2ah	**-0.01**		13.96	-0.06	**0.951415**
NM_178182	Hist1h2ai	**0.09**		15.22	0.72	**0.510010**
NM_010377	Hist1h1t	**0.14**		7.94	0.42	**0.696434**
NM_178184	Hist1h2an	**0.26**		15.46	1.64	**0.173012**
NM_175658	Hist1h2aa	**-0.53**	**-1.72**	10.81	-3.04	**0.035955**
NM_023422	Hist1h2bc	**0.15**		15.21	1.01	**0.367964**
NM_023422	Hist1h2bc	**0.11**		15.22	0.88	**0.426658**
NM_178185	Hist1h2ao	**0.06**		15.16	0.48	**0.655348**
NM_178204	Hist1h3d	**-0.24**		15.04	-1.86	**0.133156**
NM_153173	Hist1h4h	**-0.36**		7.48	-0.71	**0.514902**
NM_015786	Hist1h1c	**0.86**	**1.94**	14.13	5.42	**0.004889**
NM_178194	Hist1h2be	**0.28**		11.20	1.51	**0.203188**
NM_175657	Hist1h4m	**0.33**		12.18	2.51	**0.063089**
NM_175665	Hist1h2bk	**0.18**		14.22	1.25	**0.275794**
NM_178205	Hist1h3e	**-0.19**		15.14	-1.50	**0.205874**
NM_145073	Hist1h3g	**-0.75**		7.83	-2.72	**0.050298**
NM_178189	Hist1h2ac	**-0.03**		8.74	-0.14	**0.894723**
NM_178188	Hist1h2ad	**0.01**		15.12	0.10	**0.926093**
NM_178196	Hist1h2bg	**0.07**		9.42	0.28	**0.795373**
NM_178201	Hist1h2bn	**0.19**		15.04	1.49	**0.207222**
NM_013548	Hist1h3f	**-0.77**	**-1.89**	7.17	-4.44	**0.010104**
NM_178204	Hist1h3d	**0.28**		9.85	0.97	**0.385013**
NM_153173	Hist1h4h	**0.31**		13.48	2.54	**0.061005**
NM_178199	Hist1h2bl	**-0.08**		14.75	-0.53	**0.624600**
NM_175661	Hist1h2af	**0.12**		15.28	0.98	**0.381203**
NM_178203	Hist1h3b	**0.00**		11.64	0.00	**0.999105**
NM_175654	Hist1h4d	**-0.06**		10.41	-0.29	**0.785791**
NM_178202	Hist1h2bp	**0.11**		14.60	0.84	**0.448296**
NM_178186	Hist1h2ag	**0.08**		15.05	0.59	**0.588007**
NM_013550	Hist1h3a	**-0.01**		7.78	-0.03	**0.974586**
NM_013548	Hist1h3f	**-0.13**		7.29	-0.52	**0.626294**
NM_175653	Hist1h3c	**-0.25**		8.00	-1.21	**0.289339**
NM_020034	Hist1h1b	**0.60**	**1.77**	8.36	3.98	**0.014905**
NM_175656	Hist1h4i	**0.07**		12.78	0.55	**0.608536**
NM_178187	Hist1h2ae	**-0.56**		8.60	-2.21	**0.088468**
NM_178195	Hist1h2bf	**0.12**		14.51	0.77	**0.480539**
NM_178207	Hist1h3i	**-0.41**		9.72	-1.57	**0.188845**

Table S2. Microarray results for genes belonging to the Hist1 gene cluster from P10 Snf2h cKO cerebella. List of *Hist1* genes either significantly downregulated (blue) or upregulated (yellow) from P10 wild type and mutant cerebellar extracts from 3 microarrays per genotype. Highlighted values denote $P < 0.05$. Also refer to GEO database (GSE42371). *Related to Figure 6.*

SUPPLEMENTARY MOVIES.

Movie S1. Top view of three *Snf2h* cKO (agouti) and 2 control littermates (black) at P25. Note the altered mobility and smaller size of mutant mice (28 seconds). *Related to Figure 2.*

Movie S2. Top view of *Snf2h* cKO mouse highlighting the abnormal gait and balance and onset of severe ataxia-like symptoms at ~P20 (20 seconds). *Related to Figure 2.*

Movie S3. Close up view of *Snf2h* cKO mouse highlighting the abnormal grooming and exploratory behavior at the onset of severe ataxia-like symptoms at ~P20 (34 seconds). *Related to Figure 2.*

Movie S4. *Snf2h* cKO mouse in the elevated platform assay at P22 (11 seconds). *Related to Figure 2.*

Movie S5. Control mouse in the elevated platform assay at P22 (30 seconds). *Related to Figure 2.*

Movie S6. Three *Snf2l*$^{-/+}$*::Snf2h* cKO compound ISWI mutants (recognizable by the smaller body size, agouti and black) show an aggravated gait and sensorimotor dysfunction at P25 compared to two control littermates (agouti and black; 31 seconds). *Related to Figure 4.*

Movie S7. Sample movie of H1e-GFP recovery curve before and after photobleaching, approximately 48hrs after siSnf2h transfection of mouse Neuro2A cells (24 seconds). *Related to Figure 6.*

Movie S8. Sample movie of H1e-GFP recovery curve before and after photobleaching, approximately 48hrs after siScrambled transfection of mouse Neuro2A cells (24 seconds). *Related to Figure 6.*

CHAPTER 5: GENERAL DISCUSSION

5.1 Snf2h and Snf2l co-modulate target loci to control neural gene expression programs

The control of cerebellar morphogenesis by the *En1* and *En2* TFs (Cheng et al., 2010), or the *FoxG1*-dependent spatiotemporal control of cortical differentiation (Kumamoto et al., 2013; Miyoshi and Fishell, 2012) provides us with a glimpse of the complexity and specificity in the developmental control of neural gene expression. One phenomenon has been described in which the *Brg1*- and *Brahma*-associated chromatin remodeling subunits Baf45a/Baf53a control neural stem cell proliferation (Lessard et al., 2007). A subunit composition switch to Baf45b/Baf45c/Baf53b allows for neurons to differentiate, demonstrating that subunit composition can further modulate the spatiotemporal specificity of ATP-dependent CRCs for gene expression control (Lessard et al., 2007). However, how CRCs modify the underlying chromatin structure to mediate gene expression and brain development is unknown. Similarly, the molecular mechanisms that control chromatin compaction during lineage specification are poorly understood. In the following sections, I will discuss how mammalian ISWI are involved in the transition from a progenitor to a differentiated neuron in the mouse brain.

5.1.1 Snf2l mediates the transition from a progenitor to a differentiated neuron.

Chapter 2 described the role of the *Snf2l* chromatin remodeler in the developing forebrain. *Snf2l* loss-of-function (*Snf2l* KO hereon) mice develop a larger brain in part due to FoxG1 upregulation. FoxG1 is a critical initiator of neurogenesis through spatiotemporal control of cortical subtypes (Hanashima et al., 2004; Kumamoto et al., 2013). *Snf2l* KO display elevated FoxG1 mRNA and protein levels during mid-neurogenesis, resulting in the overproduction of nearly all cortical subtypes. However, the precise molecular mechanisms

(i.e. at the chromatin level) of how Snf2l loss resulted in the continuous upregulation of *FoxG1* levels are unknown. A tempting hypothesis is that Snf2l is triggered at the onset of cell cycle exit to remodel the FoxG1 locus, reduce gene expression and promote postmitotic identity. This could be achieved by mechanisms such as: a) eviction of variant histones associated with promoter activation (e.g. H2A.Z) (Bruce et al., 2005; Creyghton et al., 2008; Ku et al., 2012); permissiveness for deposition of variant histones involved in repressing gene activity (e.g. macro-H2A) (Chang et al., 2008; Draker and Cheung, 2009; Draker et al., 2012; Sarcinella et al., 2007); or generation of a "poised" nucleosome environment near the TSS for environmental-responsive genes (Coleman-Derr and Zilberman, 2012a; Ku et al., 2012; Voigt et al., 2012). In this regard, *Drosophila* genome-wide mapping revealed that ISWI is bound to intra- and intergenic regions, but highly enriched close to the TSS of gene promoters (Sala et al., 2011). Moreover, *Drosophila Rsf-1* mutants have reduced histone variant H2Av (the H2AX and H2A.Z orthologue in mice and humans) in euchromatic/heterochromatic boundaries (Hanai et al., 2008). Rsf-1 physically interacts with H2Av and the Tip60 complex, known to catalyze H2Av variant exchange, suggesting that Rsf-1 plays a role in histone H2Av exchange to control chromatin boundaries (Hanai et al., 2008; Kusch et al., 2004). Similarly, the histone variant macro-H2A helps maintain X inactivation and gene silencing (Ladurner, 2003). ACF has been shown to remodel macro-H2A-containing nucleosomes and H2A-containing nucleosomes at similar rates (Chang et al., 2008), while ISWI-dependent nucleosome remodeling is enhanced by H2A.Z-containing nucleosomes (Goldman et al., 2010). In mammals, the Snf2h-containing WICH CRC also phosphorylates tyrosine 142 of H2AX to activate the DNA damage response (Xiao et al., 2009). These findings support a role for Snf2h and Snf2l-dependent H2A.Z/macro-H2A

functional interactions to modify the underlying chromatin structure. Thus, ISWI-dependent chromatin remodeling may have evolved to control gene responsiveness through conformational changes to the underlying chromatin structure to repress, activate, or modulate gene expression.

5.1.2 Snf2h activates the expression of essential patterning transcription factors

Snf2h loss in neocortical or cerebellar progenitor pools resulted in enhanced cell death, supporting established roles for Snf2h during the rapid phases of cell proliferation in fly and mouse development (Deuring et al., 2000; Stopka and Skoultchi, 2003). It is noteworthy that RNAi-mediated silencing of WSTF or Snf2h (the only two members of the WICH complex) resulted in the compaction of newly replicated chromatin (Poot et al., 2004). WICH plays an essential role in DNA replication through the maintenance of highly condensed regions of chromatin (Collins et al., 2002). These observations suggest that Snf2h loss in neural progenitors results in abnormal replication of heterochromatin and therefore apoptosis. However, my results also support the idea that improper gene activation of essential patterning TFs essential for cell survival may also contribute to the increased cell mortality observed when Snf2h was ablated rom neural progenitors.

Chapter 3 described how Snf2h is involved in the activation of essential patterning TFs such FoxG1 and Satb2 during early neocortical specification. Similarly, Chapter 4 described how both Snf2h and Snf2l play a role in the spatiotemporal control of *En1* expression during PC development. These results suggest that Snf2h is essential for gene expression activation in neural populations, in part by activating essential patterning TFs, including *FoxG1*, *Satb2* and *En1*. In this regards, it is well established that *FoxG1* is essential for early progenitor specification, but also for postmitotic neuronal development

(Hanashima et al., 2004; Kumamoto et al., 2013; Shen et al., 2006a). Similarly, *En1* is essential for early cerebellar progenitor expansion, as well as postnatal foliation and afferent circuitry development (Sillitoe et al., 2010; Wurst et al., 1994). Thus, Snf2h intricately activates the expression of master TFs that are necessary for progenitor and postmitotic neuronal development.

It is noteworthy that Snf2l was found to be upregulated in both the cortex and cerebellum upon Snf2h deletion, suggesting that Snf2l provides partial compensation upon Snf2h loss. However, the cell-intrinsic effects upon *Snf2h* loss were further augmented by loss of *Snf2l* in cDKO-Emx1, cDKO-PCP2 or cDKO-Nestin mice. For example, cDKO-Nestin mice did not survive past birth, but introduction of a single *Snf2l* allele in females (*Snf2l* is X-linked), allowed for the postnatal survival of *Snf2l*$^{-/+}$*::Snf2h* cKO mice to ~P25. Similarly, cDKO-Emx1 mice have a more pronounced cortical hypoplasia relative to *Snf2h* cKO-Emx1 mice, but lifespan was unaffected amongst strains. How Snf2l provides this transient compensation upon loss of its homologue Snf2h is yet unresolved. It is feasible that Snf2l forms CRCs that mimic the role for endogenous Snf2h during DNA replication, or during postmitotic differentiation as NURF (a Snf2l-containing complex), or as the catalytic subunit of Snf2h-containing CRCs. Future studies that address the spatiotemporal expression and stoichiometry of Snf2h-containing CRCs in the developing and mature mutant brain will shed more insight into the compensatory role of Snf2l upon Snf2h loss in neural progenitors and postmitotic neurons alike.

5.1.3 Snf2h activates the clustered protocadherin genes in postmitotic neurons

Microarray experiments from the neocortex of *Snf2h* cKO-Emx1 revealed a significant downregulation of transcripts from the clustered *Pcdh-β* genes. The mouse and

human *Protocadherin (Pcdh)* genes are organized into three tandemly linked clusters, *Pcdh-α, Pcdh-β* and *Pcdh-γ* (Wu et al., 2001). The *Pcdh-α* and *Pcdh-γ* clusters are composed of 14 and 22 variable-region exons, respectively, and a common set of constant-region exons (Tasic et al., 2002; Wang et al., 2002a). Conversely, the *Pcdh-β* cluster is composed of 22 tandemly arranged single-exon genes that lack a constant region with common exons (Wu et al., 2001). Thus, *Pcdh-β* genes encode unique but similar proteins with a short cytoplasmic domain (Hirano et al., 2012). Theoretically, the multiple clustered *Pcdhs* could generate more than 3×10^{10} possible variations in each neuron and 12,720 types of cis-tetramers per neuron (Yagi, 2012). These findings provide a molecular basis for neuronal individuality that contributes to the overall development of complex neural networks.

How does Snf2h deregulation of the transcriptional activation of the *Pcdh* clusters cause neuronal arborization defects? Deregulation of *Pcdh* gene expression results in abnormal neuronal arborization, altered dendritic self-avoidance, and abnormal synaptic physiology (Lefebvre et al., 2012; Li et al., 2012; Weiner et al., 2005). Similarly, neuronal-specific *CCTC-binding factor (CTCF)* cKO mice have altered *Pcdh* gene expression, neural arborization deficits and abnormal neural physiology (Hirayama et al., 2012). CTCF has gained attention as a key regulator of DNA looping, in part by interacting with the cohesin complex, to transcriptionally activate the clustered *Pcdhs* (Golan-Mashiach et al., 2012; Guo et al., 2012; Hirayama et al., 2012; Kehayova et al., 2011). The CTCF/cohesin complex binds to two symmetrically aligned binding sites in active *Pcdh* promoters to control stochastic *Pcdh* diversity (Guo et al., 2012; Ribich et al., 2006). Interestingly, Snf2h interacts with the Rad21 subunit of the cohesin complex and seems to play a role in the loading of Rad21 onto chromatin (Hakimi et al., 2002). Thus, Snf2h-catalyzed interactions with Rad21

and CTCF may control topological 3D conformations of the *Pcdh* gene cluster to control isoform expression. Moreover, the establishment of chromatin loops may be a general function for ISWI for global gene regulation (Mitchell et al., 2013). This is further supported by evidence that the ISWI orthologue in *Hemicentrotus pulcherrimus* (sea urchin) physically interacts with the Ars1 chromatin insulator proteins that are highly conserved through evolution and play roles in gene activation (Bielinsky et al., 2001; Roth et al., 1983; Yajima et al., 2012). Thus, my findings suggest that Snf2h plays an essential enzymatic and structural role in the transcriptional modulation of gene expression programs during neuronal differentiation through clustered *Pcdh gene* activation.

5.1.4 Snf2h and Satb2 functionally interact to control neural maturation

A fundamental question in developmental neuroscience is how postmitotic neurons find their synaptic targets to establish the neural networks that form the mammalian brain. Evidence suggests that CTCF-mediated control of clustered *Pcdh* gene expression regulates neuronal arborization, barrel cortex formation and synaptic plasticity in the mouse (Hirayama et al., 2012). Deletion of clustered *Pcdh* isoforms also alters dendritic arborization through a process known as self-avoidance, in which dendritic arbors from a single neuron repel each other to minimize gaps and prevent overlaps within its own trajectory (Lefebvre et al., 2012).

Snf2h cKO-Emx1 mice displayed altered neuronal arborization, partial agenesis of corpus callosum and cognitive dysfunctions, partially phenocopying forebrain-specific *CTCF* cKO mice (Hirayama et al., 2012). Interestingly, Chapter 4 shows that Snf2h is necessary for *Satb2* expression in the developing forebrain, as well as in a differentiated Neuro2A cell culture model. Satb2 is a multifaceted protein that regulates neuronal

arborization; and specification of CaPNs at the level of higher order chromatin structure by binding to matrix attachment region (MAR) DNA elements to repress gene expression (Alcamo et al., 2008; Britanova et al., 2005; Britanova et al., 2008; Zhang et al., 2012). MARs are thought to function as mediators of loop attachments, but *in vivo* experiments suggest that they are also used in a highly selective and dynamic fashion (de Belle et al., 1998; Heng et al., 2004; Strukov et al., 2003).

My results suggest a functional link between Snf2h, an activator of gene expression; CTCF, a chromatin architectural protein; and Satb2, a MAR-associated protein, to jointly control DNA looping and clustered *Pcdh* gene activation. Indeed, hSATB2 was able to compensate for Snf2h loss in differentiated Neuro2A cells by upregulation of Snf2h mRNA and protein levels. Thus, Snf2h and Satb2 functionally cooperate to control the gene expression programs necessary for cortical development, in part through clustered *Pcdh* gene regulation. Whether Satb2 is directly interacting with CTCF is currently under investigation. Moreover, current ChIP-Seq studies will assess whether Snf2h binding overlaps CTCF and/or SATB2 binding sites in primary neuronal models.

5.1.5 Snf2h controls the assembly and function of neural networks.

Snf2h ablation in postmitotic Purkinje neurons of the cerebellum, or in neocortical progenitors, resulted in overlapping deficiencies in learning and memory, alterations in social interactions and hyperactive-like symptoms, but no motor dysfunction. Recently, deregulation of the mTOR signaling pathway in Purkinje-specific *Tsc1* cKO mice resulted in mice with hyperactivity, reduced social interactions and deficits in ultrasonic vocalization (Tsai et al., 2012b). My neurobehavioral studies support existing evidence suggesting that Purkinje and cortical dysfunction results in overlapping phenotypes with autistic-like

features (Koziol et al., 2012). The cerebellum mediates the physiology of the motor cortex through PC-derived inhibitory connections to the deep cerebellar nuclei (DCN), which has a di-synaptic excitatory pathway through the ventral thalamus to the motor cortex (Allen and Tsukahara, 1974). Therefore, inhibitory signals from PCs may result in the reduction of excitatory output from the DCN to the motor cortex to impact on its function. This phenomenon has recently been demonstrated in live human studies where cerebellar input to the cerebral cortex contributes to the cerebrocortical processing by adding "forward-model" signals (Sultan et al., 2012). These observations explain the overlapping cognitive phenotypes of *Snf2h* cKO-Emx1 and *Snf2h* cKO-PCP2 mice and provide strong evidence for the functional connection between the cerebellum and the frontal cortex through cerebrocortical networks. My results support the view that abnormalities in PC physiology underlie disorders not just of movement, but also of other cognitive skills such as associative learning, social interactions, and linguistics (Fatemi et al., 2012). Despite the severe hypoplasia of the cortex or cerebellum, *Snf2h* cKO-Emx1, cDKO-Emx1, *Snf2h* cKO-PCP2 and cDKO-PCP2 mice live past 2 years of age and do not display gross abnormalities. These mouse models with autistic-like features provide important insight into the cellular and molecular mechanisms of how mutations affecting epigenetic modulators may cause subtle cognitive deficits through abnormal neural development and connectivity.

Indeed, abnormalities in CaPN connectivity are associated with defects in higher-order associative tasks, such as abstract reasoning and problem-solving (Paul et al., 2007). Similarly, complete or partial agenesis of the corpus callosum results in cognitive deficits (Egaas et al., 1995; Herbert and Kenet, 2007). CaPN dysgenesis is one of the few pathologies consistently identified in autism spectrum disorders (Egaas et al., 1995; Frazier

and Hardan, 2009; Vidal et al., 2006). Superficial-layer CaPNs send collaterals to pyramidal neurons within layers II/III and layer V to act locally in column circuitry, but also project to the contralateral cortex through pyramidal and stellate neurons in layer VI (Garcez et al., 2007; Yorke and Caviness, 1975). Thus, CaPNs are responsible for association and integration among ipsilateral circuits and contralateral cortical hemispheres.

5.2 Snf2h controls chromatin fluidity

The linker histone H1 plays a key role in maintenance of higher-order chromatin structure. ISWI-null flies display a significant reduction in histone H1 levels (Corona et al., 2007). Similarly, a study in *Drosophila* argues for histone H1-dependent control of chromosome rearrangements (Lu et al., 2009). Nevertheless, the mammalian biology of the linker histones is much more complex since multiple histone H1 genes are encoded across three different chromosomal clusters in the mouse and human genomes (Marzluff et al., 2002). They exist in multiple isoforms and undergo a large variety of posttranslational modifications to their unstructured NH_2- and COOH-terminal tails (Harshman et al., 2013). Triple-H1-null mouse embryos (for histone H1c, H1d, and H1e) die at mid-gestation and display a global shortening of nucleosome spacing *in vivo* (Fan et al., 2003). However, triple-H1-null mouse embryonic stem (ES) cells only display modest changes in gene expression, but do present with abnormalities in chromatin compaction (Fan et al., 2005). In *Drosophila,* histone H1 physically interacts with the H3K9 methyltransferase Su(var)3-9 and is essential for heterochromatin maintenance (Lu et al., 2009; Lu et al., 2013). My cell culture experiments in Neuro2A cells (Chapter 6) demonstrate that acute Snf2h knockdown results in reduced recovery rates of tagged H1e-GFP that can be rescued by simultaneous reintroduction of human SNF2H or SNF2L. The rescue observed upon SNF2H or SNF2L

overexpression in H1e-GFP recovery rates argues for a conserved biochemical function between the mammalian ISWI proteins. However, spatiotemporal intrinsic and extrinsic cues, as well as specific interacting partners likely control their precise roles *in vivo*.

5.2.1 Snf2h governs chromatin organization

Live-cell imaging studies showed that during the G1/S-phase of the cell cycle, SNF2H binds only transiently to nucleosomes with ~10-millisecond residence times (Erdel et al., 2010). Conversely, SNF2H binding increases in the range of seconds to minutes during S-phase. These authors proposed a "continuous sampling mechanism" where SNF2H constantly scans the genome in transient binding reactions according to cellular needs (Erdel et al., 2010). Chapter 5 describes how Snf2h is essential for chromatin ultrastructural organization in progenitor and postmitotic Purkinje neurons of the cerebellum. My observations suggest that Snf2h, coupled to histone H1 deposition, is constantly remodeling the 3D topological conformation of the genome to activate gene expression in proliferative and postmitotic cells. This mechanistic role in "genome scanning and fluidity" would explain the rapid progressive deregulation of the genome in the cerebellum of *Snf2h* cKO-Nestin mice from birth to P10, as well the progressive cell death of Purkinje neurons upon postmitotic deletion of the Snf2h protein.

Chapter 5 also shows the progressive loss of histone H2A and its variants upon Snf2h ablation in the developing cerebellum. The C-terminal tail of histone H2A is required for histone H1 loading and Snf2h-dependent nucleosome translocation (Vogler et al., 2010). This raises the idea that Snf2h may promote histone H1 loading onto chromatin through interactions with the C-terminal H2A tail. This mechanism would also explain the progressive loss of macro-H2A, H2A.X and H2A.Z upon Snf2h loss in the developing

cerebellum. I propose that Snf2h loss deregulates histone H1 dynamics, and as a result of abnormal histone H1 linker deposition, H2A.Z-containing loci poised for transcriptional activation are not properly remodeled to generate NFRs (Bruce et al., 2005; Jin et al., 2009; Yen et al., 2012). Consequently, abnormal linker H1 deposition and higher order chromatin packaging and dynamics results in the progressive loss of variant histones, as well as destabilization of the core nucleosome, genome-wide hypoactivation and cell death. Similarly, the progressive loss of H2A.X and macro-H2A can also reflect alterations in the proper maintenance of heterochromatin, as Snf2h is a member of the NoRC complex involved in gene silencing (Guetg et al., 2010; Santoro et al., 2002; Strohner et al., 2001). This progressive combinatorial failure to activate target genes (i.e. *FoxG1, En1* or clustered *Pcdh* isoforms), and the abnormal de-repression of silenced genes likely underlie the complexity of the Snf2h-null neuronal phenotype through its interactions with RSF, ACF, CHRAC, WICH, and NoRC. Despite this complexity, my results suggest that Snf2h is directly involved in histone H1 dynamics *in vivo* to topologically remodel the genome for gene activity and fluidity during all stages of neural development.

5.2.2 Epigenetic control of hyperactive patterning genes.

Histone variants and modified histones work as templates for chromatin remodeling complexes to activate genes. In yeast, the H2A.Z paralogue Htz1 can be acetylated at Lysine (Lys) 3, 8, 10 and 14, where Lys 14 acetylation is most highly enriched at active gene promoters (Millar et al., 2006). Conversely, H2A.Z monoubiquitylation is a specific mark that distinguishes H2A.Z-associated heterochromatin (Sarcinella et al., 2007). Thus, the H2AZ genomic landscape is complex, but it is evident that H2A.Z is controlled at the level of PTMs, and its acetylation or ubiquitination controls its role in gene activation or

repression, respectively. Thus, Snf2h and Snf2l co-modulation of target loci may be regulated through the remodeling of nucleosomes tagged with specific post-translationally modified variant histones, such as acetylation or ubiquitination of H2A.Z, H2A.X or macro-H2A, amongst others. I thus propose that the ISWI homologues diverged in mammals to mediate the transition of a progenitor neuron to a differentiated lineage, through Snf2h- and Snf2l-dependent co-modulation and chromatin conformational changes at common target loci. I have proposed a model where Snf2h-dependent chromatin remodeling is partially initiated by its recruitment to hyperacetylated H2AZ–containing nucleosomes **(Figure 5.1)** (Draker et al., 2012; Sarcinella et al., 2007). Upon recognition and binding, Snf2h-dependent nucleosome remodeling at three-dimensional transcriptional hubs allows for transcriptional initiation and elongation. The cooperative recruitment of CRCs and TFs to hyperactive genomic loci controls embryonic progenitor expansion, neural differentiation and maturation. Upon Snf2h loss, deficient chromatin remodeling activity results in genome-wide deregulation. These events also result in the progressive destabilization of higher order chromatin structure, in part through abnormal histone H1 deposition and deregulation of chromatin fluidity. During early progenitor expansion, Snf2h loss results in abnormal DNA replication and hypoactivation of patterning TFs, whereas in postmitotic neurons the clustered *Pcdh* isoforms become hypoactivated.

An essential remaining question is how Snf2l modulates the chromatin structure to modulate gene expression and promote neural differentiation. This process could be modulated in the following ways: a) Snf2l mediates the eviction of H2A.Z/H3.3 bivalent nucleosomes to repress hyperactive loci; b) Snf2l cooperates with other histone-modifying complexes to mediate the deposition of macro-H2A and promote heterochromatin formation;

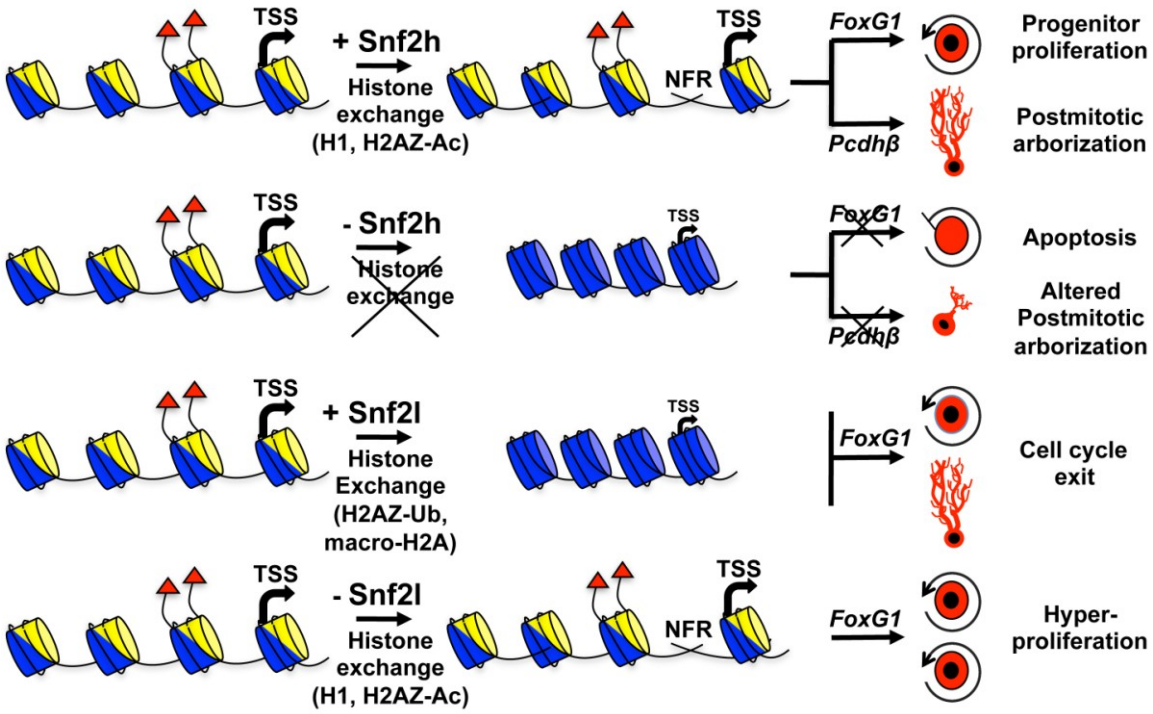

Figure 5.1. Proposed model of Snf2h- and Snf2l-dependent gene expression control during brain development.

Top Panels: Snf2h catalyzes histone exchange (e.g. histone H1) and nucleosome remodeling of hyperacetylated (red triangles) H2A.Z-containing nucleosomes (blue-yellow bins) near target transcriptional start sites (TSS) to activate gene expression (Coleman-Derr and Zilberman, 2012a, b; Ku et al., 2012; Voigt et al., 2012). Snf2h-dependent *FoxG1* activation in cortical progenitors results in cell proliferation and specification, while Snf2h-dependent *Pcdhß* gene activation results in postmitotic arborization and neural maturation. Upon Snf2h loss, histone exchange is interrupted and target genes hypoactivated (blue bins), resulting in transcriptional silencing, progenitor cell death, abnormal postmitotic arborization, and cognitive deficits.

Bottom Panels: Snf2l catalyzes histone exchange (e.g. histone H1) and nucleosome remodeling of hyperacetylated (red triangles) H2AZ-containing nucleosomes (blue-yellow bins) for transcriptional silencing of target genes (blue bins) through the deposition of H2A variant histones (Lagarou et al., 2008; Ma et al., 2011; Sin et al., 2012; Smith et al., 2004; Stock et al., 2007). Thus, coordinated spatiotemporal *FoxG1* repression results in cell cycle withdrawal and neuronal differentiation. Upon Snf2l loss, Snf2h-dependent histone exchange persists and *FoxG1* levels remain upregulated, resulting in cortical progenitor hyperproliferation and a larger brain (Yip et al., 2012).

c) or Snf2l binding to target loci inhibits Snf2h binding to prevent gene activation, but target loci remain "poised" for environmental-dependent stimuli **(Figure 5.1)** (Coleman-Derr and Zilberman, 2012a, b). Whichever the case, Snf2l-mediated chromatin remodeling plays an important role in neural differentiation by modulation in the gene expression levels of patterning TFs (Barak et al., 2003; Lazzaro and Picketts, 2001a; Yip et al., 2012). It is noteworthy that *FoxG1, En1* or clustered *Pcdh* expression is never fully turned off in differentiated mammalian neurons (Hirayama and Yagi, 2013; Shen et al., 2006a; Wilson et al., 2011), suggesting that Snf2l-mediated target repression could be reversible upon specific environmental stimuli through Snf2l de-repression and Snf2h-dependent gene activation.

5.3 Future perspectives

To gain insight into the genome-wide distribution of Snf2h and Snf2l-containing CRCs, I will perform high-throughput ChIP-Sequencing experiments in progenitor and differentiated neurons. For this end, I will assess the genome-wide binding for CTCF, Satb2, Snf2h and Snf2l in progenitor and differentiated cerebellar granule neurons. These experiments aim to unravel Snf2h and Snf2l regulatory binding sites and their relationship to CTCF- and Satb2-mediated chromatin topology.

My latest findings also revealed that voluntary running significantly rescues the motor alterations and lifespan of *Snf2h* cKO-Nestin mice for more than 1 year, which under standard laboratory conditions do not survive past ~P45. Genome-wide transcriptome analysis (RNA-Sequencing) in mutant and control runner and sedentary cerebella identified the upregulation of multiple neuropeptides and growth factors relative to sedentary controls, some of which were previously identified to be upregulated by running in the hippocampus.

My current efforts aim to identify the molecular signaling pathways behind the running-induced brain repair mechanisms observed in *Snf2h* cKO-Nestin mice through cellular, molecular and pharmacological studies.

REFERENCES

Abrams, E., Neigeborn, L., and Carlson, M. (1986). Molecular analysis of SNF2 and SNF5, genes required for expression of glucose-repressible genes in Saccharomyces cerevisiae. Molecular and cellular biology *6*, 3643-3651.

Ahn, A.H., Dziennis, S., Hawkes, R., and Herrup, K. (1994). The cloning of zebrin II reveals its identity with aldolase C. Development *120*, 2081-2090.

Alcamo, E.A., Chirivella, L., Dautzenberg, M., Dobreva, G., Farinas, I., Grosschedl, R., and McConnell, S.K. (2008). Satb2 regulates callosal projection neuron identity in the developing cerebral cortex. Neuron *57*, 364-377.

Allen, G.I., and Tsukahara, N. (1974). Cerebrocerebellar communication systems. Physiological reviews *54*, 957-1006.

Altman, J., and Bayer, S.A. (1985). Embryonic development of the rat cerebellum. III. Regional differences in the time of origin, migration, and settling of Purkinje cells. The Journal of comparative neurology *231*, 42-65.

Andersen, E.C., Lu, X., and Horvitz, H.R. (2006). C. elegans ISWI and NURF301 antagonize an Rb-like pathway in the determination of multiple cell fates. Development *133*, 2695-2704.

Angley, C., Kumar, M., Dinsio, K.J., Hall, A.K., and Siegel, R.E. (2003). Signaling by bone morphogenetic proteins and Smad1 modulates the postnatal differentiation of cerebellar cells. The Journal of neuroscience : the official journal of the Society for Neuroscience *23*, 260-268.

Arlotta, P., Molyneaux, B.J., Chen, J., Inoue, J., Kominami, R., and Macklis, J.D. (2005). Neuronal subtype-specific genes that control corticospinal motor neuron development in vivo. Neuron *45*, 207-221.

Badenhorst, P., Voas, M., Rebay, I., and Wu, C. (2002). Biological functions of the ISWI chromatin remodeling complex NURF. Genes & development *16*, 3186-3198.

Bagchi, A., Papazoglu, C., Wu, Y., Capurso, D., Brodt, M., Francis, D., Bredel, M., Vogel, H., and Mills, A.A. (2007). CHD5 is a tumor suppressor at human 1p36. Cell *128*, 459-475.

Bajpai, R., Chen, D.A., Rada-Iglesias, A., Zhang, J., Xiong, Y., Helms, J., Chang, C.P., Zhao, Y., Swigut, T., and Wysocka, J. (2010). CHD7 cooperates with PBAF to control multipotent neural crest formation. Nature *463*, 958-962.

Bakshi, R., Prakash, T., Dash, D., and Brahmachari, V. (2004). In silico characterization of the INO80 subfamily of SWI2/SNF2 chromatin remodeling proteins. Biochemical and biophysical research communications *320*, 197-204.

Banting, G.S., Barak, O., Ames, T.M., Burnham, A.C., Kardel, M.D., Cooch, N.S., Davidson, C.E., Godbout, R., McDermid, H.E., and Shiekhattar, R. (2005). CECR2, a protein involved in neurulation, forms a novel chromatin remodeling complex with SNF2L. Human molecular genetics *14*, 513-524.

Barak, O., Lazzaro, M.A., Lane, W.S., Speicher, D.W., Picketts, D.J., and Shiekhattar, R. (2003). Isolation of human NURF: a regulator of Engrailed gene expression. The EMBO journal *22*, 6089-6100.

Baranek, C., Dittrich, M., Parthasarathy, S., Bonnon, C.G., Britanova, O., Lanshakov, D., Boukhtouche, F., Sommer, J.E., Colmenares, C., Tarabykin, V.*, et al.* (2012). Protooncogene Ski cooperates with the chromatin-remodeling factor Satb2 in

specifying callosal neurons. Proceedings of the National Academy of Sciences of the United States of America *109*, 3546-3551.
Barnett, C., Yazgan, O., Kuo, H.C., Malakar, S., Thomas, T., Fitzgerald, A., Harbour, W., Henry, J.J., and Krebs, J.E. (2012). Williams Syndrome Transcription Factor is critical for neural crest cell function in Xenopus laevis. Mechanisms of development *129*, 324-338.
Barski, J.J., Dethleffsen, K., and Meyer, M. (2000). Cre recombinase expression in cerebellar Purkinje cells. Genesis *28*, 93-98.
Bedogni, F., Hodge, R.D., Elsen, G.E., Nelson, B.R., Daza, R.A., Beyer, R.P., Bammler, T.K., Rubenstein, J.L., and Hevner, R.F. (2010). Tbr1 regulates regional and laminar identity of postmitotic neurons in developing neocortex. Proceedings of the National Academy of Sciences of the United States of America *107*, 13129-13134.
Ben-Arie, N., Bellen, H.J., Armstrong, D.L., McCall, A.E., Gordadze, P.R., Guo, Q., Matzuk, M.M., and Zoghbi, H.Y. (1997). Math1 is essential for genesis of cerebellar granule neurons. Nature *390*, 169-172.
Berube, N.G., Mangelsdorf, M., Jagla, M., Vanderluit, J., Garrick, D., Gibbons, R.J., Higgs, D.R., Slack, R.S., and Picketts, D.J. (2005). The chromatin-remodeling protein ATRX is critical for neuronal survival during corticogenesis. J Clin Invest *115*, 258-267.
Bielinsky, A.K., Blitzblau, H., Beall, E.L., Ezrokhi, M., Smith, H.S., Botchan, M.R., and Gerbi, S.A. (2001). Origin recognition complex binding to a metazoan replication origin. Current biology : CB *11*, 1427-1431.
Bowen, N.J., Fujita, N., Kajita, M., and Wade, P.A. (2004). Mi-2/NuRD: multiple complexes for many purposes. Biochimica et biophysica acta *1677*, 52-57.
Boyer, L.A., Langer, M.R., Crowley, K.A., Tan, S., Denu, J.M., and Peterson, C.L. (2002). Essential role for the SANT domain in the functioning of multiple chromatin remodeling enzymes. Molecular cell *10*, 935-942.
Bozhenok, L., Wade, P.A., and Varga-Weisz, P. (2002). WSTF-ISWI chromatin remodeling complex targets heterochromatic replication foci. The EMBO journal *21*, 2231-2241.
Brancaccio, M., Pivetta, C., Granzotto, M., Filippis, C., and Mallamaci, A. (2010). Emx2 and Foxg1 inhibit gliogenesis and promote neuronogenesis. Stem Cells *28*, 1206-1218.
Brasted, A. (1941). An Analysis of the Expression of the Mutant "Engrailed" in Drosophila Melanogaster. Genetics *26*, 347-373.
Britanova, O., Akopov, S., Lukyanov, S., Gruss, P., and Tarabykin, V. (2005). Novel transcription factor Satb2 interacts with matrix attachment region DNA elements in a tissue-specific manner and demonstrates cell-type-dependent expression in the developing mouse CNS. The European journal of neuroscience *21*, 658-668.
Britanova, O., de Juan Romero, C., Cheung, A., Kwan, K.Y., Schwark, M., Gyorgy, A., Vogel, T., Akopov, S., Mitkovski, M., Agoston, D*., et al.* (2008). Satb2 is a postmitotic determinant for upper-layer neuron specification in the neocortex. Neuron *57*, 378-392.
Broccoli, V., Boncinelli, E., and Wurst, W. (1999). The caudal limit of Otx2 expression positions the isthmic organizer. Nature *401*, 164-168.
Brochu, G., Maler, L., and Hawkes, R. (1990). Zebrin II: a polypeptide antigen expressed selectively by Purkinje cells reveals compartments in rat and fish cerebellum. The Journal of comparative neurology *291*, 538-552.

Bruce, K., Myers, F.A., Mantouvalou, E., Lefevre, P., Greaves, I., Bonifer, C., Tremethick, D.J., Thorne, A.W., and Crane-Robinson, C. (2005). The replacement histone H2A.Z in a hyperacetylated form is a feature of active genes in the chicken. Nucleic acids research *33*, 5633-5639.
Bugga, L., McDaniel, I.E., Engie, L., and Armstrong, J.A. (2013). The Drosophila melanogaster CHD1 chromatin remodeling factor modulates global chromosome structure and counteracts HP1a and H3K9me2. PloS one *8*, e59496.
Bulchand, S., Grove, E.A., Porter, F.D., and Tole, S. (2001). LIM-homeodomain gene Lhx2 regulates the formation of the cortical hem. Mechanisms of development *100*, 165-175.
Bultman, S., Gebuhr, T., Yee, D., La Mantia, C., Nicholson, J., Gilliam, A., Randazzo, F., Metzger, D., Chambon, P., Crabtree, G.*, et al.* (2000). A Brg1 null mutation in the mouse reveals functional differences among mammalian SWI/SNF complexes. Molecular cell *6*, 1287-1295.
Bultman, S.J., Gebuhr, T.C., Pan, H., Svoboda, P., Schultz, R.M., and Magnuson, T. (2006). Maternal BRG1 regulates zygotic genome activation in the mouse. Genes & development *20*, 1744-1754.
Burgio, G., La Rocca, G., Sala, A., Arancio, W., Di Gesu, D., Collesano, M., Sperling, A.S., Armstrong, J.A., van Heeringen, S.J., Logie, C.*, et al.* (2008). Genetic identification of a network of factors that functionally interact with the nucleosome remodeling ATPase ISWI. PLoS Genet *4*, e1000089.
Cai, Y., Jin, J., Yao, T., Gottschalk, A.J., Swanson, S.K., Wu, S., Shi, Y., Washburn, M.P., Florens, L., Conaway, R.C.*, et al.* (2007). YY1 functions with INO80 to activate transcription. Nature structural & molecular biology *14*, 872-874.
Caric, D., Gooday, D., Hill, R.E., McConnell, S.K., and Price, D.J. (1997). Determination of the migratory capacity of embryonic cortical cells lacking the transcription factor Pax-6. Development *124*, 5087-5096.
Chang, E.Y., Ferreira, H., Somers, J., Nusinow, D.A., Owen-Hughes, T., and Narlikar, G.J. (2008). MacroH2A allows ATP-dependent chromatin remodeling by SWI/SNF and ACF complexes but specifically reduces recruitment of SWI/SNF. Biochemistry *47*, 13726-13732.
Chen, B., Wang, S.S., Hattox, A.M., Rayburn, H., Nelson, S.B., and McConnell, S.K. (2008). The Fezf2-Ctip2 genetic pathway regulates the fate choice of subcortical projection neurons in the developing cerebral cortex. Proceedings of the National Academy of Sciences of the United States of America *105*, 11382-11387.
Cheng, Y., Sudarov, A., Szulc, K.U., Sgaier, S.K., Stephen, D., Turnbull, D.H., and Joyner, A.L. (2010). The Engrailed homeobox genes determine the different foliation patterns in the vermis and hemispheres of the mammalian cerebellum. Development *137*, 519-529.
Chi, C.L., Martinez, S., Wurst, W., and Martin, G.R. (2003). The isthmic organizer signal FGF8 is required for cell survival in the prospective midbrain and cerebellum. Development *130*, 2633-2644.
Chiara, F., Badaloni, A., Croci, L., Yeh, M.L., Cariboni, A., Hoerder-Suabedissen, A., Consalez, G.G., Eickholt, B., Shimogori, T., Parnavelas, J.G.*, et al.* (2012). Early B-cell factors 2 and 3 (EBF2/3) regulate early migration of Cajal-Retzius cells from the cortical hem. Developmental biology *365*, 277-289.

Chioda, M., Vengadasalam, S., Kremmer, E., Eberharter, A., and Becker, P.B. (2010). Developmental role for ACF1-containing nucleosome remodellers in chromatin organisation. Development *137*, 3513-3522.
Cho, J.H., and Tsai, M.J. (2006). Preferential posterior cerebellum defect in BETA2/NeuroD1 knockout mice is the result of differential expression of BETA2/NeuroD1 along anterior-posterior axis. Developmental biology *290*, 125-138.
Choeiri, C., Hewitt, K., Durkin, J., Simard, C.J., Renaud, J.M., and Messier, C. (2005). Longitudinal evaluation of memory performance and peripheral neuropathy in the Ins2C96Y Akita mice. Behav Brain Res *157*, 31-38.
Coleman-Derr, D., and Zilberman, D. (2012a). Deposition of histone variant H2A.Z within gene bodies regulates responsive genes. PLoS genetics *8*, e1002988.
Coleman-Derr, D., and Zilberman, D. (2012b). DNA methylation, H2A.Z, and the regulation of constitutive expression. Cold Spring Harbor symposia on quantitative biology *77*, 147-154.
Collins, N., Poot, R.A., Kukimoto, I., Garcia-Jimenez, C., Dellaire, G., and Varga-Weisz, P.D. (2002). An ACF1-ISWI chromatin-remodeling complex is required for DNA replication through heterochromatin. Nature genetics *32*, 627-632.
Corona, D.F., Langst, G., Clapier, C.R., Bonte, E.J., Ferrari, S., Tamkun, J.W., and Becker, P.B. (1999). ISWI is an ATP-dependent nucleosome remodeling factor. Molecular cell *3*, 239-245.
Corona, D.F., Siriaco, G., Armstrong, J.A., Snarskaya, N., McClymont, S.A., Scott, M.P., and Tamkun, J.W. (2007). ISWI regulates higher-order chromatin structure and histone H1 assembly in vivo. PLoS biology *5*, e232.
Cote, J., Quinn, J., Workman, J.L., and Peterson, C.L. (1994). Stimulation of GAL4 derivative binding to nucleosomal DNA by the yeast SWI/SNF complex. Science *265*, 53-60.
Creyghton, M.P., Markoulaki, S., Levine, S.S., Hanna, J., Lodato, M.A., Sha, K., Young, R.A., Jaenisch, R., and Boyer, L.A. (2008). H2AZ is enriched at polycomb complex target genes in ES cells and is necessary for lineage commitment. Cell *135*, 649-661.
Cuadrado, A., Remeseiro, S., Gomez-Lopez, G., Pisano, D.G., and Losada, A. (2012). The specific contributions of cohesin-SA1 to cohesion and gene expression: implications for cancer and development. Cell Cycle *11*, 2233-2238.
Cubelos, B., Sebastian-Serrano, A., Beccari, L., Calcagnotto, M.E., Cisneros, E., Kim, S., Dopazo, A., Alvarez-Dolado, M., Redondo, J.M., Bovolenta, P.*, et al.* (2010). Cux1 and Cux2 regulate dendritic branching, spine morphology, and synapses of the upper layer neurons of the cortex. Neuron *66*, 523-535.
de Belle, I., Cai, S., and Kohwi-Shigematsu, T. (1998). The genomic sequences bound to special AT-rich sequence-binding protein 1 (SATB1) in vivo in Jurkat T cells are tightly associated with the nuclear matrix at the bases of the chromatin loops. The Journal of cell biology *141*, 335-348.
Deuring, R., Fanti, L., Armstrong, J.A., Sarte, M., Papoulas, O., Prestel, M., Daubresse, G., Verardo, M., Moseley, S.L., Berloco, M.*, et al.* (2000). The ISWI chromatin-remodeling protein is required for gene expression and the maintenance of higher order chromatin structure in vivo. Molecular cell *5*, 355-365.

Diesinger, P.M., and Heermann, D.W. (2008). The influence of the cylindrical shape of the nucleosomes and H1 defects on properties of chromatin. Biophysical journal *94*, 4165-4172.
Dingwall, A.K., Beek, S.J., McCallum, C.M., Tamkun, J.W., Kalpana, G.V., Goff, S.P., and Scott, M.P. (1995). The Drosophila snr1 and brm proteins are related to yeast SWI/SNF proteins and are components of a large protein complex. Molecular biology of the cell *6*, 777-791.
Dirscherl, S.S., Henry, J.J., and Krebs, J.E. (2005). Neural and eye-specific defects associated with loss of the imitation switch (ISWI) chromatin remodeler in Xenopus laevis. Mechanisms of development *122*, 1157-1170.
Dirscherl, S.S., and Krebs, J.E. (2004). Functional diversity of ISWI complexes. Biochem Cell Biol *82*, 482-489.
Dou, C.L., Li, S., and Lai, E. (1999). Dual role of brain factor-1 in regulating growth and patterning of the cerebral hemispheres. Cereb Cortex *9*, 543-550.
Draker, R., and Cheung, P. (2009). Transcriptional and epigenetic functions of histone variant H2A.Z. Biochemistry and cell biology = Biochimie et biologie cellulaire *87*, 19-25.
Draker, R., Ng, M.K., Sarcinella, E., Ignatchenko, V., Kislinger, T., and Cheung, P. (2012). A combination of H2A.Z and H4 acetylation recruits Brd2 to chromatin during transcriptional activation. PLoS genetics *8*, e1003047.
Duckett, S., and Pearse, A.G. (1968). The cells of Cajal-Retzius in the developing human brain. Journal of anatomy *102*, 183-187.
Eagleson, K.L., Schlueter McFadyen-Ketchum, L.J., Ahrens, E.T., Mills, P.H., Does, M.D., Nickols, J., and Levitt, P. (2007). Disruption of Foxg1 expression by knock-in of cre recombinase: effects on the development of the mouse telencephalon. Neuroscience *148*, 385-399.
Eberharter, A., Ferrari, S., Langst, G., Straub, T., Imhof, A., Varga-Weisz, P., Wilm, M., and Becker, P.B. (2001). Acf1, the largest subunit of CHRAC, regulates ISWI-induced nucleosome remodelling. The EMBO journal *20*, 3781-3788.
Eberharter, A., Vetter, I., Ferreira, R., and Becker, P.B. (2004). ACF1 improves the effectiveness of nucleosome mobilization by ISWI through PHD-histone contacts. The EMBO journal *23*, 4029-4039.
Edwards, M.A., Yamamoto, M., and Caviness, V.S., Jr. (1990). Organization of radial glia and related cells in the developing murine CNS. An analysis based upon a new monoclonal antibody marker. Neuroscience *36*, 121-144.
Efroni, S., Duttagupta, R., Cheng, J., Dehghani, H., Hoeppner, D.J., Dash, C., Bazett-Jones, D.P., Le Grice, S., McKay, R.D., Buetow, K.H.*, et al.* (2008). Global transcription in pluripotent embryonic stem cells. Cell stem cell *2*, 437-447.
Egaas, B., Courchesne, E., and Saitoh, O. (1995). Reduced size of corpus callosum in autism. Archives of neurology *52*, 794-801.
Egan, C.M., Nyman, U., Skotte, J., Streubel, G., Turner, S., O'Connell, D.J., Rraklli, V., Dolan, M.J., Chadderton, N., Hansen, K.*, et al.* (2013). CHD5 Is Required for Neurogenesis and Has a Dual Role in Facilitating Gene Expression and Polycomb Gene Repression. Developmental cell *26*, 223-236.

Eisen, J.A., Sweder, K.S., and Hanawalt, P.C. (1995). Evolution of the SNF2 family of proteins: subfamilies with distinct sequences and functions. Nucleic acids research *23*, 2715-2723.
Elfring, L.K., Deuring, R., McCallum, C.M., Peterson, C.L., and Tamkun, J.W. (1994). Identification and characterization of Drosophila relatives of the yeast transcriptional activator SNF2/SWI2. Molecular and cellular biology *14*, 2225-2234.
Ellenberg, J., Siggia, E.D., Moreira, J.E., Smith, C.L., Presley, J.F., Worman, H.J., and Lippincott-Schwartz, J. (1997). Nuclear membrane dynamics and reassembly in living cells: targeting of an inner nuclear membrane protein in interphase and mitosis. J Cell Biol *138*, 1193-1206.
Ellerman, J.M., Flament, D., Kim, S.G., Fu, Q.G., Merkle, H., Ebner, T.J., and Ugurbil, K. (1994). Spatial patterns of functional activation of the cerebellum investigated using high field (4 T) MRI. NMR in biomedicine *7*, 63-68.
Engelkamp, D., Rashbass, P., Seawright, A., and van Heyningen, V. (1999). Role of Pax6 in development of the cerebellar system. Development *126*, 3585-3596.
Englund, C., Kowalczyk, T., Daza, R.A., Dagan, A., Lau, C., Rose, M.F., and Hevner, R.F. (2006). Unipolar brush cells of the cerebellum are produced in the rhombic lip and migrate through developing white matter. The Journal of neuroscience : the official journal of the Society for Neuroscience *26*, 9184-9195.
Erdel, F., and Rippe, K. (2011). Chromatin remodelling in mammalian cells by ISWI-type complexes--where, when and why? The FEBS journal *278*, 3608-3618.
Erdel, F., Schubert, T., Marth, C., Langst, G., and Rippe, K. (2010). Human ISWI chromatin-remodeling complexes sample nucleosomes via transient binding reactions and become immobilized at active sites. Proceedings of the National Academy of Sciences of the United States of America *107*, 19873-19878.
Fame, R.M., MacDonald, J.L., and Macklis, J.D. (2011). Development, specification, and diversity of callosal projection neurons. Trends Neurosci *34*, 41-50.
Fan, Y., Nikitina, T., Morin-Kensicki, E.M., Zhao, J., Magnuson, T.R., Woodcock, C.L., and Skoultchi, A.I. (2003). H1 linker histones are essential for mouse development and affect nucleosome spacing in vivo. Molecular and cellular biology *23*, 4559-4572.
Fan, Y., Nikitina, T., Zhao, J., Fleury, T.J., Bhattacharyya, R., Bouhassira, E.E., Stein, A., Woodcock, C.L., and Skoultchi, A.I. (2005). Histone H1 depletion in mammals alters global chromatin structure but causes specific changes in gene regulation. Cell *123*, 1199-1212.
Fasano, C.A., Phoenix, T.N., Kokovay, E., Lowry, N., Elkabetz, Y., Dimos, J.T., Lemischka, I.R., Studer, L., and Temple, S. (2009). Bmi-1 cooperates with Foxg1 to maintain neural stem cell self-renewal in the forebrain. Genes Dev *23*, 561-574.
Fatemi, S.H., Aldinger, K.A., Ashwood, P., Bauman, M.L., Blaha, C.D., Blatt, G.J., Chauhan, A., Chauhan, V., Dager, S.R., Dickson, P.E.*, et al.* (2012). Consensus paper: pathological role of the cerebellum in autism. Cerebellum *11*, 777-807.
Fazzio, T.G., Kooperberg, C., Goldmark, J.P., Neal, C., Basom, R., Delrow, J., and Tsukiyama, T. (2001). Widespread collaboration of Isw2 and Sin3-Rpd3 chromatin remodeling complexes in transcriptional repression. Mol Cell Biol *21*, 6450-6460.
Feng, W., Khan, M.A., Bellvis, P., Zhu, Z., Bernhardt, O., Herold-Mende, C., and Liu, H.K. (2013). The Chromatin Remodeler CHD7 Regulates Adult Neurogenesis via Activation of SoxC Transcription Factors. Cell stem cell *13*, 62-72.

Fink, A.J., Englund, C., Daza, R.A., Pham, D., Lau, C., Nivison, M., Kowalczyk, T., and Hevner, R.F. (2006). Development of the deep cerebellar nuclei: transcription factors and cell migration from the rhombic lip. The Journal of neuroscience : the official journal of the Society for Neuroscience *26*, 3066-3076.
Flanagan, J.F., Mi, L.Z., Chruszcz, M., Cymborowski, M., Clines, K.L., Kim, Y., Minor, W., Rastinejad, F., and Khorasanizadeh, S. (2005). Double chromodomains cooperate to recognize the methylated histone H3 tail. Nature *438*, 1181-1185.
Foucher, I., Mione, M., Simeone, A., Acampora, D., Bally-Cuif, L., and Houart, C. (2006). Differentiation of cerebellar cell identities in absence of Fgf signalling in zebrafish Otx morphants. Development *133*, 1891-1900.
Frazier, T.W., and Hardan, A.Y. (2009). A meta-analysis of the corpus callosum in autism. Biological psychiatry *66*, 935-941.
Fritsch, O., Benvenuto, G., Bowler, C., Molinier, J., and Hohn, B. (2004). The INO80 protein controls homologous recombination in Arabidopsis thaliana. Molecular cell *16*, 479-485.
Fujita, S. (1967). Quantitative analysis of cell proliferation and differentiation in the cortex of the postnatal mouse cerebellum. The Journal of cell biology *32*, 277-287.
Fujita, S., Shimada, M., and Nakamura, T. (1966). H3-thymidine autoradiographic studies on the cell proliferation and differentiation in the external and the internal granular layers of the mouse cerebellum. The Journal of comparative neurology *128*, 191-208.
Fukumitsu, H., Ohtsuka, M., Murai, R., Nakamura, H., Itoh, K., and Furukawa, S. (2006). Brain-derived neurotrophic factor participates in determination of neuronal laminar fate in the developing mouse cerebral cortex. J Neurosci *26*, 13218-13230.
Fyodorov, D.V., Blower, M.D., Karpen, G.H., and Kadonaga, J.T. (2004). Acf1 confers unique activities to ACF/CHRAC and promotes the formation rather than disruption of chromatin in vivo. Genes & development *18*, 170-183.
Garcez, P.P., Henrique, N.P., Furtado, D.A., Bolz, J., Lent, R., and Uziel, D. (2007). Axons of callosal neurons bifurcate transiently at the white matter before consolidating an interhemispheric projection. The European journal of neuroscience *25*, 1384-1394.
Garrett, A.M., Schreiner, D., Lobas, M.A., and Weiner, J.A. (2012). gamma-protocadherins control cortical dendrite arborization by regulating the activity of a FAK/PKC/MARCKS signaling pathway. Neuron *74*, 269-276.
Gaspar-Maia, A., Alajem, A., Polesso, F., Sridharan, R., Mason, M.J., Heidersbach, A., Ramalho-Santos, J., McManus, M.T., Plath, K., Meshorer, E.*, et al.* (2009). Chd1 regulates open chromatin and pluripotency of embryonic stem cells. Nature *460*, 863-868.
Gebre, S.A., Reeber, S.L., and Sillitoe, R.V. (2012). Parasagittal compartmentation of cerebellar mossy fibers as revealed by the patterned expression of vesicular glutamate transporters VGLUT1 and VGLUT2. Brain structure & function *217*, 165-180.
Gerlitz, G., Livnat, I., Ziv, C., Yarden, O., Bustin, M., and Reiner, O. (2007). Migration cues induce chromatin alterations. Traffic *8*, 1521-1529.
Gkikopoulos, T., Schofield, P., Singh, V., Pinskaya, M., Mellor, J., Smolle, M., Workman, J.L., Barton, G.J., and Owen-Hughes, T. (2011). A role for Snf2-related nucleosome-spacing enzymes in genome-wide nucleosome organization. Science *333*, 1758-1760.

Golan-Mashiach, M., Grunspan, M., Emmanuel, R., Gibbs-Bar, L., Dikstein, R., and Shapiro, E. (2012). Identification of CTCF as a master regulator of the clustered protocadherin genes. Nucleic acids research *40*, 3378-3391.
Goldman, J.A., Garlick, J.D., and Kingston, R.E. (2010). Chromatin remodeling by imitation switch (ISWI) class ATP-dependent remodelers is stimulated by histone variant H2A.Z. The Journal of biological chemistry *285*, 4645-4651.
Gossett, A.J., and Lieb, J.D. (2012). In vivo effects of histone H3 depletion on nucleosome occupancy and position in Saccharomyces cerevisiae. PLoS genetics *8*, e1002771.
Gotz, M., and Huttner, W.B. (2005). The cell biology of neurogenesis. Nat Rev Mol Cell Biol *6*, 777-788.
Grune, T., Brzeski, J., Eberharter, A., Clapier, C.R., Corona, D.F., Becker, P.B., and Muller, C.W. (2003). Crystal structure and functional analysis of a nucleosome recognition module of the remodeling factor ISWI. Molecular cell *12*, 449-460.
Guetg, C., Lienemann, P., Sirri, V., Grummt, I., Hernandez-Verdun, D., Hottiger, M.O., Fussenegger, M., and Santoro, R. (2010). The NoRC complex mediates the heterochromatin formation and stability of silent rRNA genes and centromeric repeats. The EMBO journal *29*, 2135-2146.
Guibert, S., and Weber, M. (2013). Functions of DNA methylation and hydroxymethylation in mammalian development. Current topics in developmental biology *104*, 47-83.
Guillemot, F. (2007). Spatial and temporal specification of neural fates by transcription factor codes. Development *134*, 3771-3780.
Guo, H., Hong, S., Jin, X.L., Chen, R.S., Avasthi, P.P., Tu, Y.T., Ivanco, T.L., and Li, Y. (2000). Specificity and efficiency of Cre-mediated recombination in Emx1-Cre knock-in mice. Biochemical and biophysical research communications *273*, 661-665.
Guo, Y., Monahan, K., Wu, H., Gertz, J., Varley, K.E., Li, W., Myers, R.M., Maniatis, T., and Wu, Q. (2012). CTCF/cohesin-mediated DNA looping is required for protocadherin alpha promoter choice. Proceedings of the National Academy of Sciences of the United States of America *109*, 21081-21086.
Gupta, A., Tsai, L.H., and Wynshaw-Boris, A. (2002). Life is a journey: a genetic look at neocortical development. Nat Rev Genet *3*, 342-355.
Guschin, D., Geiman, T.M., Kikyo, N., Tremethick, D.J., Wolffe, A.P., and Wade, P.A. (2000). Multiple ISWI ATPase complexes from xenopus laevis. Functional conservation of an ACF/CHRAC homolog. The Journal of biological chemistry *275*, 35248-35255.
Gyorgy, A.B., Szemes, M., de Juan Romero, C., Tarabykin, V., and Agoston, D.V. (2008). SATB2 interacts with chromatin-remodeling molecules in differentiating cortical neurons. The European journal of neuroscience *27*, 865-873.
Hakimi, M.A., Bochar, D.A., Schmiesing, J.A., Dong, Y., Barak, O.G., Speicher, D.W., Yokomori, K., and Shiekhattar, R. (2002). A chromatin remodelling complex that loads cohesin onto human chromosomes. Nature *418*, 994-998.
Hall, J.A., and Georgel, P.T. (2007). CHD proteins: a diverse family with strong ties. Biochemistry and cell biology = Biochimie et biologie cellulaire *85*, 463-476.
Hamby, M.E., Coskun, V., and Sun, Y.E. (2008). Transcriptional regulation of neuronal differentiation: the epigenetic layer of complexity. Biochim Biophys Acta *1779*, 432-437.

Han, W., Kwan, K.Y., Shim, S., Lam, M.M., Shin, Y., Xu, X., Zhu, Y., Li, M., and Sestan, N. (2011). TBR1 directly represses Fezf2 to control the laminar origin and development of the corticospinal tract. Proceedings of the National Academy of Sciences of the United States of America *108*, 3041-3046.
Hanai, K., Furuhashi, H., Yamamoto, T., Akasaka, K., and Hirose, S. (2008). RSF governs silent chromatin formation via histone H2Av replacement. PLoS genetics *4*, e1000011.
Hanashima, C., Li, S.C., Shen, L., Lai, E., and Fishell, G. (2004). Foxg1 suppresses early cortical cell fate. Science *303*, 56-59.
Harshman, S.W., Young, N.L., Parthun, M.R., and Freitas, M.A. (2013). H1 histones: current perspectives and challenges. Nucleic acids research.
Hartlepp, K.F., Fernandez-Tornero, C., Eberharter, A., Grune, T., Muller, C.W., and Becker, P.B. (2005). The histone fold subunits of Drosophila CHRAC facilitate nucleosome sliding through dynamic DNA interactions. Molecular and cellular biology *25*, 9886-9896.
Hattori, N., Niwa, T., Kimura, K., Helin, K., and Ushijima, T. (2013). Visualization of multivalent histone modification in a single cell reveals highly concerted epigenetic changes on differentiation of embryonic stem cells. Nucleic acids research.
Hauk, G., and Bowman, G.D. (2011). Structural insights into regulation and action of SWI2/SNF2 ATPases. Current opinion in structural biology *21*, 719-727.
Hawkins, R.D., Hon, G.C., Lee, L.K., Ngo, Q., Lister, R., Pelizzola, M., Edsall, L.E., Kuan, S., Luu, Y., Klugman, S.*, et al.* (2010). Distinct epigenomic landscapes of pluripotent and lineage-committed human cells. Cell stem cell *6*, 479-491.
Hebert, J.M., and McConnell, S.K. (2000). Targeting of cre to the Foxg1 (BF-1) locus mediates loxP recombination in the telencephalon and other developing head structures. Developmental biology *222*, 296-306.
Heng, H.H., Goetze, S., Ye, C.J., Liu, G., Stevens, J.B., Bremer, S.W., Wykes, S.M., Bode, J., and Krawetz, S.A. (2004). Chromatin loops are selectively anchored using scaffold/matrix-attachment regions. Journal of cell science *117*, 999-1008.
Herbert, M.R., and Kenet, T. (2007). Brain abnormalities in language disorders and in autism. Pediatric clinics of North America *54*, 563-583, vii.
Higashi, T., Matsunaga, S., Isobe, K., Morimoto, A., Shimada, T., Kataoka, S., Watanabe, W., Uchiyama, S., Itoh, K., and Fukui, K. (2007). Histone H2A mobility is regulated by its tails and acetylation of core histone tails. Biochemical and biophysical research communications *357*, 627-632.
Hirano, K., Kaneko, R., Izawa, T., Kawaguchi, M., Kitsukawa, T., and Yagi, T. (2012). Single-neuron diversity generated by Protocadherin-beta cluster in mouse central and peripheral nervous systems. Frontiers in molecular neuroscience *5*, 90.
Hirayama, T., Tarusawa, E., Yoshimura, Y., Galjart, N., and Yagi, T. (2012). CTCF is required for neural development and stochastic expression of clustered Pcdh genes in neurons. Cell reports *2*, 345-357.
Hirayama, T., and Yagi, T. (2013). Clustered protocadherins and neuronal diversity. Progress in molecular biology and translational science *116*, 145-167.
Hirschhorn, J.N., Brown, S.A., Clark, C.D., and Winston, F. (1992). Evidence that SNF2/SWI2 and SNF5 activate transcription in yeast by altering chromatin structure. Genes & development *6*, 2288-2298.

Ho, L., and Crabtree, G.R. (2010). Chromatin remodelling during development. Nature *463*, 474-484.
Ho, L., Jothi, R., Ronan, J.L., Cui, K., Zhao, K., and Crabtree, G.R. (2009a). An embryonic stem cell chromatin remodeling complex, esBAF, is an essential component of the core pluripotency transcriptional network. Proceedings of the National Academy of Sciences of the United States of America *106*, 5187-5191.
Ho, L., Ronan, J.L., Wu, J., Staahl, B.T., Chen, L., Kuo, A., Lessard, J., Nesvizhskii, A.I., Ranish, J., and Crabtree, G.R. (2009b). An embryonic stem cell chromatin remodeling complex, esBAF, is essential for embryonic stem cell self-renewal and pluripotency. Proceedings of the National Academy of Sciences of the United States of America *106*, 5181-5186.
Hood, R.L., Lines, M.A., Nikkel, S.M., Schwartzentruber, J., Beaulieu, C., Nowaczyk, M.J., Allanson, J., Kim, C.A., Wieczorek, D., Moilanen, J.S.*, et al.* (2012). Mutations in SRCAP, encoding SNF2-related CREBBP activator protein, cause Floating-Harbor syndrome. American journal of human genetics *90*, 308-313.
Huh, M.S., Price O'Dea, T., Ouazia, D., McKay, B.C., Parise, G., Parks, R.J., Rudnicki, M.A., and Picketts, D.J. (2012). Compromised genomic integrity impedes muscle growth after Atrx inactivation. The Journal of clinical investigation *122*, 4412-4423.
Hurd, E.A., Capers, P.L., Blauwkamp, M.N., Adams, M.E., Raphael, Y., Poucher, H.K., and Martin, D.M. (2007). Loss of Chd7 function in gene-trapped reporter mice is embryonic lethal and associated with severe defects in multiple developing tissues. Mammalian genome : official journal of the International Mammalian Genome Society *18*, 94-104.
Iida, T., and Araki, H. (2004). Noncompetitive counteractions of DNA polymerase epsilon and ISW2/yCHRAC for epigenetic inheritance of telomere position effect in Saccharomyces cerevisiae. Molecular and cellular biology *24*, 217-227.
Ito, T., Bulger, M., Pazin, M.J., Kobayashi, R., and Kadonaga, J.T. (1997). ACF, an ISWI-containing and ATP-utilizing chromatin assembly and remodeling factor. Cell *90*, 145-155.
Jin, C., Zang, C., Wei, G., Cui, K., Peng, W., Zhao, K., and Felsenfeld, G. (2009). H3.3/H2A.Z double variant-containing nucleosomes mark 'nucleosome-free regions' of active promoters and other regulatory regions. Nature genetics *41*, 941-945.
Jin, J., Cai, Y., Yao, T., Gottschalk, A.J., Florens, L., Swanson, S.K., Gutierrez, J.L., Coleman, M.K., Workman, J.L., Mushegian, A.*, et al.* (2005). A mammalian chromatin remodeling complex with similarities to the yeast INO80 complex. The Journal of biological chemistry *280*, 41207-41212.
Joyner, A.L., Herrup, K., Auerbach, B.A., Davis, C.A., and Rossant, J. (1991). Subtle cerebellar phenotype in mice homozygous for a targeted deletion of the En-2 homeobox. Science *251*, 1239-1243.
Kai, N., Mishina, M., and Yagi, T. (1997). Molecular cloning of Fyn-associated molecules in the mouse central nervous system. Journal of neuroscience research *48*, 407-424.
Kaji, K., Caballero, I.M., MacLeod, R., Nichols, J., Wilson, V.A., and Hendrich, B. (2006). The NuRD component Mbd3 is required for pluripotency of embryonic stem cells. Nature cell biology *8*, 285-292.
Kaji, K., Nichols, J., and Hendrich, B. (2007). Mbd3, a component of the NuRD co-repressor complex, is required for development of pluripotent cells. Development *134*, 1123-1132.

Kawauchi, S., Calof, A.L., Santos, R., Lopez-Burks, M.E., Young, C.M., Hoang, M.P., Chua, A., Lao, T., Lechner, M.S., Daniel, J.A*., et al.* (2009). Multiple organ system defects and transcriptional dysregulation in the Nipbl(+/-) mouse, a model of Cornelia de Lange Syndrome. PLoS genetics *5*, e1000650.
Kehayova, P., Monahan, K., Chen, W., and Maniatis, T. (2011). Regulatory elements required for the activation and repression of the protocadherin-alpha gene cluster. Proceedings of the National Academy of Sciences of the United States of America *108*, 17195-17200.
Kehle, J., Beuchle, D., Treuheit, S., Christen, B., Kennison, J.A., Bienz, M., and Muller, J. (1998). dMi-2, a hunchback-interacting protein that functions in polycomb repression. Science *282*, 1897-1900.
Kennison, J.A., and Tamkun, J.W. (1988). Dosage-dependent modifiers of polycomb and antennapedia mutations in Drosophila. Proceedings of the National Academy of Sciences of the United States of America *85*, 8136-8140.
Khavari, P.A., Peterson, C.L., Tamkun, J.W., Mendel, D.B., and Crabtree, G.R. (1993). BRG1 contains a conserved domain of the SWI2/SNF2 family necessary for normal mitotic growth and transcription. Nature *366*, 170-174.
Kobor, M.S., Venkatasubrahmanyam, S., Meneghini, M.D., Gin, J.W., Jennings, J.L., Link, A.J., Madhani, H.D., and Rine, J. (2004). A protein complex containing the conserved Swi2/Snf2-related ATPase Swr1p deposits histone variant H2A.Z into euchromatin. PLoS biology *2*, E131.
Kohmura, N., Senzaki, K., Hamada, S., Kai, N., Yasuda, R., Watanabe, M., Ishii, H., Yasuda, M., Mishina, M., and Yagi, T. (1998). Diversity revealed by a novel family of cadherins expressed in neurons at a synaptic complex. Neuron *20*, 1137-1151.
Konev, A.Y., Tribus, M., Park, S.Y., Podhraski, V., Lim, C.Y., Emelyanov, A.V., Vershilova, E., Pirrotta, V., Kadonaga, J.T., Lusser, A*., et al.* (2007). CHD1 motor protein is required for deposition of histone variant H3.3 into chromatin in vivo. Science *317*, 1087-1090.
Konig, N., Valat, J., Fulcrand, J., and Marty, R. (1977). The time of origin of Cajal-Retzius cells in the rat temporal cortex. An autoradiographic study. Neuroscience letters *4*, 21-26.
Koziol, L.F., Budding, D.E., and Chidekel, D. (2012). From movement to thought: executive function, embodied cognition, and the cerebellum. Cerebellum *11*, 505-525.
Ku, M., Jaffe, J.D., Koche, R.P., Rheinbay, E., Endoh, M., Koseki, H., Carr, S.A., and Bernstein, B.E. (2012). H2A.Z landscapes and dual modifications in pluripotent and multipotent stem cells underlie complex genome regulatory functions. Genome biology *13*, R85.
Kumamoto, T., Toma, K., Gunadi, McKenna, W.L., Kasukawa, T., Katzman, S., Chen, B., and Hanashima, C. (2013). Foxg1 coordinates the switch from nonradially to radially migrating glutamatergic subtypes in the neocortex through spatiotemporal repression. Cell reports *3*, 931-945.
Kusch, T., Florens, L., Macdonald, W.H., Swanson, S.K., Glaser, R.L., Yates, J.R., 3rd, Abmayr, S.M., Washburn, M.P., and Workman, J.L. (2004). Acetylation by Tip60 is required for selective histone variant exchange at DNA lesions. Science *306*, 2084-2087.
Kwan, K.Y., Lam, M.M., Krsnik, Z., Kawasawa, Y.I., Lefebvre, V., and Sestan, N. (2008). SOX5 postmitotically regulates migration, postmigratory differentiation, and

projections of subplate and deep-layer neocortical neurons. Proceedings of the National Academy of Sciences of the United States of America *105*, 16021-16026.
Kwan, K.Y., Sestan, N., and Anton, E.S. (2012). Transcriptional co-regulation of neuronal migration and laminar identity in the neocortex. Development *139*, 1535-1546.
Ladurner, A.G. (2003). Inactivating chromosomes: a macro domain that minimizes transcription. Molecular cell *12*, 1-3.
Lagarou, A., Mohd-Sarip, A., Moshkin, Y.M., Chalkley, G.E., Bezstarosti, K., Demmers, J.A., and Verrijzer, C.P. (2008). dKDM2 couples histone H2A ubiquitylation to histone H3 demethylation during Polycomb group silencing. Genes & development *22*, 2799-2810.
Lan, L., Ui, A., Nakajima, S., Hatakeyama, K., Hoshi, M., Watanabe, R., Janicki, S.M., Ogiwara, H., Kohno, T., Kanno, S*., et al.* (2010). The ACF1 complex is required for DNA double-strand break repair in human cells. Molecular cell *40*, 976-987.
Landry, J., Sharov, A.A., Piao, Y., Sharova, L.V., Xiao, H., Southon, E., Matta, J., Tessarollo, L., Zhang, Y.E., Ko, M.S*., et al.* (2008). Essential role of chromatin remodeling protein Bptf in early mouse embryos and embryonic stem cells. PLoS genetics *4*, e1000241.
Landry, J.W., Banerjee, S., Taylor, B., Aplan, P.D., Singer, A., and Wu, C. (2011). Chromatin remodeling complex NURF regulates thymocyte maturation. Genes & development *25*, 275-286.
Larsell, O. (1952). The morphogenesis and adult pattern of the lobules and fissures of the cerebellum of the white rat. The Journal of comparative neurology *97*, 281-356.
Larsell, O., and Whitlock, D.G. (1952). Further observations on the cerebellum of birds. The Journal of comparative neurology *97*, 545-566.
Lasalle, J.M., Powell, W.T., and Yasui, D.H. (2013). Epigenetic layers and players underlying neurodevelopment. Trends in neurosciences.
Lazzaro, M.A., Pepin, D., Pescador, N., Murphy, B.D., Vanderhyden, B.C., and Picketts, D.J. (2006). The imitation switch protein SNF2L regulates steroidogenic acute regulatory protein expression during terminal differentiation of ovarian granulosa cells. Mol Endocrinol *20*, 2406-2417.
Lazzaro, M.A., and Picketts, D.J. (2001a). Cloning and characterization of the murine Imitation Switch (ISWI) genes: differential expression patterns suggest distinct developmental roles for Snf2h and Snf2l. Journal of neurochemistry *77*, 1145-1156.
Lazzaro, M.A., and Picketts, D.J. (2001b). Cloning and characterization of the murine Imitation Switch (ISWI) genes: differential expression patterns suggest distinct developmental roles for Snf2h and Snf2l. J Neurochem *77*, 1145-1156.
Lazzaro, M.A., Todd, M.A., Lavigne, P., Vallee, D., De Maria, A., and Picketts, D.J. (2008). Characterization of novel isoforms and evaluation of SNF2L/SMARCA1 as a candidate gene for X-linked mental retardation in 12 families linked to Xq25-26. BMC medical genetics *9*, 11.
Ledderose, J., Dieter, S., and Schwarz, M.K. (2013). Maturation of postnatally generated olfactory bulb granule cells depends on functional gamma-protocadherin expression. Scientific reports *3*, 1514.
Lefebvre, J.L., Kostadinov, D., Chen, W.V., Maniatis, T., and Sanes, J.R. (2012). Protocadherins mediate dendritic self-avoidance in the mammalian nervous system. Nature *488*, 517-521.
LeRoy, G., Orphanides, G., Lane, W.S., and Reinberg, D. (1998). Requirement of RSF and FACT for transcription of chromatin templates in vitro. Science *282*, 1900-1904.

Lessard, J., Wu, J.I., Ranish, J.A., Wan, M., Winslow, M.M., Staahl, B.T., Wu, H., Aebersold, R., Graef, I.A., and Crabtree, G.R. (2007). An essential switch in subunit composition of a chromatin remodeling complex during neural development. Neuron *55*, 201-215.
Lewandoski, M., Wassarman, K.M., and Martin, G.R. (1997). Zp3-cre, a transgenic mouse line for the activation or inactivation of loxP-flanked target genes specifically in the female germ line. Current biology : CB *7*, 148-151.
Li, E., Bestor, T.H., and Jaenisch, R. (1992). Targeted mutation of the DNA methyltransferase gene results in embryonic lethality. Cell *69*, 915-926.
Li, H., Tao, W., and Lai, E. (1996). Characterization of the structure and function of the gene for transcription factor BF-1, an essential regulator of forebrain development. Brain Res Mol Brain Res *37*, 96-104.
Li, J.Y., Lao, Z., and Joyner, A.L. (2002). Changing requirements for Gbx2 in development of the cerebellum and maintenance of the mid/hindbrain organizer. Neuron *36*, 31-43.
Li, M., Belozerov, V.E., and Cai, H.N. (2010). Modulation of chromatin boundary activities by nucleosome-remodeling activities in Drosophila melanogaster. Mol Cell Biol *30*, 1067-1076.
Li, Y., Xiao, H., Chiou, T.T., Jin, H., Bonhomme, B., Miralles, C.P., Pinal, N., Ali, R., Chen, W.V., Maniatis, T.*, et al.* (2012). Molecular and functional interaction between protocadherin-gammaC5 and GABAA receptors. The Journal of neuroscience : the official journal of the Society for Neuroscience *32*, 11780-11797.
Lim, D.A., Huang, Y.C., Swigut, T., Mirick, A.L., Garcia-Verdugo, J.M., Wysocka, J., Ernst, P., and Alvarez-Buylla, A. (2009). Chromatin remodelling factor Mll1 is essential for neurogenesis from postnatal neural stem cells. Nature *458*, 529-533.
Lin, J.J., Lehmann, L.W., Bonora, G., Sridharan, R., Vashisht, A.A., Tran, N., Plath, K., Wohlschlegel, J.A., and Carey, M. (2011). Mediator coordinates PIC assembly with recruitment of CHD1. Genes & development *25*, 2198-2209.
Liu, A., and Joyner, A.L. (2001a). Early anterior/posterior patterning of the midbrain and cerebellum. Annual review of neuroscience *24*, 869-896.
Liu, A., and Joyner, A.L. (2001b). EN and GBX2 play essential roles downstream of FGF8 in patterning the mouse mid/hindbrain region. Development *128*, 181-191.
Lu, X., Wontakal, S.N., Emelyanov, A.V., Morcillo, P., Konev, A.Y., Fyodorov, D.V., and Skoultchi, A.I. (2009). Linker histone H1 is essential for Drosophila development, the establishment of pericentric heterochromatin, and a normal polytene chromosome structure. Genes & development *23*, 452-465.
Lu, X., Wontakal, S.N., Kavi, H., Kim, B.J., Guzzardo, P.M., Emelyanov, A.V., Xu, N., Hannon, G.J., Zavadil, J., Fyodorov, D.V.*, et al.* (2013). Drosophila H1 regulates the genetic activity of heterochromatin by recruitment of Su(var)3-9. Science *340*, 78-81.
Lusser, A., Urwin, D.L., and Kadonaga, J.T. (2005). Distinct activities of CHD1 and ACF in ATP-dependent chromatin assembly. Nature structural & molecular biology *12*, 160-166.
Ma, M.K., Heath, C., Hair, A., and West, A.G. (2011). Histone crosstalk directed by H2B ubiquitination is required for chromatin boundary integrity. PLoS genetics *7*, e1002175.
Machold, R., and Fishell, G. (2005). Math1 is expressed in temporally discrete pools of cerebellar rhombic-lip neural progenitors. Neuron *48*, 17-24.

Maier, V.K., Chioda, M., Rhodes, D., and Becker, P.B. (2008). ACF catalyses chromatosome movements in chromatin fibres. The EMBO journal *27*, 817-826.
Mao, X., Fujiwara, Y., and Orkin, S.H. (1999). Improved reporter strain for monitoring Cre recombinase-mediated DNA excisions in mice. Proc Natl Acad Sci U S A *96*, 5037-5042.
Maren, S. (2001). Neurobiology of Pavlovian fear conditioning. Annual review of neuroscience *24*, 897-931.
Marfella, C.G., Ohkawa, Y., Coles, A.H., Garlick, D.S., Jones, S.N., and Imbalzano, A.N. (2006). Mutation of the SNF2 family member Chd2 affects mouse development and survival. Journal of cellular physiology *209*, 162-171.
Marmorstein, R., and Berger, S.L. (2001). Structure and function of bromodomains in chromatin-regulating complexes. Gene *272*, 1-9.
Martinez, S., Crossley, P.H., Cobos, I., Rubenstein, J.L., and Martin, G.R. (1999). FGF8 induces formation of an ectopic isthmic organizer and isthmocerebellar development via a repressive effect on Otx2 expression. Development *126*, 1189-1200.
Martynoga, B., Morrison, H., Price, D.J., and Mason, J.O. (2005). Foxg1 is required for specification of ventral telencephalon and region-specific regulation of dorsal telencephalic precursor proliferation and apoptosis. Dev Biol *283*, 113-127.
Marzban, H., and Hawkes, R. (2011). On the architecture of the posterior zone of the cerebellum. Cerebellum *10*, 422-434.
Marzluff, W.F., Gongidi, P., Woods, K.R., Jin, J., and Maltais, L.J. (2002). The human and mouse replication-dependent histone genes. Genomics *80*, 487-498.
Matsumoto, K., Nishihara, S., Kamimura, M., Shiraishi, T., Otoguro, T., Uehara, M., Maeda, Y., Ogura, K., Lumsden, A., and Ogura, T. (2004). The prepattern transcription factor Irx2, a target of the FGF8/MAP kinase cascade, is involved in cerebellum formation. Nature neuroscience *7*, 605-612.
Matsunaga, E., Katahira, T., and Nakamura, H. (2002). Role of Lmx1b and Wnt1 in mesencephalon and metencephalon development. Development *129*, 5269-5277.
McConnell, S.K., and Kaznowski, C.E. (1991). Cell cycle dependence of laminar determination in developing neocortex. Science *254*, 282-285.
McDaniel, I.E., Lee, J.M., Berger, M.S., Hanagami, C.K., and Armstrong, J.A. (2008). Investigations of CHD1 function in transcription and development of Drosophila melanogaster. Genetics *178*, 583-587.
McKenna, W.L., Betancourt, J., Larkin, K.A., Abrams, B., Guo, C., Rubenstein, J.L., and Chen, B. (2011). Tbr1 and Fezf2 regulate alternate corticofugal neuronal identities during neocortical development. The Journal of neuroscience : the official journal of the Society for Neuroscience *31*, 549-564.
McMahon, A.P., and Bradley, A. (1990). The Wnt-1 (int-1) proto-oncogene is required for development of a large region of the mouse brain. Cell *62*, 1073-1085.
Melcer, S., Hezroni, H., Rand, E., Nissim-Rafinia, M., Skoultchi, A., Stewart, C.L., Bustin, M., and Meshorer, E. (2012). Histone modifications and lamin A regulate chromatin protein dynamics in early embryonic stem cell differentiation. Nature communications *3*, 910.
Melicharek, D.J., Ramirez, L.C., Singh, S., Thompson, R., and Marenda, D.R. (2010). Kismet/CHD7 regulates axon morphology, memory and locomotion in a Drosophila model of CHARGE syndrome. Human molecular genetics *19*, 4253-4264.

Meshorer, E., Yellajoshula, D., George, E., Scambler, P.J., Brown, D.T., and Misteli, T. (2006). Hyperdynamic plasticity of chromatin proteins in pluripotent embryonic stem cells. Developmental cell *10*, 105-116.
Miale, I.L., and Sidman, R.L. (1961). An autoradiographic analysis of histogenesis in the mouse cerebellum. Experimental neurology *4*, 277-296.
Mielke, J.G., Nicolitch, K., Avellaneda, V., Earlam, K., Ahuja, T., Mealing, G., and Messier, C. (2006). Longitudinal study of the effects of a high-fat diet on glucose regulation, hippocampal function, and cerebral insulin sensitivity in C57BL/6 mice. Behav Brain Res *175*, 374-382.
Millar, C.B., Xu, F., Zhang, K., and Grunstein, M. (2006). Acetylation of H2AZ Lys 14 is associated with genome-wide gene activity in yeast. Genes & development *20*, 711-722.
Mitchell, A.C., Bharadwaj, R., Whittle, C., Krueger, W., Mirnics, K., Hurd, Y., Rasmussen, T., and Akbarian, S. (2013). The Genome in Three Dimensions: A New Frontier in Human Brain Research. Biological psychiatry.
Miyoshi, G., and Fishell, G. (2012). Dynamic FoxG1 expression coordinates the integration of multipolar pyramidal neuron precursors into the cortical plate. Neuron *74*, 1045-1058.
Mizuguchi, G., Shen, X., Landry, J., Wu, W.H., Sen, S., and Wu, C. (2004). ATP-driven exchange of histone H2AZ variant catalyzed by SWR1 chromatin remodeling complex. Science *303*, 343-348.
Molofsky, A.V., He, S., Bydon, M., Morrison, S.J., and Pardal, R. (2005). Bmi-1 promotes neural stem cell self-renewal and neural development but not mouse growth and survival by repressing the p16Ink4a and p19Arf senescence pathways. Genes Dev *19*, 1432-1437.
Molofsky, A.V., Pardal, R., Iwashita, T., Park, I.K., Clarke, M.F., and Morrison, S.J. (2003). Bmi-1 dependence distinguishes neural stem cell self-renewal from progenitor proliferation. Nature *425*, 962-967.
Molyneaux, B.J., Arlotta, P., Hirata, T., Hibi, M., and Macklis, J.D. (2005). Fezl is required for the birth and specification of corticospinal motor neurons. Neuron *47*, 817-831.
Molyneaux, B.J., Arlotta, P., Menezes, J.R., and Macklis, J.D. (2007). Neuronal subtype specification in the cerebral cortex. Nature reviews Neuroscience *8*, 427-437.
Monuki, E.S., Porter, F.D., and Walsh, C.A. (2001). Patterning of the dorsal telencephalon and cerebral cortex by a roof plate-Lhx2 pathway. Neuron *32*, 591-604.
Morales, D., and Hatten, M.E. (2006). Molecular markers of neuronal progenitors in the embryonic cerebellar anlage. The Journal of neuroscience : the official journal of the Society for Neuroscience *26*, 12226-12236.
Morata, G., and Lawrence, P.A. (1975). Control of compartment development by the engrailed gene in Drosophila. Nature *255*, 614-617.
Morrison, A.J., Highland, J., Krogan, N.J., Arbel-Eden, A., Greenblatt, J.F., Haber, J.E., and Shen, X. (2004). INO80 and gamma-H2AX interaction links ATP-dependent chromatin remodeling to DNA damage repair. Cell *119*, 767-775.
Muzio, L., Di Benedetto, B., Stoykova, A., Boncinelli, E., Gruss, P., and Mallamaci, A. (2002). Emx2 and Pax6 control regionalization of the pre-neuronogenic cortical primordium. Cereb Cortex *12*, 129-139.

Muzio, L., and Mallamaci, A. (2005). Foxg1 confines Cajal-Retzius neuronogenesis and hippocampal morphogenesis to the dorsomedial pallium. The Journal of neuroscience : the official journal of the Society for Neuroscience *25*, 4435-4441.
Narlikar, G.J., Sundaramoorthy, R., and Owen-Hughes, T. (2013). Mechanisms and functions of ATP-dependent chromatin-remodeling enzymes. Cell *154*, 490-503.
Neale, B.M., Kou, Y., Liu, L., Ma'ayan, A., Samocha, K.E., Sabo, A., Lin, C.F., Stevens, C., Wang, L.S., Makarov, V.*, et al.* (2012). Patterns and rates of exonic de novo mutations in autism spectrum disorders. Nature *485*, 242-245.
Neigeborn, L., and Carlson, M. (1984). Genes affecting the regulation of SUC2 gene expression by glucose repression in Saccharomyces cerevisiae. Genetics *108*, 845-858.
Nishiyama, M., Oshikawa, K., Tsukada, Y., Nakagawa, T., Iemura, S., Natsume, T., Fan, Y., Kikuchi, A., Skoultchi, A.I., and Nakayama, K.I. (2009). CHD8 suppresses p53-mediated apoptosis through histone H1 recruitment during early embryogenesis. Nature cell biology *11*, 172-182.
Nishiyama, M., Skoultchi, A.I., and Nakayama, K.I. (2012). Histone H1 recruitment by CHD8 is essential for suppression of the Wnt-beta-catenin signaling pathway. Molecular and cellular biology *32*, 501-512.
Nissim-Rafinia, M., and Meshorer, E. (2011). Photobleaching assays (FRAP & FLIP) to measure chromatin protein dynamics in living embryonic stem cells. J Vis Exp.
Nogami, T., Beppu, H., Tokoro, T., Moriguchi, S., Shioda, N., Fukunaga, K., Ohtsuka, T., Ishii, Y., Sasahara, M., Shimada, Y.*, et al.* (2011). Reduced expression of the ATRX gene, a chromatin-remodeling factor, causes hippocampal dysfunction in mice. Hippocampus *21*, 678-687.
O'Roak, B.J., Vives, L., Fu, W., Egertson, J.D., Stanaway, I.B., Phelps, I.G., Carvill, G., Kumar, A., Lee, C., Ankenman, K.*, et al.* (2012a). Multiplex targeted sequencing identifies recurrently mutated genes in autism spectrum disorders. Science *338*, 1619-1622.
O'Roak, B.J., Vives, L., Girirajan, S., Karakoc, E., Krumm, N., Coe, B.P., Levy, R., Ko, A., Lee, C., Smith, J.D.*, et al.* (2012b). Sporadic autism exomes reveal a highly interconnected protein network of de novo mutations. Nature *485*, 246-250.
Orvis, G.D., Hartzell, A.L., Smith, J.B., Barraza, L.H., Wilson, S.L., Szulc, K.U., Turnbull, D.H., and Joyner, A.L. (2012). The engrailed homeobox genes are required in multiple cell lineages to coordinate sequential formation of fissures and growth of the cerebellum. Developmental biology *367*, 25-39.
Papamichos-Chronakis, M., Watanabe, S., Rando, O.J., and Peterson, C.L. (2011). Global regulation of H2A.Z localization by the INO80 chromatin-remodeling enzyme is essential for genome integrity. Cell *144*, 200-213.
Paul, L.K., Brown, W.S., Adolphs, R., Tyszka, J.M., Richards, L.J., Mukherjee, P., and Sherr, E.H. (2007). Agenesis of the corpus callosum: genetic, developmental and functional aspects of connectivity. Nature reviews Neuroscience *8*, 287-299.
Pena, P.V., Davrazou, F., Shi, X., Walter, K.L., Verkhusha, V.V., Gozani, O., Zhao, R., and Kutateladze, T.G. (2006). Molecular mechanism of histone H3K4me3 recognition by plant homeodomain of ING2. Nature *442*, 100-103.
Peterson, C.L., and Herskowitz, I. (1992). Characterization of the yeast SWI1, SWI2, and SWI3 genes, which encode a global activator of transcription. Cell *68*, 573-583.

Phair, R.D., Gorski, S.A., and Misteli, T. (2004). Measurement of dynamic protein binding to chromatin in vivo, using photobleaching microscopy. Methods Enzymol *375*, 393-414.
Poot, R.A., Bozhenok, L., van den Berg, D.L., Steffensen, S., Ferreira, F., Grimaldi, M., Gilbert, N., Ferreira, J., and Varga-Weisz, P.D. (2004). The Williams syndrome transcription factor interacts with PCNA to target chromatin remodelling by ISWI to replication foci. Nature cell biology *6*, 1236-1244.
Poot, R.A., Dellaire, G., Hulsmann, B.B., Grimaldi, M.A., Corona, D.F., Becker, P.B., Bickmore, W.A., and Varga-Weisz, P.D. (2000). HuCHRAC, a human ISWI chromatin remodelling complex contains hACF1 and two novel histone-fold proteins. The EMBO journal *19*, 3377-3387.
Postepska-Igielska, A., Krunic, D., Schmitt, N., Greulich-Bode, K.M., Boukamp, P., and Grummt, I. (2013). The chromatin remodelling complex NoRC safeguards genome stability by heterochromatin formation at telomeres and centromeres. EMBO reports.
Raedler, E., and Raedler, A. (1978). Autoradiographic study of early neurogenesis in rat neocortex. Anatomy and embryology *154*, 267-284.
Randazzo, F.M., Khavari, P., Crabtree, G., Tamkun, J., and Rossant, J. (1994). brg1: a putative murine homologue of the Drosophila brahma gene, a homeotic gene regulator. Developmental biology *161*, 229-242.
Rangasamy, S., D'Mello, S.R., and Narayanan, V. (2013). Epigenetics, autism spectrum, and neurodevelopmental disorders. Neurotherapeutics : the journal of the American Society for Experimental NeuroTherapeutics *10*, 742-756.
Rapsomaniki, M.A., Kotsantis, P., Symeonidou, I.E., Giakoumakis, N.N., Taraviras, S., and Lygerou, Z. (2012). easyFRAP: an interactive, easy-to-use tool for qualitative and quantitative analysis of FRAP data. Bioinformatics *28*, 1800-1801.
Raymond, C.S., and Soriano, P. (2010). ROSA26Flpo deleter mice promote efficient inversion of conditional gene traps in vivo. Genesis *48*, 603-606.
Reith, R.M., McKenna, J., Wu, H., Hashmi, S.S., Cho, S.H., Dash, P.K., and Gambello, M.J. (2013). Loss of Tsc2 in Purkinje cells is associated with autistic-like behavior in a mouse model of tuberous sclerosis complex. Neurobiology of disease *51*, 93-103.
Remeseiro, S., Cuadrado, A., Gomez-Lopez, G., Pisano, D.G., and Losada, A. (2012). A unique role of cohesin-SA1 in gene regulation and development. The EMBO journal *31*, 2090-2102.
Reyes, J.C., Barra, J., Muchardt, C., Camus, A., Babinet, C., and Yaniv, M. (1998). Altered control of cellular proliferation in the absence of mammalian brahma (SNF2alpha). The EMBO journal *17*, 6979-6991.
Rhinn, M., Dierich, A., Shawlot, W., Behringer, R.R., Le Meur, M., and Ang, S.L. (1998). Sequential roles for Otx2 in visceral endoderm and neuroectoderm for forebrain and midbrain induction and specification. Development *125*, 845-856.
Ribich, S., Tasic, B., and Maniatis, T. (2006). Identification of long-range regulatory elements in the protocadherin-alpha gene cluster. Proceedings of the National Academy of Sciences of the United States of America *103*, 19719-19724.
Robinson, P.J., An, W., Routh, A., Martino, F., Chapman, L., Roeder, R.G., and Rhodes, D. (2008). 30 nm chromatin fibre decompaction requires both H4-K16 acetylation and linker histone eviction. Journal of molecular biology *381*, 816-825.

Rogers, T.D., Dickson, P.E., McKimm, E., Heck, D.H., Goldowitz, D., Blaha, C.D., and Mittleman, G. (2013). Reorganization of circuits underlying cerebellar modulation of prefrontal cortical dopamine in mouse models of autism spectrum disorder. Cerebellum *12*, 547-556.
Ronan, J.L., Wu, W., and Crabtree, G.R. (2013). From neural development to cognition: unexpected roles for chromatin. Nature reviews Genetics *14*, 347-359.
Roth, G.E., Blanton, H.M., Hager, L.J., and Zakian, V.A. (1983). Isolation and characterization of sequences from mouse chromosomal DNA with ARS function in yeasts. Molecular and cellular biology *3*, 1898-1908.
Routh, A., Sandin, S., and Rhodes, D. (2008). Nucleosome repeat length and linker histone stoichiometry determine chromatin fiber structure. Proceedings of the National Academy of Sciences of the United States of America *105*, 8872-8877.
Ruhl, D.D., Jin, J., Cai, Y., Swanson, S., Florens, L., Washburn, M.P., Conaway, R.C., Conaway, J.W., and Chrivia, J.C. (2006). Purification of a human SRCAP complex that remodels chromatin by incorporating the histone variant H2A.Z into nucleosomes. Biochemistry *45*, 5671-5677.
Ryan, D.P., and Owen-Hughes, T. (2011). Snf2-family proteins: chromatin remodellers for any occasion. Current opinion in chemical biology *15*, 649-656.
Ryan, D.P., Sundaramoorthy, R., Martin, D., Singh, V., and Owen-Hughes, T. (2011). The DNA-binding domain of the Chd1 chromatin-remodelling enzyme contains SANT and SLIDE domains. The EMBO journal *30*, 2596-2609.
Sala, A., Toto, M., Pinello, L., Gabriele, A., Di Benedetto, V., Ingrassia, A.M., Lo Bosco, G., Di Gesu, V., Giancarlo, R., and Corona, D.F. (2011). Genome-wide characterization of chromatin binding and nucleosome spacing activity of the nucleosome remodelling ATPase ISWI. The EMBO journal *30*, 1766-1777.
Sanchez-Molina, S., Mortusewicz, O., Bieber, B., Auer, S., Eckey, M., Leonhardt, H., Friedl, A.A., and Becker, P.B. (2011). Role for hACF1 in the G2/M damage checkpoint. Nucleic acids research *39*, 8445-8456.
Santoro, R., Li, J., and Grummt, I. (2002). The nucleolar remodeling complex NoRC mediates heterochromatin formation and silencing of ribosomal gene transcription. Nature genetics *32*, 393-396.
Sarachana, T., and Hu, V.W. (2013). Genome-wide identification of transcriptional targets of RORA reveals direct regulation of multiple genes associated with autism spectrum disorder. Molecular autism *4*, 14.
Sarcinella, E., Zuzarte, P.C., Lau, P.N., Draker, R., and Cheung, P. (2007). Monoubiquitylation of H2A.Z distinguishes its association with euchromatin or facultative heterochromatin. Molecular and cellular biology *27*, 6457-6468.
Schnetz, M.P., Bartels, C.F., Shastri, K., Balasubramanian, D., Zentner, G.E., Balaji, R., Zhang, X., Song, L., Wang, Z., Laframboise, T.*, et al.* (2009). Genomic distribution of CHD7 on chromatin tracks H3K4 methylation patterns. Genome research *19*, 590-601.
Schuster, E.F., and Stoger, R. (2002). CHD5 defines a new subfamily of chromodomain-SWI2/SNF2-like helicases. Mammalian genome : official journal of the International Mammalian Genome Society *13*, 117-119.
Scott, T.G. (1963). A Unique Pattern of Localization within the Cerebellum. Nature *200*, 793.

Seelig, H.P., Moosbrugger, I., Ehrfeld, H., Fink, T., Renz, M., and Genth, E. (1995). The major dermatomyositis-specific Mi-2 autoantigen is a presumed helicase involved in transcriptional activation. Arthritis and rheumatism *38*, 1389-1399.
Shen, L., Nam, H.S., Song, P., Moore, H., and Anderson, S.A. (2006a). FoxG1 haploinsufficiency results in impaired neurogenesis in the postnatal hippocampus and contextual memory deficits. Hippocampus *16*, 875-890.
Shen, Q., Wang, Y., Dimos, J.T., Fasano, C.A., Phoenix, T.N., Lemischka, I.R., Ivanova, N.B., Stifani, S., Morrisey, E.E., and Temple, S. (2006b). The timing of cortical neurogenesis is encoded within lineages of individual progenitor cells. Nat Neurosci *9*, 743-751.
Shioda, N., Beppu, H., Fukuda, T., Li, E., Kitajima, I., and Fukunaga, K. (2011). Aberrant calcium/calmodulin-dependent protein kinase II (CaMKII) activity is associated with abnormal dendritic spine morphology in the ATRX mutant mouse brain. The Journal of neuroscience : the official journal of the Society for Neuroscience *31*, 346-358.
Siegenthaler, J.A., and Miller, M.W. (2005). Transforming growth factor beta 1 promotes cell cycle exit through the cyclin-dependent kinase inhibitor p21 in the developing cerebral cortex. J Neurosci *25*, 8627-8636.
Siegenthaler, J.A., Tremper-Wells, B.A., and Miller, M.W. (2007). Foxg1 Haploinsufficiency Reduces the Population of Cortical Intermediate Progenitor Cells: Effect of Increased p21 Expression. Cereb Cortex.
Siegenthaler, J.A., Tremper-Wells, B.A., and Miller, M.W. (2008). Foxg1 haploinsufficiency reduces the population of cortical intermediate progenitor cells: effect of increased p21 expression. Cereb Cortex *18*, 1865-1875.
Sillitoe, R.V., and Joyner, A.L. (2007). Morphology, molecular codes, and circuitry produce the three-dimensional complexity of the cerebellum. Annual review of cell and developmental biology *23*, 549-577.
Sillitoe, R.V., Stephen, D., Lao, Z., and Joyner, A.L. (2008). Engrailed homeobox genes determine the organization of Purkinje cell sagittal stripe gene expression in the adult cerebellum. The Journal of neuroscience : the official journal of the Society for Neuroscience *28*, 12150-12162.
Sillitoe, R.V., Vogel, M.W., and Joyner, A.L. (2010). Engrailed homeobox genes regulate establishment of the cerebellar afferent circuit map. The Journal of neuroscience : the official journal of the Society for Neuroscience *30*, 10015-10024.
Simic, R., Lindstrom, D.L., Tran, H.G., Roinick, K.L., Costa, P.J., Johnson, A.D., Hartzog, G.A., and Arndt, K.M. (2003). Chromatin remodeling protein Chd1 interacts with transcription elongation factors and localizes to transcribed genes. The EMBO journal *22*, 1846-1856.
Sims, R.J., 3rd, Millhouse, S., Chen, C.F., Lewis, B.A., Erdjument-Bromage, H., Tempst, P., Manley, J.L., and Reinberg, D. (2007). Recognition of trimethylated histone H3 lysine 4 facilitates the recruitment of transcription postinitiation factors and pre-mRNA splicing. Molecular cell *28*, 665-676.
Sin, H.S., Barski, A., Zhang, F., Kartashov, A.V., Nussenzweig, A., Chen, J., Andreassen, P.R., and Namekawa, S.H. (2012). RNF8 regulates active epigenetic modifications and escape gene activation from inactive sex chromosomes in post-meiotic spermatids. Genes & development *26*, 2737-2748.

Siriaco, G., Deuring, R., Chioda, M., Becker, P.B., and Tamkun, J.W. (2009). Drosophila ISWI regulates the association of histone H1 with interphase chromosomes in vivo. Genetics *182*, 661-669.
Smart, I.H. (1984). Histogenesis of the mesocortical area of the mouse telencephalon. Journal of anatomy *138 (Pt 3)*, 537-552.
Smart, I.H. (1985a). Differential growth of the cell production systems in the lateral wall of the developing mouse telencephalon. Journal of anatomy *141*, 219-229.
Smart, I.H. (1985b). A localised growth zone in the wall of the developing mouse telencephalon. Journal of anatomy *140 (Pt 3)*, 397-402.
Smart, I.H., and McSherry, G.M. (1982). Growth patterns in the lateral wall of the mouse telencephalon. II. Histological changes during and subsequent to the period of isocortical neuron production. Journal of anatomy *134*, 415-442.
Smart, I.H., and Smart, M. (1982). Growth patterns in the lateral wall of the mouse telencephalon: I. Autoradiographic studies of the histogenesis of the isocortex and adjacent areas. Journal of anatomy *134*, 273-298.
Smith, K.P., Byron, M., Clemson, C.M., and Lawrence, J.B. (2004). Ubiquitinated proteins including uH2A on the human and mouse inactive X chromosome: enrichment in gene rich bands. Chromosoma *113*, 324-335.
Smolle, M., Venkatesh, S., Gogol, M.M., Li, H., Zhang, Y., Florens, L., Washburn, M.P., and Workman, J.L. (2012). Chromatin remodelers Isw1 and Chd1 maintain chromatin structure during transcription by preventing histone exchange. Nature structural & molecular biology *19*, 884-892.
Srinivasan, K., Leone, D.P., Bateson, R.K., Dobreva, G., Kohwi, Y., Kohwi-Shigematsu, T., Grosschedl, R., and McConnell, S.K. (2012). A network of genetic repression and derepression specifies projection fates in the developing neocortex. Proceedings of the National Academy of Sciences of the United States of America *109*, 19071-19078.
Srinivasan, R., Mager, G.M., Ward, R.M., Mayer, J., and Svaren, J. (2006). NAB2 represses transcription by interacting with the CHD4 subunit of the nucleosome remodeling and deacetylase (NuRD) complex. The Journal of biological chemistry *281*, 15129-15137.
Srinivasan, S., Armstrong, J.A., Deuring, R., Dahlsveen, I.K., McNeill, H., and Tamkun, J.W. (2005). The Drosophila trithorax group protein Kismet facilitates an early step in transcriptional elongation by RNA Polymerase II. Development *132*, 1623-1635.
Srinivasan, S., Dorighi, K.M., and Tamkun, J.W. (2008). Drosophila Kismet regulates histone H3 lysine 27 methylation and early elongation by RNA polymerase II. PLoS genetics *4*, e1000217.
Stock, J.K., Giadrossi, S., Casanova, M., Brookes, E., Vidal, M., Koseki, H., Brockdorff, N., Fisher, A.G., and Pombo, A. (2007). Ring1-mediated ubiquitination of H2A restrains poised RNA polymerase II at bivalent genes in mouse ES cells. Nature cell biology *9*, 1428-1435.
Stokes, D.G., and Perry, R.P. (1995). DNA-binding and chromatin localization properties of CHD1. Molecular and cellular biology *15*, 2745-2753.
Stopka, T., and Skoultchi, A.I. (2003). The ISWI ATPase Snf2h is required for early mouse development. Proc Natl Acad Sci U S A *100*, 14097-14102.
Stoykova, A., Treichel, D., Hallonet, M., and Gruss, P. (2000). Pax6 modulates the dorsoventral patterning of the mammalian telencephalon. The Journal of neuroscience : the official journal of the Society for Neuroscience *20*, 8042-8050.

Strohner, R., Nemeth, A., Jansa, P., Hofmann-Rohrer, U., Santoro, R., Langst, G., and Grummt, I. (2001). NoRC--a novel member of mammalian ISWI-containing chromatin remodeling machines. The EMBO journal *20*, 4892-4900.
Strukov, Y.G., Wang, Y., and Belmont, A.S. (2003). Engineered chromosome regions with altered sequence composition demonstrate hierarchical large-scale folding within metaphase chromosomes. The Journal of cell biology *162*, 23-35.
Sudarov, A., and Joyner, A.L. (2007). Cerebellum morphogenesis: the foliation pattern is orchestrated by multi-cellular anchoring centers. Neural development *2*, 26.
Sultan, F., Augath, M., Hamodeh, S., Murayama, Y., Oeltermann, A., Rauch, A., and Thier, P. (2012). Unravelling cerebellar pathways with high temporal precision targeting motor and extensive sensory and parietal networks. Nature communications *3*, 924.
Surmeli, G., Akay, T., Ippolito, G.C., Tucker, P.W., and Jessell, T.M. (2011). Patterns of spinal sensory-motor connectivity prescribed by a dorsoventral positional template. Cell *147*, 653-665.
Talkowski, M.E., Rosenfeld, J.A., Blumenthal, I., Pillalamarri, V., Chiang, C., Heilbut, A., Ernst, C., Hanscom, C., Rossin, E., Lindgren, A.M*., et al.* (2012). Sequencing chromosomal abnormalities reveals neurodevelopmental loci that confer risk across diagnostic boundaries. Cell *149*, 525-537.
Tan, S.S., and Breen, S. (1993). Radial mosaicism and tangential cell dispersion both contribute to mouse neocortical development. Nature *362*, 638-640.
Tasic, B., Nabholz, C.E., Baldwin, K.K., Kim, Y., Rueckert, E.H., Ribich, S.A., Cramer, P., Wu, Q., Axel, R., and Maniatis, T. (2002). Promoter choice determines splice site selection in protocadherin alpha and gamma pre-mRNA splicing. Molecular cell *10*, 21-33.
Thompson, P.M., Gotoh, T., Kok, M., White, P.S., and Brodeur, G.M. (2003). CHD5, a new member of the chromodomain gene family, is preferentially expressed in the nervous system. Oncogene *22*, 1002-1011.
Tian, C., Gong, Y., Yang, Y., Shen, W., Wang, K., Liu, J., Xu, B., Zhao, J., and Zhao, C. (2012). Foxg1 has an essential role in postnatal development of the dentate gyrus. The Journal of neuroscience : the official journal of the Society for Neuroscience *32*, 2931-2949.
Todd, M.A., and Picketts, D.J. (2012). PHF6 interacts with the nucleosome remodeling and deacetylation (NuRD) complex. Journal of proteome research *11*, 4326-4337.
Todd, P.H., and Smart, I.H. (1982). Growth patterns in the lateral wall of the mouse telencephalon: III. Studies of the chronologically ordered column hypothesis of isocortical histogenesis. Journal of anatomy *134*, 633-642.
Tong, J.K., Hassig, C.A., Schnitzler, G.R., Kingston, R.E., and Schreiber, S.L. (1998). Chromatin deacetylation by an ATP-dependent nucleosome remodelling complex. Nature *395*, 917-921.
Tsai, P.T., Hull, C., Chu, Y., Greene-Colozzi, E., Sadowski, A.R., Leech, J.M., Steinberg, J., Crawley, J.N., Regehr, W.G., and Sahin, M. (2012a). Autistic-like behaviour and cerebellar dysfunction in Purkinje cell Tsc1 mutant mice. Nature *488*, 647-651.
Tsai, P.T., Hull, C., Chu, Y., Greene-Colozzi, E., Sadowski, A.R., Leech, J.M., Steinberg, J., Crawley, J.N., Regehr, W.G., and Sahin, M. (2012b). Autistic-like behaviour and cerebellar dysfunction in Purkinje cell Tsc1 mutant mice. Nature.
Tsukiyama, T., Daniel, C., Tamkun, J., and Wu, C. (1995). ISWI, a member of the SWI2/SNF2 ATPase family, encodes the 140 kDa subunit of the nucleosome remodeling factor. Cell *83*, 1021-1026.

Tsukiyama, T., Palmer, J., Landel, C.C., Shiloach, J., and Wu, C. (1999). Characterization of the imitation switch subfamily of ATP-dependent chromatin-remodeling factors in Saccharomyces cerevisiae. Genes & development *13*, 686-697.
Tsukiyama, T., and Wu, C. (1995). Purification and properties of an ATP-dependent nucleosome remodeling factor. Cell *83*, 1011-1020.
van Attikum, H., Fritsch, O., Hohn, B., and Gasser, S.M. (2004). Recruitment of the INO80 complex by H2A phosphorylation links ATP-dependent chromatin remodeling with DNA double-strand break repair. Cell *119*, 777-788.
van Bokhoven, H., and Kramer, J.M. (2010). Disruption of the epigenetic code: an emerging mechanism in mental retardation. Neurobiol Dis *39*, 3-12.
Varga-Weisz, P.D., Wilm, M., Bonte, E., Dumas, K., Mann, M., and Becker, P.B. (1997). Chromatin-remodelling factor CHRAC contains the ATPases ISWI and topoisomerase II. Nature *388*, 598-602.
Vary, J.C., Jr., Gangaraju, V.K., Qin, J., Landel, C.C., Kooperberg, C., Bartholomew, B., and Tsukiyama, T. (2003). Yeast Isw1p forms two separable complexes in vivo. Molecular and cellular biology *23*, 80-91.
Vernay, B., Koch, M., Vaccarino, F., Briscoe, J., Simeone, A., Kageyama, R., and Ang, S.L. (2005). Otx2 regulates subtype specification and neurogenesis in the midbrain. The Journal of neuroscience : the official journal of the Society for Neuroscience *25*, 4856-4867.
Vidal, C.N., Nicolson, R., DeVito, T.J., Hayashi, K.M., Geaga, J.A., Drost, D.J., Williamson, P.C., Rajakumar, N., Sui, Y., Dutton, R.A.*, et al.* (2006). Mapping corpus callosum deficits in autism: an index of aberrant cortical connectivity. Biological psychiatry *60*, 218-225.
Vissers, L.E., van Ravenswaaij, C.M., Admiraal, R., Hurst, J.A., de Vries, B.B., Janssen, I.M., van der Vliet, W.A., Huys, E.H., de Jong, P.J., Hamel, B.C.*, et al.* (2004). Mutations in a new member of the chromodomain gene family cause CHARGE syndrome. Nature genetics *36*, 955-957.
Vogel-Ciernia, A., Matheos, D.P., Barrett, R.M., Kramar, E.A., Azzawi, S., Chen, Y., Magnan, C.N., Zeller, M., Sylvain, A., Haettig, J.*, et al.* (2013). The neuron-specific chromatin regulatory subunit BAF53b is necessary for synaptic plasticity and memory. Nature neuroscience *16*, 552-561.
Vogler, C., Huber, C., Waldmann, T., Ettig, R., Braun, L., Izzo, A., Daujat, S., Chassignet, I., Lopez-Contreras, A.J., Fernandez-Capetillo, O.*, et al.* (2010). Histone H2A C-terminus regulates chromatin dynamics, remodeling, and histone H1 binding. PLoS genetics *6*, e1001234.
Voigt, P., LeRoy, G., Drury, W.J., 3rd, Zee, B.M., Son, J., Beck, D.B., Young, N.L., Garcia, B.A., and Reinberg, D. (2012). Asymmetrically modified nucleosomes. Cell *151*, 181-193.
Voogd, J. (1967). Comparative aspects of the structure and fibre connexions of the mammalian cerebellum. Progress in brain research *25*, 94-134.
Wade, P.A., Jones, P.L., Vermaak, D., and Wolffe, A.P. (1998). A multiple subunit Mi-2 histone deacetylase from Xenopus laevis cofractionates with an associated Snf2 superfamily ATPase. Current biology : CB *8*, 843-846.
Wallace, V.A. (1999). Purkinje-cell-derived Sonic hedgehog regulates granule neuron precursor cell proliferation in the developing mouse cerebellum. Current biology : CB *9*, 445-448.

Wang, V.Y., Rose, M.F., and Zoghbi, H.Y. (2005). Math1 expression redefines the rhombic lip derivatives and reveals novel lineages within the brainstem and cerebellum. Neuron *48*, 31-43.
Wang, V.Y., and Zoghbi, H.Y. (2001). Genetic regulation of cerebellar development. Nature reviews Neuroscience *2*, 484-491.
Wang, X., Su, H., and Bradley, A. (2002a). Molecular mechanisms governing Pcdh-gamma gene expression: evidence for a multiple promoter and cis-alternative splicing model. Genes & development *16*, 1890-1905.
Wang, X., Weiner, J.A., Levi, S., Craig, A.M., Bradley, A., and Sanes, J.R. (2002b). Gamma protocadherins are required for survival of spinal interneurons. Neuron *36*, 843-854.
Wang, Y., Zhang, H., Chen, Y., Sun, Y., Yang, F., Yu, W., Liang, J., Sun, L., Yang, X., Shi, L.*, et al.* (2009). LSD1 is a subunit of the NuRD complex and targets the metastasis programs in breast cancer. Cell *138*, 660-672.
Weiner, J.A., Wang, X., Tapia, J.C., and Sanes, J.R. (2005). Gamma protocadherins are required for synaptic development in the spinal cord. Proceedings of the National Academy of Sciences of the United States of America *102*, 8-14.
Williams, C.J., Naito, T., Arco, P.G., Seavitt, J.R., Cashman, S.M., De Souza, B., Qi, X., Keables, P., Von Andrian, U.H., and Georgopoulos, K. (2004). The chromatin remodeler Mi-2beta is required for CD4 expression and T cell development. Immunity *20*, 719-733.
Wilson, S.L., Kalinovsky, A., Orvis, G.D., and Joyner, A.L. (2011). Spatially restricted and developmentally dynamic expression of engrailed genes in multiple cerebellar cell types. Cerebellum *10*, 356-372.
Wong, M.M., Cox, L.K., and Chrivia, J.C. (2007). The chromatin remodeling protein, SRCAP, is critical for deposition of the histone variant H2A.Z at promoters. The Journal of biological chemistry *282*, 26132-26139.
Wood, J.G., Martin, S., and Price, D.J. (1992). Evidence that the earliest generated cells of the murine cerebral cortex form a transient population in the subplate and marginal zone. Brain research Developmental brain research *66*, 137-140.
Woodage, T., Basrai, M.A., Baxevanis, A.D., Hieter, P., and Collins, F.S. (1997). Characterization of the CHD family of proteins. Proceedings of the National Academy of Sciences of the United States of America *94*, 11472-11477.
Wu, J.I., Lessard, J., Olave, I.A., Qiu, Z., Ghosh, A., Graef, I.A., and Crabtree, G.R. (2007). Regulation of dendritic development by neuron-specific chromatin remodeling complexes. Neuron *56*, 94-108.
Wu, Q., Zhang, T., Cheng, J.F., Kim, Y., Grimwood, J., Schmutz, J., Dickson, M., Noonan, J.P., Zhang, M.Q., Myers, R.M.*, et al.* (2001). Comparative DNA sequence analysis of mouse and human protocadherin gene clusters. Genome research *11*, 389-404.
Wurst, W., Auerbach, A.B., and Joyner, A.L. (1994). Multiple developmental defects in Engrailed-1 mutant mice: an early mid-hindbrain deletion and patterning defects in forelimbs and sternum. Development *120*, 2065-2075.
Wurst, W., and Bally-Cuif, L. (2001). Neural plate patterning: upstream and downstream of the isthmic organizer. Nature reviews Neuroscience *2*, 99-108.
Wysocka, J., Swigut, T., Xiao, H., Milne, T.A., Kwon, S.Y., Landry, J., Kauer, M., Tackett, A.J., Chait, B.T., Badenhorst, P.*, et al.* (2006). A PHD finger of NURF couples histone H3 lysine 4 trimethylation with chromatin remodelling. Nature *442*, 86-90.

Xi, R., and Xie, T. (2005). Stem cell self-renewal controlled by chromatin remodeling factors. Science *310*, 1487-1489.
Xiao, A., Li, H., Shechter, D., Ahn, S.H., Fabrizio, L.A., Erdjument-Bromage, H., Ishibe-Murakami, S., Wang, B., Tempst, P., Hofmann, K.*, et al.* (2009). WSTF regulates the H2A.X DNA damage response via a novel tyrosine kinase activity. Nature *457*, 57-62.
Xie, W., Schultz, M.D., Lister, R., Hou, Z., Rajagopal, N., Ray, P., Whitaker, J.W., Tian, S., Hawkins, R.D., Leung, D.*, et al.* (2013). Epigenomic analysis of multilineage differentiation of human embryonic stem cells. Cell *153*, 1134-1148.
Xuan, S., Baptista, C.A., Balas, G., Tao, W., Soares, V.C., and Lai, E. (1995). Winged helix transcription factor BF-1 is essential for the development of the cerebral hemispheres. Neuron *14*, 1141-1152.
Xue, Y., Wong, J., Moreno, G.T., Young, M.K., Cote, J., and Wang, W. (1998). NURD, a novel complex with both ATP-dependent chromatin-remodeling and histone deacetylase activities. Molecular cell *2*, 851-861.
Yadon, A.N., and Tsukiyama, T. (2011). SnapShot: Chromatin remodeling: ISWI. Cell *144*, 453-453 e451.
Yagi, T. (2012). Molecular codes for neuronal individuality and cell assembly in the brain. Frontiers in molecular neuroscience *5*, 45.
Yajima, M., Fairbrother, W.G., and Wessel, G.M. (2012). ISWI contributes to ArsI insulator function in development of the sea urchin. Development *139*, 3613-3622.
Yao, Y.L., and Yang, W.M. (2003). The metastasis-associated proteins 1 and 2 form distinct protein complexes with histone deacetylase activity. The Journal of biological chemistry *278*, 42560-42568.
Yasui, D., Miyano, M., Cai, S., Varga-Weisz, P., and Kohwi-Shigematsu, T. (2002). SATB1 targets chromatin remodelling to regulate genes over long distances. Nature *419*, 641-645.
Yen, K., Vinayachandran, V., Batta, K., Koerber, R.T., and Pugh, B.F. (2012). Genome-wide nucleosome specificity and directionality of chromatin remodelers. Cell *149*, 1461-1473.
Yip, D.J., Corcoran, C.P., Alvarez-Saavedra, M., DeMaria, A., Rennick, S., Mears, A.J., Rudnicki, M.A., Messier, C., and Picketts, D.J. (2012). Snf2l regulates Foxg1-dependent progenitor cell expansion in the developing brain. Developmental cell *22*, 871-878.
Yip, D.J., and Picketts, D.J. (2003). Increasing D4Z4 repeat copy number compromises C2C12 myoblast differentiation. FEBS Lett *537*, 133-138.
Yokota, S., Hirayama, T., Hirano, K., Kaneko, R., Toyoda, S., Kawamura, Y., Hirabayashi, M., Hirabayashi, T., and Yagi, T. (2011). Identification of the cluster control region for the protocadherin-beta genes located beyond the protocadherin-gamma cluster. The Journal of biological chemistry *286*, 31885-31895.
Yorke, C.H., Jr., and Caviness, V.S., Jr. (1975). Interhemispheric neocortical connections of the corpus callosum in the normal mouse: a study based on anterograde and retrograde methods. The Journal of comparative neurology *164*, 233-245.
Yoshimura, K., Kitagawa, H., Fujiki, R., Tanabe, M., Takezawa, S., Takada, I., Yamaoka, I., Yonezawa, M., Kondo, T., Furutani, Y.*, et al.* (2009). Distinct function of 2 chromatin remodeling complexes that share a common subunit, Williams syndrome transcription factor (WSTF). Proceedings of the National Academy of Sciences of the United States of America *106*, 9280-9285.

Yoshinaga, S.K., Peterson, C.L., Herskowitz, I., and Yamamoto, K.R. (1992). Roles of SWI1, SWI2, and SWI3 proteins for transcriptional enhancement by steroid receptors. Science *258*, 1598-1604.
Yu, Y., Chen, Y., Kim, B., Wang, H., Zhao, C., He, X., Liu, L., Liu, W., Wu, L.M., Mao, M.*, et al.* (2013). Olig2 targets chromatin remodelers to enhancers to initiate oligodendrocyte differentiation. Cell *152*, 248-261.
Zentner, G.E., and Henikoff, S. (2013). Regulation of nucleosome dynamics by histone modifications. Nature structural & molecular biology *20*, 259-266.
Zentner, G.E., Tsukiyama, T., and Henikoff, S. (2013). ISWI and CHD chromatin remodelers bind promoters but act in gene bodies. PLoS genetics *9*, e1003317.
Zhang, L., Song, N.N., Chen, J.Y., Huang, Y., Li, H., and Ding, Y.Q. (2012). Satb2 is required for dendritic arborization and soma spacing in mouse cerebral cortex. Cereb Cortex *22*, 1510-1519.
Zhang, Y., LeRoy, G., Seelig, H.P., Lane, W.S., and Reinberg, D. (1998). The dermatomyositis-specific autoantigen Mi2 is a component of a complex containing histone deacetylase and nucleosome remodeling activities. Cell *95*, 279-289.
Zhao, C., Guan, W., and Pleasure, S.J. (2006). A transgenic marker mouse line labels Cajal-Retzius cells from the cortical hem and thalamocortical axons. Brain research *1077*, 48-53.
Zhou, Z., Hong, E.J., Cohen, S., Zhao, W.N., Ho, H.Y., Schmidt, L., Chen, W.G., Lin, Y., Savner, E., Griffith, E.C.*, et al.* (2006). Brain-specific phosphorylation of MeCP2 regulates activity-dependent Bdnf transcription, dendritic growth, and spine maturation. Neuron *52*, 255-269.
Zhu, Y., van Essen, D., and Saccani, S. (2012). Cell-type-specific control of enhancer activity by H3K9 trimethylation. Molecular cell *46*, 408-423.

APPENDIX (COPYRIGHT PERMISSIONS)

ELSEVIER LICENSE
TERMS AND CONDITIONS
Nov 29, 2013

This is a License Agreement between Matias A Alvarez-Saavedra ("You") and Elsevier ("Elsevier") provided by Copyright Clearance Center ("CCC"). The license consists of your order details, the terms and conditions provided by Elsevier, and the payment terms and conditions.

All payments must be made in full to CCC. For payment instructions, please see information listed at the bottom of this form.

Supplier	Elsevier Limited The Boulevard,Langford Lane Kidlington,Oxford,OX5 1GB,UK
Registered Company Number	1982084
Customer name	Matias A Alvarez-Saavedra
Customer address	195 Lennox Park Avenue Ottawa, ON K1G 0K3
License number	3185510464799
License date	Jul 10, 2013
Licensed content publisher	Elsevier
Licensed content publication	Developmental Cell
Licensed content title	Snf2l Regulates Foxg1-Dependent Progenitor Cell Expansion in the Developing Brain
Licensed content author	Darren J. Yip,Chelsea P. Corcoran,Matías Alvarez-Saavedra,Adriana DeMaria,Stephen Rennick,Alan J. Mears,Michael A. Rudnicki,Claude Messier,David J. Picketts
Licensed content date	17 April 2012
Licensed content volume number	22
Licensed content issue number	4
Number of pages	8
Start Page	871
End Page	878
Type of Use	reuse in a thesis/dissertation
Portion	full article
Format	both print and electronic

Are you the author of this Elsevier article?	Yes
Will you be translating?	No
Title of your thesis/dissertation	The Snf2l and Snf2h chromatin remodeling proteins co-modulate gene expression to govern brain development, neuronal circuitry assembly and cognitive functions.
Expected completion date	Sep 2013
Estimated size (number of pages)	
Elsevier VAT number	GB 494 6272 12
Permissions price	0.00 USD
VAT/Local Sales Tax	0.00 USD / 0.00 GBP
Total	0.00 USD

Terms and Conditions

NATURE PUBLISHING GROUP LICENSE
TERMS AND CONDITIONS

Aug 30, 2013

This is a License Agreement between Matias A Alvarez-Saavedra ("You") and Nature Publishing Group ("Nature Publishing Group") provided by Copyright Clearance Center ("CCC"). The license consists of your order details, the terms and conditions provided by Nature Publishing Group, and the payment terms and conditions.

All payments must be made in full to CCC. For payment instructions, please see information listed at the bottom of this form.

License Number	3218650653650
License date	Aug 30, 2013
Licensed content publisher	Nature Publishing Group
Licensed content publication	Nature
Licensed content title	Chromatin remodelling during development
Licensed content author	Lena Ho and Gerald R. Crabtree
Licensed content date	Jan 27, 2010
Volume number	463
Issue number	7280
Type of Use	reuse in a thesis/dissertation
Requestor type	academic/educational
Format	print and electronic
Portion	figures/tables/illustrations
Number of figures/tables /illustrations	1
High-res required	no
Figures	Figure 2.
Author of this NPG article	no
Your reference number	
Title of your thesis / dissertation	The Snf2l and Snf2h chromatin remodeling proteins co-modulate gene expression to govern brain development, neuronal circuitry assembly and cognitive functions.
Expected completion date	Sep 2013
Estimated size (number of pages)	300
Total	0.00 USD

ELSEVIER LICENSE
TERMS AND CONDITIONS

Aug 30, 2013

This is a License Agreement between Matias A Alvarez-Saavedra ("You") and Elsevier ("Elsevier") provided by Copyright Clearance Center ("CCC"). The license consists of your order details, the terms and conditions provided by Elsevier, and the payment terms and conditions.

All payments must be made in full to CCC. For payment instructions, please see information listed at the bottom of this form.

Supplier	Elsevier Limited The Boulevard,Langford Lane Kidlington,Oxford,OX5 1GB,UK
Registered Company Number	1982084
Customer name	Matias A Alvarez-Saavedra
Customer address	195 Lennox Park Avenue Ottawa, ON K1G 0K3
License number	3218650761542
License date	Aug 30, 2013
Licensed content publisher	Elsevier
Licensed content publication	Cell
Licensed content title	SnapShot: Chromatin Remodeling: ISWI
Licensed content author	Adam N. Yadon,Toshio Tsukiyama
Licensed content date	4 February 2011
Licensed content volume number	144
Licensed content issue number	3
Number of pages	2
Start Page	453
End Page	453.e1
Type of Use	reuse in a thesis/dissertation
Intended publisher of new work	other
Portion	figures/tables/illustrations

NATURE PUBLISHING GROUP LICENSE
TERMS AND CONDITIONS

Aug 30, 2013

This is a License Agreement between Matias A Alvarez-Saavedra ("You") and Nature Publishing Group ("Nature Publishing Group") provided by Copyright Clearance Center ("CCC"). The license consists of your order details, the terms and conditions provided by Nature Publishing Group, and the payment terms and conditions.

All payments must be made in full to CCC. For payment instructions, please see information listed at the bottom of this form.

License Number	3218650460032
License date	Aug 30, 2013
Licensed content publisher	Nature Publishing Group
Licensed content publication	Nature Reviews Neuroscience
Licensed content title	Neuronal subtype specification in the cerebral cortex
Licensed content author	Bradley J. Molyneaux, Paola Arlotta, Joao R. L. Menezes and Jeffrey D. Macklis
Licensed content date	Jun 1, 2007
Volume number	8
Issue number	6
Type of Use	reuse in a thesis/dissertation
Requestor type	academic/educational
Format	print and electronic
Portion	figures/tables/illustrations
Number of figures/tables /illustrations	1
High-res required	no
Figures	Figure 2.
Author of this NPG article	no
Your reference number	
Title of your thesis / dissertation	The Snf2l and Snf2h chromatin remodeling proteins co-modulate gene expression to govern brain development, neuronal circuitry assembly and cognitive functions.
Expected completion date	Sep 2013
Estimated size (number of pages)	300

Confirmation Number: 11119846

Special Rightsholder Terms & Conditions

The following terms & conditions apply to the specific publication under which they are listed

ANNUAL REVIEW OF CELL AND DEVELOPMENTAL BIOLOGY
Permission type: Republish or display content
Type of use: Republish in a thesis/dissertation

TERMS AND CONDITIONSThe following terms are individual to this publisher:

None

Other Terms and Conditions:NoneSTANDARD TERMS AND CONDITIONS1. Description of Service; Defined Terms. T
Republication License enables the User to obtain licenses for republication of one or more copyrighted works as
described in detail on the relevant Order Confirmation (the "Work(s)"). Copyright Clearance Center, Inc. ("CCC") g
licenses through the Service on behalf of the rightsholder identified on the Order Confirmation (the "Rightsholder".
"Republication", as used herein, generally means the inclusion of a Work, in whole or in part, in a new work or wo
also as described on the Order Confirmation. "User", as used herein, means the person or entity making such
republication.2. The terms set forth in the relevant Order Confirmation, and any terms set by the Rightsholder witl
respect to a particular Work, govern the terms of use of Works in connection with the Service. By using the Servic
person transacting for a republication license on behalf of the User represents and warrants that he/she/it (a) has
duly authorized by the User to accept, and hereby does accept, all such terms and conditions on behalf of User, ar
shall inform User of all such terms and conditions. In the event such person is a "freelancer" or other third party
independent of User and CCC, such party shall be deemed jointly a "User" for purposes of these terms and conditi
any event, User shall be deemed to have accepted and agreed to all such terms and conditions if User republishes
Work in any fashion.3. Scope of License; Limitations and Obligations.3.1 All Works and all rights therein, including
copyright rights, remain the sole and exclusive property of the Rightsholder. The license created by the exchange
Order Confirmation (and/or any invoice) and payment by User of the full amount set forth on that document inclu
only those rights expressly set forth in the Order Confirmation and in these terms and conditions, and conveys no
rights in the Work(s) to User. All rights not expressly granted are hereby reserved.3.2 General Payment Terms: Yo
pay by credit card or through an account with us payable at the end of the month. If you and we agree that you m
establish a standing account with CCC, then the following terms apply: Remit Payment to: Copyright Clearance Ce
Dept 001, P.O. Box 843006, Boston, MA 02284-3006. Payments Due: Invoices are payable upon their delivery to
upon our notice to you that they are available to you for downloading). After 30 days, outstanding amounts will be
subject to a service charge of 1-1/2% per month or, if less, the maximum rate allowed by applicable law. Unless
otherwise specifically set forth in the Order Confirmation or in a separate written agreement signed by CCC, invoic
due and payable on "net 30" terms. While User may exercise the rights licensed immediately upon issuance of the
Confirmation, the license is automatically revoked and is null and void, as if it had never been issued, if complete
payment for the license is not received on a timely basis either from User directly or through a payment agent, su
credit card company.3.3 Unless otherwise provided in the Order Confirmation, any grant of rights to User (i) is
"one-time" (including the editions and product family specified in the license), (ii) is non-exclusive and non-transfe
and (iii) is subject to any and all limitations and restrictions (such as, but not limited to, limitations on duration of
circulation) included in the Order Confirmation or invoice and/or in these terms and conditions. Upon completion o
licensed use, User shall either secure a new permission for further use of the Work(s) or immediately cease any ne
of the Work(s) and shall render inaccessible (such as by deleting or by removing or severing links or other locator
further copies of the Work (except for copies printed on paper in accordance with this license and still in User's sto
the end of such period).3.4 In the event that the material for which a republication license is sought includes third

FINIS